
Development of a hierarchically detailed
chemical reaction mechanism from
 C_3 to C_5 hydrocarbons

Von der Fakultät für Maschinenbau, Elektro- und
Energiesysteme der Brandenburgischen Technischen Universität
Cottbus-Senftenberg zur Erlangung des akademischen Grades eines
Doktors der Ingenieurwissenschaften

genehmigte Dissertation

vorgelegt von

M.Sc.

Larisa León de Syniawa (geb. León Viloría)

geboren am 06.08.1981 in Valencia, Venezuela

Vorsitzender: Prof. Dr.-Ing. Heiko Schmidt

Gutachter: Prof. Dr.-Ing. Fabian Mauß

Gutachter: Dr. George Skevis

Gutachter: Apl. Prof. Dr. Thomas Zeuch

Tag der mündlichen Prüfung: 17.03.2022

DOI: 10.26127/BTUOpen-6157

Contents

Nomenclature	v
List of Abbreviations	vi
Acknowledgements	vii
1 Introduction	1
2 Theoretical part	5
2.1 Chemical kinetics	5
2.1.1 Rate law and reaction order	5
2.1.2 Relation of forward and reverse reactions	6
2.1.3 Elementary reactions, molecularity of a reaction	7
2.1.4 Temperature dependence of rate coefficients.	8
2.1.5 Pressure dependence of rate coefficients	10
2.2 Thermochemistry	12
2.3 Reaction mechanism	13
2.4 Analysis of a reaction mechanism	14
2.4.1 Sensitivity analysis	14
2.4.2 Reaction Flow analyses	15
2.5 Chemical kinetics in mass and energy conservation	17
2.5.1 Constant volume reactor	17
2.5.2 Constant pressure reactor	21
2.5.3 Perfectly stirred reactor (PSR)	23
2.5.4 Laminar premixed flames	24
2.5.5 Premixed freely propagating flames	25
2.5.6 Premixed burner-stabilized flames	26
2.6 Computational Tool-LOGEresearch	27
2.7 Naming rules for species in the mechanism	27
3 Influence of thermodynamic data on reaction fluxes, and prediction by chemical reaction mechanism	31
3.1 Propane and Propene ignition delay time and sensitivity results.	32
3.2 Propane and Propene ignition delay time and sensitivity results using updated thermodynamic data.	37
3.3 Ignition delay time, laminar flame speed and burner-stabilized flame validation for propene and propane.	44

4	Combustion chemistry of isomers of butane	49
4.1	High temperature chemistry for the C ₄ H ₁₀ isomers	51
4.1.1	Class 1: Unimolecular fuel decomposition	51
4.1.2	Class 2: H-atom abstraction from fuel	52
4.1.3	Class 3: Alkyl radical decomposition	53
4.1.4	Class 4: Alkyl radical + O ₂ direct formation of olefin and HO ₂	54
4.1.5	Class 5: Alkyl radical isomerization	54
4.2	Experiments	55
4.3	Burner-stabilized flame validation of <i>n</i> -butane (C ₄ H ₁₀) and <i>iso</i> -butane (C ₄ H ₁₀ -Me ₂).	55
4.3.1	Major Species	58
4.3.2	Intermediate species	58
4.3.3	Smaller decomposition pathways	61
4.4	Ignition delay time and laminar flame speed validation for <i>n</i> -butane (C ₄ H ₁₀) and <i>iso</i> -butane (C ₄ H ₁₀ -Me ₂)	66
5	Combustion chemistry of the butene isomers	71
5.1	High-temperature chemistry of C ₄ H ₈ isomers	73
5.1.1	Class 1: Unimolecular fuel decomposition	73
5.1.2	Class 2: H-atom abstraction from fuel	74
5.1.3	Class 3: Alkenyl radical decomposition	76
5.1.4	Class 4: Alkenyl radical + O ₂ direct formation of di-olefin and HO ₂	76
5.1.5	Class 5: Alkene isomerization	76
5.2	Experiments	77
5.3	Burner-stabilized flame validation of C ₄ H ₈ isomers: <i>1</i> -butene (C ₄ H ₈ -D1), <i>trans</i> -2-butene (T-C ₄ H ₈ -D2), and <i>iso</i> -butene (C ₄ H ₈ -D1Me ₂).	77
5.3.1	Major Species	81
5.3.2	Intermediate species	82
5.4	Ignition delay time and laminar flame speed validation for butene (C ₄ H ₈) isomers.	92
6	Combustion chemistry of C₅ linear and branched species	102
6.1	High temperature chemistry for <i>n</i> -Pentane (C ₅ H ₁₂) and C ₅ H ₁₀ isomers	109
6.1.1	Class 1: Unimolecular fuel decomposition	109
6.1.2	Class 2: H-atom abstraction from fuel	110
6.1.3	Class 3: Alkyl and alkenyl radical decomposition	114
6.1.4	Class 4: Alkenyl radical + O ₂ direct formation of di-olefin and HO ₂	116
6.1.5	Class 5: Alkyl and alkenyl radical isomerization	116
6.1.6	Class 6: Abstraction reactions from bi-olefin	118
6.1.7	Class 7: Addition of radical species to Olefin	118
6.1.8	Class 8: Radical decomposition	119
6.1.9	Class 9: Di-olefin decomposition	119
6.2	Reaction pathways for aromatic formation	120
6.3	Thermodynamic data	121

6.4	Validation of burner-stabilized flame experiments: 2-Methyl-2-butene (C ₅ H ₁₀ -D ₂ Me ₂) and n-Pentane (C ₅ H ₁₂).	124
6.4.1	Major Species	127
6.4.2	Intermediate species	128
6.4.3	Aromatic ring formation and precursors	133
6.4.4	Influence of C ₅ chemistry on premixed butene flames	145
6.5	Validation of shock tube and Laminar flame speed experiments for 2-Methyl-2-butene and n-Pentane	148
7	Conclusion	153
	Bibliography	156
A	Appendix - Class 2: H-atom abstraction from fuel	169
B	Appendix - Nomenclature	172
B.1	Species containing no carbon	172
B.2	C ₁ species	173
B.3	C ₂ species	175
B.4	C ₃ species	178
B.5	C ₄ species	182
B.6	C ₅ species	193
B.7	C ₆ species	198
B.8	C ₇ species	199
B.9	C ₈ species	200
B.10	C ₉ Species	202
B.11	C ₁₀ Species	202
B.12	C ₁₁ Species	203
B.13	C ₁₂ Species	203
B.14	C ₁₄ species	204

Nomenclature

Roman alphabet

n_A	amount of substance
k	rate coefficient of chemical reaction
A	pre-exponential factor
A	frequency factor (pre-exponential factor)
b	temperature exponent
R	gases constant
E_a	activation energy
Y_i	species mass fraction
W_i	molar mass
T_w	wall temperature
V	volume
A	heat transfer area
h_c	specific enthalpy of convection
c_v	specific heat at constant volume
W_i	molar mass
u	gas velocity component
J_i	diffusion flux
\dot{m}_i	production rate of species i
c_p	heat capacity at constant pressure
h_i	specific enthalpy of species i
N_s	total number of species
T_0	temperature of the surroundings
f_r	radiation factor
G	Gibbs free energy
H	enthalpy
S	entropy
T	temperature
U	internal energy
ΔP	maximun pressure cocentration
ΔCO_2	maximun CO ₂ concentration

Greek Symbols

ε	emissivity factor
ν	reaction rate (also known as R , r and ω_i)
ξ	rate of conversion
ρ	density
σ	Stefan-Boltzmann constant
τ	residence time
ν	number of moles
ϕ	fuel equivalence ratio
λ	thermal conductivity
α	Planck's constant
σ	Stefan Boltzmann constant

List of abbreviations

Bp	Boiling point
C1	Carbon number is 1
C2	Carbon number is 2
C3	Carbon number is 3
C4	Carbon number is 4
C5	Carbon number is 5
HHV	High heating value
IDT	Ignition delay time
JSR	Jet-stirred reactor
LHV	Low heating value
LOGEsoft	Scientific software for modelling of chemical kinetic systems
LPG	Liquefied petroleum gas
MON	Motor octane number
MW	Molecular weight
PSR	Perfectly stirred reactor
RON	Research octane number
Ta	Adiabatic temperature
VPFR	Variable pressure flow reactor

Acknowledgment.

This work has been a great Journey and the first line is too say thank you to everyone who helped me along the way. I have had the opportunity to meet brilliant and passionate people from all over the world that share the same curiosity and desire to understand a science that represents a drop from a big ocean.

I would like to thank Prof. Fabian Mauss for giving me the chance to belong to his team and accept the responsibility to supervise my work during this time. Being part of the chair of thermodynamics has given me the opportunity to learn not only from combustion science but also to grow and develop my skills as a professional. I also want to thank Dr. George Skevis and Prof. Thomas Zeuch for agreeing to act as examiners.

Being a woman in combustion is a challenge. I am inspired by great women who are by my side and actively participate building their ways. Some of them have become close friends and I am thankful to have them in my life.

I also want to thank my mother Magaly, my father Nerio, Milla and Franca for their love, support and education. To Berni and Werner for their continued support with Santiago and Alejandro. To my cousin Soraya for always being there for me.

This thesis is dedicated to Alejandro, Santiago and Ray.

Chapter 1

Introduction

About 84% of the world's energy comes from the combustion of fossil fuels. The energy is needed for industrial processes, heating in buildings, electricity generation and transportation (sea, land, air) [1]. If we take into account the growth of the population and their energetic needs, time and effort is required to generate a real change in the energy sources (renewable energy supply based on wind, water and sun) as it is discussed in Kohse-Höinghaus (2018) [2]. As a result, Global CO₂ emissions have increased from 23 Gt in 1996 to 36 Gt in 2016 [3]. CO₂ emissions represent approximately 75% of the total greenhouse gas emissions which are responsible for global warming which cause the interest of the society and governments in the development of regulations to control. Combustion processes and fuels are responsible for the chemical composition of the emissions. Fuel properties together with combustion conditions determine the composition of the exhaust stream and the GHG concentration. There are other molecules that also contribute to the GHG emissions such as: Methane (CH₄), NO_x, formaldehyde CH₂O among others. New limits for these two pollutants have been proposed by CLOVE for Euro 7 [4].

The oxidation of fuel molecules can be described by using a reaction mechanism, a model that combines thermodynamic and transport properties with reaction rates to predict the behavior and sub-products at different temperatures, pressures and equivalence ratios. A detailed reaction mechanism helps to understand the fuel-specific pollutant formation process [2]. The aim of this doctoral thesis is to generate a hierarchically-detailed chemical reaction mechanism from C₃ to C₅ hydrocarbons that can be used to understand the reaction decomposition pathways for different fuels at high temperature, e.g. propene, propane, butane isomers, butene isomers and pentene isomers. The compilation strategy was used and it aims to continuously increase the number and type of targets for mechanism validation.

A big challenge at the moment of the development of a kinetic model is the nomenclature that is used to name species that will conform the reactions. Each group that makes kinetics has started the development of their models and over time new experiments have emerged for fuels that had not been measured before. As a consequence, the models must be expanded and there is no convention having a chemical basis. Another limitation is the fact that this

model will be read in a program where a maximum number of characters is required. As part of this thesis, a nomenclature based in the IUPAC rules, has been developed and implemented. The naming follows the order of priority for choosing a principal characteristic group. These naming rules and some examples are explained here and are also published in the work of Leon et al. [5]. I wish people from scientific community feel identified in how important is to have a nomenclature that can be interpreted while reading the name. This species naming can be also useful for scientists who calculates the thermodynamic data making the implementation to our work more friendly. This nomenclature is not a finished product but the first step for its development, I invite you all to test it and expand their application.

Regarding the reaction mechanism developed in this doctor thesis, it is motivated and based in the work of Hoyermann et al. [6] where the chemical coupling among C_1-C_3 species was validated on acetylene and propene burner stabilized flame experiments. Laminar flame velocities and ignition delay times for a numerous number of C_1-C_4 fuels were also well predicted. The model was extended, to include the high temperature oxidation of *n*-butane (C_4H_{10}) and *iso*-butane (C_4H_{10} -Me2) in Oskwald et al. (2011) [7]. The high-temperature oxidation of C_4 hydrocarbon species (but-1-ene (C_4H_8 -D1), (*Z*)-but-2-ene (T- C_4H_8 -D2) and *iso*-butene (C_4H_8 -D1Me2) was included in the mechanism and presented by Schenk et al. (2013) [8]. In this work, it was noted that C_3 -species are sensitive towards their thermodynamic data. Therefore, propane and propene chemistry were investigated in cooperation with Elke Goos and thermodynamic data for sensitive species were verified.

In chapter 3, sensitivity analysis for propane and propene ignition delay times on heat of formation ($\Delta_f H_{298}^0$) were performed to find the most sensitive species. The species that showed the highest sensitivity are propene (C_3H_6 -D1), allyl (C_3H_5 -R1D2), propargyl (C_3H_3 -R1T2), and ethyl radical (C_2H_5 -R1). Their thermodynamic data were scientifically verified and adjusted by Goos. Using this new data, an improvement in the calculated ignition delay times for propane and propene are observed. The results of the sensitivity analysis together with ignition delay times show that a small change on the thermodynamic data of a key specie involved during fuel decomposition can have a big impact on the calculation target. This was observed by comparing ignition delay times and flow analysis calculations before and after the implementation of the verified thermodynamic data. The flow analysis show that mayor and minor consumption pathways for the fuel decomposition changed after implementation of the new polynomials. Reaction rates sensitivity analysis were performed before and after the thermodynamic data correction observing that the sensitivity of the reactions was also changing. The investigation also included the validation for laminar flame speed and burner stabilized flame experiments using both data set. Thermodynamic data changes show no big impact for laminar flame speed. In the case of burner stabilized flame experiments, a high sensitivity for species profiles was found after using the verified data. To conclude, the enthalpy sensitivity analysis tool has a big potential to improve kinetics models and help to have a better understanding of the decomposition pathways of the fuels when the thermodynamic data of the key radicals involved in the fuel decomposition can be determined using a refined calculation method e.g: benchmarked G3B3

method and further improved.

Revised thermochemical data from chapter 3 are used in chapter 4, chapter 5 and chapter 6. In chapter 4, most C_4 species were updated, using the thermochemical data of the database by Goos and Burcat (Goos et al. [9]). Burner stabilized flames presented in the work of Oswald et al. (2011) [7] were recalculated and analyzed. Auto-ignition experiments and laminar flame speed for each butane isomer and their mixtures (*n*-butane (C_4H_{10}) and *iso*-butane (C_4H_{10} -Me2)) as fuel were calculated. A very good agreement between model and experiments is shown.

The chemistry of the butene (C_4H_8) isomers have been revised in chapter 5. A correction taking into account the *H* – *atom* allyl abstraction is implemented following the recommendation from Nawdiyal 2018 [10]. Experiments of burner stabilized flame performed in the work of Schenk et al. 2013 [8] were recalculated using updated thermodynamic data and rates. Prediction of the stable and intermediate species are within the error measurements and it was discussed that the mechanism could not represent successfully the C_5 chemistry. Flow analysis are performed and show decomposition pathways for branched and linear species. The chapter includes validation of laminar flame speeds and ignition delay times for the different isomers.

Chapter 6 is an extended version from the reaction mechanism development of the work presented in the publication of Leon et al. 2019 [5] where a new experiment for a burner stabilized flame for *n*-Pentane (C_5H_{12}) was compared with a burner stabilized 2-Methyl-2-butene (C_5H_{10} -D2Me2) measured in the publication of Ruwe et al. [11]. 2-Methyl-2-butene (C_5H_{10} -D2Me2) is the most interesting C_5 isomer because 9 of its 10 *C* – *H* atoms are in allylic position which makes this fuel having a higher sooting tendency. This work was in cooperation with Prof. Kohse-Höinghaus, Lena ruwe, Nils Hansen, Kai Moshhammer, Krishna Shrestha and Lars Seidel.

From my side, the high-temperature chemistry for branched and linear C_5H_{10} species (2-Methyl-1-butene (C_5H_{10} -D1Me2), 2-Methyl-2-butene (C_5H_{10} -D2Me2), 3-Methyl-1-butene (C_5H_{10} -D1Me3), *n*-Pentene (C_5H_{10} -D1), and *cis*-2-Pentene (C_5H_{10} -D2)) is implemented in the model. *n*-Pentane (C_5H_{12}) chemistry was revised and updated. Thermodynamic data for newly introduced species and their C_5 degradation products were updated using the database of Goos et al. 2013 [9] and Gao et al. [12].

After the reactions in the mechanism were updated, discrepancies between experimental and modeling results for several key species were still observed. For example, only 1,3-butadiene (C_4H_6 -D1D3) was detected experimentally. The work from Ruwe et al. [13] states that a fast isomerization from C_4H_6 -D1-D2 to C_4H_6 -D1D3 may occur. Model prediction shows similar concentrations of 1,3-butadiene (C_4H_6 -D1D3) and 1,2-butadiene (C_4H_6 -D1-D2). Based on these observations, the sub-mechanism for C_4H_6 isomers was revised. Due to the big uncertainty arising from using thermodynamic data from different sources (different calculation methods), a new set of thermodata using the program MOPAC 2016 [14] were calculated and implemented for all the related C_5 species. The

change of the thermodata resulted in a change of the fuel decomposition flow. The validation of ignition delay time, and laminar flame speed experiments for these fuels are also presented and discussed.

Chapter 2

Theoretical part

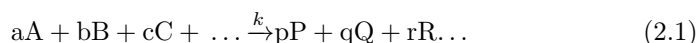
This chapter will lay out the theoretical background required to understand the different steps to develop and validate the detailed chemical reaction mechanism presented presented in this doctoral thesis.

2.1 Chemical kinetics

2.1.1 Rate law and reaction order

Chemical reactions take place at a certain rate and depend on the system's conditions. The significant conditions are concentration of reactants, temperature, radiation effects and the presence of catalysts or inhibitors. It is possible that the reaction rate is expressed in terms of either the concentration of any of the reacting substances or the concentration of any of the products. The rate can be indicated as the decrease of concentration of the reactant or as the rate of increase of concentration of a product [15].

A chemical reaction can be described by:



where: A, B, C, \dots represent different species involved in the reaction; a, b, c, \dots represent the reaction order with respect to A, B , and C species and k is the rate coefficient of the reaction. A rate law defines an experimental conception of the *reaction rate*, i.e: the rate of formation or consumption of species A as it can be observed in the expression 2.2 [16].

$$\frac{d[A]}{dt} = -k \cdot [A]^a [B]^b [C]^c \dots \quad (2.2)$$

Some species may be present in the reaction in excessive amounts. E.g. if the concentration of B and C , $[B]$ and $[C]$, do not change significantly, a typical rate coefficient can be set up from the concentration, $k_{\text{exp}} = -k \cdot [B]^b [C]^c$. Thus, simplifying eq. 2.2 to

$$\frac{d[A]}{dt} = -k_{\text{exp}} \cdot [A]^a \quad (2.3)$$

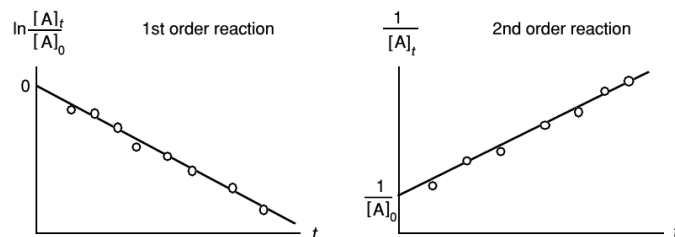


Figure 2.1: Time behavior of the concentrations for first- and second-order reactions [16]

By integrating the differential equation 2.3, the change in $[A]$ can be calculated over time. Assuming a positive integer reaction order, $[A]_0$ as the initial concentration of A and $[A]_t$ as the concentration of A at time t [16].

(a) **First-order reaction (a=1)**

$$\ln \frac{[A]_t}{[A]_0} = -k_{\text{exp}}(t-t_0) \quad (2.4)$$

(b) **Second-order reaction (a=2)**

$$\frac{1}{[A]_t} - \frac{1}{[A]_0} = k_{\text{exp}}(t-t_0) \quad (2.5)$$

(c) **Third-order reaction (a=3)**

$$\frac{1}{[A]_t^2} - \frac{1}{[A]_0^2} = 2k_{\text{exp}}(t-t_0) \quad (2.6)$$

The reaction order \mathbf{a} can only be solved empirically since it is based upon experiments. An example of species concentration time behavior for first- and second-order reactions is shown in Figure 2.1. In these cases, the larger the gradient, the higher the rate.

2.1.2 Relation of forward and reverse reactions

Looking at the reverse reaction of 2.1, the rate law for the production of A is:

$$\frac{d[A]}{dt} = -k^{(r)} \cdot [P]^p [Q]^q [R]^r \dots \quad (2.7)$$

On a microscopic level at chemical equilibrium, forward and backward reactions may have the same rate, whereas at a macroscopic level no net reaction is observed [16]. In such cases, $k^{(f)} \cdot [A]^a [B]^b [C]^c \dots = k^{(r)} \cdot [D]^d [E]^e [F]^f \dots$ or

$$\frac{[P]^p [Q]^q [R]^r \dots}{[A]^a [B]^b [C]^c \dots} = \frac{k^{(f)}}{k^{(r)}} \quad (2.8)$$

The left side corresponds to the equilibrium constant of the reaction, which can be calculated from thermodynamic data, leading to the expression eq.2.8:

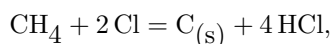
$$k_c = \frac{k^{(f)}}{k^{(r)}} = \exp(-\Delta_R \bar{A}^0 RT) \quad (2.9)$$

A similar expression to eq. 2.8 can be derived as a function of pressure:

$$k_p = \frac{k^{(f)}}{k^{(r)}} = \exp(-\Delta_R \bar{G}^0 RT) \quad (2.10)$$

2.1.3 Elementary reactions, molecularity of a reaction

Considering a chemical reaction (balanced or global reaction),



The left side shows a picture of the system before the reaction occurs, while the right side is a picture of the final system. These two conditions do not provide information on what happens in between. Information regarding the process of the reaction itself, between the before and after states, is, however, necessary for engineering and optimization. This involves knowing the details of more than just the one global reaction.

Additionally, global reactions may have complicated rate laws: the reaction orders a, b, c, \dots need not be integers, may even be negative and depend on time and reaction conditions. Extrapolations to conditions where no experiments exist are not reliable and are the consequence of a large number of elementary reactions. Elementary reactions have a constant reaction order and can be easily determined considering the molecularity of the reaction (number of species that form the reaction complex). Three possible values of the reaction molecularity are observed:

- (a) **Unimolecular reaction:** describes the rearrangement or dissociation of a molecule and has first-order behavior.



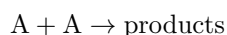
If the initial concentration is doubled, the reaction rate is also doubled.

First-order reactions lose importance with increasing pressure. ($[A] = \frac{y_1^{\text{ae}}}{RT}$)

- (b) **Bimolecular reaction:** it is the most common reaction type and describes the rearrangement of two molecules



or

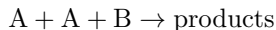


It has a second-order rate; doubling the concentration of each reaction partner quadruples the reaction rate.

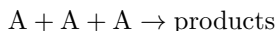
(c) **Trimolecular reactions:** they are usually recombination reactions.



or

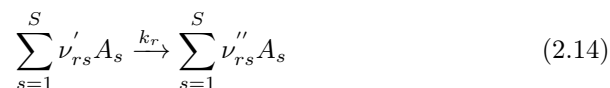


or



They obey a third-order rate law. The molecularity equals the order for elementary reactions.

The generalized equation of an elementary reaction r is given by:

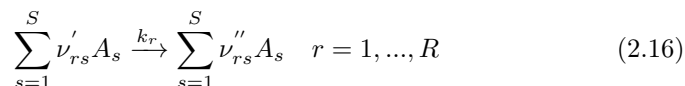


where ν'_{rs} and ν''_{rs} are stoichiometric coefficients of reactants and products respectively; A_s denotes the different species involved in the reaction r , and k_r is the specific reaction rate coefficient. Also, the rate law for the formation of species i in reaction r is:

$$\left(\frac{\partial c_i}{\partial t} \right)_{chem,r} = k_r \left(\nu''_{ri} - \nu'_{ri} \right) \prod_{s=1}^S c_s^{\nu'_{rs}} \quad (2.15)$$

where: ν'_{ri} and ν''_{ri} are stoichiometric coefficients of reactants and products respectively; c_i is the concentration of the species i , and c_s is the concentration of the s different species S .

Rate laws can always be specified for elementary reaction mechanisms. For an elementary mechanism composed of R reactions and S species, it is given by:



The rate of formation of a species i is given by the summation over the rate equation 2.15 of all elementary reactions [16]:

$$\left(\frac{\partial c_i}{\partial t} \right)_{chem} = \sum_{r=1}^R k_r \left(\nu''_{ri} - \nu'_{ri} \right) \prod_{s=1}^S c_s^{\nu'_{rs}} \quad (2.17)$$

2.1.4 Temperature dependence of rate coefficients.

The rate coefficients of chemical reactions depend strongly in a non-linear way on the temperature. According to Arrhenius (1889), the temperature dependence can be described by the formula (eq. 2.18) [16]:

$$k = A' \cdot \exp\left(\frac{-E_a}{RT}\right) \quad (2.18)$$

Further studies showed that the temperature dependence of the pre-exponential factor, also called factor A' , is normally small if compared to the exponential dependence. This can be observed in eq. 2.19:

$$k = AT^b \cdot \exp\left(\frac{-E_a}{RT}\right) \quad (2.19)$$

where A (mol, cm, second) is called the pre-exponential factor or frequency factor, b (-) is the temperature exponent, R (kJ/mol) is the universal gas constant, T is the temperature and E_a is the activation energy. The activation energy E_a matches an energy barrier that is overcome during the reaction (see fig 2.2). The binding energy in the molecule represents the maximum value for this barrier .

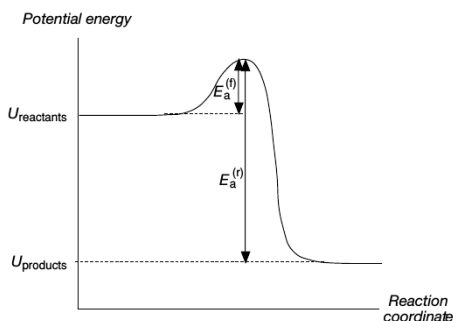


Figure 2.2: Energy diagram for a chemical reaction. The reaction coordinate is the path of minimum potential energy from reactants to products with respect to changing inter-atomic distance [17]

In dissociation reactions, the activation energy is approximately equal to the binding energy. It can also be lower or even zero, if new bonds are formed simultaneously with the breaking of an old bond [16].

In Figure 2.3, the logarithms of the rate coefficients versus the reciprocal temperature are plotted. A linear dependence is obtained from equation 2.19 $\log(k) = \log(A) - \text{const}/T$; the temperature dependence of the pre-exponential factor $A \cdot T^b$ can be neglected due to experimental uncertainty. Due to very high temperatures, the exponential term approaches 1 and the rate coefficient is dominated by the pre-exponential factor A' or $A \cdot T^b$ [16].

Meaning of pre-exponential factor A for uni-, bi-, and trimolecular reactions.

In Unimolecular reactions it corresponds to the mean lifespan of an activated (Reactive) molecule. In dissociation reactions, this lifespan is determined by the frequency of the vibration of the bond that breaks.

$$A \left[\frac{1}{s} \right]$$

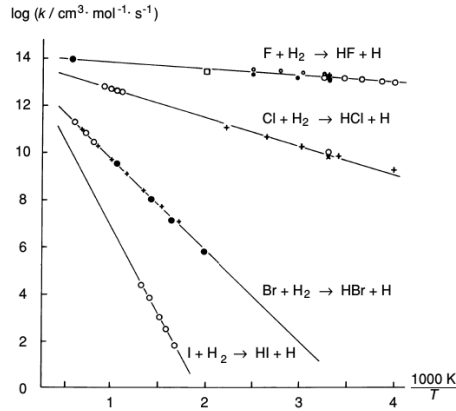


Figure 2.3: Arrhenius plot $k=k(T)$ for reactions of halogen atoms with H_2 [17]

In Bimolecular reactions it corresponds to a product of the collision rate and the probability of reaction. This collision rate is an upper limit for the reaction rate

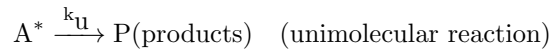
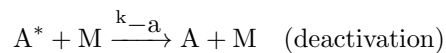
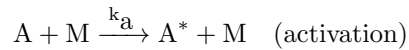
$$A \left[\frac{cm^3 \cdot s}{mol} \right]$$

In Trimolecular reactions, a third collision partner M , i. e: H_2O , CO_2 , CH_4 , H_2 , CO , has to remove the energy from the reaction. In detail, a three-body reaction is two bimolecular reactions in rapid succession. [16].

$$A \left[\frac{cm^6 \cdot s^2}{mol^2} \right]$$

2.1.5 Pressure dependence of rate coefficients

The pressure dependence of rate coefficients can be explained using the Lindemann model (1922) [18]. Consistent with this, a unimolecular decomposition is only possible if the energy of the molecule is sufficient to break the bond. Before any decomposition reaction, energy is added to the molecule by collision with other molecules M . After this, the excited molecule may decompose into the products or become deactivated through a collision [16]:



The rate equations for this case are:

$$\frac{d[P]}{dt} = k_u[A^*] \quad \text{and} \quad \frac{d[A^*]}{dt} = k_a[A][M] - k_{-a}[A^*][M] - k_u[A^*] \quad (2.20)$$

Assuming that the concentration of the reactive intermediate A^* is in a quasi-steady state

$$\frac{d[A^*]}{dt} \approx 0, \quad (2.21)$$

the concentration of the activated species $[A^*]$ and the formation of the products P result as follows:

$$[A^*] = \frac{k_a[A][M]}{k_{-a}[M] + k_u} \quad (2.22)$$

and

$$\frac{d[P]}{dt} = \frac{k_u k_a [A][M]}{k_{-a}[M] + k_u}$$

The tendency in different extreme conditions such as low and high pressures can be observed.

- Low pressure limit: it assumes $k_{-a}[M] \ll k_u$, with the collision partners M being very small, obtaining an apparent second-order rate law

$$\frac{d[P]}{dt} = k_a \cdot [A][M] = k_0 \cdot [A][M] \quad (2.23)$$

where k_0 is the low-pressure rate coefficient. The reaction rate is proportional to the concentrations of species A and the collision partner M, since activation is slow at low pressures [16].

- High pressure limit: it assumes $k_{-a}[M] \gg k_u$. The collision partner M has a high concentration, obtaining an apparent first-order rate law

$$\frac{d[P]}{dt} = \frac{k_u k_a}{k_{-a}} [A] = k_\infty \cdot [A] \quad (2.24)$$

where k_∞ is a high pressure rate coefficient. In this case the reaction rate does not depend on the concentration of the collision partners. The decomposition of the activated molecule $[A^*]$ is rate-limiting step instead of the activation [16].

Figure 2.4 shows the dependence of the reaction rate for different pressures. Due to the fact that many experiments on combustion are performed under low or elevated pressures, it is very important to describe correctly the pressure-dependence of reactions. The most commonly used formalism is the TROE approach, where ten parameters are used to determine a rate coefficient at specific temperature and pressure [16].

In table 2.1, the first line contains the reaction equation and high-pressure parameters; the second line, the low-pressure modified parameters and the third line contains four parameters a , T^{***} , T^* and T^{**} that are used to determine the F-center value, describing the center of the falloff range [16].

$$F_{cent} = a \cdot \exp\left(\frac{-T}{T^*}\right) + \exp\left(\frac{-T^{**}}{T}\right) + (1 - a) \cdot \exp\left(\frac{-T}{T^{***}}\right) \quad (2.25)$$

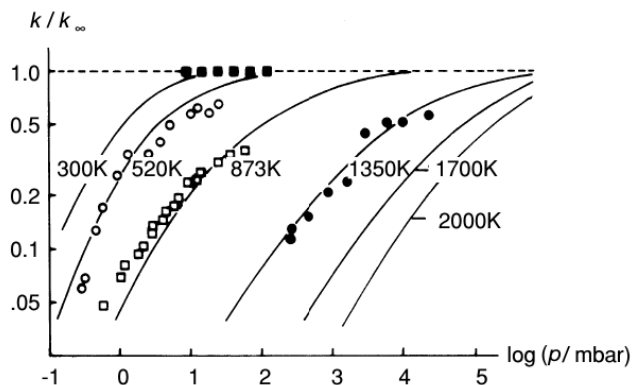


Figure 2.4: Falloff curves for the unimolecular reaction $C_2H_6 \longrightarrow CH_3 + CH_3$ [16]

Reaction	A [cm, mol, s]	b	E_a [kJ.mol ⁻¹]
OH+OH+M(1)=H2O2 + M(1)	1.57E+13	0.00	0.00
LOW	5.98E+19	-0.80	0.00
TROE	0.50 0.0	0.0	0.0

Table 2.1: Example of Arrhenius parameters for pressure-dependent reactions [16]

This is used to calculate the value F using equation 2.26:

$$\log F = \log F_{cent} \left\{ 1 + \left[\frac{\log P_r + c}{n - d \cdot (\log P_r + c)} \right]^2 \right\}^{-1} \quad (2.26)$$

where $c = -0.4 - 0.67 \log F_{cent}$, $n = 0.75 - 1.27 \log F_{cent}$, $d = 0.14$ and $P_r = k_0 \cdot [M] / k_\infty$, which together can be solved to obtain the following expression:

$$k = k_\infty \cdot \left(\frac{P_r}{1 + P_r} \right) \cdot F. \quad (2.27)$$

2.2 Thermochemistry

Thermodynamic temperature-dependent functions of enthalpy, entropy, Gibbs free energy and heat capacities are obtained from reliable molecular and spectroscopic properties through the calculation of partition functions with statistical methods as proposed by Goos and Burcat 2010 [19]. The resulting thermochemical data are fitted into the well-known NASA polynomial format [16] for easy use in modeling software. Coefficients of the NASA polynomials are available in Goos, Burcat, Ruscic’s “Extended Third Millennium Thermodynamic Database for Combustion and Air-Pollution Use with updates from Active Thermochemical Tables” (Goos et al. 2013 [9]).

The NASA polynomials have the form

$$\bar{C}_p^0/R = a_1 + a_2T + a_3T^2 + a_4T^3 + a_5T^4 \quad (2.28)$$

$$\bar{H}_T^0(T)/R = a_6 + a_1T + \frac{a_2}{2}T^2 + \frac{a_3}{3}T^3 + \frac{a_4}{4}T^4 + \frac{a_5}{5}T^5 \quad (2.29)$$

$$\bar{S}_T^0(T)/R = a_7 + a_1\ln T + a_2T + \frac{a_3}{2}T^2 + \frac{a_4}{3}T^3 + \frac{a_5}{4}T^4 \quad (2.30)$$

The molar heat capacities are expressed as five-term polynomials of fourth order in T . The enthalpy at any temperature T follows from integration of the heat capacity. The entropy at any temperature T follows from integration of the heat capacity divided by temperature T . Usually two different polynomials are used for high (First seven coefficients) and low temperature (second set of seven coefficients) separated by a switch temperature, normally $T = 1000K$. The first row has specific information, such as: species symbol, date of generation, state, lowest and highest temperature of validity.

2.3 Reaction mechanism

Theoretical, numerical, experimental methods, and any combination of them are used to solve combustion problems. Combustion modeling aims to simulate combustion processes, to develop predictivity capability for combustion systems under operating conditions, to help in interpreting combustion phenomena, and to substitute for difficult or expensive experiments. The theoretical model should be validated by comparison with reliable experimental data before it is used for prediction and evaluation of the influence of any parameters [20].

A reaction mechanism is a set of elementary reactions by which overall chemical change occurs [21] describing the process from reactants to products, including a characterization as complete as possible of the composition, structure, energy and other properties of reaction intermediates, products and transition states [17]. A theoretical model is composed of three files:

- A gas state file where elements, species, and reactions are listed.
- A state function file where thermodynamic information (enthalpy, entropy, and heat capacity) are provided for each species in form of seven NASA polynomials for low and high temperature.
- A molecular data file where the transport properties of each species are provided.

When the conditions in the experiments change, some reactions become insignificant while others become more important. For that reason, a reaction mechanism is limited to the range of experimental conditions to which it applies, e.g. low, intermediate or high temperature regime; lean or rich combustion according to the equivalence ratio, or working pressure range, respectively. If some credible elementary reaction is not incorporated in the mechanism, it is not implied that the reaction does not occur, but rather that it is not significant under the specified conditions and thus is not taken into account.

2.4 Analysis of a reaction mechanism

2.4.1 Sensitivity analysis

Sensitivity analyses are a time-efficient approach to investigate chemical models based on the direct relationships between input parameters and model predictions. They identify the rate-determining step or rate-limiting step in a reaction mechanism [16]. Species thermodynamic properties and rate coefficients of elementary reactions with high sensitivities should be well known and studied because they have a big influence on the results of the mathematical model. This work presents sensitivity analysis for species enthalpies and reaction rates on the ignition delay time and burner-stabilized flame.

Enthalpy influence on the ignition delay time

The sensitivity analyses of species enthalpies of formation on ignition delay times were performed to identify species whose thermo-chemical data influence the simulation results significantly. In praxis, this was achieved by incrementing the value of the 6th and 13th term of each seven-term NASA polynomial introduced beforehand by $10kJ/mol$. Ignition delay times were calculated for every perturbation. The relative sensitivity [16] for the heat of formation is defined in the present study as

$$S_i = \frac{LHV_{fuel}}{\tau_{ref}R} \left(\frac{\tau_i - \tau_{ref}}{\Delta\bar{h}_i} \right) \quad (2.31)$$

Here, S_i is the sensitivity of species i on the heat of formation, defined as the relative change in the ignition delay time τ . τ_{ref} is the ignition delay time calculated with the original thermochemical data and LHV_{fuel} is the lower heating value of the fuel at $298K$. The lower heating value of the fuel was applied, and not the heat of formation of the individual species as reference, since the selection of the zero point in enthalpy is arbitrary. $\tau_i - \tau_{ref}$ is the absolute change of the ignition delay time calculated with the updated thermochemical data of the species i respectively to τ_{ref} . $\Delta\bar{h}_i$ is the change of enthalpy of formation in reference i to original enthalpy provided.

Enthalpy influence on maximum concentration profiles in burner-stabilized flames

The sensitivity analyses of species enthalpies of formation on species concentration profiles for major and minor species in burner-stabilized flames were performed to identify species whose thermochemical data influence the simulation results significantly. In praxis, this was achieved by incrementing the value of the 6th and 13th term of each seven-term NASA polynomial by $1kJ/mol$. Concentration profiles were calculated for every perturbation. The relative sensitivity [16] for the heat of formation is defined in the present study as

$$S_{i,j} = \frac{LHV_{fuel}}{c_{ref}R} \left(\frac{\Delta c_i}{\Delta\bar{h}_{Tj}} \right) \quad (2.32)$$

where: $S_{i,j}$ is the sensitivity of species j on the heat of formation, defined as a relative change in the maximum value of the peak concentration of species i , c_{ref}

is the maximum value of the concentration of the reference species i , calculated with the original thermochemical data and LHV_{fuel} is the lower heating value of the fuel at $298K$. Δc_i is the absolute change of the maximum concentration calculated with the updated thermochemical data of the species j respectively to c_{ref} . Δh_{T_j} is the change of enthalpy of formation of species j at temperature T , at the position of maximum reference concentration of species i .

Reaction rates influence on ignition delay time

The sensitivity analyses of reaction rates influence on ignition delay times were performed to determine which reaction had the largest influence on the simulation results. The sensitivity analysis was performed by incrementing the pre-exponential factor A (see Arrhenius law 2.19) in each reaction by 20%. A complete ignition delay time computation for every perturbation was made. The reaction rate sensitivity is defined as

$$S_k = \frac{A_k}{\tau_{ref}} \left(\frac{\tau_{ref} - \tau_k}{\Delta A_k} \right) \quad (2.33)$$

S_k is the rate sensitivity of a reaction, defined as a relative change in the ignition delay τ of reaction k when the Arrhenius pre-exponential factor of the reaction is increased by 20%. A_k is the current Arrhenius pre-exponential factor, τ_{ref} is the ignition delay time without changing the Arrhenius pre-exponential factor, $\Delta\tau$ is the change against the reference ignition delay time ($\Delta\tau = \tau_{ref} - \tau_k$) and ΔA_k is the absolute change in the pre-exponential factor. In this study, a positive sensitivity is equivalent to a shorter ignition delay time, while a negative sensitivity describes a longer ignition delay time.

2.4.2 Reaction Flow analyses

Flow analyses are used to determine the characteristic reaction paths of a reaction mechanism. In numerical simulations of combustion processes, there are available software packages that automatically perform this analysis [16].

A flow analysis considers the percentage of the contributions of different reactions r ($r = 1, \dots, R$) to formation (or consumption) of the chemical species s ($s = 1, \dots, S$). An example can be seen in table 2.2, where 5% of formation of species 1, can be attributed to reaction 2. The percentage in the columns must add up to 100% [16]. Fig.2.5 shows one example of the output of a flow analysis from LOGEsoft program.

Reaction ↓	Species ⇒			
	1	2	...	S
1	30%	3%	...	10%
2	5%	60%	...	90%
3	65%	0%	...	60%

Table 2.2: Illustration of the output of a reaction flow analysis.

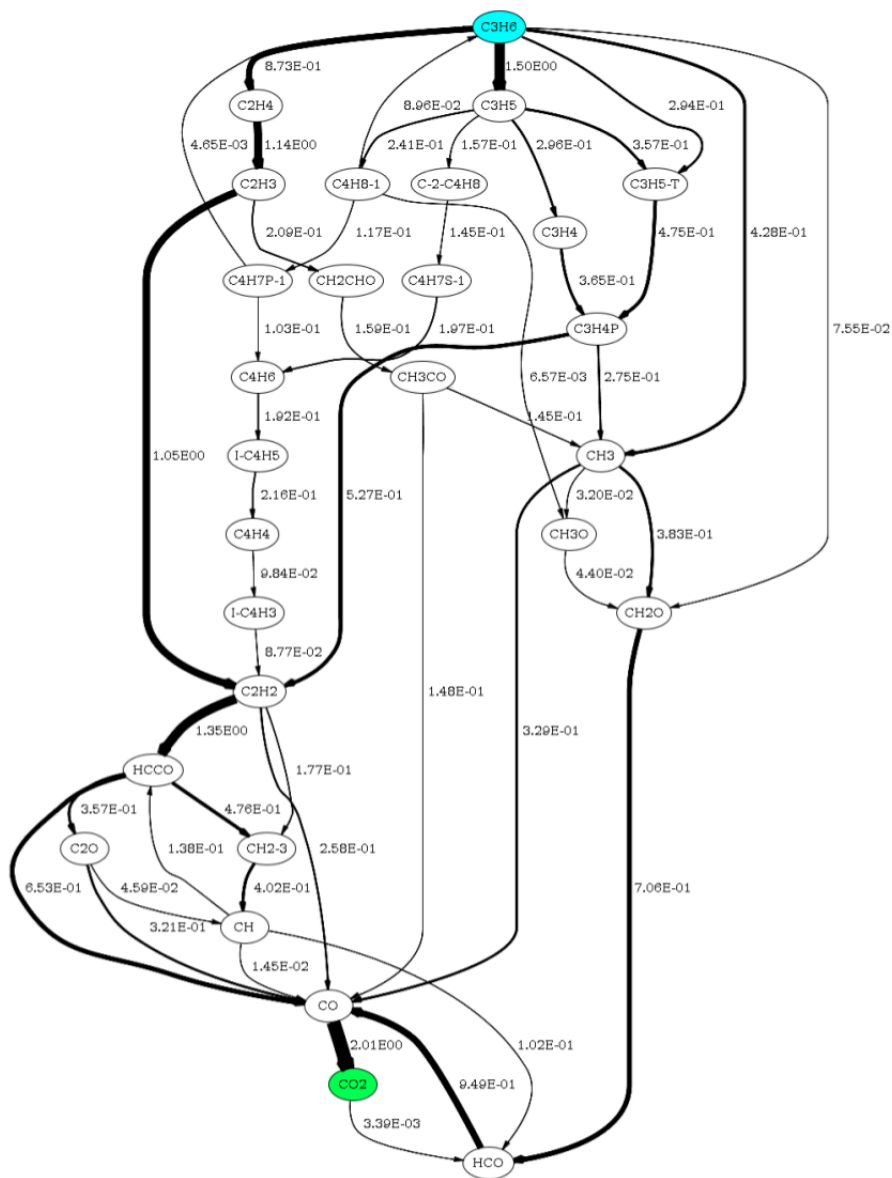


Figure 2.5: Example of a flow analysis at 50% of max. flux. Flux values are in $\text{mol}/\text{cm}^3/\text{s}$ at 50% of fuel consumption (propene) in a constant volume reactor simulating a shock tube.

2.5 Chemical kinetics in mass and energy conservation

Chemical reactions such as those described by equation 2.1 are nothing else than a representation of the principle of mass conservation. In the most general case, conservation laws can be derived from the application of the Reynolds Transport Theorem (RTT) to arbitrarily chosen Lagrangian Control Volumes (CV) representing closed systems V_ψ . We use ψ to symbolize the chosen conserved intensive property in such systems, e.g. mass or energy,

$$\frac{d}{dt} \int_{V_\psi} \rho\psi dV = \int_V \frac{\partial(\rho\psi)}{\partial t} dV + \int_S \rho\psi \vec{v}_\psi \cdot d\vec{S}. \quad (2.34)$$

At a given time t , the system V_ψ coincides with a fixed constant volume (CV) V , which has boundary S with a normal area vector $d\vec{S}$. The LHS of equation 2.34 represents the sources or sinks of ψ in the CV V_ψ . The first term on the RHS of equation 2.34 represents the instantaneous change of $\rho\psi$ in a fixed point in space, and the second term on the RHS symbolizes the incoming or outgoing fluxes of ψ across the boundary S .

In the following subsections, some special cases for the generalized equation 2.34 are analyzed in detail. These cases have practical relevance for this thesis given their regular use within the computational tool LOGEsoft.

2.5.1 Constant volume reactor

The constant volume reactor is constituted by a closed rigid vessel in which the combustion occurs, the volume is maintained constant and the pressure increases. This device is often employed for calorimetric studies to determine the heat of formations of various fuels. It is used to simulate shock tube experiments. The constant volume reactor is a closed system. There are no mass fluxes going in or out of the system [22].

As the definition implies, customizing equation 2.34 for $\psi = 1$ (intensive property of mass), results in the following expression for conservation of mass in a constant volume reactor:

$$\frac{d}{dt} \int_{V_\psi} \rho dV = \frac{dm_{V_\psi}}{dt} = \int_V \frac{\partial \rho}{\partial t} dV. \quad (2.35)$$

Equation 2.35 is equal to zero due to the absence of sources or sinks of mass in the universe according to the standard model of physics. Equation 2.35 can also be expressed in differential terms, taking the limit $dV \rightarrow 0$ in the RHS,

$$\frac{d\rho}{dt} = 0, \quad \text{or alternatively} \quad \frac{dm}{dt} = 0. \quad (2.36)$$

According to the continuity equation, the mass balance of a single chemical species i in a system is given by three terms describing the mass flux and the formation and consumption of said species, see Eq.2.37. The first two terms on the right hand side represent the total flux of mass entering and leaving the control volume V . The last term describes the formation (consumption) of the species by chemical reactions.

$$\frac{\partial m_i}{\partial t} = \sum_{l=1}^{N_{in}} \dot{m}_{i,l} - \sum_{k=1}^{N_{out}} \dot{m}_{i,k} + \omega_i^* W_i \quad (2.37)$$

Here W_i is the species molecular weight in $\frac{kg}{mol}$ and ω_i^* is the species net reaction rate in $\frac{mol}{s}$. The balance equations for the total mass is derived through summation of the total number of chemical species present in the reactor where the last equality comes from the fact that the total formation and consumption of all species mass has to be zero.

$$\frac{\partial m}{\partial t} = \sum_{i=1}^{N_s} \frac{\partial m_i}{\partial t} = \sum_{i=1}^{N_s} \left(\sum_{l=1}^{N_{in}} \dot{m}_{i,l} - \sum_{k=1}^{N_{out}} \dot{m}_{i,k} + \omega_i^* W_i \right) = \sum_{l=1}^{N_{in}} \dot{m}_l - \sum_{K=1}^{N_{out}} \dot{m}_k \quad (2.38)$$

In multi-component systems (multi-component chemical system), V_ψ does not coincide with the fixed constant volume V . In this case, $\psi = Y_i$ and equation 2.34 is not zero in contrast to the general mass case. The partial mass of every component needs to be tracked. The balance equation for the mass fraction Y_i of species i is derived in a way similar to that of the balance equation of total mass with two terms describing change due to in- and outflow and one term describing species production (consumption). The following holds:

$$\frac{\partial Y_i}{\partial t} = \frac{\partial \frac{m_i}{m}}{\partial t} = \frac{1}{m} \frac{\partial m_i}{\partial t} - \frac{m_i}{m^2} \frac{\partial m}{\partial t} \quad (2.39)$$

Using Eqs.2.38 and 2.39 together with the definition of density $\rho = \frac{m}{V}$. Thus, a sink or source $\omega_i W_i$ of the mass fraction Y_i or, conversely, of the partial density ρ_i is required ($\omega_i = \frac{\omega_i^*}{V}$ is the species reaction rate in $\frac{mol}{m^3 s}$ and W_i is the species molecular weight in $\frac{kg}{mol}$). Eq. 2.39 can be rewritten as:

$$\frac{dY_i}{dt} = \frac{1}{m} \left(\sum_{l=1}^{N_{in}} (\dot{m}_{i,l} - \dot{m}_l Y_i) - \sum_{k=1}^{N_{out}} (\dot{m}_{i,k} - \dot{m}_k Y_i) \right) + \frac{\omega_i W_i}{\rho}. \quad (2.40)$$

The species mass fractions of the gas exiting the volume $Y_{i,k}$ are the same as that of the gas inside the volume Y_i . The expression for change in mass fraction is:

$$\frac{dY_i}{dt} = \sum_{l=1}^{N_{in}} \frac{\dot{m}_l}{m} (Y_{i,l} - Y_i) + \frac{\omega_i W_i}{\rho}. \quad (2.41)$$

For energy conservation, the first law of thermodynamics demands the net internal energy of V_ψ to be equal to the difference between heat fluxes and work done by or on the system. The change of energy in a system depends on the heat transfer to and from the surroundings, performed work, chemical reactions and transport phenomena:

$$\frac{dE}{dt} = \dot{Q} + \dot{W} + \sum_{l=1}^{N_{in}} \dot{m}_l (h + e_k + e_p)_l - \sum_{k=1}^{N_{out}} \dot{m}_k (h + e_k + e_p)_k \quad (2.42)$$

where E is the total energy of the system. On the right hand side of 2.42, the terms \dot{Q} and \dot{W} are the heat and work transfer rates between the control volume

and the environment. The two sums represent the total energy transferred into and out of the control volume by flow through the inlets and outlets. The in- and outlets are denoted by l and k , and h , e_k and e_p are the specific enthalpy, kinetic energy and potential energy of the mass flows, respectively. Eq. 2.42 can be rewritten as follows. Considering the left side of Eq. 2.42, the total energy is the sum of internal, kinetic and potential energy. However, it is assumed that changes in kinetic and potential energy are negligible so the energy differential can be approximated as:

$$\frac{dE}{dt} \approx \frac{dU}{dt}$$

The total heat transfer rate \dot{Q} is given by $\dot{Q} = \dot{Q}_{conv} + \dot{Q}_{rad}$, where \dot{Q}_{conv} is the convective heat exchange with reactor walls in $\frac{J}{s}$ and \dot{Q}_{rad} is the heat transferred through radiation in $\frac{J}{s}$.

$$\dot{Q}_{conv} = h_c A (T - T_w) \quad (2.43)$$

$$\dot{Q}_{rad} = \rho \epsilon A (T^4 - T_w^4) \quad (2.44)$$

whereby A is the heat transfer area in m^2 , h_c is the heat transfer coefficient in $\frac{W}{m^2K}$, ϵ is the emissivity factor [-], and T_w is the wall temperature. The work rate \dot{W} is the change of volume V with pressure p in $\frac{J}{s}$:

$$\dot{W} = -p \frac{dV}{dt} \quad (2.45)$$

Since kinetic and potential energy is negligible compared to enthalpy, energy transport in and out of the system can be approximated by $(h + e_k + e_p) \approx h$ in $\frac{J}{kg}$. Consequently, the last two terms of Eq. 2.42 become:

$$\sum_{l=1}^{N_{in}} \dot{m}_l h_l - \sum_{k=1}^{N_{out}} \dot{m}_k h_k = \sum_{l=1}^{N_{in}} \dot{m}_l \sum_{i=1}^{N_s} Y_{i,l} h_{i,l} - \sum_{k=1}^{N_{out}} \dot{m}_k \sum_{i=1}^{N_s} Y_{i,k} h_{i,k}$$

Eq. 2.42 can now be rewritten as:

$$\frac{dU}{dt} = \dot{Q} - p \frac{dV}{dt} + \sum_{l=1}^{N_{in}} \dot{m}_l \sum_{i=1}^{N_s} Y_{i,l} h_{i,l} - \sum_{k=1}^{N_{out}} \dot{m}_k \sum_{i=1}^{N_s} Y_{i,k} h_{i,k} \quad (2.46)$$

From the expression of instantaneous energy change,

$$\frac{dE}{dt} \approx \frac{dU}{dt} = \frac{d(mu)}{dt} = m \frac{du}{dt} + u \frac{dm}{dt} \quad (2.47)$$

For specific internal energy $\psi = u$, the heat fluxes are expressed by the outgoing (incoming) radiation heat flux, which are compensated by the endothermic (exothermic) heats of reaction, the term du/dt can be rewritten as follows:

$$\frac{du}{dt} = \frac{d}{dt} \left(\sum_{i=1}^{N_s} Y_i u_i \right) = \sum_{i=1}^{N_s} Y_i \frac{du_i}{dt} + \sum_{i=1}^{N_s} u_i \frac{dY_i}{dt} \quad (2.48)$$

To evaluate species internal energy u_i in $\frac{J}{kg}$, the calorific equation of state is used:

$$u_i = u_i^0 + \int_{T^0}^{T'} c_{v,i} dT \quad (2.49)$$

Assuming ideal gas behaviour, $u_i = u_i(T)$:

$$\frac{du_i}{dt} = \frac{\partial u_i}{dT} \frac{dT}{dt} = c_{v,i} \frac{dT}{dt} \quad (2.50)$$

u_i^0 is the internal energy at reference temperature T^0 and $c_{v,i}$ is the specific heat capacity ($\frac{J}{kgK}$) at constant volume for species i .

$$\frac{du}{dt} = \sum_{i=1}^{N_s} Y_i c_{v,i} \frac{dT}{dt} + \sum_{i=1}^{N_s} u_i \frac{dY_i}{dt} \quad (2.51)$$

With the terms dm/dt and dY_i/dt from Eqs. 2.37 and 2.41, utilising $c_v = \sum_{i=1}^{N_s} Y_i c_{v,i}$, $u = \sum_{i=1}^{N_s} Y_i u_i$, in equation 2.47 one gets:

$$\begin{aligned} \frac{dU}{dt} = m \frac{du}{dt} + u \frac{dm}{dt} = m c_v \frac{dT}{dt} + m \sum_{i=1}^{N_s} u_i \left(\sum_{l=1}^{N_{in}} \frac{\dot{m}_l}{m} (Y_{i,l} - Y_i) + \frac{\omega_i W_i}{\rho} \right) + \\ \sum_{i=1}^{N_s} Y_i u_i \left(\sum_{l=1}^{N_{in}} \dot{m}_l - \sum_{k=1}^{N_{out}} \dot{m}_k \right) \end{aligned} \quad (2.52)$$

Introducing the internal molar energy $U_i = W_i u_i$ and expressing all terms explicitly, one gets

$$\frac{dU}{dt} = m \frac{du}{dt} + u \frac{dm}{dt} = m c_v \frac{dT}{dt} + \sum_{i=1}^{N_s} u_i \sum_{l=1}^{N_{in}} \dot{m}_l Y_{i,l} + \frac{m}{\rho} \sum_{i=1}^{N_s} \omega_i U_i - \sum_{i=1}^{N_s} Y_i u_i \sum_{k=1}^{N_{out}} \dot{m}_k \quad (2.53)$$

Setting the right hand side of Eq. 2.53 equal to Energy equation 2.46 and using the definition of enthalpy, $h = u + pv$, yields:

$$\begin{aligned} m c_v \frac{dT}{dt} + \sum_{i=1}^{N_s} u_i \sum_{l=1}^{N_{in}} \dot{m}_l Y_{i,l} + \frac{m}{\rho} \sum_{i=1}^{N_s} \omega_i U_i \\ = \dot{Q} - p \frac{dV}{dt} + \sum_{l=1}^{N_{in}} \dot{m}_l \sum_{i=1}^{N_s} Y_{i,l} u_{i,l} + \sum_{l=1}^{N_{in}} \dot{m}_l \sum_{i=1}^{N_s} Y_{i,l} p v - \sum_{k=1}^{N_{out}} \dot{m}_k \sum_{i=1}^{N_s} Y_{i,k} p v \end{aligned} \quad (2.54)$$

Again, $Y_{i,k} u_{i,k} = Y_i u_i$ is valid for all outlets so rearranging, dividing by volume and assuming constant volume, including the heat transfer rate \dot{Q}_{conv} using Eq. 2.43 and \dot{Q}_{rad} 2.44, ideal gas law $p v = \frac{RT}{W}$, Eq. 2.54 can be simplified to:

$$\begin{aligned} \rho c_v \frac{dT}{dt} = \sum_{l=1}^{N_{in}} \frac{\dot{m}_l}{V} \sum_{i=1}^{N_s} Y_{i,l} (u_{i,l} - u_i) - \sum_{i=1}^{N_s} \omega_i U_i + \sum_{l=1}^{N_{in}} \frac{\dot{m}_l}{V} \frac{R_0 T_l}{W_l} \\ - \sum_{k=1}^{N_{out}} \frac{\dot{m}_k}{V} \frac{R_0 T_k}{W_k} + \frac{h_c A}{V} (T - T_w) + \sigma \epsilon \frac{A}{V} (T^4 - T_w^4) \end{aligned} \quad (2.55)$$

With appropriate simplifications and considering that mass flow $\dot{m} = 0$ (closed system), one obtains:

$$\rho c_v \frac{dT}{dt} = \frac{h_c A}{V} (T - T_w) + \rho \epsilon \frac{A}{V} (T^4 - T_w^4) - \sum_{i=1}^{N_s} \omega_i U_i, \quad (2.56)$$

whereby A is the heat transfer area, h_c is the heat transfer coefficient, ϵ is the emissivity factor, T_w is the wall temperature and U_i are the partial molar internal energies resulting from the chemical reactions.

2.5.2 Constant pressure reactor

The constant pressure reactor represents a gas that is allowed to expand freely in the reactor volume. Examples of constant pressure reactors are tubes, closed at one end and with a movable piston at the other, ensuring constant pressure during combustion. Mass conservation in equation 2.34 implies that

$$\int_V \frac{\partial \rho}{\partial t} dV + \int_S \rho \vec{v}_\psi \cdot d\vec{S} = 0. \quad (2.57)$$

This case is idealized as a 1-D system with an inlet and an outlet of equal cross-sectional area. $\int_S \rho \vec{v}_\psi \cdot d\vec{S} = \rho_{out} v_{out} A - \rho_{in} v_{in} A$ due to the 1-D assumption, where only the velocity aligned with the surface vector is considered and this velocity is uniform across the CV boundary. Additionally, with $v_{in} = v_{out}$ and assuming homogeneous flow properties $\rho_{in} = \rho_{out}$, the expression results in the same equation 2.36 for a CVR.

For energy conservation (see Eq. 2.46), it can be expressed using the definition of enthalpy (h) $h = u + pv$ where u is the specific internal energy, p the pressure and v the specific volume. Volume is given by $V = vm$ in m^3 .

$$\begin{aligned} \frac{dE}{dt} &= \frac{dU}{dt} = \frac{d(mu)}{dt} = m \frac{du}{dt} + u \frac{dm}{dt} = m \frac{d(h - pv)}{dt} + (h - pv) \frac{dm}{dt} \\ &= m \frac{dh}{dt} - m \frac{dpv}{dt} + h \frac{dm}{dt} - pv \frac{dm}{dt} = m \frac{dh}{dt} + h \frac{dm}{dt} - \frac{d(mpv)}{dt} \end{aligned} \quad (2.58)$$

The first term on the right hand side of Eq. 2.58 represents the change in energy due to a change in enthalpy dh/dt . Using the explicit expression for total enthalpy (given as the sum over all species molecular enthalpies by their mass fractions), this can be rewritten as:

$$m \frac{dh}{dt} = m \frac{d}{dt} \left(\sum_{i=1}^{N_s} Y_i h_i \right) = m \left(\sum_{i=1}^{N_s} Y_i \frac{dh_i}{dt} + \sum_{i=1}^{N_s} h_i \frac{dY_i}{dt} \right) \quad (2.59)$$

To evaluate the species enthalpy, h_i , the calorific equation of state is used:

$$h_i = h_i^0 + \int_{T^0}^{T'} c_{p,i} dT \quad (2.60)$$

with h_i^0 being the enthalpy at reference temperature T^0 and $c_{p,i}$ the specific heat capacity at constant pressure for species i . Assuming ideal gas behaviour, $h_i = h_i(T)$:

$$\frac{dh_i}{dt} = \frac{\partial h_i}{\partial T} \frac{dT}{dt} = c_{p,i} \frac{dT}{dt} \quad (2.61)$$

Replacing dh_i/dt and dY_i/dt in Eq. 2.59:

$$m \frac{dh}{dt} = m \sum_{i=1}^{N_s} Y_i c_{p,i} \frac{dT}{dt} + m \sum_{i=1}^{N_s} h_i \left(\sum_{l=1}^{N_{in}} \frac{\dot{m}_l}{m} (Y_{i,l} - Y_i) + \frac{\omega_i W_i}{\rho} \right) \quad (2.62)$$

Considering that $c_p = \sum_i^{N_s} Y_i c_{p,i}$, then yields:

$$m \frac{dh}{dt} = m c_p \frac{dT}{dt} + m \sum_{i=1}^{N_s} h_i \left(\sum_{l=1}^{N_{in}} \frac{\dot{m}_l}{m} (Y_{i,l} - Y_i) + \frac{\omega_i W_i}{\rho} \right) \quad (2.63)$$

Replacing Eq. 2.63, 2.38 and Volume $V = vm$ into Eq. 2.58 gives:

$$\begin{aligned} \frac{dU}{dt} &= m \frac{dh}{dt} + h \frac{dm}{dt} - \frac{dmpv}{dt} \\ &= m c_p \frac{dT}{dt} + m \sum_{i=1}^{N_s} h_i \left(\sum_{l=1}^{N_{in}} \frac{\dot{m}_l}{m} (Y_{i,l} - Y_i) + \frac{\omega_i W_i}{\rho} \right) \\ &\quad + \left(\sum_{i=1}^{N_s} Y_i h_i \right) \left(\sum_{l=1}^{N_{in}} \dot{m}_l - \sum_{k=1}^{N_{out}} \dot{m}_k \right) - \frac{d(pV)}{dt} \end{aligned} \quad (2.64)$$

Setting the result from Eq. 2.64 equal to general energy equation 2.46, one gets:

$$\begin{aligned} & m c_p \frac{dT}{dt} + m \sum_{i=1}^{N_s} h_i \left(\sum_{l=1}^{N_{in}} \frac{\dot{m}_l}{m} (Y_{i,l} - Y_i) + \frac{\omega_i W_i}{\rho} \right) \\ & + \left(\sum_{i=1}^{N_s} Y_i h_i \right) \left(\sum_{l=1}^{N_{in}} \dot{m}_l - \sum_{k=1}^{N_{out}} \dot{m}_k \right) - \frac{d(pV)}{dt} = \\ & \dot{Q} - p \frac{dV}{dt} + \sum_{l=1}^{N_{in}} \dot{m}_l \sum_{i=1}^{N_s} Y_{i,l} h_{i,l} - \sum_{k=1}^{N_{out}} \dot{m}_k \sum_{i=1}^{N_s} Y_{i,k} h_{i,k} \end{aligned} \quad (2.65)$$

Simplifying and introducing the molar enthalpy from species $H_i = W_i h_i$ (J/mol), one gets:

$$m c_p \frac{dT}{dt} - \sum_{i=1}^{N_s} h_{i,l} \sum_{l=1}^{N_{in}} \dot{m}_l Y_{i,l} + \frac{m}{\rho} \sum_{i=1}^{N_s} \omega_i H_i - V \frac{dp}{dt} = \dot{Q} - \sum_{k=1}^{N_{out}} \dot{m}_k \sum_{i=1}^{N_s} Y_{i,k} h_{i,k} \quad (2.66)$$

Utilising that $Y_{i,k} h_{i,k} = Y_i h_i$ for all outlets, dividing by volume and assuming constant pressure. The total heat transfer rate \dot{Q} is given by $\dot{Q} = \dot{Q}_{conv} + \dot{Q}_{rad}$, where the heat transfer rate of convection \dot{Q}_{conv} is included using Eq. 2.43 and

heat transfer rate of radiation \dot{Q}_{rad} is included using Eq.2.44. Equation 2.66 can be simplified to:

$$\rho c_p \frac{dT}{dt} = \sum_{l=1}^{N_{in}} \frac{\dot{m}_l}{V} \sum_{i=1}^{N_s} Y_{i,l} (h_{i,l} - h_i) - \sum_{i=1}^{N_s} \omega_i H_i + \frac{h_c A}{V} (T - T_w) + \sigma \epsilon \frac{A}{V} (T^4 - T_w^4) \quad (2.67)$$

The energy conservation equation is expressed in terms of specific enthalpy. Since mass flow $\dot{m} = 0$ (closed system), the energy equation becomes:

$$\rho c_p \frac{dT}{dt} = \frac{h_c A}{V} (T - T_w) + \rho \epsilon \frac{A}{V} (T^4 - T_w^4) - \sum_{i=1}^{N_s} \omega_i H_i, \quad (2.68)$$

Given the assumption of flow homogeneity and equal inlet and outlet velocities, the net momentum of the system is zero. Therefore, no balance equation for momentum has to be solved [22].

2.5.3 Perfectly stirred reactor (PSR)

The perfectly stirred reactor model (PSR) is frequently used to simulate toroidal jet-stirred reactors, that are used in laboratories to investigate ignition processes [22].

This model is used frequently to study aspects of combustion, such as flame stabilization and NO_x formation. The PSR is a constant pressure vessel with inlet and outlet ducts, with or without thermal isolation. A steady flow gas with a certain composition and temperature is introduced through the inlets. After a certain residence time, the reacted gas products exit the chamber through the outlets. The PSR can be regarded as a vessel in which there is extremely strong mixing. The reactive time-scales can be considered negligible in comparison to the mechanical time-scales. This allows steady-state solutions for the balance equations [23].

As in the CPR, mass conservation is given by equation 2.57. The same considerations as in the CPR apply; however, the inlets and outlets are now generalized under any number N_{in} of inlets and any number N_{out} of outlets. This case is a 0-D idealization and thus, all integrals can be expressed as the corresponding algebraic multiplication of constant properties,

$$\frac{d\rho}{dt} V + \sum_{k=1}^{N_{out}} \rho_k v_k A - \sum_{l=1}^{N_{in}} \rho_l v_l A = 0, \quad (2.69)$$

which can be rewritten as

$$\frac{dm}{dt} = \sum_{l=1}^{N_{in}} \dot{m}_l - \sum_{k=1}^{N_{out}} \dot{m}_k. \quad (2.70)$$

The gas flowing continuously in the chamber is a mixture of combusted and unburned gas. Homogeneity inside the chamber means that the gas composition exiting the vessel is the same as the one inside, i.e. $Y_{i,l} = Y_i$, for all outlets.

Following this assumption and substituting equation 2.69, the balance equation for species mass fractions is,

$$\frac{d(\rho Y_i)}{dt} V + \sum_{k=1}^{N_{out}} \rho_k Y_{i,k} v_k A - \sum_{l=1}^{N_{in}} \rho_l Y_{i,l} v_l A = \rho \frac{dY_i}{dt} V + \sum_{l=1}^{N_{in}} \rho_l Y_i v_l A - \sum_{l=1}^{N_{in}} \rho_l Y_{i,l} v_l A. \quad (2.71)$$

This expression is equal to the sinks or sources of Y_i and can be rewritten as,

$$\rho \frac{dY_i}{dt} V + \sum_{l=1}^{N_{in}} \rho_l v_l A (Y_i - Y_{i,l}) = \omega_i W_i V, \quad \text{or} \quad \frac{dY_i}{dt} = \frac{\omega_i W_i}{\rho} - \sum_{l=1}^{N_{in}} \frac{\dot{m}_l}{m} (Y_{i,l} - Y_i). \quad (2.72)$$

Therefore, the rate of change of the mass fraction, Y_i , depends on the production rate by chemical reactions (the first term on the RHS), and the influx to the PSR (the second term on the RHS) [22].

The change in energy corresponds to the change of enthalpy due to incoming and outgoing heat fluxes (radiation and convection), endothermic and exothermic heats of reaction and the enthalpy of the incoming flow to the PSR [24]. The equation is obtained similarly to equation 2.68 and analogously to equation 2.72,

$$\begin{aligned} \rho \frac{dh}{dt} &= - \sum_{i=1}^{N_s} \omega_i H_i + \sum_{i=1}^{N_s} h_i \left[\sum_{l=1}^{N_{in}} \frac{\dot{m}_l}{V} (Y_{i,l} - Y_i) \right] - \sum_{l=1}^{N_{in}} \frac{\dot{m}_l}{V} (h_l - h) \\ &\quad + \frac{h_c A}{V} (T - T_w) + \sigma \varepsilon \frac{A}{V} (T^4 - T_w^4). \end{aligned} \quad (2.73)$$

Here, h_i symbolizes the specific enthalpy of species i and h_c is the heat convection coefficient.

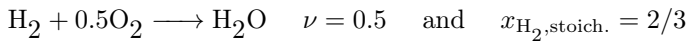
2.5.4 Laminar premixed flames

A flame is the visible gaseous part of a fire. It is caused by a highly exothermic reaction taking place in a thin reaction zone [24]. In the case of laminar premixed flames, the fuel and the oxidizer are premixed before the combustion and the flow is laminar. A premixed flame is stoichiometric if the fuel and the oxidizer are consumed completely forming carbon dioxide and water. If there is an excess of fuel, the system is called fuel-rich, and if there is an excess of oxygen the system is called fuel-lean [16].

If the reaction equation is written down so as to describe exactly the reaction of 1 mol fuel, the mole fraction of the fuel in a stoichiometric mixture can be calculated as

$$x_{\text{fuel,stoich.}} = \frac{1}{1 + \nu}. \quad (2.74)$$

Here ν denotes the number of moles of O_2 in the reaction equation for a complete reaction to CO_2 and H_2O . An example is:



The use of air as an oxidizer has to be made taking into consideration that dry air contains about 21% oxygen (78% nitrogen, 1% noble gases) [16]. For a stoichiometric mixture with air, the fuel mole fraction is

$$\begin{aligned} x_{\text{fuel,stoich.}} &= \frac{1}{1 + \nu \cdot 4.762}, x_{\text{O}_2,\text{stoich.}} \\ &= \nu \cdot x_{\text{fuel,stoich.}}, \quad x_{\text{N}_2,\text{stoich.}} = 3.762 \cdot x_{\text{O}_2,\text{stoich.}} \end{aligned} \quad (2.75)$$

Air equivalence ratio (air number) or the reciprocal value of the fuel equivalence ratio $\phi = 1/\lambda$, is the number used to describe premixtures of fuel and air

$$\begin{aligned} \lambda &= (x_{\text{air}}/x_{\text{fuel}})/(x_{\text{air,stoich.}}/x_{\text{fuel,stoich.}}) \\ &= (W_{\text{air}}/W_{\text{fuel}})/(W_{\text{air,stoich.}}/W_{\text{fuel,stoich.}}) \end{aligned} \quad (2.76)$$

This formula can be rewritten to allow the evaluation of mole fractions in a mixture from ϕ by

$$x_{\text{fuel}} = \frac{a}{1 + \frac{4.762 \cdot \nu}{\phi}}, \quad x_{\text{air}} = 1 - x_{\text{fuel}}, \quad x_{\text{O}_2} = x_{\text{air}}/4.762, \quad x_{\text{N}_2} = x_{\text{O}_2} \cdot 3.762 \quad (2.77)$$

The air and fuel equivalence ratios allow the classification of premixed combustion processes in three groups,

- rich combustion: $\phi > 1$, $\lambda < 1$
- stoichiometric combustion: $\phi = 1$, $\lambda = 1$
- lean combustion: $\phi < 1$, $\lambda > 1$

2.5.5 Premixed freely propagating flames

This 1-D model represents a stationary, flat and infinitely large flame front propagating through a premixed medium. The medium is presumed of infinite length and the total energy of the system can be considered constant. There are no flame strain or mass transfer (in the direction normal to the flow field of the fuel and oxidizer) phenomena present [25]. The balance equations for the freely propagating flame can also be derived from the RTT. These are:

- Continuity equation:

$$\frac{d(\rho u)}{dz} = 0. \quad (2.78)$$

- Balance of species mass fraction:

$$\rho u \frac{dY_i}{dz} = -\frac{dj_i}{dz} + \dot{m}_i. \quad (2.79)$$

- Balance of energy:

$$\begin{aligned} \rho u c_p \frac{dT}{dz} &= \frac{d}{dz} \left(\lambda \frac{dT}{dz} \right) - \sum_{i=1}^{N_s} h_i \dot{m}_i - \sum_{i=1}^{N_s} c_p j_i \frac{dT}{dz} \\ &\quad - 4\alpha\sigma (T^4 - T_0^4) V f_r \end{aligned} \quad (2.80)$$

In equations 2.78 and 2.79, u is the gas velocity, j_i is the diffusion flux and \dot{m}_i the production rate of species i . The diffusion flux is, per definition, $j_i = \rho V_i Y_i$, with V_i being the diffusion velocity of species i . In equation 2.80, λ is the thermal conductivity, α is Planck's constant, σ is the Stefan Boltzmann constant, T_0 is the temperature of the surroundings and f_r a radiation factor. The rest of the terms were described above [25].

In the LOGE package, the flame configuration can be chosen. The transport model specifies the relation between heat diffusion and mass diffusion due to concentration gradients (Lewis number).

- Unity Lewis number: thermal and species diffusion are constant and equal for all the species
- Constant Lewis number: sets constant values for Lewis number for all species.
- Variable Lewis number: the Lewis number is calculated from the transport data individually for each species.

Thermodiffusion: allows to calculate the diffusion of the species due to temperature gradients.

Radiation: is used for calculating the heat loss due to radiation. Taking into account that H_2O and CO_2 are final products of combustion, these are the species with the biggest radiation.

The laminar burning velocity (flame speed or flame velocity) is a characteristic of the freely burning premixed laminar flat flames into the unburnt mixture. It is the velocity at which unburned gases move through the combustion wave in direction normal to the wave surface. The burning velocity depends solely on the mixture composition of equivalence ratio ϕ , the pressure P , and the initial temperature T [15].

2.5.6 Premixed burner-stabilized flames

This model reproduces the low-pressure flat-flame burner experiments to observe the species profiles within the flame structure. Species profiles are typically determined experimentally by quartz micro-probe sampling and gas chromatography for stable species, molecular beam sampling mass spectrometry for both stable and radical species and electron or spin resonance for H, O and OH [24].

The balance equations for the burner-stabilized flames are the same as those that were used for premixed freely propagating flames. In these calculations, the energy conservation has not been solved; instead, the experimentally determined temperature profile has been used. Temperatures are generally measured in the experiments with a radiation-corrected thermocouple [16].

2.6 Computational Tool-LOGEresearch

LOGEresearchv1.10-000 is the tool used in this work to perform the calculations to simulate the different experiments and its conditions. It allows the analysis of complex chemistry in engineering applications, providing easy access to complex chemical models [26]. Among many features, LOGEresearch includes a wide range of 0-D reactor models and 1-D flame calculations. LOGEresearch can be used to:

- Read and visualize existing reaction mechanisms
- Perform sensitivity, flow and lifetime analysis
- Reduce reaction mechanisms

For this investigation, the constant volume reactor, constant pressure reactor, jet stirred reactor, premixed burner-stabilized flames and premixed freely propagating flames were all models used for simulations.

2.7 Naming rules for species in the mechanism

The mechanisms related to this thesis follow the naming presented in table 2.3. You may find the structure representation very simplified. Resonance structures are not presented, bond angles are not correct and the 3D structure is completely ignored. A new nomenclature has been implemented and developed for species, derived from IUPAC rules, and following the order of priority for choosing a principal characteristic group. These naming rules were published in the work of Leon et al. [5] in supplementary material 2.

The nomenclature that is used in this mechanism for non-aromatic species starting from C_2 is in some points related to the IUPAC nomenclature of organic chemistry¹. The functional groups and the respective abbreviations used in our mechanism are listed in Tab. 2.3 in decreasing order of priority. The italic *X* and *Y* behind the abbreviation are used as placeholder for the position number of the functional group.

There are a few steps that needs to be considered to derive the correct species name in our mechanism and these steps are explained in the following:

First of all, the parent hydrocarbon chain must be identified. It should have the maximum length, maximum number of functional groups, as well as the maximum number of multiple and single bonds. The parent hydrocarbon chain must then be numbered. This is done by first numbering the chain in both directions (left to right as well as right to left) and then selecting the numbering where the sum of all locants is the smallest. Locants are the numbers on the carbon atoms to which the substituent is directly attached.

¹Henri A. Favre, Warren H. Powell. Nomenclature of Organic Chemistry: IUPAC Recommendations and Preferred Names 2013. Chapter 4 and chapter 5.

Example: $\text{CH}_3\text{—}\dot{\text{C}}\text{=CH—CH}_3$
 Right: C4H7-R2D2
 Wrong: C4H7-R3D3

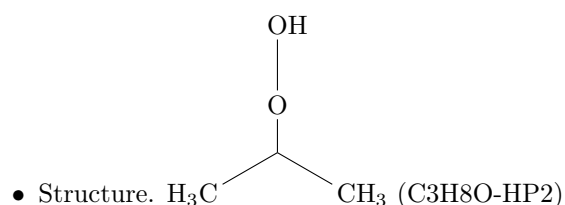
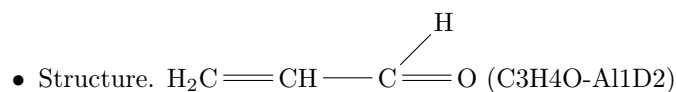
The radical is on the second carbon when counting from left to right. By naming the species, the positional number of a functional group should be minimized.

Afterwards, all functional groups needs to be identified and ordered according their priorities (see Tab. 2.3).

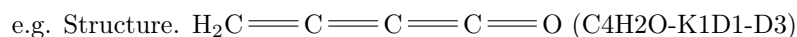
Following our nomenclature, the species name is subdivided in two parts that are divided by an hyphen. The sum formula of the respective molecule is given in front of the hyphen, whereas molecule specific information (e.g. functional groups, binding situations, ...) are stated behind the hyphen with a number giving the specific position of the functional group in the molecule. Behind the hyphen, the abbreviation of each functional group is listed in the name and the different groups are ordered with decreasing priority.

$$C_XH_Y - (\text{FunctionalgroupA})(\text{PositionA})(\text{FunctionalgroupB})(\text{PositionB}) \quad (2.81)$$

e.g.

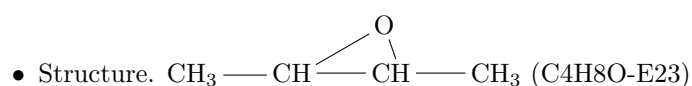
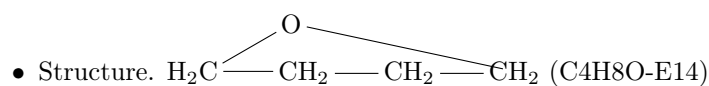
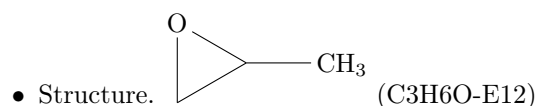
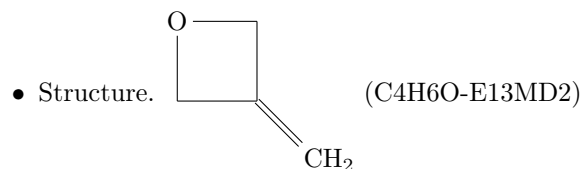


In the case of cumulative double bonds, the naming is abbreviated by only mentioning the first and last of the adjacent double bonds.



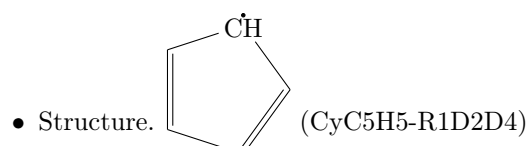
In case of cyclic ethers, the position numbers of the two carbon atoms X and Y that are bridged by the ether function are listed behind the abbreviation of the ether group (E).

e.g.



In case of cyclic species, the species name is subdivided in two parts that are divided by an hyphen. The initials **CY** followed by sum formula of the respective molecule is given in front of the hyphen, whereas molecule specific information are stated behind the hyphen (as for linear molecules).

e.g.



Another cyclic molecules are named after the nomenclature presented by Frenklach et al. 1988² where benzene is represented by **A1** and naphthalene **A2**.

²M. Frenklach, W.C. Gardiner, S.E. Stein, D.W. Clary and T. Yuan, 1986, Mechanism of Soot Formation in Acetylene-Oxygen Mixtures, Combustion Science and Technology, 50:1-3, 79-115

Group	Special Case	General Structure	Abbreviation Position of Functional Group
Radical	-	$(R')_3C^*$	R X
Alkoxy radical	-	$(R) - O^*$	O X
Peroxy radical	-	$(R) - OO^*$	OO X
Carboxylic acid	-	$RCOOH$	Ac X
Ester	-	$RCOOR'$	Es X
Aldehyde	-	$RCHO$	Al X
Ketone	-	$R - CO - R'$	K X
Alcohol	-	$R - OH$	OH X
Hydroperoxid	-	$R - OOH$	HP X
Ether	-	$R - O - R'$	E X
-	Cyclic ether	$R - O - R'$	EX Y
Alkene	-	$R - CH = CH - R'$	D X
-	Methylene group	$R - C = CH_2$	MD X
-	Cumulative double bonds	$R - CH = C = CH - R'$	DX-DY
Alkyne	-	$R - C \equiv C - R'$	T X
Peroxid	-	$R - O - O - R'$	P X
Alkanes	-	$R - (CH_2)_n - R'$	-
-	Methyl	$R - CH_3$	Me X
-	Ethyl	$R - CH_2 - CH_3$	Et X
-	Propyl	$R - (CH_2)_2 - CH_3$	Pr X
-	Butyl	$R - (CH_2)_3 - CH_3$	Bu X

Table 2.3: *Priority list following nomenclature [5]. * :This is a suggested abbreviation since these molecules are not part of the mechanism.*

Chapter 3

Influence of thermodynamic data on reaction fluxes, and prediction by chemical reaction mechanism

The work presented in this chapter aims at improving the propane (C₃H₈) and propene (C₃H₆-D1) chemistry of the reaction mechanism by evaluating the influence of the thermodynamic data (enthalpy of formation at 298 K) on the simulation of ignition delay times measured in shock tube experiments. Propane and propene are frequently used as fuel and can be found as a compound of natural gas, propene is studied for a better understanding of critical precursors of benzene formation, such as the propargyl radical (see Atakan et al. (1998) [27] and Hoyermann et al. (2004) [6]).

The chemical mechanism presented in Schenk et al. (2013) [8] was used for all calculations. It consists of 163 species and 1055 reversible reactions with 94 non-reversible forward reactions.

The assumption of microscopic reversibility of chemical steps is widely applied in kinetic simulations of combustion processes. The rate coefficients for backward reactions are typically calculated from the thermodynamic properties of the reactants involved. However, systematic studies of the influence of thermodynamic data (assumptions) on kinetic simulations are scarce, e. g: Hughes et al. (2006) [28] and Goos et al. (2013) [29]. The crucial role of the thermochemistry of the NCN radical on modeling NO_x formation in flames was exemplified in Goos et al. (2013b) [29].

The experimental data validated in the present study for propane as fuel was measured in: Burcat et al. (1971) [30], Brown and Thomas (1999) [31], Herzler et al. (2004) [32], Zhukov et al. (2005) [33] and Lam et al. (2011) [34] in a variety of temperatures ranging from 900 K to 1850 K, with pressures from 1 atm to 500 atm and equivalence ratios from 0.5 to 1.8. In the case of propene as

fuel, Burcat and Radhakrishnan (1985) [35] investigated an experimental range from 1271 K to 1900 K, a pressure from 1 atm to 6 atm and equivalence ratios from 0.5 to 2.0. Qin et al. (2001) [36] studied propene auto-ignition in temperatures ranging from 1270 to 1820 K, with pressures from 0.95 to 4.7 atm and equivalence ratios from 0.5 to 2.0, and, recently, Burke et al. (2015) [37] studied propene auto-ignition in temperatures ranging from 1100 to 1750 K, with pressures from 2 to 40 atm and equivalence ratios from 0.5 to 2.0.

The laminar burning velocities for propane/air mixtures at a temperature of 298 K, ambient pressure and equivalence ratios from 0.5 to 1.8 were also validated using the measurements from Metghalchi and Keck (1980) [38], Egolfopoulos et al. (1991) [39], Vagelopoulos et al. (1994) [40], Vagelopoulos and Egolfopoulos (1998) [41], Davis and Law (1998) [42], Hassan et al. (1998) [43], Bosschaart and Goey (2004) [44], Jomaas et al. (2005) [45], Huzayyin et al. (2008) [46], Wu et al. (2011) [47], Lowry et al. (2011) [48], and Dirrenberger et al. (2011) [49]. In the case of propene/air mixtures, experimental measurements presented in Davis and Law (1998) [42], Davis et al. (1999) [50], and Jomaas et al. (2005) [45] were used for validation of the model at a temperature of 298 K, ambient pressure and equivalence ratios from 0.5 to 1.7.

3.1 Propane and Propene ignition delay time and sensitivity results.

The mechanism is validated against a shock tube experiment performed by Qin et al. (2001) [36] for propene, and against a shock tube experiment from Burcat et al. (1971) [30] for propane as fuel. Maximum pressure rise was the criterion for determining the propene ignition delay time and maximum formation of carbon dioxide (CO₂) was the criterion for the propane ignition delay time as described in the experimental conditions of the original sources [36] and [30].

Figure 3.1 a) shows results for propene ignition delay time where the simulation results are 62.8% lower than the experimental data at 1440 K; the ignition timing slope, however, follows the experimental data behavior. Figure 3.1 b) shows the results for propane ignition delay time where the values of the simulation results are 54% lower than the experimental data at 1380 K. These deviations from experimental data are large in comparison to deviations for other fuels using the reaction mechanism (Hoyermann et al. (2004) [6], Schenk et al. (2013) [8], and Oßwald et al. (2011) [7]).

Figure 3.2 a) shows results for the sensitivity analysis of enthalpy of formation on ignition delay time for propene as fuel at 1440 K, 1540 K, and 1660 K. It is observed that species sensitivity towards enthalpy changes are temperature-dependent and the strongest sensitivity is found at 1440 K. Allyl (C₃H₅-R1D2) and propene (C₃H₆) are the most sensitive species with C₃H₅-R1D2 showing a positive sensitivity and C₃H₆-D1 showing a negative sensitivity. Also, propargyl (C₃H₃-R1T2) shows an influence on the ignition delay time targets under these conditions. Lower sensitivities were observed for C₃H₄-T1, C₂H₅-R1, C₂H₄-D1 and CH₃.

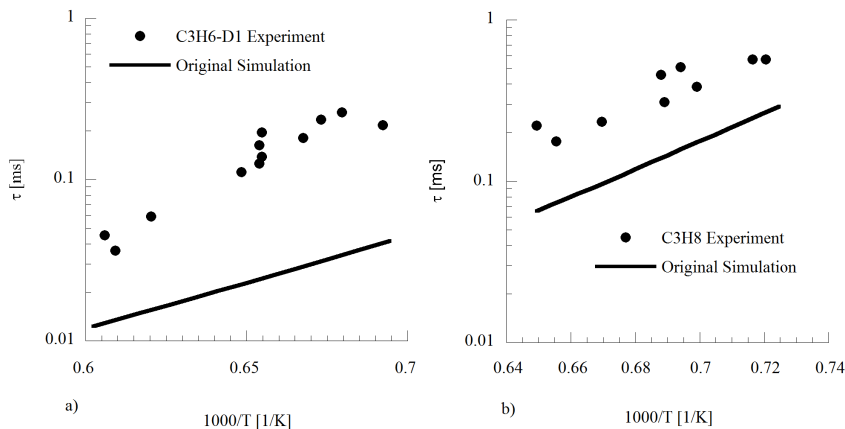


Figure 3.1: a) Ignition delay time of 1.6% C3H6-D1/ 7.2% O₂ mixture in Ar in a shock tube at 4 bar and a temperature range of 1440-1660 K. Symbols represent experimental data ([36]). b) Ignition delay time of 0.84% C3H8 / 2.1% O₂ mixture in Ar in a shock tube at 7.5 bar and a temperature range of 1380-1540 K. Symbols represent experimental data ([30]). Black lines are simulation results.

Figure 3.2 b) presents the sensitivity analysis of enthalpy of formation on ignition delay time for propane as fuel at 1380 K, 1460 K and 1540 K. The H radical is the most sensitive species and a change of its thermodata will affect the prediction of all the mechanism targets. This study will not address the H-atom sensitivity because the availability of experimental data for H-atom concentration-time-profiles is limited, although it is well known that this is an important issue in kinetic modeling (see discussion in Goos et al. (2013) [29]). A negative sensitivity to enthalpy changes for C3H8 and C3H6-D1 was observed, while C2H5-R1, C2H4-D1, CH4 and CH3 exhibit a positive sensitivity to enthalpy changes. CH3 has a positive sensitivity for 1380 K and 1460 K but a change to negative sensitivity at 1540 K. C2H5-R1 shows the most largest sensitivity value after the H-atom.

Sensitivity analyses of reaction rates were performed for propene as fuel at 1440 K, 1540 K and 1660 K (see Figure 3.3) which are, respectively, the lowest, medium and highest temperatures in the experimental data. The most sensitive reactions with a positive tendency are

- $\text{H} + \text{O}_2 \rightleftharpoons \text{O} + \text{OH}$ (R1),
- $\text{HO}_2 + \text{C}_3\text{H}_5\text{-R1D2} \rightleftharpoons \text{O}_2 + \text{C}_3\text{H}_6\text{-D1}$ (R292),
- $\text{C}_3\text{H}_3\text{-R1T2} + \text{O}_2 \rightarrow \text{CH}_2\text{O} + \text{HCCO}$ (R243),
- $\text{C}_3\text{H}_5\text{-R1D2} + \text{C}_3\text{H}_5\text{-R1D2} \rightarrow \text{H} + \text{H} + \text{C}_6\text{H}_8\text{-D1T5}$ (R496), and
- $\text{H} + \text{C}_3\text{H}_5\text{-R1D2} \rightleftharpoons \text{C}_3\text{H}_4\text{-D1D2} + \text{H}_2$ (R269)

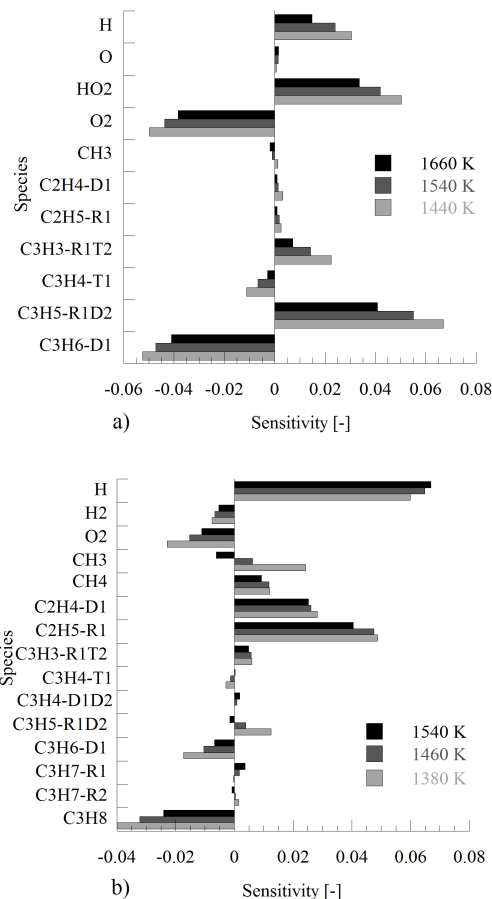


Figure 3.2: a) Sensitivity analysis of enthalpy on ignition delay time for propene as fuel (1.6% C3H6-D1/ 7.2% O₂ mixture in Ar at 4 bar ([36]) for 1440 K, 1540 K and 1660 K. b) Sensitivity analysis of enthalpy on ignition delay time for propane as fuel (0.84% C3H8/ 2.1% O₂ mixture in Ar at 7.5 bar ([30]) for 1380 K, 1460 K and 1540 K.

H + C3H5-R1T2 \rightleftharpoons C3H4-D1D2 + H₂ (R269) is the most sensitive reaction, which shows a negative sensitivity. In general, higher sensitivities are observed in the reactions where C3H3-R1T2, C3H5-R1D2 and C3H6-D1 molecules are involved, and such analysis confirms the information obtained from the enthalpy sensitivity (Fig 3.2 a)), where allyl and propene were found as the most sensitive species.

Propane reaction rate sensitivity analyses were performed for 1380 K, 1460 K, and 1540 K (Fig. 3.4)). The most sensitive reactions with a positive tendency are:

- H + O₂ \rightleftharpoons O + OH (R1),

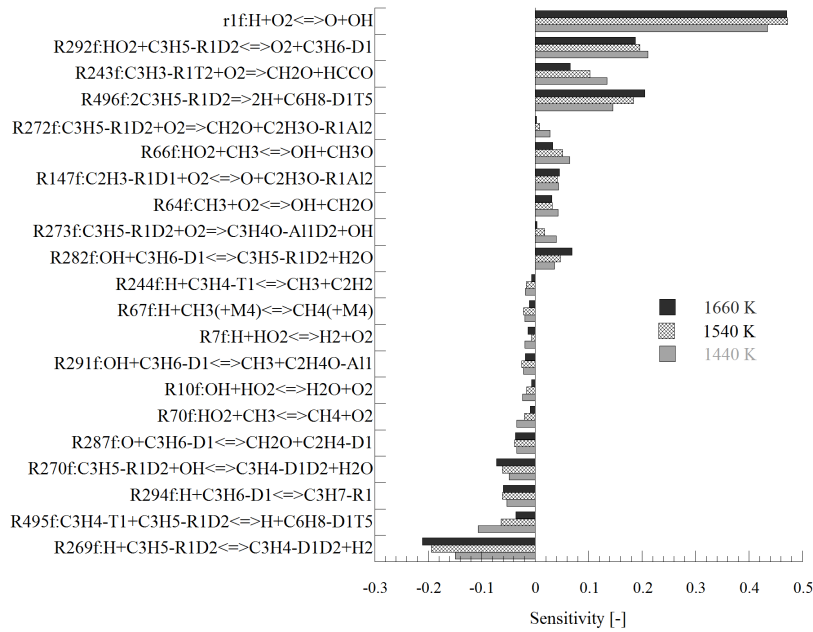


Figure 3.3: Net sensitivity analysis of reaction rates on ignition delay time for propene as fuel (1.6% C₃H₆-D1/ 7.2% O₂ mixture in Ar at 4 bar ([36])) for 1440K, 1540K and 1660K.

- CH₃ + C₂H₅-R1 \rightleftharpoons C₃H₈ (R300),
- C₂H₃-R1D1 + O₂ \rightleftharpoons CH₂O + HCCO (R147), and
- H + C₂H₄-D1 \rightleftharpoons C₂H₃-R1D1 + H₂ (R162),

while negative sensitivities are observed for

- H + C₃H₈ \rightleftharpoons C₃H₇-R2 + H₂ (R301),
- H + C₃H₈ \rightleftharpoons C₃H₇-R1 + H₂ (R302),
- H + C₃H₅ \rightleftharpoons C₃H₄-D1D2 + H₂ (R269), and
- CH₃ + CH₃ \rightleftharpoons C₂H₅-R1 + H (R188).

The reaction rate sensitivity for propane shows species (C₃H₈, C₃H₆-D1, C₃H₅-R1D2, C₃H₃-R1T2, C₂H₅-R1, C₂H₄-D1, CH₄, and CH₃) observed in the enthalpy sensitivity analysis.

There are 163 species in the reaction mechanism used in this study, which is equivalent to 163 perturbations for the enthalpy sensitivity analysis. In the case of the reaction sensitivity analysis, there are 2204 perturbations (1055 reversible reactions plus 94 forward reactions). The calculation time needed for the enthalpy sensitivity analysis is shorter than the calculation time needed for the reaction rate sensitivity analysis. The enthalpy sensitivity analysis is a useful strategy that can be implemented to determine the sensitive species and related

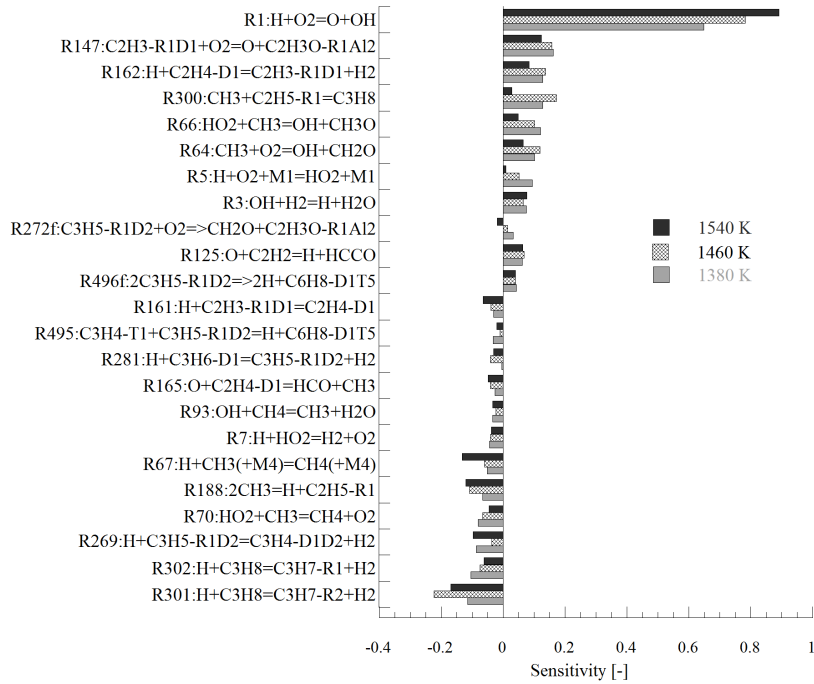


Figure 3.4: Net sensitivity analysis of reaction rates towards ignition delay time for propane as fuel (0.84% C3H8 / 2.1% O₂ mixture in Ar at 7.5 bar ([30])) for 1380K, 1460K and 1540K.

reactions that are affecting the oxidation process of the fuel. Based on the observations of the sensitivity analysis of enthalpy and reaction rates on ignition delay times for propane and propene as fuels, the thermodata of propene (C3H6-D1), allyl (C3H5-R1D2), propargyl (C3H3-R1T2), and ethyl radical (C2H5-R1) molecules were reviewed.

Original polynomials for propene (C3H6-D1), allyl (C3H5-R1D2), propargyl (C3H3-R1T2), and ethyl radical (C2H5-R1) thermodata were taken from the work of Burcat 1984 [51] and the implemented polynomials from the database by Goos and Burcat [9]. Both the original and implemented values for $\Delta_f H_{298}^0$ are presented in table 3.1.

	$\Delta_f H_{298}^0$ (kJ/mol)			
	C3H6-D1	C3H5-R1D2	C3H3-R1T2	C2H5-R1
Original	20.57	134.31	320	117
Implemented	19.67	163.71	351	119

Table 3.1: Original [51] and implemented [9] values of $\Delta_f H_{298}^0$ for propene (C3H6-D1), allyl (C3H5-R1D2), propargyl (C3H3-R1T2) and ethyl radical (C2H5-R1).

3.2 Propane and Propene ignition delay time and sensitivity results using updated thermodynamic data.

Figure 3.5 shows a comparison of simulation results for propene as fuel using: a) original thermodynamic data, b) updated thermodata of the C₂H₅-R1 molecule, c) updated thermodata of the C₃H₃-R1T2 molecule, d) updated thermodata of the C₃H₅-R1D2 molecule, e) updated thermodata of the C₃H₆-D1 molecule and f) updated thermochemical data of C₂H₅-R1, C₃H₃-R1T2, C₃H₅-R1D2, and C₃H₆-D1 at once.

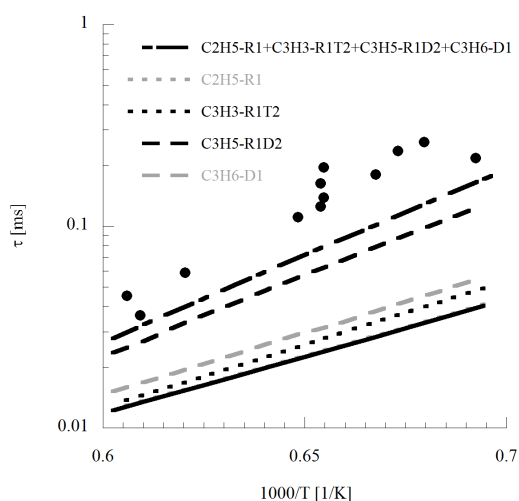


Figure 3.5: Ignition delay time of 1.6% C₃H₆-D1/ 7.2% O₂ mixture in Ar in a shock tube at 4 bar and a temperature range of 1440-1660 K. Symbols represent experimental data ([36]). Black solid line: original simulation result, dark gray line: updated C₃H₃-R1T2 thermodynamic data, light gray dotted line: updated C₃H₆-D1 thermodynamic data, black dotted line: updated C₃H₅-R1D2 and black dashed line: updated C₂H₅-R1, C₃H₃-R1T2, C₃H₅-R1D2, and C₃H₆-D1 thermodynamic data.

The greatest influence on ignition delay time was observed for the updated thermodata of the allyl molecule (C₃H₅-R1D2) (black dashed line). The replacement of the thermodata for the propene (C₃H₆-D1) molecule resulted in lower values for $\Delta_f H_{298}^0$ (C₃H₆-D1) than the ones used in the original thermodata, which leads to an increase of the ignition delay time (gray dashed line). The change in the thermodata for propargyl (C₃H₃-R1T2) increases the ignition delay time (black dotted line). Changing the value of thermodata for $\Delta_f H_{298}^0$ (C₂H₅-R1) does not influence the ignition delay time (gray dotted dashed line). The black dashed line shows the predicted ignition delay time result using all the thermodynamic data calculated in this work (C₂H₅-R1, C₃H₃-R1T2, C₃H₅-R1D2 and C₃H₆-D1) and is closer to the experimental measurements.

Figure 3.6 presents the results for propane as fuel. The use of the updated

thermochemical data results in an improvement of the modeling predictions for ignition delay times obtained in the shock tube experiment from Burcat et al. 1971 [30] for propane as fuel. In this case, the main influence comes from the change in the value of thermodata for ethyl radical (C2H5-R1). The biggest influence of the change on ignition delay time has been observed at 1380 K.

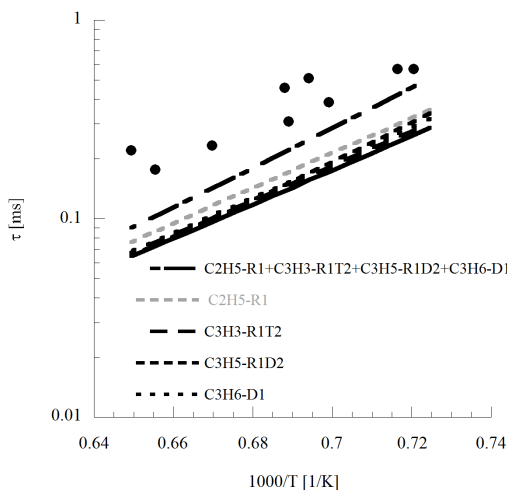


Figure 3.6: Ignition delay time of 0.84% C3H8/ 2.1% O₂ mixture in Ar in a shock tube at 7.5 bar and a temperature range of 1380-1540 K. Symbols represent experimental data ([30]). Black solid line: original simulation result, dark gray line: updated C3H3-R1T2 thermodynamic data, light gray dotted line: updated C3H6-D1 thermodynamic data, black dotted line: updated C3H5-R1D2, black dashed line: updated C2H5-R1, C3H3-R1T2, C3H5-R1D2, C3H6-D1 thermodynamic data.

An Integral flow analysis for propene as fuel at 1440 K and propane as fuel at 1380 K (using original and updated thermodata) is presented in figures 3.7 and 3.8. The flow analysis in this study visualizes the flow of carbon atoms and was introduced in the work by Schenk et al. 2013 [8]. Percentage numbers presented in the Figures are the number of C-atoms consumed by the respective reaction from the reactant molecule to the product molecule(s). The flux is normalized with the total flux of carbon atoms consumed by reactions with the reactant molecule. In the Figures, the minor reaction pathways are filtered out and therefore, the flows do not total 100%.

Figure 3.7 shows the flow corresponding to the propene decomposition. Every flow has two values. The first value corresponds to the original thermodata (normal script) and the second value corresponds to the updated thermodata (bold script).

The consumption of C3H6-D1 using the original thermodata (normal script) is dominated by abstraction of H-atom in allylic position producing 55.8% of the resonance-stabilized allyl radical (C3H5-R1D2). Other minor decomposition pathways for propene are H-atom abstraction from double bond producing

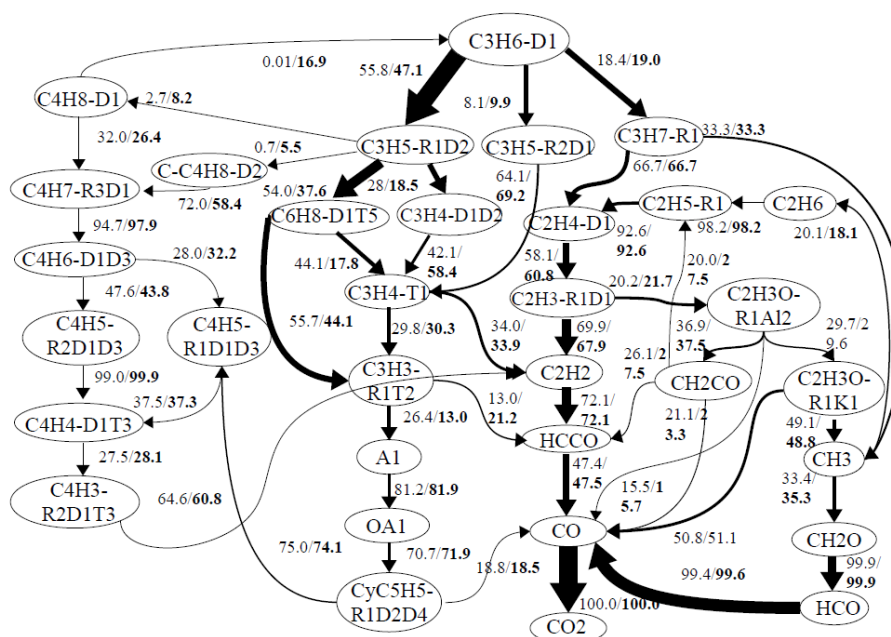


Figure 3.7: Integral reaction flux analysis for propene as fuel (1.6% C3H6-D1/ 7.2% O₂ mixture in Ar at 4 bar at 1440K ([36])). The first value corresponds to the original thermodata (normal script) and the second value corresponds to the updated thermodata (bold script). The contributions of individual pathways in the consumption of a species are indicated by percentages next to the arrows. The thickness of the arrows indicates the contribution of the respective pathway to the total flux of C-atoms.

8.1% of C3H5-R2D1 and H-atom addition to double bond producing 18.4% of C3H7-R1. The resonance-stabilized allyl radical (C3H5-R1D2) follows two main reaction pathways: The first one via reactions R495, R496 and R497 to form 54.4% of C6H8-D1T5 and the second one via H-atom abstraction to form 28% of allene (C3H4-D1D2). There are other two minor reaction pathways via methyl addition that result in 2.7% of the adduct of 1-butene (R354) and 0.7% of cis-2-butene (R400) that feed the C₄ route. The propyne (C3H4-T1) destruction channel contributes with 34% of its flow to the C₂ species pool.

Propargyl (C3H3-R1T2) is mainly formed by C6H8-D1T5 (R497) with 55.7% of the flow and propyne (C3H4-T1) with 29.8% of the flow. 26.4% of the Propargyl (C3H3-R1T2) recombines to produce benzene, which follows the destruction channel via the C₅ route feeding the C₄ route or contributing to the C₁ route, forming CO.

The alkyl radical C3H7-R1 is formed by 66.7% of ethene (C2H4-D1) and 33.3% of methyl CH₃ radical. The 20.1% of methyl radical recombines to form ethane C₂H₆, which decomposes via H-atom abstraction to ethyl C₂H₅-R1 radical; C₂H₅-R1 continues a subsequent dehydrogenation chain via H-atom abstraction up to acetylene (C₂H₂). A main contribution to ketyl radical formation is

attributed to acetylene (C2H2), with 72% of the flow.

Methyl radical follows another important pathway via O-atom addition to produce formaldehyde (CH2O), which subsequently forms formyl radical (HCO), which contributes to carbon monoxide (CO) formation. Final oxidation is reached when CO converts to carbon dioxide (CO2).

After the previously outlined update in the thermodynamic data of propene (C3H6-D1), allyl radical (C3H5-R1D2), propargyl (C3H3-R1T2), and ethyl radical (C2H5-R1), the impact in the carbon flow was investigated. The major decomposition pathways remain unchanged and the new values are presented in figure 3.7 in bold script.

The main differences are: a decrease in the flow formed by the abstraction of H-atom in allylic position from the propene molecule reaching 47.1% of resonance-stabilized allyl radical (C3H5-R1D2), an increase in the flow of C3H5-R2D1 and C3H7-R1 to 9.9% and 18.8% respectively. The reaction pathway responsible for propyne C3H4-T1 formation via C6H8-D1T5 decreased the flow to 17.8%, and direct propargyl formation via C6H8-D1T5 was reduced to 44.1%. In the same way, an increase in the flow that contributes to the consumption of propargyl C3H3-R1T2 via HCCO to 21.2% was observed and the reaction pathway responsible for benzene (A1) flow formation decreased to 13%. An increase in the flows forming 1-butene (C4H8-D1) to 8.2% and cis-2-butene (C-C4H8-D2) to 5.5% was observed. Furthermore, the decomposition reaction pathway from 1-butene (C4H8-D1) by removal of methyl radical gains relevance and this flow is responsible for 16.9% of propene (C3H6-D1) formation. The main path between propene (C3H6-D1) and allyl radical (C3H5-R1D2) has been slowed down. The contribution of this flow affects the ignition delay time.

In the case of propane (original mechanism), fuel consumption is dominated by abstraction of hydrogen in allylic position, producing 39.5% alkyl radical C3H7-R2 (R301) and 32.2% C3H7-R1 (R302). The unimolecular decomposition of the fuel molecule leads to the formation of 18.5% C2H5-R1 and 9.2% CH3 (R300). C3H7-R2 forms 96.2% of C3H6-D1 by H-atom abstraction and this flow follows the same decomposition pathways as discussed in Figure 3.7. Alkyl radical C3H7-R1 decomposes into 66.7% C2H4-D1 and 33.3% of CH3. 56.1% of the methyl radical recombines to form C2H6, marking the beginning of a subsequent dehydrogenation chain for C₂ route. Ethane molecules decompose via H-atom abstraction to form 97.3% C2H5-R1 flow and further H-atom abstraction forms 94.8% of C2H4-D1 flow. Ethene molecules decompose to form 69.5% of C2H3-R1D1 and 19.8% of C2H5O-R1OH2. C2H3-R1D1 flow forms 69.5% of acetylene C2H2 and 19.8% of C2H3O-R1A12. C2H5O-R1OH2 converts completely to acetaldehyde C2H4O-A11. C2H3O-R1A12 forms mainly two products, first 48.2% of C2H2O-K1D1 and second 11.3% of C2H4O-A11. C2H2O-K1D1 contributes to HCCO flow and CO flow, while C2H3O-R1K1 contributes to CO flow and methyl CH3 flow. Acetylene decomposition follows the reaction pathway that forms HCCO, forming CO and finally carbon dioxide CO2.

After the previously outlined update in the thermodynamic data of propene (C3H6-D1), allyl radical (C3H5-R1D2), propargyl (C3H3-R1T2), and ethyl ra-

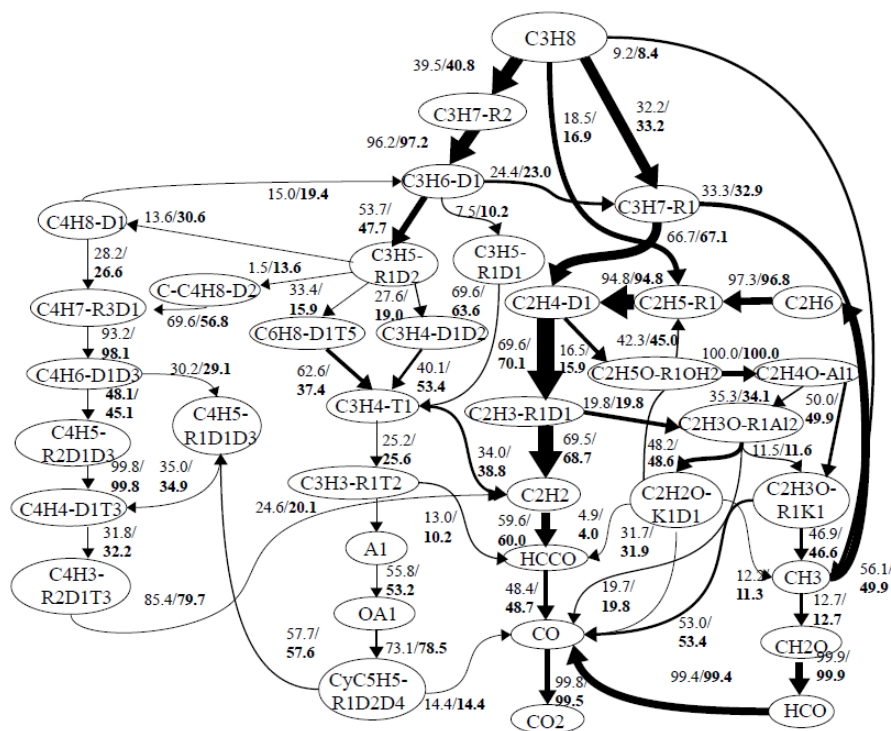


Figure 3.8: Integral reaction flux analysis for propane as fuel (0.84% C₃H₈/ 2.1% O₂ mixture in Ar at 7.5 bar at 1380 K ([30])). The first value corresponds to the original thermodata (normal script) and the second value corresponds to the updated thermodata (bold script). The contributions of individual pathways in the consumption of a species are indicated by percentages next to the arrows. The thickness of the arrows indicates the contribution of the respective pathway to the total flux of C-atoms.

dical (C₂H₅-R₁), the impact in the carbon flow was investigated. The major decomposition pathways remain unchanged and the new values are presented in the bold script in figure 3.8. Propane converts to 40.8% of alkyl radical C₃H₇-R₂ and 33.2% C₃H₇-R₁ for the abstraction of hydrogen. A decrease in the flows resulting from unimolecular fuel decomposition to produce 16.9% of C₂H₅-R₁ and 8.4% of CH₃ is observed. Propene destruction flow decreased to 47.7%. The reaction path leading to C₆H₈-D₁T₅ decreased to 15.9% and the path to form C₃H₄-D₁D₂ decreased to 19%. An opposite behavior was observed for C₄ species, where the reaction pathway that leads to butene (C₄H₈-D₁) formation increased up to 30% and the reaction pathway to form 2-butene (cis) C-C₄H₈-D₂ to 14%. Propyne (C₃H₄-T₁) decomposition to ethylene showed no significant changes.

After updating the thermodata, reaction rate sensitivity analyses were repeated for propene (figure 3.9) and propane (figure 3.10) as fuel. In the case of propene, several reactions show changes in their sensitivities to ignition delay times. We observed an increment in the sensitive values using the updated thermodata for

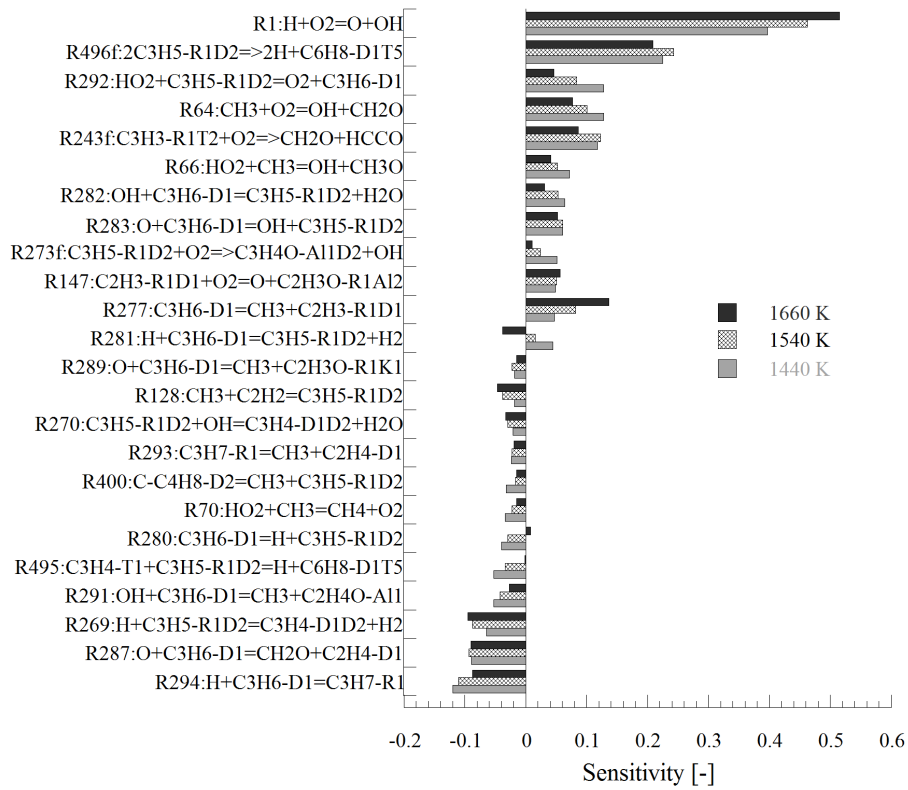


Figure 3.9: Net sensitivity analysis of reaction rates on ignition delay time for propene as fuel (1.6% C3H6-D1 / 7.2% O₂ mixture in Ar at 4 bar ([36])) for 1440 K, 1540 K and 1660 K.

the reactions:

- $\text{H} + \text{C3H6-D1} \rightleftharpoons \text{C3H7-R1}$ (R294)
- $\text{O} + \text{C3H6-D1} \rightleftharpoons \text{CH2O} + \text{C2H4-D1}$ (R287)
- $\text{O} + \text{C3H6-D1} \rightleftharpoons \text{OH} + \text{C3H5-R1D2}$ (R283)
- $\text{C3H6-D1} \rightleftharpoons \text{CH3} + \text{C2H3-R1D1}$ (R277)
- $2\text{C3H5-R1D2} \rightleftharpoons 2\text{H} + \text{C6H8-D1T5}$ (R496),

and a decrease in the sensitivity values for the reactions:

- $\text{H} + \text{C3H5-R1D2} \rightleftharpoons \text{C3H4-D1D2} + \text{H2}$ (R269) and
- $\text{HO2} + \text{C3H5-R1D2} \rightleftharpoons \text{O2} + \text{C3H6-D1}$ (R292).

For propane as fuel, reactions $\text{CH3} + \text{C2H5-R1} \rightleftharpoons \text{C3H8}$ (R300) and $\text{H} + \text{C3H8} \rightleftharpoons \text{C3H7-R2} + \text{H2}$ (R301) show an increase in the sensitivity values, with the most sensitive temperature for R300 being 1380 K and for R301 1380 K. Reactions $\text{H} + \text{C3H8} \rightleftharpoons \text{C3H7-R1} + \text{H2}$ (R302),

$\text{H} + \text{C}_3\text{H}_5\text{-R1D2} \rightleftharpoons \text{C}_3\text{H}_4\text{-D1D2} + \text{H}_2$ (R269), and
 $\text{CH}_3 + \text{CH}_3 \rightleftharpoons \text{C}_2\text{H}_5\text{-R1} + \text{H}$ (R188) showed a decrease in their sensitivity.

The reaction rate sensitivity analysis for some reactions does not follow a monotonic relation with the change of the temperature (e.g.: R496 in figure 3.9). For further understanding, a more detailed investigation was carried out for smaller temperature intervals and it was found that a clear trend appears with the maximum value of 1540 K. We have observed that in such cases, the perturbation of this reaction causes a change in the curvature of the reaction rate sensitivity on ignition delay time as shown on figure 3.11.

New thermodynamic data for C3H6-D1, C3H5-R1D2, C3H3-R1T2 and C2H5-R1 are available and have been included in our reaction mechanism. A change in thermodata has direct influence on the reactions sensitivities, which results in a change in the ignition delays time under these operating conditions.

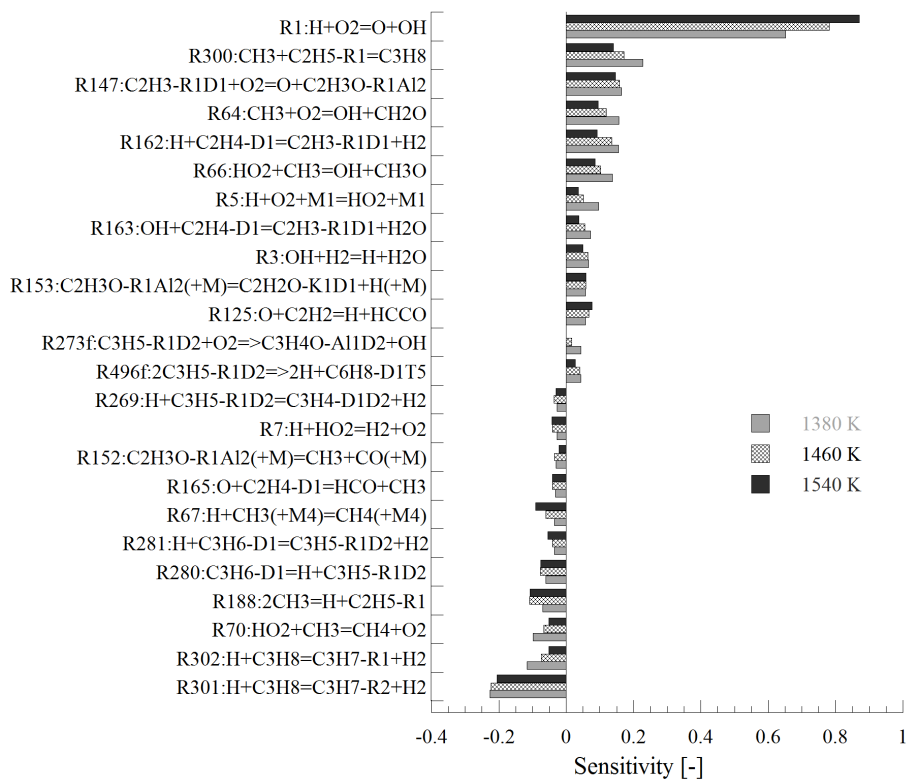


Figure 3.10: Net sensitivity analysis of reaction rates on ignition delay time for propane as fuel (0.84% C3H8/ 2.1% O₂ mixture in Ar at 7.5 bar ([30])) for 1380 K, 1460 K and 1540 K.

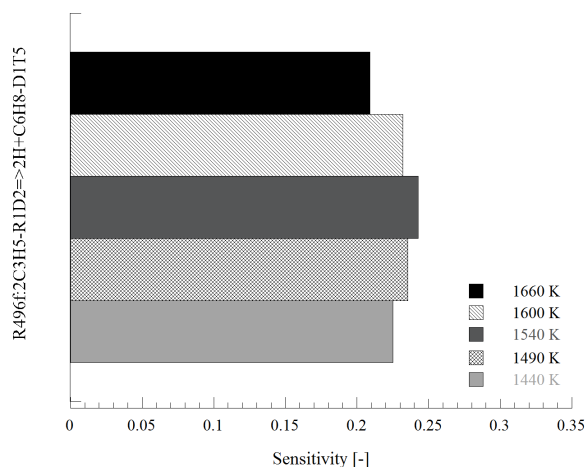


Figure 3.11: Net sensitivity analysis of reaction rates on ignition delay time for propene as fuel (1.6% C₃H₆-D1/ 7.2% O₂ mixture in Ar at 4 bar ([36])) for 1440 K, 1500 K, 1540 K, 1600 K and 1660 K.

3.3 Ignition delay time, laminar flame speed and burner-stabilized flame validation for propene and propane.

The mechanism with the updated thermodata has been further validated against several shock tube experiments, laminar flame speeds and burner-stabilized flames.

The results for propene are discussed in Figure 3.12 a), where simulations of ignition delay times for stoichiometric ($\phi=1$) conditions at 1 bar and fuel rich conditions ($\phi=2$) at 4 bar in the temperature range from 1500 to 1820 K were performed (see table 3.2). The experimental data are taken from Qin et al. (2001) [36] and Burcat and Radhakrishnan (1985) [35]. The measurements of [35] show a longer ignition delay time than the one observed by Qin et al. (2001) for similar conditions. A good agreement between simulation results using the updated model and experiments from [36] and [35] were found in this study.

Figure 3.12 b) shows a comparison of modeling results and experimental ignition delay times for propane by [31], [32], [33], and [34]. In general, a good predictability of the mechanism is found for the different experimental conditions at high temperatures. At lower temperatures, an offset is observed between the experimental and calculated results due to the missing low temperature reaction pathways for propane in the current version of the mechanism.

Simulations of premixed laminar flame speed using the updated thermodynamic data from this study were performed and compared to experiments from Davis and Law (1998) [42], Davis et al. (1999) [50], and Jomaas et al. (2005) [45] for propene as fuel (Figure 3.13.a)), and from Egolfopoulos et al. (1991) [39], Boss-

	Mixture	ϕ	Temperature K	pressure (bar)	Ref.
A	1.6% C3H6-D1/7.2% O ₂ in Ar	1	1500-1820	1	[36]
B	1.6% C3H6-D1/7.2% O ₂ in Ar	1	1500-1820	1	[35]
C	0.8% C3H6-D1/7.2% O ₂ in Ar	2	1440-1720	4	[36]
D	0.8% C3H6-D1/7.2% O ₂ in Ar	2	1440-1720	4	[35]
E	0.8% C3H8/8% O ₂ in Ar	0.5	900-1400	60	[34]
F	4.16% C3H8/20.84% O ₂ in N ₂	1	1250-1550	4.2	[31]
G	2.1% C3H8/20.6% O ₂ in Ar	0.5	900-1330	4.6	[32]
H	2% C3H8/20.58% O ₂ in Ar	0.5	1250-1650	4.6	[33]

Table 3.2: Ignition delay time experiments used for propane and propene validation.

chaart and Goey (2004) [44], Hassan et al. (1998) [43], Jomaas et al. (2005) [45], and Dirrenberger et al. (2011) [49] for propane as fuel (Figure 3.13.b)). No significant influence of the updated thermodata on the prediction of the laminar flame speed for propene/air and propane/air mixtures at 1 bar and 298 K in an equivalence ratio range from 0.2 to 2.0 is observed. This indicates that the C₃ flame chemistry is less sensitive on thermodata of the C₂, C₃ radical pool compared to the ignition process.

Numerical calculation of burner-stabilized flames from C₄ hydrocarbon species (*1*-butene (C4H8-D1), *2*-butene (T-C4H8-D2) and *iso*-butene (C4H8-D1Me2)) were repeated using the updated thermodata from this study and compared to the experimental and simulation results reported in Schenk et al. (2013) [8]. Main species profiles remained constant for all the flames, and it was found that C3H6-D1 and C3H4-D1D2 isomers (allene and propyne) are the most sensitive profiles to the thermodata changes.

Figure 3.14 shows propene (C3H6-D1) and C3H4-D1D2 isomers (allene and propyne) mole fraction profiles for the three butene isomers, a decrease in the prediction of C3H4-D1D2 mole fraction for the *1*-butene (C4H8-D1) and *2*-butene (T-C4H8-D2) flames was observed in comparison to the profiles predicted using the Schenk et al. (2013) [8] mechanism. No significant influence in the prediction of *iso*-butene (C4H8-D1Me2) profile is observed. For propene (C3H6-D1), an increase in the mole fraction for *2*-butene (T-C4H8-D2) and *iso*-butene (C4H8-D1Me2) is observed respectively, which results in an improvement of the prediction of experimental measurements. *1*-butene (C4H8-D1) mole fraction profile shows a decrease in the molar fraction prediction, but it still remains in the error range of the experimental measurement. Using the updated thermodata, the simulated profiles are closer to the experimental measurements.

Species enthalpy sensitivities on ignition delay times were calculated. We found several species with significant sensitivities of their heat of formation, namely propene (C3H6-D1), allyl (C3H5-R1D2), propyne (C3H4-D1D2), propargyl (C3H3-R1T2), oxygen (O2) and hydroperoxy radical (HO2) for propene auto ignition. Propane (C3H8), propene (C3H6-D1), allyl (C3H5-R1D2), propargyl (C3H3-R1T2), ethyl radical (C2H5-R1), ethylene (C2H4-D1), methane (CH4), methyl radical (CH3), oxygen (O2) and hydroperoxy radical (HO2) were identified as sensitive species for the propane auto ignition. A reaction rate sensitivity anal-

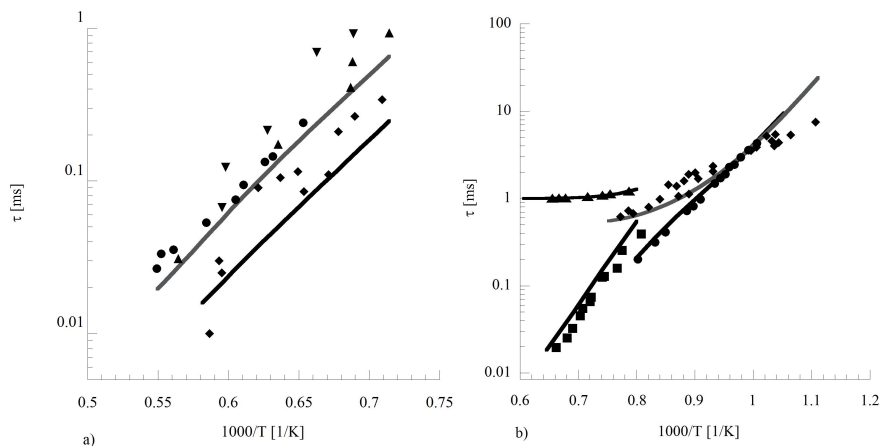


Figure 3.12: a) Experimental and calculated ignition delay times. Mixture compositions, equivalence ratio, pressures, temperature range, and references for experiments: ●: A, ▼: B, ◆: C, ▲: D, b) ●: E, ■: F, ◆: G $N=0.5$, ▲: H $N=1$. N offset of τ . Lines are simulation results using the combination of thermodynamic data corresponding to species $C_2H_5-R_1$, $C_3H_3-R_1T_2$, $C_3H_5-R_1D_2$ and $C_3H_6-D_1$ from this study.

ysis on ignition delay time was calculated before and after the update in the thermodata and a direct influence on the reaction rate sensitivity results coming from the change in the thermodata was found.

Thermodynamic data of Propene ($C_3H_6-D_1$), allyl ($C_3H_5-R_1D_2$), propargyl ($C_3H_3-R_1T_2$), and ethyl radical ($C_2H_5-R_1$) molecules were calculated and replaced in the reaction mechanism. The thermochemistry was derived from a combination of reliable molecular and spectroscopic properties, quantum chemical calculations and consistency tests based on thermochemical networks. As a result, a better agreement of model predictions of ignition delay times under different experimental conditions was observed.

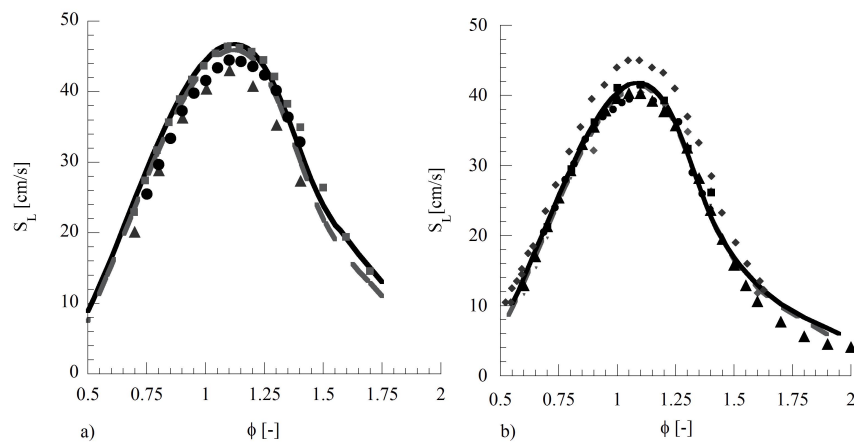


Figure 3.13: a) Numerical and determined laminar flame speeds as a function of the equivalence ratio for propene/air mixture at $T_u = 298$ K and $p = 1$ atm. The black line shows calculations using the original scheme, the gray dashed line shows calculations using the thermodynamic data for C_2H_5-R1 , C_3H_3-R1T2 , C_3H_5-R1D2 , C_3H_6-D1 calculated in this study. Experiments: \bullet [45], \blacksquare [50] and \blacktriangle [42] b) Numerically and determined laminar flame speeds as a function of the equivalence ratio for propane/air mixture at $T_u = 298$ K and $p = 1$ atm. The black line shows calculations using the original scheme, the gray dashed line shows calculations using the thermodynamic data for C_2H_5-R1 , C_3H_3-R1T2 , C_3H_5-R1D2 and C_3H_6-D1 calculated in this study. Experiments: \blacklozenge [39], \blacklozenge [43]), \bullet [41]), \blacktriangledown [44], \blacksquare [45], and \blacktriangle [49].

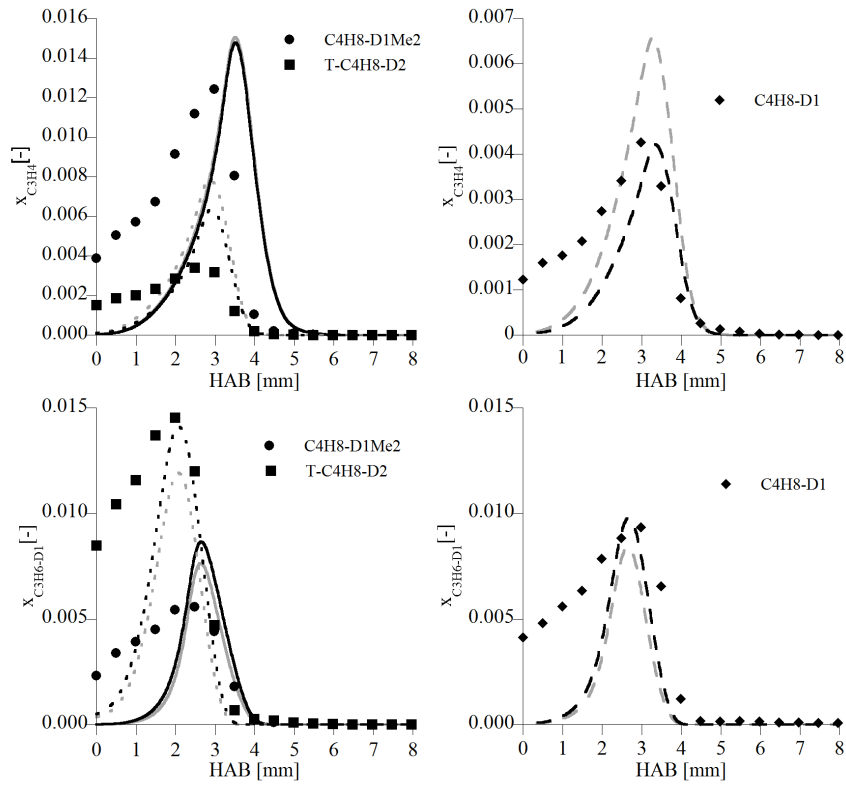


Figure 3.14: Propene (C_3H_6-D1) and C_3H_4-D1D2 isomers (allene and propyne) mole fraction profiles in premixed-low pressure (40 mbar) flat argon-diluted (25%) flame of the three butene isomers ($\phi=1.7$). The symbols represent the experimental measurements [8]: \bullet iso-butene ($C_4H_8-D1Me_2$), \blacksquare 2-butene ($T-C_4H_8-D2$), \blacklozenge 1-butene (C_4H_8-D1). Filled lines correspond to $C_4H_8-D1Me_2$, dotted lines correspond to $T-C_4H_8-D2$, and dashed lines correspond to C_4H_8-D1 . Gray lines are the validation using Schenk et al. (2013) [8] mechanism and black lines are the validation using the updated thermodata from this study.

Chapter 4

Combustion chemistry of isomers of butane

In this chapter, chemistry for *n*-butane (C₄H₁₀) and *iso*-butane (C₄H₁₀-Me₂) on burner-stabilized flames, ignition delay times and laminar flame speed will be revised. Thermodynamic data from chapter 3 has been included and most of the C₄ species were updated, using the thermochemical data of the database by Goos and Burcat (Goos et al. [9]).

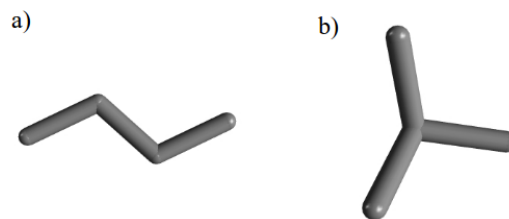


Figure 4.1: 3D model of butane molecules: a) *n*-butane [52] and b) *iso*-butane [53]

Butane is an alkane that has four carbon atoms with the formula C₄H₁₀. There are two structural isomers (see figure 4.1): a) an unbranched structure *n*-butane, and b) a branched structure, *iso*-butane, also known as 2-methylpropane [1].

Fuel	MW (g/mol)	LHV (KJ/g)	Bp (C)	T _a (K)	RON	MON
<i>n</i> -C ₄ H ₁₀	58.123	45.742	-0.5	2270	93.5	89
<i>iso</i> -C ₄ H ₁₀	58.123	45.742	-12	2246	100.1	96.8

Table 4.1: Physical and chemical properties of *n*-butane [52] and *iso*-butane [53]. RON and MON number [54]

The physical and chemical properties of both isomers ([52], [53]) are presented

in table 4.1. Both isomers are different compounds, *iso*-butane has higher RON and MON number and is used by refineries to increase the octane number of motor gasoline. Meanwhile, *n*-butane is known as an important component in LPG and natural gas. Butanes are highly flammable, colorless, easily liquified gases.

Several studies to understand the behavior of C₄H₁₀ isomers have been published: premixed flat flames for *n*-butane and *iso*-butane were measured by Osswald et al. 2011 [7] under equal fuel rich conditions at low-pressure. Tran et al. 2017 [55] measured *n*-butane/oxygen/argon premixed flat flames at similar conditions of [7]. Marinov et al. 1998 [56] measured an *n*-butane/oxygen/argon rich, sooting burner-stabilized flame at equivalence ratio $\phi=2.6$.

Laminar burning velocities were measured by Davis and Law 1998 [42], Bosschaert and de Goey [44], Hirasawa et al. 2001 [57], Dirrenberg et al. 2012 [49], Tang et al. 2011 [58] and Wu et al. 2014 [59] for *n*-butane (C₄H₁₀) and *iso*-butane at 298 K, ambient pressure, and equivalence ratios from 0.7 to 1.7. Veloo et al. 2010 [60], and Wang et al. 2011 [61] measured the laminar flame speeds for *n*-butane-air mixtures at 343 K and 403 K respectively at ambient pressure and an equivalence ratio from 0.7 to 1.5.

Herbinet et al. 2011 [62], Dagaut et al. 2000 [63], Cathonnet et al. 1981 [64], and Chakir et al. 1898 [65] studied the low-temperature oxidation of *n*-butane in a jet-stirred reactor (JSR), using a range of temperatures from 550 to 1300K, a pressure range from 1 to 10 bar, and an equivalence ratio from 0.15 to 2.0. Dagaut et al. 2000 [66] studied the low-temperature oxidation of *n*-butane in a JSR, using a range of temperatures from 1000 to 1300K, at atmospheric pressure, and with an equivalence ratio $\phi=1$.

Burcat et al. 1971 [30], Horning et al. 2002 [67], and Healy et al. 2010 [68] measured ignition delay times for *n*-butane at temperatures ranging from 950 to 1700 K, and pressures from 1 to 40 bar, using equivalence ratios from 0.3 to 2.0. Oehlschlaeger et al. 2004 [69] and Healy et al. 2010 [70] performed measurements of *iso*-butane at temperatures ranging from 950 to 2009 K, pressures ranging from 1 to 30 atm, and equivalence ratios from 0.25 to 2.0. Ogura et al. 2007 [71] and Donado et al. 2009 [72] measured ignition delay times of the isomers mixtures (*n*- and *iso*-butane) at temperatures ranging from 1050 to 1550 K, pressure of 2 bar and an equivalence ratio of $\phi=0.3-2.0$.

Gersen et al. 2010 [73] studied the autoignition of *n*-butane and *iso*-butane. The measurements were done in a Rapid Compression Machine in a temperature range from 660 to 1010 K, at pressures varying from 14 to 36 bar and at equivalence ratios $\phi=1.0$ and $\phi=0.5$. Both butane isomers exhibit a negative-temperature-coefficient (NTC) region and, at low temperatures, two-stage ignition.

Oehlschlaeger et al. 2004 [74] studied the decomposition rates of *iso*-butane and *n*-butane in the falloff regime at high temperatures in a shock tube using UV narrow-line laser absorption of CH₃ at 216.6 nm. Experimental conditions ranged from 1297 to 1601 K and 0.20 to 8.8 atm with mixtures varying in

concentration from 198 to 400 *ppm* of *iso*-butane or *n*-butane diluted in argon. Decomposition rate coefficients were determined by monitoring the formation rate of CH₃ immediately behind shock waves and modeling the CH₃ formation with detailed kinetic mechanisms.

4.1 High temperature chemistry for the C₄H₁₀ isomers

In this section, the updated reaction rates that have been implemented for the high temperature sub-mechanisms of *n*-butane (C₄H₁₀) and *iso*-butane (C₄H₁₀-Me₂) fuel molecules will be discussed in detail. Rate constants are expressed in the form of the Arrhenius equation (see eq. 2.19) with the units *cm*³, *mol*, *s*, *cal*; \longrightarrow indicates that only forward reaction is considered; \rightleftharpoons indicates that also the reverse reaction is considered, as well as the data to calculate the pressure dependency (see 2.1).

4.1.1 Class 1: Unimolecular fuel decomposition

n-butane (C₄H₁₀) and *iso*-butane (C₄H₁₀-Me₂) unimolecular decomposition rates for C–C bond breaking reactions were updated using the kinetic data calculated by Oehlschlaeger et al. [74] whereby pressure dependency was provided by TROE formalism. Third body efficiencies were taken from Griffiths and Barnard 1985 [75]. In order to compensate for the energy in the system, a decrease of the pre-exponential factors for some reactions was implemented (See tables 4.2 and 4.3).

In the case of reactions with C–H bond breaking, the study from Dean 1985 [76] provided measurements for both linear isomers. The rates have also been included in our model. Regarding the branched molecule, the rates have been taken from the investigation of Curran et al. 2002 [77].

	A	n	Ea	Ref
C ₄ H ₁₀ (+ M) \rightleftharpoons C ₂ H ₅ -R1 + C ₂ H ₅ -R1 (+ M)	2.092E+15	0.0	7.561E+04	^a
LOW/	3.631E+18	0.0	4.958E+04	
TROE/ 0.72 1500.0 1.00E-07/				
H ₂ / 1.0/H ₂ O/ 6.40/CO ₂ / 1.50/O ₂ / 0.45/N ₂ / 0.40/AR/ 0.35/				[75]
C ₄ H ₁₀ (+ M) \rightleftharpoons C ₃ H ₇ -R1 + CH ₃ (+ M)	4.280E+14	0.0	6.990E+04	[74]
LOW/	5.340E+17	0.0	4.296E+04	
TROE/ 0.72 1500.0 1.00E-07/				
H ₂ / 1.0/H ₂ O/ 6.40/CO ₂ / 1.50/O ₂ / 0.45/N ₂ / 0.40/AR/ 0.35/				[75]
C ₄ H ₁₀ \rightleftharpoons C ₄ H ₉ -R1 + H	1.580E+16	0.0	9.796E+04	[76]
C ₄ H ₁₀ \rightleftharpoons C ₄ H ₉ -R2 + H	1.000E+16	0.0	9.499E+04	[76]

Table 4.2: Unimolecular fuel decomposition for *n*-butane (C₄H₁₀). ^a: The pre-exponential factor A is the original value from [74] by 1.3 uncertainty factor.

	A	n	Ea	Ref
C4H10-Me2 (+ M) <=> C3H7-R1 + CH3 (+ M)	7.550E+15	0.0	7.991E+04	^a
LOW/	3.766E+18	0.0	5.258E+04	
TROE/ 0.25 1500.0 1.00E-07/				
H2/ 1.0/H2O/ 6.40/CO2/ 1.50/O2/ 0.45/N2/ 0.40/AR/ 0.35/				[75]
C4H10-Me2 <=> C4H9-R1Me2 + H	2.510E+98	-23.81	1.453E+05	[77]
C4H10-Me2 <=> C4H9-R2Me2 + H	9.850E+95	-23.11	1.453E+05	[77]

Table 4.3: Unimolecular fuel decomposition for iso-butane (C_4H_{10} -Me2). ^a: The pre-exponential factor A is the original value from [74] by 6.4 uncertainty factor

4.1.2 Class 2: H-atom abstraction from fuel

Reaction rates change depending on the type of hydrogen atom that can be abstracted from the alkyl radical (primary, secondary, or tertiary site). In this model, ten radicals are considered: H, OH, O, CH3, HO2, CH3O, O2, C2H3-R1D1, C2H5-R1, and CH3O2. Reactions are expressed in equilibrium.

	A	n	Ea	Ref
C4H10 + H <=> C4H9-R1 + H2	2.640E+14	0.00	9.380E+03	^a
C4H10 + H <=> C4H9-R2 + H2	3.920E+14	0.00	7.949E+03	^a
C4H10 + O <=> C4H9-R1 + OH	2.260E+14	0.00	7.858E+03	^b
C4H10 + O <=> C4H9-R2 + OH	1.124E+13	0.00	5.207E+03	^b
C4H10 + OH <=> C4H9-R1 + H2O	2.695E+06	2.00	4.510E+02	^c
C4H10 + OH <=> C4H9-R2 + H2O	2.600E+06	2.00	-6.140E+02	^c
C4H10 + HO2 <=> C4H9-R1 + H2O2	4.080E+01	3.59	1.716E+04	[78]
C4H10 + HO2 <=> C4H9-R2 + H2O2	1.264E+02	3.37	1.372E+04	[78]
C4H10 + CH3 <=> C4H9-R1 + CH4	1.300E+12	0.00	1.161E+04	[79]
C4H10 + CH3 <=> C4H9-R2 + CH4	8.000E+11	0.00	9.506E+03	[79]
C4H10 + O2 <=> C4H9-R1 + HO2	2.500E+13	0.00	4.901E+04	[79]
C4H10 + O2 <=> C4H9-R2 + HO2	4.000E+13	0.00	4.760E+04	[79]
C4H10 + CH3O <=> C4H9-R1 + CH3OH	3.000E+11	0.00	6.998E+03	[79]
C4H10 + CH3O <=> C4H9-R2 + CH3OH	6.000E+11	0.00	6.998E+03	[79]
C4H10 + CH3O2 <=> C4H9-R1 + CH3O2H	1.700E+13	0.00	2.046E+04	[80]
C4H10 + CH3O2 <=> C4H9-R2 + CH3O2H	1.120E+13	0.00	1.770E+04	[80]
C4H10 + C2H3-R1D1 <=> C4H9-R1 + C2H4-D1	1.000E+12	0.00	1.800E+04	[81]
C4H10 + C2H3-R1D1 <=> C4H9-R2 + C2H4-D1	8.000E+11	0.00	1.680E+04	[81]
C4H10 + C2H5-R1 <=> C4H9-R1 + C2H6	3.162E+11	0.00	1.230E+04	[82]
C4H10 + C2H5-R1 <=> C4H9-R2 + C2H6	1.000E+11	0.00	1.040E+04	[82]

Table 4.4: H-atom abstraction for n -butane (C_4H_{10}). ^a: The pre-exponential factor is 2 times the original value from [83], ^b: The pre-exponential factor is 2 times the original value from [79], ^c: The pre-exponential factor is the original value from [84] divided by 2.

The rates for n -butane (C_4H_{10}) are presented in table 4.4. Original rates were taken from the work of Westbrook et al. 1989 [79]. Modifications were applied as follows: H-atom rates were taken from the work of Baldwin and Walker [83]. OH-atom rates were updated from the work of Atkinson [84]. HO2 rates were taken from the work of Aguilera et al. [78]. CH3O2 rates were taken from the work of Carstensen et al 2007 [80]. C2H5-R1 rates were taken from Allara and Shaw [82], and C2H3-R1D1 rates were written following n -heptane rules from

Ahmed et al. 2007 [81]. Finally, H, O, and OH reaction rates have been adjusted within the experimental uncertainty in order to improve the prediction of the mechanism.

The rates for *iso*-butane (C4H10-Me2) are presented in table 4.5. Original rates are taken from Tsang et al. 1989 [85]. OH rates were updated using the rates from Cohen et al. 1991 [86], HO2 rates were updated using the rates from Aguilera et al 2008 [78] and CH3O2 rates were taken from the work of Carstensen et al 2007 [80].

	A	n	Ea	Ref
C4H10-Me2 + H <=> C4H9-R2Me2 + H2	6.025E+05	2.40	2.583E+03	[85]
C4H10-Me2 + H <=> C4H9-R1Me2 + H2	1.810E+06	2.54	6.757E+03	[85]
C4H10-Me2 + O <=> C4H9-R2Me2 + OH	1.570E+05	2.50	1.113E+03	[85]
C4H10-Me2 + O <=> C4H9-R1Me2 + OH	4.280E+05	2.50	3.637E+03	[85]
C4H10-Me2 + OH <=> C4H9-R2Me2 + H2O	5.140E+06	1.90	-1.451E+01	^a
C4H10-Me2 + OH <=> C4H9-R1Me2 + H2O	3.427E+07	1.80	1.451E+03	^b
C4H10-Me2 + HO2 <=> C4H9-R1Me2 + H2O2	6.100E+01	3.59	1.728E+04	[78]
C4H10-Me2 + HO2 <=> C4H9-R2Me2 + H2O2	6.504E+02	3.01	1.210E+04	[78]
C4H10-Me2 + CH3 <=> C4H9-R2Me2 + CH4	0.904E+00	3.46	4.590E+03	[85]
C4H10-Me2 + CH3 <=> C4H9-R1Me2 + CH4	1.360E+00	3.65	7.154E+04	[85]
C4H10-Me2 + O2 <=> C4H9-R1Me2 + HO2	4.040E+13	0.00	5.087E+04	[85]
C4H10-Me2 + O2 <=> C4H9-R2Me2 + HO2	3.970E+13	0.00	4.390E+04	[85]
C4H10-Me2 + CH3O <=> C4H9-R1Me2 + CH3OH	4.820E+11	0.00	7.313E+03	[85]
C4H10-Me2 + CH3O <=> C4H9-R2Me2 + CH3OH	2.290E+10	0.00	2.881E+03	[85]
C4H10-Me2 + CH3O2 <=> C4H9-R1Me2 + CH3O2H	5.958E+02	3.75	1.690E+04	[80]
C4H10-Me2 + CH3O2 <=> C4H9-R2Me2 + CH3O2H	2.620E+02	3.12	1.110E+04	[80]
C4H10-Me2 + C2H3-R1D1 <=> C4H9-R1Me2 + C2H4-D1	1.360E+00	3.65	5.167E+03	[85]
C4H10-Me2 + C2H3-R1D1 <=> C4H9-R2Me2 + C2H4-D1	0.904E+00	3.46	2.603E+03	[85]
C4H10-Me2 + C2H5-R1 <=> C4H9-R1Me2 + C2H6	1.390E+00	3.65	9.141E+04	[85]
C4H10-Me2 + C2H5-R1 <=> C4H9-R2Me2 + C2H6	0.540E+00	3.46	5.962E+03	[85]

Table 4.5: *H*-atom abstraction for *iso*-butane (C4H10-Me2). ^a: The pre-exponential factor is 2 times the original value from [86]. ^b: The pre-exponential factor is the original value from [86] by 1.5

4.1.3 Class 3: Alkyl radical decomposition

The rates for *n*-butane (C4H10) and *iso*-butane (C4H10-Me2) are presented in table 4.6. This reaction class is characterized by the breakdown of the C–C and C–H bond in β -position of the carbon atom carrying the radical center [87]. Original rates for the linear and branched molecules are taken from Chakir et al. 1989 [65] and Tsang 1989 [85] respectively. Updated rates were taken from the work of Curran 2006 [88].

	A	n	Ea	Ref
C4H9-R1 \rightleftharpoons C2H4-D1 + C2H5-R1	2.500+13	0.00	2.880E+04	[65]
C4H9-R1 \rightleftharpoons H + C4H8-D1	1.260E+13	0.00	3.860E+04	[65]
C4H9-R2 \rightleftharpoons H + T-C4H8-D2	2.850E+11	0.34	3.552E+04	[88]
C4H9-R2 \rightleftharpoons H + C4H8-D1	2.990E+11	0.00	3.682E+04	[88]
C4H9-R2 \rightleftharpoons CH3 + C3H6-D1	9.582E+10	1.04	3.036E+04	[88]
C4H9-R2Me2 \rightleftharpoons H + C4H8-D1Me2	8.300E+13	0.00	3.815E+04	[85]
C4H9-R1Me2 \rightleftharpoons C3H6-D1 + CH3	9.504E+11	0.773	3.070E+04	[88]
C4H9-R1Me2 \rightleftharpoons C4H8-D1Me2 + H	1.710E+13	0.12	3.368E+04	[88]

Table 4.6: Alkyl radical decomposition for *n*-butane (C4H10) and iso-butane (C4H10-Me2).

4.1.4 Class 4: Alkyl radical + O2 direct formation of olefin and HO2

This class allows the alkyl radical to react via several pathways adding the O2. The elimination of RO2 produces the conjugated alkene. Reaction rates are presented in table 4.7. Original values are taken from Chakir et al. 1989 [65] and Curran et al. 2002 [77].

	A	n	Ea	Ref
C4H9-R1 + O2 \rightleftharpoons HO2 + C4H8-D1	1.000E+12	0.00	2.006E+03	[65]
C4H9-R2 + O2 \rightleftharpoons HO2 + C4H8-D1	2.000E+12	0.00	4.490E+03	[65]
C4H9-R2 + O2 \rightleftharpoons HO2 + T-C4H8-D2	5.000E+12	0.00	4.251E+03	^a
C4H9-R2 + O2 \rightleftharpoons HO2 + C-C4H8-D2	5.000E+12	0.00	4.251E+03	^a
C4H9-R2Me2 + O2 \rightleftharpoons C4H8-D1Me2 + HO2	7.500E-19	0.00	5.020E+03	[77]
C4H9-R1Me2 + O2 \rightleftharpoons C4H8-D1Me2 + HO2	1.500E-19	0.00	2.000E+03	[77]

Table 4.7: Alkyl radical + O2 for *n*-butane (C4H10) and iso-butane (C4H10-Me2).
^a: The pre-exponential factor is the original value from [65] by 4.

4.1.5 Class 5: Alkyl radical isomerization

The alkyl radical can transfer any H-atoms to the radical site [77]. This reaction occurs through the formation of a cyclic transition state that usually includes four to eight carbon atoms. The reaction rate depends on the type of bond that needs to be broken, and on the distance from the ring. For these small molecules, the rates were taken from the work of Matheu et al. 2003 ([89]).

	A	n	Ea	Ref
C4H9-R1 \rightleftharpoons C4H9-R2	3.560E+10	0.88	3.730E+04	[89]
C4H9-R1 \rightleftharpoons C4H9-R2	3.800E+10	0.67	3.660E+04	[89]
C4H9-R1Me2 \rightleftharpoons C4H9-R2Me2	3.560E+10	0.88	3.464E+04	[89]

Table 4.8: Alkyl radical isomerization for *n*-butane (C4H10) and iso-butane (C4H10-Me2).

Abstraction reactions from olefin (class 6), Alkenyl radical decomposition (class 8), and olefin decomposition (class 9) are presented in the following chapter

combustion chemistry of the butene isomers, where the chemistry of but-1-ene (C4H8-D1), (Z)-but-2-ene (T-C4H8-D2), and *iso*-butene (C4H8-D1Me2) are discussed in detail.

The mechanism used for flame simulations in the present study consists of 277 species and 1387 irreversible reactions (forward and backward reactions are accounted for separately as individual, irreversible reactions). The kinetic, thermodynamic and transport data are available on the supplementary material. All calculations were performed with the current version of the LOGEsoft software package [26].

4.2 Experiments

In the present study, *n*-butane and *iso*-butane as fuel were validated against premixed flat flames, ignition delay times and laminar flame speed experiments.

Osswald et al. 2011 [7] measured *n*-butane and *iso*-butane premixed flat flames under equal fuel rich ($\phi=1.71$) conditions at low-pressure (40 *mbar*). Laminar burning velocities were validated against measurements done by Hirasawa et al. 2001 [57], Dirrenberg et al. 2012 [49], Tang et al. 2011 [58] and Wu et al. 2014 [59] for *n*-butane at 298 *K*, ambient pressure, and equivalence ratios from 0.7 to 1.5. Davis and Law 1998 [42], Bosschaart and de Goey [44] measured *n*-butane and *iso*-butane as fuel at 298 *K*, ambient pressure, and equivalence ratios from 0.6 to 1.7. Veloo et al. 2010 [60], and Wang et al. 2011 [61] measured the laminar flame speeds for *n*-butane/air mixtures at 343 *K* and 403 *K* respectively, ambient pressure and an equivalence ratio from 0.7 to 1.5.

Autoignition experiments of butane isomers and their mixtures have been included in this study. Burcat et al. 1971 [30], Healy et al. 2010 [68], and Ogura et al. 2007 [71] were used for *n*-butane validation at temperatures ranging from 950 to 1700 *K*, pressures ranging from 1 to 40 *bar* and equivalence ratios from 0.3 to 2.0. Healy et al. 2010 [70] and Ogura et al. 2007 [71] performed measurements of *iso*-butane at temperatures ranging from 950 to 2009 *K*, pressures ranging from 1 to 30 *atm* and equivalence ratios from 0.3 to 2.0. Ogura et al. 2007 [71] investigated the ignition behavior of pure *n*-butane and *iso*-butane and its mixtures (70%C4H10/ 30%C4H10-Me2, 50%C4H10/50%C4H10-Me2, and 30%C4H10/70%C4H10-Me2) at 2 *bar*, at temperatures ranging from 1050 to 1550 *K* and equivalence ratio of 0.72.

4.3 Burner-stabilized flame validation of *n*-butane (C4H10) and *iso*-butane (C4H10-Me2).

The results regarding species profiles measured in a burner-stabilized flame will be discussed in this section. Experimental conditions from Osswald et al. 2011 [7] for *n*-butane and *iso*-butane were simulated using the Freely propagating module. For the simulation, the overall mass conservation equation and N-1 species conservation equations are solved, where N is the total number of

species. The energy equation is solved by means of a given temperature profile. by the means of a given temperature profile. The diffusion transport coefficient was calculated by the mixture-averaged diffusion method. The gas composition, pressure and disturbed temperature profiles were given as input parameters. Measured temperature profiles were used as parameterized input curves without any shift between measurement and simulation. Both flames have the same experimental conditions, the *n*-butane flame has a 100 K higher temperature peak in comparison to the *iso*-butane flame.

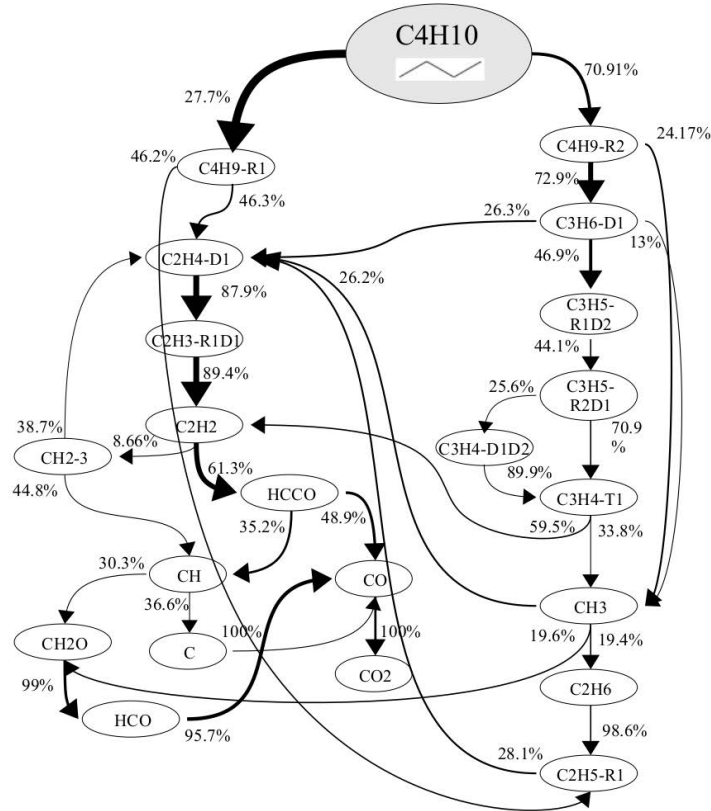


Figure 4.2: Integrated flow analysis of *n*-butane (C_4H_{10}) consumption. The thickness of the arrows indicates the contribution of the respective pathway to the total flux of C-atoms (contributions of the destruction of the individual molecule are indicated by percentages next to the arrows) [7].

Figures 4.2 and 4.3 show the detailed flow analysis for *n*-butane (C_4H_{10}) and *iso*-butane ($C_4H_{10}-Me_2$) respectively. Main fluxes for the discussion are presented. The thickness of the arrow is approximately scaled to represent the flux of C-atoms from one species to another. The contribution of individual pathways in consuming a chemical species are indicated by the percentages next to the arrows. The flux analysis was filtered in a C-atom. Fluxes below 10% of the total flow are not shown.

Some differences can be observed by comparing both schemes. *n*-butane (C_4H_{10}) decomposition is initiated by hydrogen abstraction forming 70.91% 2-butyl radical ($C_4H_9-R_2$) and 27.7% 1-butyl radical ($C_4H_9-R_1$). 72.9% 2-butyl radical decomposes via C-C β -scission to propene ($C_3H_6-D_1$) and methyl radical ($C_4H_9-R_2 = C_3H_6-D_1 + CH_3$). 46.9% of propene decomposes via H-abstraction to forms allyl radical ($C_3H_5-R_1D_2$), which by further oxidation contributes to the C_1 and C_2 routes. 27.7% 1-butyl radical via C-C β -scission forms ethene ($C_2H_4-D_1$) and 46.2% of ethyl radical ($C_2H_5-R_1$) ($C_4H_9-R_1 = C_2H_4-D_1 + C_2H_5-R_1$). 87.9% of ethene ($C_2H_4-D_1$) undergoes oxidation by H-atom abstraction to give vinyl radical ($C_2H_3-R_1D_1$), which by further dehydrogenation forms acetylene (C_2H_2). 61.3 % of acetylene decomposes to ethynyl radical ($HCCO$). Further oxidation follows via Formaldehyde (CH_2O) and bicarbonate (HCO), contributing to carbon monoxide (CO) and carbon dioxide CO_2 .

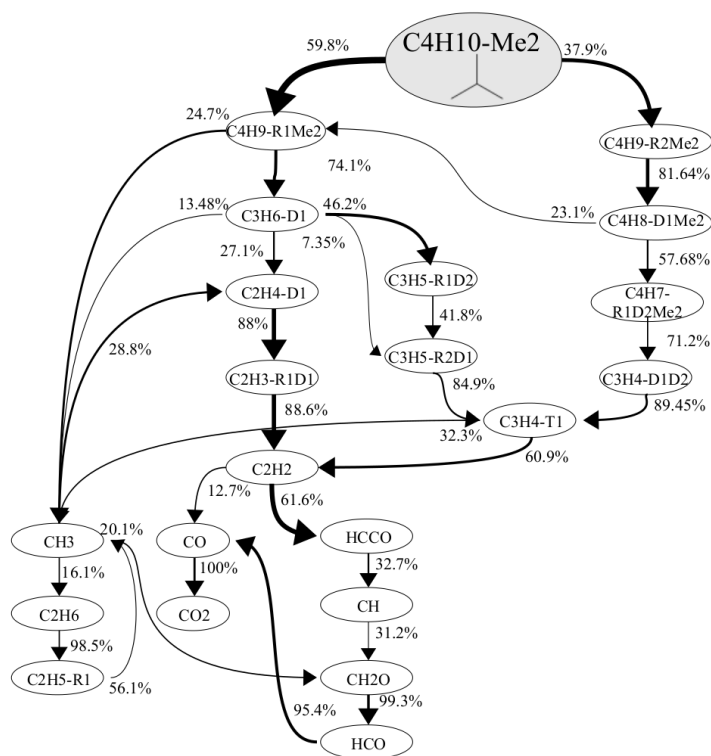


Figure 4.3: Reaction path analysis for iso-butane ($C_4H_{10}-Me_2$) flame. The contribution of individual pathways in consuming a species are indicated by percentage next to the arrows; C-atom fluxes below 10% are not shown [7].

For the *iso*-butane ($C_4H_{10}-Me_2$) flame, the decomposition is initiated by H-atom abstraction where 59.8% forms iso-butyl radical ($C_4H_9-R_1Me_2$) and 37.9% forms *t*-butyl radical ($C_4H_9-R_2Me_2$). 74.1% of iso-butyl radical forms propene ($C_3H_6-D_1$) and methyl radical (CH_3) via C-C β -scission. Propene contributes to C_1 , C_2 and C_3 routes. 81.64% of *t*-butyl radical via H-atom abstraction forms iso-butene ($C_4H_8-D_1Me_2$), which triggers H-atom abstraction to form 2-

methylallyl radical ($C_4H_7-R1D2Me_2$), further contributing to C_3 and C_1 routes. Reactions towards acetylene (C_2H_2) and ethynyloxidanyl ($HCCO$), and further oxidation then proceeds towards CO and CO_2 . Thermal decomposition can be neglected.

Experiments will be presented below along with the modeling results of selected species mole fraction profiles following the reaction pathways identified for the two fuels in the flow analysis.

4.3.1 Major Species

Major species profiles (butane, O_2 , Ar, CO , CO_2 , H_2 , and H_2O) have been compared for both flames. The model can predict the major species mole fractions well. Equilibrium mole fractions are reached in the exhaust gases, therefore the temperature profile can be assumed to be the correct one. No position shift has been applied between the experiment and the model.

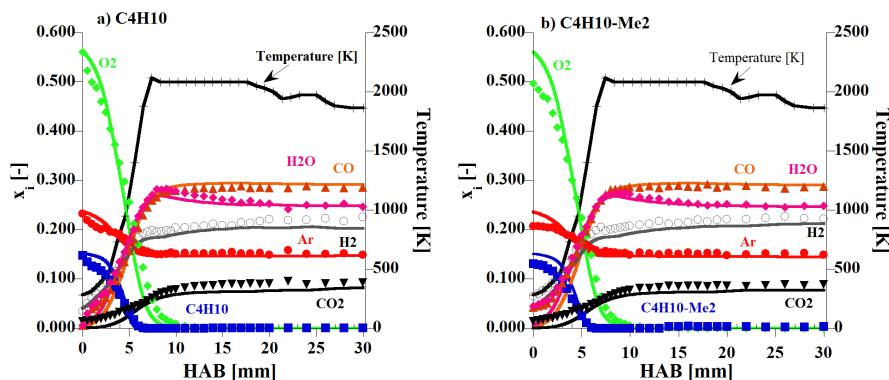


Figure 4.4: Major species mole fractions plotted vs. height above the burner (HAB); a) *n*-butane (C_4H_{10}) flame and b) *iso*-butane ($C_4H_{10}-Me_2$) flame. The symbols are from the EI-MBMS experiment [7]; lines represent simulations with the model. mole fractions are shown in the exhaust.

4.3.2 Intermediate species

In this section, the model and experimental results obtained are discussed by comparing the trends between both butane fuels. Figure 4.5 shows the C_4 intermediates, represented by the formula C_4H_8 (*iso*-butene ($C_4H_8-D1Me_2$), 1-butene (C_4H_8-D1), *trans*-2-butene (T- C_4H_8-D2), and *cis*-2-butene (C- C_4H_8-D2)) and the formula C_4H_6 (1,3-Butadiene (C_4H_6-D1D3) and 1,2-Butadiene ($C_4H_6-D1-D2$)), as products of dehydrogenation reactions.

The predicted mole fraction of C_4H_8 isomers from the model matches the peak position and magnitude. Here we can observe that the *iso*-butane flame pro-

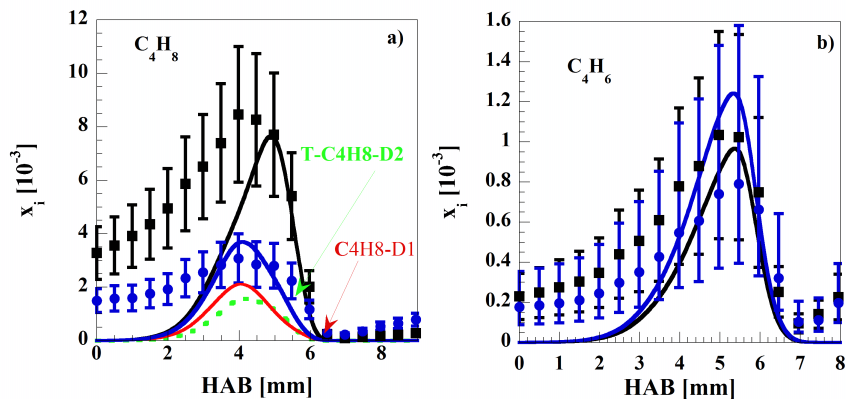


Figure 4.5: Mole fraction profiles of C_4H_8 and C_4H_6 isomers. Symbols represent experimental data: *n*-butane (C_4H_{10}) (\bullet) and *iso*-butane (C_4H_{10} -Me2) (\blacksquare) flame. Solid lines represent modeling results and the corresponding error bars show the experimental error.

duces a higher amount of C_4H_8 , which comes mainly from *iso*-butene (C4H8-D1Me2). Conversely, in the *n*-butane flame the amount is lower by a factor 4 and mainly originates from linear isomers *1*-butene and *2*-butene. To understand these results better, the flow analysis on Fig. 4.3 demonstrates that the initial decomposition of *iso*-butane follows a path via *t*-butyl radical (C4H9-R2Me2), which forms C4H8-D1Me2 by H-atom abstraction removal. By observing the analysis for *n*-butane (see Fig. 4.2), it is observed that the main decomposition pathway favors the path to *2*-butyl radical (C4H9-R2), which will favor C_3 and C_2 reaction pathways.

The experimental results show that C_4H_6 corresponds mainly to 1,3-butadiene in both flames, being 26% higher for the *iso*-butane flame. This is a very interesting observation since there are no direct dehydrogenation pathways that lead to 1,3-butadiene (C4H6-D1D3) in the *iso*-butane flame. Modeling results are in good agreement with respect to the peak position, and 1-3-butadiene is the isomer with the highest predicted concentration, which is consistent with the experimental findings.

Figure 4.6 shows the mole fraction profiles of some unsaturated species, such as: acetylene (C_2H_2), vinylacetylene (C_4H_4 -D1T3) and diacetylene (C_4H_2 -T1T3). Mole fraction measurements are very similar for both flames. In the case of acetylene, the profiles are in good agreement with the experimental values at the peak. Similar consistent shapes and peak positions can be observed for C_4H_2 -T1T3 and C_4H_4 -D1T3. Diacetylene (C_4H_2 -T1T3) has a deviation of factor 3 with respect to the experimental results for both flames and vinylacetylene (C_4H_4 -D1T3) by factor 2. Peak and shape are in good agreement with the experimental measurement, considering that the model prediction is

within the experimental error limit.

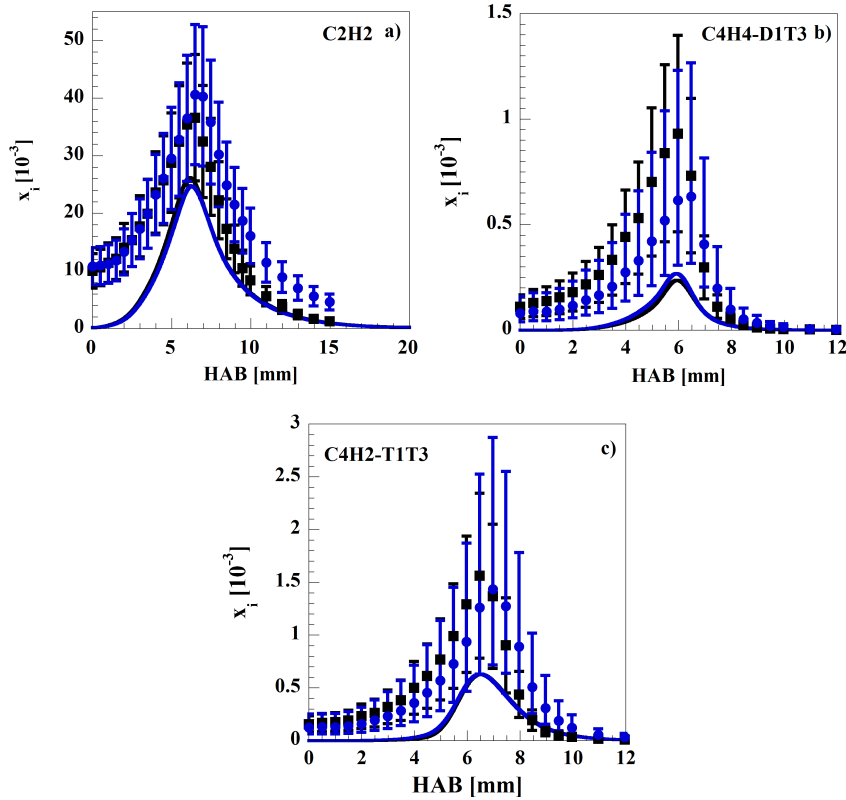


Figure 4.6: Mole fraction profiles of selected unsaturated species: acetylene (C_2H_2), vinylacetylene (C_4H_4 -D1T3) and diacetylene (C_4H_2 -T1T3). Symbols represent experimental data: *n*-butane (C_4H_{10}) (\bullet) and iso-butane (C_4H_{10} -Me2) (\blacksquare) flame. Solid lines represent modeling results and the corresponding bars show the experimental error.

Results corresponding to unsaturated species C_6H_2 and C_6H_4 are presented in Figure 4.7. C_6H_2 according to the model and experimental measurements corresponds to hexa-1,5-diyne-3-ene. It shows a good agreement in shape and position of the peak with a deviation factor 2 from the experimental results. Regarding C_6H_4 , several isomers are possible, but the energy scan of mass 76 does not allow unambiguous identification because of poor signal-to-noise ratio [7]. The model includes two radicals, namely: hexa-1,5-diyne-3-ene or hexa-1,3-diyne-5-ene (C_6H_4 -D3T1T5) as well as cyclic benzyne (CYC_6H_4 -D1D3T5). Further development of the model to predict C_6 growth of linear and branched products depends primarily on reliable species identification as provided by the GC analysis. However, the development of a full C_6 sub-mechanism for linear and branched species is beyond the scope of the present work.

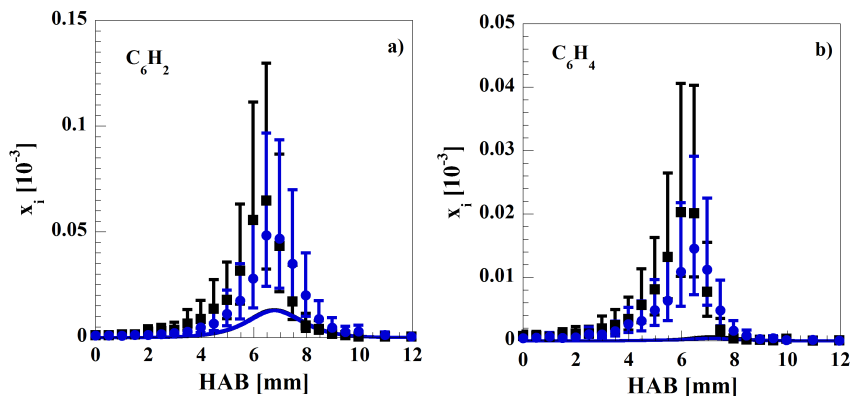


Figure 4.7: Mole fraction profiles of selected unsaturated species C_6H_2 and C_6H_4 . Symbols represent experimental data: *n*-butane (C_4H_{10}) (●) and *iso*-butane (C_4H_{10} -Me2) (■) flame. Solid lines represent modeling results and the corresponding bars show the experimental error.

4.3.3 Smaller decomposition pathways

Figure 4.8 shows main C_2 and C_3 species which are a very important decomposition pathway for both flames. Decomposition of C_4 via C-C scission may lead to a combination of C_3+C_1 and C_2+C_2 species. Propene (C_3H_6 -D1) can be formed from both fuels via H-atom abstraction. For *n*-butane, it is formed from 2-butyl radical (C_4H_9 -R2) and for *iso*-butane it is done via *iso*-butyl radical (C_4H_9 -R1Me2).

- C_4H_9 -R2 \rightleftharpoons C_3H_6 -D1 + CH_3
- C_4H_9 -R1Me2 \rightleftharpoons C_3H_6 -D1 + CH_3

In both flames, almost the same amount of propene was detected while slightly higher values were measured for *iso*-butane. The mole fraction of allyl radical (C_3H_5 -R1D2) follows the same trend as propene. The decomposition pathway is the result of H-atom abstraction. The propene mole fraction is 9% over-predicted by the model for *n*-butane and 23% under-predicted by the model for *iso*-butane. The trends as well as the peak locations match well in the simulations. As seen in Figure 4.2, C_2 species production is favored in the *n*-butane flame due to β -scission of 1-butyl radical (C_4H_9 -R1) radical towards ethene (C_2H_4 -D1) and ethyl radical (C_2H_5 -R1). In this model, ethene (C_2H_4 -D1) is under-predicted by 30% for the *n*-butane flame.

Figure 4.9 shows some important oxygenated species. Formaldehyde (CH_2O) was found in both flames in similar concentrations. The model can predict the mole fraction for both fuels with a deviation of 30% for *n*-butane and 50% for *iso*-butane flame. The model shows excellent agreement of the peak mole fraction ratio for all species. The profile maxima and shape are well predicted,

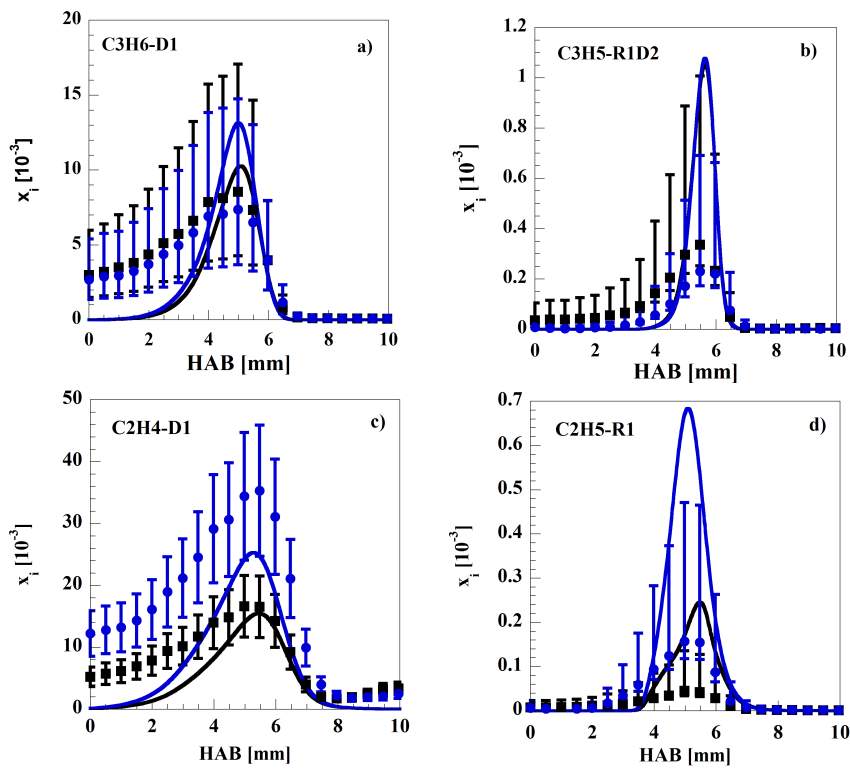


Figure 4.8: Mole fraction profiles of propene (C3H6-D1), allyl radical (C3H5-R1D2), ethyl radical (C2H5-R1), and ethene (C2H4-D1). Symbols represent experimental data: n -butane (C4H10) (\bullet) and iso-butane (C4H10-Me2) (\blacksquare) flame. Solid lines represent modeling results and the corresponding bars show the experimental error.

except for HCO, where significant differences between model and experiment are seen in the cooler regime close to the burner. Ketene (C_2H_2O -K1D1) is under-predicted by 60% for both flames. Acetaldehyde (C_2H_4O -A11) is over-predicted by 60% in both flames. All the profiles are within the experimental error.

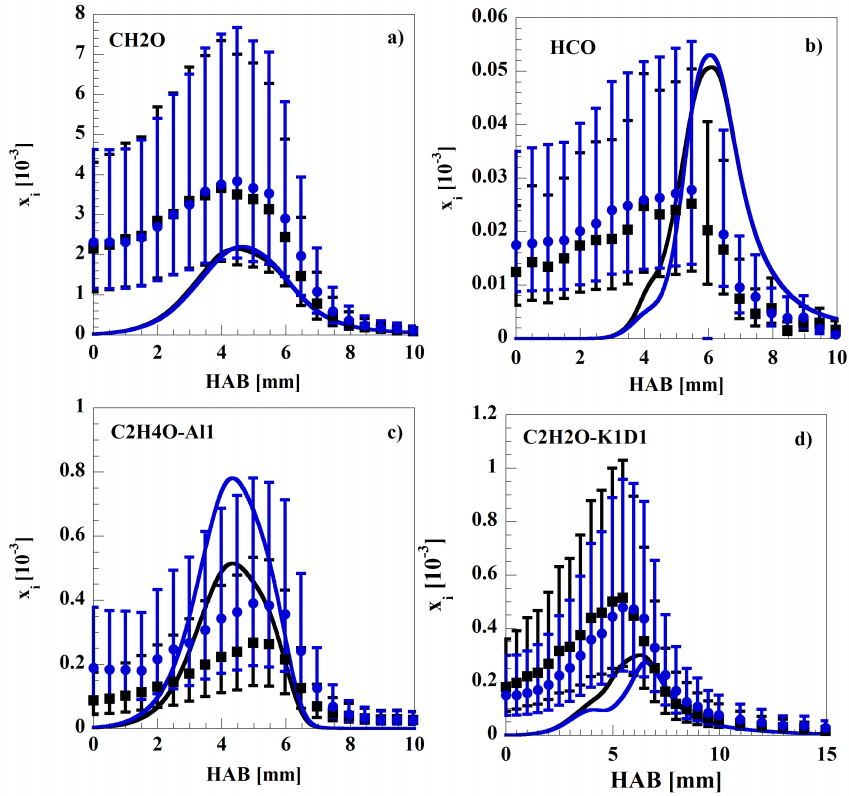


Figure 4.9: Mole fraction profiles of selected oxygenated species formaldehyde (CH_2O), HCO, acetaldehyde (C_2H_4O -A11), and ketene (C_2H_2O -K1D1). Symbols represent experimental data: *n*-butane (C_4H_{10}) (●) and *iso*-butane (C_4H_{10} -Me2) (■) flame. Solid lines represent modeling results and the corresponding bars show the experimental error.

Methyl radical (CH_3), ethane (C_2H_6 -D1) and methane (CH_4) are presented in figure 4.10. All species profiles can reproduce the shape and peak of the mole fraction. For methane, the model under-predicts the mole fraction by 30% and 40% for *n*-butane and *iso*-butane respectively. Ethane (C_2H_6) is a recombination product of methyl radical (CH_3). In this case, the prediction of the mole fraction for *iso*-butane is very good and differs from the measurement by 3%. There is a 40% over-prediction for *n*-butane. The methyl radical is over-predicted by a factor 3 in both flames. Considering that these species are

formed along minor pathways in both flames (see flow analyses 4.3 and 4.2), the prediction is reasonable.

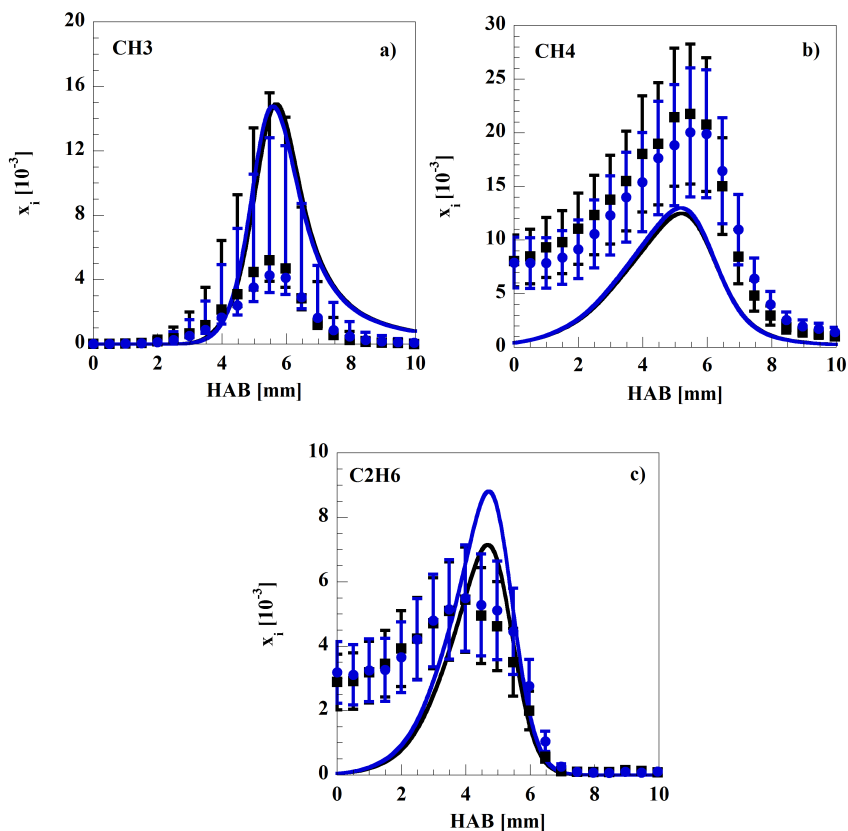


Figure 4.10: Mole fraction profiles of methyl radical (CH_3), ethane (C_2H_6) and methane (CH_4). Symbols represent experimental data: *n*-butane (C_4H_{10}) (\bullet) and *iso*-butane (C_4H_{10} -Me2) (\blacksquare) flame. Solid lines represent modeling results and the corresponding bars show the experimental error.

Figure 4.11 presents some soot precursors: propargyl (C_3H_3 -R1T2), C_3H_4 isomers, C_6H_6 isomers, and toluene (A1CH3). In the plot, C_3H_4 shows the sum of allene (C_3H_4 -D1D2) and propyne (C_3H_4 -T1). For *iso*-butane, almost only allene was detected, where the mole fraction is double in the *n*-butane flame as in the *iso*-butane flame. The shape and absolute mole fraction are in good agreement with the model. There are deviations of 20% for *n*-butane and 11% for *iso*-butane respectively. Propargyl (C_3H_3 -R1T2) is not well captured by the model. The peak is in the right position but the model over-predicts the *n*-butane mole fraction by factor 3 and the *iso*-butane flame by factor 2. Recombination of propargyl leads to formation of benzene. C_6H_6 isomers are

benzene (A1) and fulvene (FC6H6). The peak and shape of the mole fractions are in good agreement with the experimental measures but the model under-predicts the experimental results by factor 2 for *n*-butane and *iso*-butane. The methyl radical and benzene lead to toluene, where peak and shape are in good agreement with the experimental measurement. There is a deviation of 35% for *n*-butane flame and a deviation of 54% for *iso*-butane .

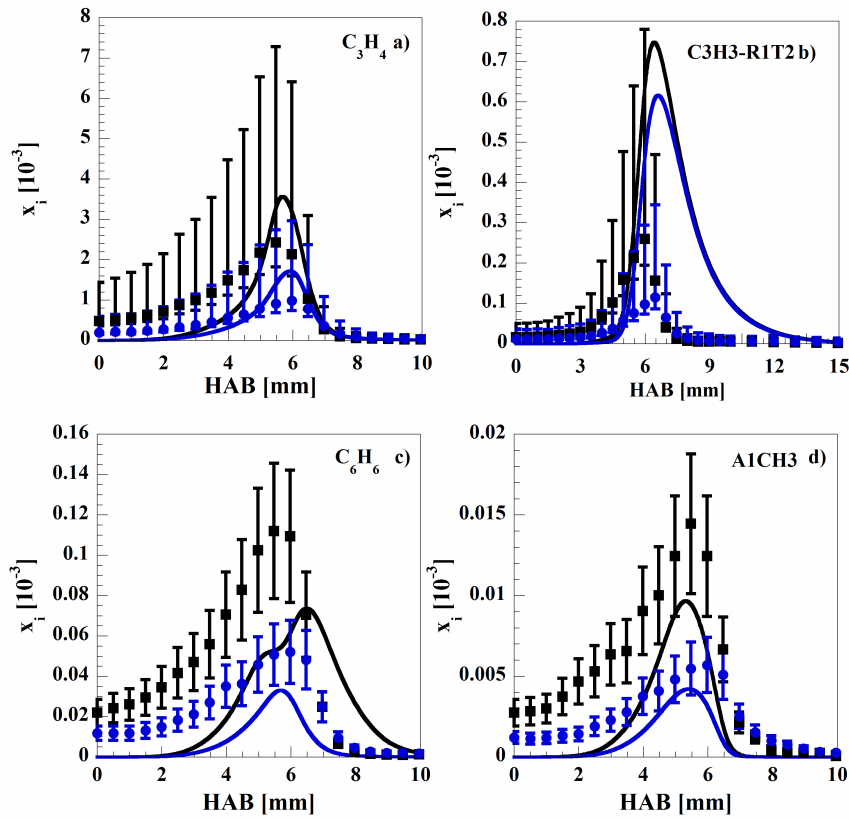


Figure 4.11: Mole fraction profiles of selected soot precursor species propargyl (C_3H_3 -R1T2), C_3H_4 isomers, C_6H_6 isomers and toluene (A1CH3). The symbols represent experimental data: *n*-butane (C_4H_{10}) (\bullet) and *iso*-butane (C_4H_{10} -Me2) (\blacksquare) flame. Solid lines represent modeling results and the corresponding bars show the experimental error.

4.4 Ignition delay time and laminar flame speed validation for *n*-butane (C₄H₁₀) and *iso*-butane (C₄H₁₀-Me₂)

The mechanism with the updated thermo chemistry has been further validated against several shock tube experiments and laminar flame speeds.

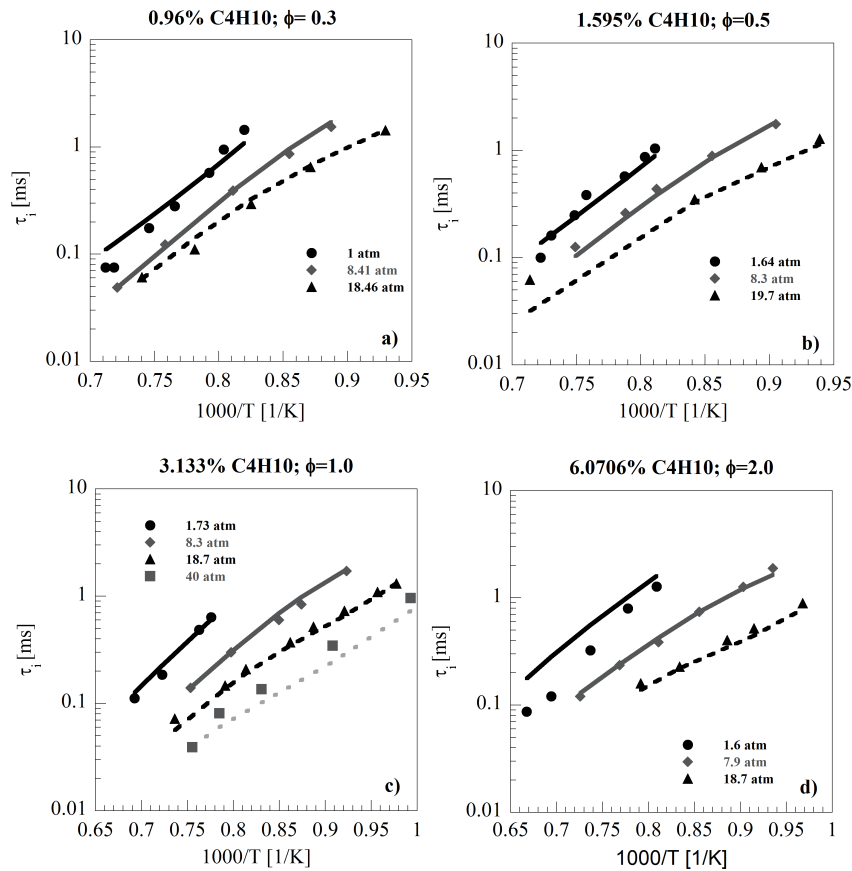


Figure 4.12: Experimental and calculated ignition delay times. Mixture compositions, temperature range, equivalence ratio, pressures and references for experiments: a) 0.96% C₄H₁₀ in Ar, 1000-1450 K, $\phi=0.3$; ●: 1 atm, ◆: 8.3 atm, and ▲: 18.4 atm. b) 1.595% C₄H₁₀ in Ar, 950-1450 K, $\phi=0.5$; ●: 1.6 atm, ◆: 8.3 atm, and ▲: 19.7 atm. c) 3.133% C₄H₁₀ in Ar, 950-1500 K, $\phi=1.0$; ●: 1.73 atm, ◆: 8.3 atm, ▲: 18.7 atm, and ■: 40 atm. d) 6.0706% C₄H₁₀ in Ar, 1000-1500 K, $\phi=2.0$; ●: 1.6 atm, ◆: 7.9 atm, and ▲: 18.7 atm. The lines are simulation results and the symbols are experiments by Healy et al. (2010) [68].

The results for *n*-butane (C4H10) are discussed in Figure 4.12. Simulations were carried out for ignition delay times for different stoichiometries ($\phi= 0.3, 0.5, 1.0,$ and 2.0) as a function of the pressure (1 to 40 *atm*) in the temperature range from 1050 to 1500 *K*. The experimental data are taken from Healy et al. (2010) [68]. Figures 4.12 a) and b) show ignition delay times for lean conditions ($\phi= 0.3$ and 0.5), where pressure dependency and trends are well predicted by the mechanism. At 1 *atm* and $\phi=0.3$ and 0.5 , slightly faster ignition delay times are predicted by the model at 1250 *K*. At higher pressure (19.7 *atm*) and $\phi=0.5$, the model predicts faster ignition delay times than experimental measurements at 1428 *K*.

For the stoichiometry condition ($\phi=1.0$), in the pressure range from 1.7 to 18.7 *atm*, slope and pressure dependency are well represented by the model. At 40 *atm* the model predicts slightly faster ignition delay times (see Figure 4.12 c). Finally, for rich mixtures ($\phi=2.0$), a very good agreement between model predictions and experiments was found in this study (see Figure 4.12 d).

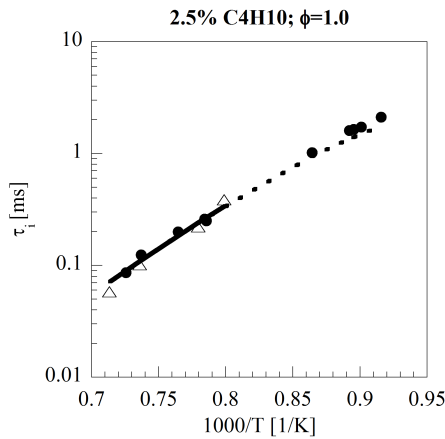


Figure 4.13: Ignition delay times of 2.5% C4H10 in Ar, $\phi=1.0$ at 10 *atm* and a temperature range from 1000 to 1400 *K*. The lines are simulation results and the symbols are experiments: \blacklozenge by Healy et al. (2010) [68] and \triangle by Burcat et al. 1971 [30].

Figure 4.13 shows the experimental measurements of *n*-butane (C4H10) in Ar, $\phi=1.0$ at 10 *atm* and a temperature range from 1200 to 1400 *K* by Burcat et al. 1971 [30]. The same conditions were tested by Healy et al. 2010 [68] and the temperature range was extended from 1000 to 1400 *K*. Both experimental measurements are in good agreement and the model has a good agreement with the experimental measurements.

Ignition delay times for *iso*-butane (C4H10-Me2) for different equivalence ratios ($\phi= 0.3, 0.5, 1.0,$ and 2.0) as a function of the pressure (1-40 *atm*) in a temperature range from 950 to 1600 *K* were measured by Healy et al. 2010 [70]. The simulation results for these conditions are shown in Figure 4.14 for lean condi-

tions ($\phi=0.3$ and 0.5 , see Figure 4.14 a) and b)). The model captures very well the trend and the pressure dependency; nevertheless, all the predicted ignition delay times are slightly faster than the experimental measurements. Figures 4.14 c) and d) show the results for stoichiometric ($\phi=1.0$) and rich conditions ($\phi=2.0$) respectively. Slope and pressure dependency are well represented by the model. At high pressure (35.83 atm), the predicted ignition is faster than the experimental measurements.

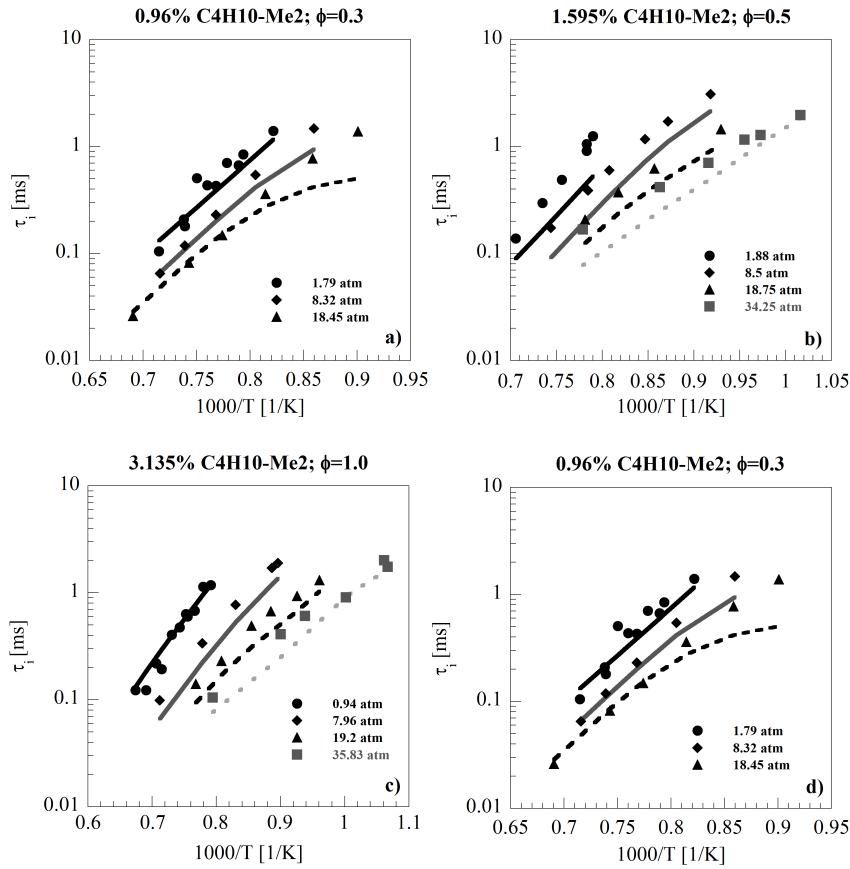


Figure 4.14: Experimental and calculated ignition delay times. Mixture compositions, temperature range, equivalence ratio, pressures and references for experiments: a) 0.96% C₄H₁₀-Me₂ in Ar, 1100-1500 K, $\phi=0.3$; ●: 1.79 atm, ◆: 8.32 atm, and ▲: 18.45 atm. b) 1.595% C₄H₁₀-Me₂ in Ar, 1000-1500 K, $\phi=0.5$; ●: 1.88 atm, ◆: 8.75 atm, ▲: 18.75 atm, and ■: 34.25 atm. c) 3.135% C₄H₁₀-Me₂ in Ar, 950-1500 K, $\phi=1.0$; ●: 0.94 atm, ◆: 7.96 atm, ▲: 19.2 atm, and ■: 35.83 atm. d) 6.08% C₄H₁₀-Me₂ in Ar, 1000-1600 K, $\phi=2.0$; ●: 1.58 atm, ◆: 7.81 atm, and ▲: 17.62 atm. The lines are simulation results and the symbols are experiments: by Healy et al. 2010 [70].

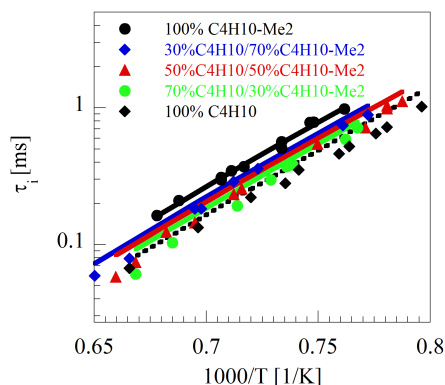


Figure 4.15: Ignition delay times of *n*-butane, *iso*-butane and its mixtures in Ar, $\phi=0.72$ at 2 bar and a temperature range from 1250 to 1500 K. The lines are simulation results and the symbols are experiments: by Ogura et al. 2007 [71]; \bullet : 100% C_4H_{10} -Me2 in Ar, \blacklozenge : 30% C_4H_{10} /70% C_4H_{10} -Me2 in Ar, \blacktriangle : 50% C_4H_{10} /50% C_4H_{10} -Me2 in Ar, \bullet : 50% C_4H_{10} /50% C_4H_{10} -Me2 in Ar, and \blacklozenge : 100% C_4H_{10} in Ar.

Figure 4.15 shows pure *n*-butane, *iso*-butane and its mixtures in Ar at a lean equivalence ratio $\phi = 0.72$, 2 bar and a temperature range from 1250 to 1500 K. The mechanism can predict well the transition from pure *n*-butane to *iso*-butane. It has been experimentally proven that ignition delay times for *iso*-butane are longer than for *n*-butane ([68], [70], [71]). This model can reproduce the same behavior. *n*-butane model predictions are slightly slower than experimental measurements.

Premixed laminar flame speed simulations using the updated model for the *n*-butane/air mixture at $T_u = 298$ K and $p = 1$ atm were performed and compared to experiments from Davis et al. 1998 [42], Hirasawa et al. 2002 [90], Dirrenberg et al. 2011 [49], Bosschart et al. 2004 [44], Tang et al. 2011 [58], and Wu et al. 2014 [59] (300 K). A good agreement with respect to the experimental points is observed (see Figure 4.16 a)). For very rich mixtures, the predicted laminar flame speed follows the measurements of Dirrenberg et al. 2011 [49].

Figure 4.16 b) shows premixed laminar flame speed simulations for a *n*-butane/air mixture at $p = 1$ atm and $T_u = 343$ K and 403 K. The model was compared to experiments from Veloo et al. 2010 [60] (343 K) and Wang et al. 2011 [61] (403 K), respectively. The simulation results follow experimental measurements after $\phi = 1.2$. In the lean side of the flame, the model is faster than the experimental measurements.

A calculated *iso*-butane / air mixture at $p = 1$ and $T_u = 298$ K and experimental profiles are presented in figure 4.17. Experiments from Davis et al. 1998 [42] and Bosschart et al. 2004 [44] were used for comparison purposes. In general, the laminar flame speeds predicted by the model are in the upper limit for the lean side. After an equivalence ratio of 1.2, the velocity decreases compared to the experimental measurements.

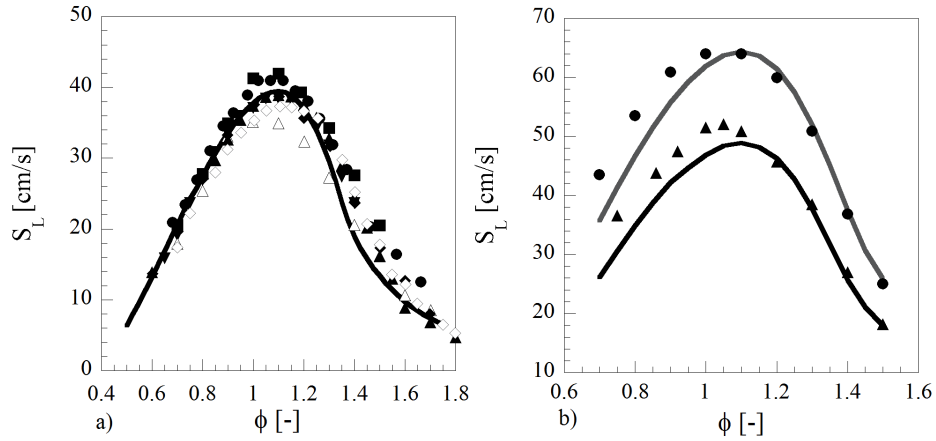


Figure 4.16: a) Numerically determined laminar flame speeds as a function of the equivalence ratio for n-butane/air mixture at $T_u = 298$ K and $p = 1$ atm. The black lines are simulation results in this study. Experiments by: ● Davis et al. 1998 [42], ■ Hirasawa et al. 2002 [90], ▲ Dirrenberg et al. 2011 [49], ▼ Bosschart et al. 2004 [44], ◆, ◇ Tang et al. 2011 [58], and △ Wu et al. 2014 [59] (300 K). b) Numerically determined laminar flame speeds as a function of the equivalence ratio for n-butane/air mixture at $p = 1$ atm and $T_u = 343$ K and 403 K. The lines show simulation results in this study. Experiments by: ▲ Veloo et al. 2010 [60] (343 K) and ● Wang et al. 2011 [61] (403 K).

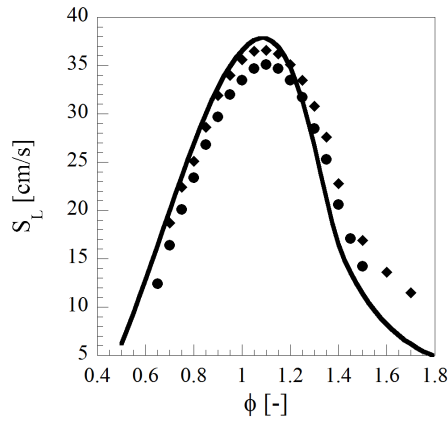


Figure 4.17: Numerically determined laminar flame speeds as a function of the equivalence ratio for iso-butane/air mixture at $T_u = 298$ K and $p = 1$ atm. Black lines are simulation results in this study. Experiments by: ◆ Davis et al. 1998 [42] and ● Bosschart et al. 2004 [44].

Chapter 5

Combustion chemistry of the butene isomers

In this chapter, thermodynamic data from chapter 3 and 4 are used to recalculate the data from Schenk et al. (2013) [8] and the influence of the updated chemistry for butene (C_4H_8) isomers on burner stabilized flames, ignition delay times and laminar flame speed will be discussed. Allyl abstraction was included in the mechanism and rates were taken in analogy to those presented in the work of Nawdiyal 2018 [10].

Butenes are alkenes that have four carbon atoms with the formula C_4H_8 and a double bond in their molecules. There are four structural isomers shown in fig. 5.1. But-1-ene (C_4H_8 -D1) is an unbranched structure, *iso*-butene (C_4H_8 -D1Me2) is a branched structure, (*Z*)-but-2-ene (T - C_4H_8 -D2) and (*E*)-but-2-ene (C - C_4H_8 -D2) are the simplest alkene molecules that show *cis/trans*-isomerism [1].

Physical and chemical properties of both isomers are presented in table 5.1. Molecular weight and low heating value are similar for all the isomers. The boiling points of *trans/cis* isomers are very close, and for that reason, it is difficult to separate them by distillation in two products. *cis*-butene has the higher RON number followed by *n*-butene and finally by *iso*-butene.

Fuel	MW (g/mol)	LHV (KJ/g)	Bp (C)	T_a (K)	RON	MON
<i>n</i> - C_4H_8	56.11	45.319	-6.47	2204	99	80.8
<i>iso</i> - C_4H_8	56.11	45.319	-6.9	1972	88	87
<i>trans</i> - C_4H_8	56.11	45.319	0.9	2328	-	83
<i>cis</i> - C_4H_8	56.11	45.319	3.7	2332	100	-

Table 5.1: Physical and chemical properties of but-1-ene (C_4H_8 -D1), *iso*-butene (C_4H_8 -D1Me2), (*Z*)-but-2-ene (T - C_4H_8 -D2), and (*E*)-but-2-ene (C - C_4H_8 -D2) [1].

Industrial uses of butene isomers cover

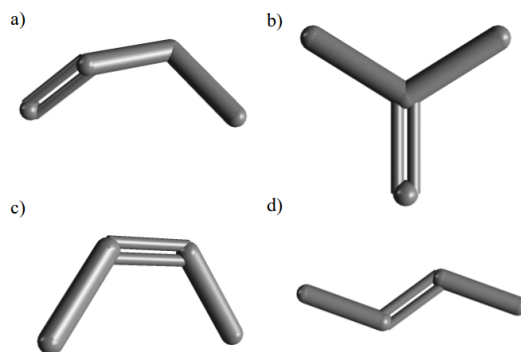


Figure 5.1: 3D model of butene molecules: *but-1-ene* (C_4H_8-D1) [91], *iso-butene* ($C_4H_8-D1Me_2$) [92], *(Z)-but-2-ene* ($T-C_4H_8-D2$) [93], and *(E)-but-2-ene* ($C-C_4H_8-D2$) [94]

- *Iso-butene*: fuels and fuel additives, intermediates, lubricants and lubricant additives, solvents [92],
- *n-butene*: adhesives and sealant chemicals, fuels and fuel additives, intermediates, plasticizers and process regulators [91],
- *trans-2-butene*: fuels, fuel additives, and intermediates [94] and
- *cis-2-butene*: fuels, fuel additives and intermediates [93].

Methods of production are mainly recovery from C_4 stream in petroleum refining. Gas mixtures containing considerable *iso-butene* are obtained by fractionation of refinery gases resulting from cracking petroleum [92]. Gases with an appreciable content of *1-butene* along with other butene and butane hydrocarbons are obtained by fractional distillation of refinery gas and can also be produced directly from ethylene [91]. $T-C_4H_8-D2$ (*trans*) is obtained by extractive distillation of the butane/butylene fraction produced by cracking crude oil [94]. $C-C_4H_8-D2$ (*cis*) gases containing appreciable concentrations of *cis-butene-2*, along with other butene and butane hydrocarbons, are obtained by fractional distillation of refinery gas [93].

In the last years, several experimental measurements have been conducted to understand the oxidation process of the butene isomers as fuel. Dias and Vandoren 2010 [95] studied a lean *iso-butene*/oxygen/argon flame of equivalence ratio $\phi=0.225$ at low pressure (40 *mbar*). Schenk et al. 2013 [8] presented measurements of the three butene isomers (*1-butene*, *trans-2-butene* and *iso-butene*) under fuel-rich ($\phi = 1.7$) conditions and low-pressure (40 *mbar*). Experimental data shows different destruction pathways for the butene isomers

and the different combustion behavior of the isomeric flames.

Curran et al. 1992 [96], Bauge et al. 1998 [97], and Yasunaga et al. 2009 [98] measured ignition delay times for *iso*-butene in a range of temperatures from 1000 to 1900 K, of pressure from 2 to 10.5 bar and equivalence ratios from 0.4 to 3.0. Heyberger et al. 2002 [99] and Pan et al. 2015 [100] measured ignition delay time for *n*-butene in a range of temperatures from 1000 to 1950 K, pressures from 1.2 to 16 bar and equivalence ratios from 0.5 to 2.0.

Dagaut and Cathonnet 1998 [101], Bauge et al. 1998 [97] studied the oxidation of *iso*-butene in a jet-stirred reactor at high temperature and pressures from 1 to 10 atm, and the equivalence ratio was varied from 0.15 to 6. Fenard et al. 2015 [102] studied the oxidation of *trans*-2-butene in a jet-stirred reactor from 900 to 1450 K at atmospheric pressure, over a range of equivalence ratios from 0.5 to 2.0.

Laminar burning velocities were measured by Davis and Law 1998 [42] for 1-butene and *iso*-butene at 298 K, ambient pressure, and equivalence ratios from 0.6 to 1.7; by Zhao et al. 2014 [103] for 1-butene, *iso*-butene and *trans*-2-butene at 298 K, normal and elevated pressures (1, 2, 5 and 10 bar), and equivalence ratios from 0.7 to 1.8, and by Fenard et al. 2015 [102] for *trans*-2-butene at 300 K, ambient pressure and equivalence ratios from 0.7 to 1.4.

5.1 High-temperature chemistry of C₄H₈ isomers

In this section, updates in the reaction rates that have been implemented for the high-temperature sub-mechanisms of but-1-ene (C4H8-D1), *iso*-butene (C4H8-D1Me2), and (Z)-but-2-ene (T-C4H8-D2) fuel molecules published in Schenk et al. 2013 [8] will be discussed in detail. Rate constants are expressed in the Arrhenius equation form (see eq. 2.19) $k = AT^b \cdot \exp\left(\frac{-E_a}{RT}\right)$ with the units cm^3 , *mol*, *s*, *cal*. -> indicates that only forward reaction is considered; <=> indicates that also the reverse reaction is considered and the data to calculate the pressure dependency (see table 2.1).

5.1.1 Class 1: Unimolecular fuel decomposition

Fuel consumption at high temperatures is initiated by C–C and C–H bond cleavage as discussed in Curran et al. 1998 [104] and Ahmed et al. 2007 [81]). Reaction rates for but-1-ene (C4H8-D1), (Z)-but-2-ene (T-C4H8-D2) and *iso*-butene (C4H8-D1Me2) are presented in table 5.2.

The rate corresponding to C–C bond breaking reaction

$C3H5-R1D2 + CH3 (+ M) <=> C4H8-D1 (+ M)$ was updated following the suggestion of Wang et al. [105] and the rate corresponding to reaction

$C4H8-D1 <=> C2H3-R1D1 + C2H5-R1$ followed the suggestion from Chakir et al. [106]. Furthermore, the reaction rates from Chakir et al. [106] were followed for (Z)-but-2-ene (T-C4H8-D2). Finally, the reaction rates from Yasunaga et al. [98] were followed for *iso*-butene (C4H8-D1Me2).

Reactions	A	n	Ea	Ref
C3H5-R1D2 + CH3 (+ M) <=> C4H8-D1 (+ M)	1.100E+14	-0.32	-2.620E+02	[105]
LOW /	3.910E+60	-12.81	6.250E+03	
TROE / 0.104 1.606E+03 6.00E+04 6.118E+03				
C4H8-D1 <=> C2H3-R1D1 + C2H5-R1	2.000E+18	-1.00	9.678E+04	[106]
C4H8-D1 <=> H + C4H7-R1D3	4.110E+18	-1.00	9.738E+07	[106]
C4H8-D1 <=> H + C4H7-R3D1	1.260E+15	0.00	8.250E+04	[76]
T-C4H8-D2 <=> H + C4H7-R3D1	4.110E+18	-1.00	9.738E+04	[106]
T-C4H8-D2 <=> CH3 + C3H5-R1D2	6.500E+13	0.00	7.125E+04	[106]
C4H8-D1Me2 <=> C3H5-R2D1 + CH3	3.300E+21	-1.2	9.772E+04	[98]
C4H8-D1Me2 <=> C4H7-R1D2Me2 + H	1.500E+15	0.00	8.340E+04	[98]

Table 5.2: Unimolecular fuel decomposition reaction rates for but-1-ene (C4H8-D1), (Z)-but-2-ene (T-C4H8-D2) and iso-butene (C4H8-D1Me2).

5.1.2 Class 2: H-atom abstraction from fuel

H-atom abstraction from the fuel molecules can take place at primary, secondary, tertiary and allyl sites forming alkenyl radicals. Vinylic site abstractions are not considered in the development of this model. Tables 5.3 and 5.4 show the reaction rates corresponding to but-1-ene (C4H8-D1) and (Z)-but-2-ene (T-C4H8-D2) respectively, where rates from Chakir et al. [106] have been applied. Nine radicals, H, OH, O, CH3, HO2, CH3O, O2, C2H5-R1, and C4H7-R3D1 are considered, and reactions are expressed in equilibrium.

For linear fuels, the formation of two different radicals, namely But-3-en-1-yl radical (C4H7-R1D3) and But-3-en-2-yl (C4H7-R3D1) have been considered. These radicals were introduced in the work of Schenk et al. 2013 [8], where no differences between the allyl, primary or secondary H-atom abstraction reaction rates were applied in the model. In this work, a correction to the original reaction rates for the allylic position (formation of But-3-en-2-yl radical (C4H7-R3D1)) was implemented following the recommendation from Mehl et al. 2008 [107] and further Nawdiyal 2018 [10]. The original activation energy was decreased by 2000 cal compared to the activation energy of the primary C-H atom abstraction for all considered radicals and no correction for the pre-exponential factor was needed.

Reaction rates corresponding to iso-butene (C4H8-D1Me2) are presented in table 5.5. Twelve radicals were considered: H, OH, O, CH3, HO2, O2, C3H5-R1D2, C3H5-R2D1, CH3O, CH3O2, and C2H3-R1D1. Reactions are expressed in equilibrium. Updates using newer data available in the literature were done as follows. For the OH radical, the work of Sun and Law 2010 [110] was implemented. The methyl radical (CH3) rate was taken from the work of Yasunaga et al. 2009 [98]. The HO2 radical was updated using the rate from Zador et al. 2011 [111]. The O2 radical was updated using the rate from Chen and Bozzeli 2000 [112]. The C2H3-R1D1 radical reaction rate was updated using the coefficients from Goldsmith et al. 2009 [109].

	A	n	Ea	Ref
H + C4H8-D1 <=> C4H7-R1D3 + H2	5.000E+13	0.00	3.893E+03	[106]
H + C4H8-D1 <=> C4H7-R3D1 + H2	5.000E+13	0.00	1.893E+03	^a
O + C4H8-D1 <=> OH + C4H7-R1D3	1.300E+13	0.00	4.490E+03	[106]
O + C4H8-D1 <=> OH + C4H7-R3D1	1.300E+13	0.00	2.490E+03	^a
OH + C4H8-D1 <=> C4H7-R1D3 + H2O	1.750E+13	0.00	6.950E+03	[106]
OH + C4H8-D1 <=> C4H7-R3D1 + H2O	1.750E+13	0.00	4.950E+03	^a
CH3 + C4H8-D1 <=> CH4 + C4H7-R1D3	1.00E+11	0.00	7.309E+03	[106]
CH3 + C4H8-D1 <=> CH4 + C4H7-R3D1	1.00E+11	0.00	5.309E+03	^a
C4H8-D1 + O2 <=> HO2 + C4H7-R1D3	4.000E+12	0.00	3.998E+04	[106]
C4H8-D1 + O2 <=> HO2 + C4H7-R3D1	4.000E+12	0.00	3.798E+04	^a
HO2 + C4H8-D1 <=> H2O2 + C4H7-R1D3	1.000E+11	0.00	1.705E+04	[106]
HO2 + C4H8-D1 <=> H2O2 + C4H7-R3D1	1.000E+11	0.00	1.505E+04	^a
C2H5-R1 + C4H8-D1 <=> C2H6 + C4H7-R1D3	1.000E+11	0.00	8.001E+03	[106]
C2H5-R1 + C4H8-D1 <=> C2H6 + C4H7-R3D1	1.000E+11	0.00	6.001E+03	^a
C3H5-R1D2 + C4H8-D1 <=> C3H6-D1 + C4H7-R1D3	8.000E+10	0.00	1.240E+04	[106]
C3H5-R1D2 + C4H8-D1 <=> C3H6-D1 + C4H7-R3D1	8.000E+10	0.00	1.040E+04	^a
C4H7-R3D1 + C4H8-D1 <=> C4H7-R1D3 + T-C4H8-D2	3.980E+10	0.00	1.240E+04	[106]
C4H7-R3D1 + C4H8-D1 <=> C4H7-R1D3 + C-C4H8-D2	3.980E+10	0.00	1.240E+04	[106]

Table 5.3: *H*-atom abstraction reaction rates for but-1-ene (C4H8-D1). ^a: Activation energy decreased by 2000 cal from its original value following Naudiyal 2018 [10].

	A	n	Ea	Ref
H + T-C4H8-D2 <=> C4H7-R3D1 + H2	7.000E+12	0.00	1.487E+03	^a
OH + T-C4H8-D2 <=> C4H7-R3D1 + H2O	6.021E+01	3.19	1.516E+03	[108]
CH3 + T-C4H8-D2 <=> C4H7-R3D1 + CH4	1.000E+11	0.00	6.192E+03	^a
O + T-C4H8-D2 <=> C4H7-R3D1 + OH	1.300E+13	0.00	2.490E+03	^a
O2 + T-C4H8-D2 <=> C4H7-R3D1 + HO2	4.000E+12	0.00	3.798E+04	^a
HO2 + T-C4H8-D2 <=> C4H7-R3D1 + H2O2	1.000E+11	0.00	1.505E+04	^a
C2H3-R1D1 + T-C4H8-D2 <=> C4H7-R3D1 + C2H4-D1	3.880E+03	2.80	5.400E+03	[109]
C2H5-R1 + T-C4H8-D2 <=> C4H7-R3D1 + C2H6	1.000E+11	0.00	6.001E+03	^a

Table 5.4: *H*-atom abstraction reaction rates for (*Z*)-but-2-ene (T-C4H8-D2). ^a: Activation energy decreased by 2000 cal from its original value following Naudiyal 2018 [10].

	A	n	Ea	Ref
C4H8-D1Me2 + H <=> C4H7-R1D2Me2 + H2	1.724E+14	0.00	8.000E+03	[85]
C4H8-D1Me2 + O <=> C4H7-R1D2Me2 + OH	1.75E+11	0.70	5.882E+03	[85]
C4H8-D1Me2 + OH <=> C4H7-R1D2Me2 + H2O	3.860E+01	3.59	-1.071E+03	[110]
C4H8-D1Me2 + CH3 <=> C4H7-R1D2Me2 + CH4	1.510E+12	0.00	1.000E+04	[98]
C4H8-D1Me2 + HO2 <=> C4H7-R1D2Me2 + H2O2	0.292E+00	4.12	1.280E+04	[111]
C4H8-D1Me2 + O2 <=> C4H7-R1D2Me2 + HO2	9.300E+08	1.301	4.094E+04	[112]
C4H8-D1Me2 + C3H5-R1D2 <=> C4H7-R1D2Me2 + C3H6-D1	7.940E+11	0.00	2.050E+04	[77]
C4H8-D1Me2 + C3H5-R2D1 <=> C4H7-R1D2Me2 + C3H6-D1	7.940E+11	0.00	2.050E+04	[77]
C4H8-D1Me2 + CH3O <=> C4H7-R1D2Me2 + CH3OH	8.990E+01	2.95	1.198E+04	[85]
C4H8-D1Me2 + CH3O2 <=> C4H7-R1D2Me2 + CH3O2H	1.990E+12	0.00	1.710E+04	[85]
C4H8-D1Me2 + C2H3-R1D1 <=> C4H7-R1D2Me2 + C2H4-D1	7.230E+11	0.00	4.3720E+03	[109]

Table 5.5: *H*-atom abstraction reaction rates for iso-butene (C4H8-D1Me2).

5.1.3 Class 3: Alkenyl radical decomposition

Table 5.6 shows the reaction rates corresponding to the alkenyl radical decomposition, where a diene and a H-atom or two small molecules are formed. For But-3-en-1-yl radical (C4H7-R1D3) and But-3-en-2-yl radical (C4H7-R3D1), the original rates from Chakir et al. 1989 [106] were kept in the model. In the case of the 2-Methylallyl radical (C4H7-R1D2Me2), the rate coefficient for the reaction $C4H7-R1D2Me2 \rightleftharpoons C3H4-D1D2 + CH3$ was updated using the suggestion of Zheng et al. 2005 [113].

	A	n	Ea	Ref
C4H7-R1D3 \rightleftharpoons H + C4H6-D1D3	1.200E+14	0.00	4.930E+04	[106]
C4H7-R1D3 \rightleftharpoons C2H3-R1D1 + C2H4-D1	1.000E+11	0.00	3.700E+04	[106]
C4H7-R3D1 \rightleftharpoons H + C4H6-D1D3	1.200E+14	0.00	4.930E+04	[106]
C4H7-R1D3 \rightleftharpoons C3H4-D1D2 + CH3	1.000E+11	0.00	3.700E+04	[106]
C4H7-R1D2Me2 \rightleftharpoons C3H4-D1D2 + CH3	7.100E+10	1.38	5.636E+04	[113]

Table 5.6: Alkenyl radical decomposition reaction rates for but-1-ene (C4H8-D1), (Z)-but-2-ene (T-C4H8-D2) and iso-butene (C4H8-D1Me2).

5.1.4 Class 4: Alkenyl radical + O2 direct formation of di-olefin and HO2

In this class, the alkyl radical reacts via O2 and H, giving a conjugated alkane [81]. Reaction rates are presented in table 5.7. Original rates for But-3-en-1-yl radical (C4H7-R1D3) and But-3-en-2-yl (C4H7-R3D1) were taken from Chakir et al. 1989 [106]. The rate coefficient for 2-Methylallyl radical (C4H7-R1D2Me2) was updated using the rate proposed by Curran et al. 2002 [77].

	A	n	Ea	Ref
C4H7-R1D3 + O2 \rightleftharpoons HO2 + C4H6-D1D3	1.000E+11	0.00	0.000E+00	[106]
C4H7-R3D1 + O2 \rightleftharpoons HO2 + C4H6-D1D3	1.000E+11	0.00	0.000E+00	[106]
H + C4H7-R1D3 \rightleftharpoons C4H6-D1D3 + H2	3.160E+13	0.00	0.000E+00	[106]
H + C4H7-R3D1 \rightleftharpoons C4H6-D1D3 + H2	3.160E+13	0.00	0.000E+00	[106]

Table 5.7: Reaction rates for direct formation of olefin.

5.1.5 Class 5: Alkene isomerization

The alkenyl radical can transfer any H-atoms to the radical site [81]. This reaction occurs through the formation of a cyclic transition state which usually includes four to eight atoms of carbons. The reaction rate depends on the type of bond that needs to be broken, and the distance formed from the ring. Table 5.8 shows rates for but-1-ene (C4H8-D1), (Z)-but-2-ene (T-C4H8-D2) and iso-butene (C4H8-D1Me2) that were taken from the work of Chakir et al [106]. Beside these changes, newly calculated reaction rates from Li et al. [114], [115] for H-atom addition to the *trans*-2-butene and addition to 1-butene respectively (R522: T-C4H8-D2 + H \rightleftharpoons C3H6-D1 + CH3 and R509: C4H8-D1 + H \rightleftharpoons C3H6-D1 + CH3) were implemented in the model.

	A	n	Ea	Ref
C4H8-D1 \rightleftharpoons T-C4H8-D2	4.000E+11	0.00	5.995E+04	[106]
C4H8-D1 \rightleftharpoons C-C4H8-D2	4.000E+11	0.00	5.995E+04	[106]
C-C4H8-D2 \rightleftharpoons T-C4H8-D2	1.000E+13	0.00	6.196E+04	[106]

Table 5.8: Alkene isomerization reaction rates.

The mechanism used for simulations in the present study consists of 277 species and 1387 irreversible reactions. The mechanism file, thermodynamic file, and transport-data file are available in the Supplementary Material.

5.2 Experiments

In this work, the chemistry of the butene isomers was validated considering the experimental work detailed next. Measurements of the three butene isomers (*1*-butene, *trans-2*-butene and *i*-butene) under fuel-rich ($\phi = 1.7$) conditions and low-pressure (40 *mbar*) by Schenk et al. 2013 [8]. Shock tubes measurements for *iso*-butene done by Curran et al. 1992 [96], Bauge et al. 1998 [97], and Yasunaga et al. 2009 [98] in temperatures ranging from 1000 *K* to 1900 *K*, pressures from 2 to 10.5 *bar* and equivalence ratios from 0.4 to 3.0. Shock tubes measurements for *1*-butene done by Heyberger et al. 2002 [99] and Pan et al. 2015 [100], and Li et al. [115] in temperatures ranging from 1000 to 1950 *K*, pressures from 1.2 to 50 *bar* and equivalence ratios from 0.5 to 2.0. Shock tubes measurements for *2*-butene from Li et al. [114] in temperatures ranging from 1000 to 1900 *K*, pressures from 10 to 50 *bar* and equivalence ratios from 0.5 to 2.0. Finally, laminar burning velocities were measured by Davis and Law 1998 [42] for *1*-butene and *iso*-butene at 298 *K*, ambient pressure, and equivalence ratios from 0.6 to 1.7, Zhao et al. 2014 [103] for *1*-butene, *iso*-butene and *trans-2*-butene at 298 *K*, normal and elevated pressures (1, 2, 5 and 10 *bar*), and equivalence ratios from 0.7 to 1.8, and Fenard et al. 2015 [116] for *trans-2*-butene at 300 *K*, ambient pressure and equivalence ratios from 0.7 to 1.4.

5.3 Burner-stabilized flame validation of C₄H₈ isomers: *1*-butene (C4H8-D1), *trans-2*-butene (T-C4H8-D2), and *iso*-butene (C4H8-D1Me2).

In this section, burner-stabilized flame experiments of *1*-butene, *trans-2*-butene, and *iso*-butene with a composition of butene/oxygen/argon (16.5 mol%/58.5 mol%/25.0 mol%) ($\phi=1.7$) at 40.0 *mbar* and 300 *K* performed by Schenk et al. [8] were used to extend and validate the C₄ subset of the chemical model.

Flow analysis for butene fuels are presented in Figs. 5.2, 5.3, and 5.4. Normally, the destruction pathways of fuel molecules is characterized by C-C bond cleavage or abstraction of H-atom by small radicals (H, O, OH, etc.) from the hydrocarbon backbone [8]. The flow analysis visualizes the flow of carbon

atoms. Percentage numbers presented in the figures are the number of C-atoms consumed by the respective reaction from the reactant molecule to the product molecule(s). The flux is normalized with the total flux of carbon atoms consumed by reactions with the reactant molecule. The figures filtered out minor reaction pathways, and the numbers do not total 100% [8].

Decomposition of *1*-butene (C4H8-D1) (see Fig. 5.2) is initiated by H-atom abstraction from the fuel molecule in allyl position and H-atom abstraction in primary position forming 21% of but-*3-en-2-yl* (C4H7-R3D1) and 16.5% of but-*3-en-1-yl* (C4H7-R1D3) radicals, respectively. These radicals decompose to form 1,3-butadiene (C4H6-D1D3). Butadiene contributes to C₄ backbone via a subsequent dehydrogenation chain. The second most important destruction channel is the formation of 38.1 % of propene (C3H6-D1) and 10.04% of methyl (CH3) (R509: C4H8-D1 + H \rightleftharpoons C3H6-D1 + CH3), contributing to the C₃ destruction pathway. Final oxidation is achieved through C₂ and C₁ reaction sequences. Ethene (C2H4-D1) marks the start of the C₂ route. It reacts via the vinyl radical (C2H2) and the ketyl radical (HCCO). Finally, the C₁ chain begins with methyl (CH3), which reacts to form 23.2% of formaldehyde (CH2O). Formaldehyde contributes mainly to formyl radical (HCO) towards CO and CO₂. There are a lot of connections between the C₁ and C₂ paths, and both routes are fed from different species of the C₄ and the C₃ destruction channels.

Figure 5.3 shows the *trans-2*-butene (T-C4H8-D2) flow analysis. The H-induced breakdown towards propene is the dominating consumption pathway for this fuel (R522: T-C4H8-D2 + H \rightleftharpoons C3H6-D1 + CH3) forming 60.7% of propene. The second destruction pathway is H-atom abstraction of the fuel molecule to form 15.2% of but-*3-en-2-yl* (C4H7-R3D1), which via H-atom abstraction forms 63.7 % of 1,3-butadiene (C4H6-D1D3) contributing to the C₄ destruction route. The final oxidation follows the same reaction channels for C₁ and C₂ decomposition as in the *1*-butene (C4H8-D1) flame. The C₄ destruction pathway seems of minor importance for this fuel compared to the *1*-butene flame.

Flow analysis corresponding to *iso*-butene (C4H8-D1Me2) is presented in Figure 5.4. Compared to the other two butene isomers, *iso*-butene has a branched structure which influences the decompositions pathways. The main reaction pathway is the H-atom abstraction from the methyl group forming 43.8% of 2-methyl allyl radical (C4H7-R1D2Me2). 2-methyl allyl radical via C-C scission forms 66.1% of allene (C3H4-D1D2). A second decomposition pathway is the H-atom addition to the fuel forming 24% of *iso*-butyl radical (C4H9-R1Me2). *iso*-Butyl radical decomposition will contribute with 74.45% of propene (C3H6-D1) formation, which will further contribute to the C₃ species pool. The direct formation of propene from *iso*-butene is not implemented as a single-step reaction (see tables 5.2-5.8). A third reaction pathway is the C-C bond breaking forming 9.14% of C3H5-R2D1 and 3.9% of methyl radical. C3H5-R2D1 further dehydrogenation opens a pathway to propyne (C3H4-T1).

Due to the fuel structure, it is not possible to achieve a sequential dehydrogenation to form 1,3-butadiene and the related C₄ products. In this flame, C₄ hydrocarbons must be formed from growth products [8]. Looking at the flow,

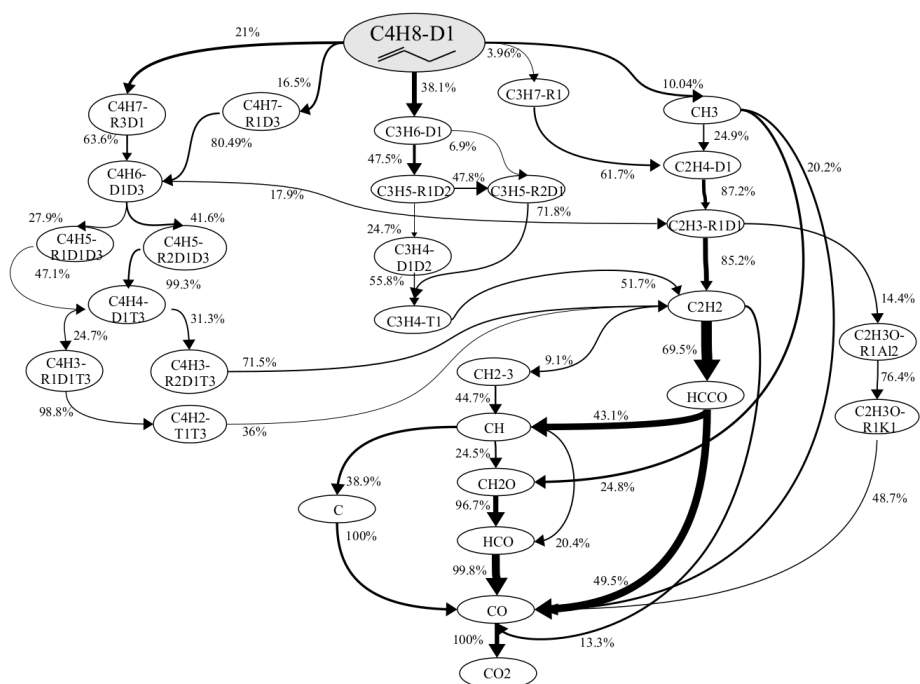


Figure 5.2: Integrated flow analysis of 1-butene ($C_4H_8-D_1$) consumption. The thickness of the arrows indicates the contribution of the respective pathway to the total flux of C-atoms (contributions of the destruction of the individual molecule are indicated by percentages next to the arrows) [8].

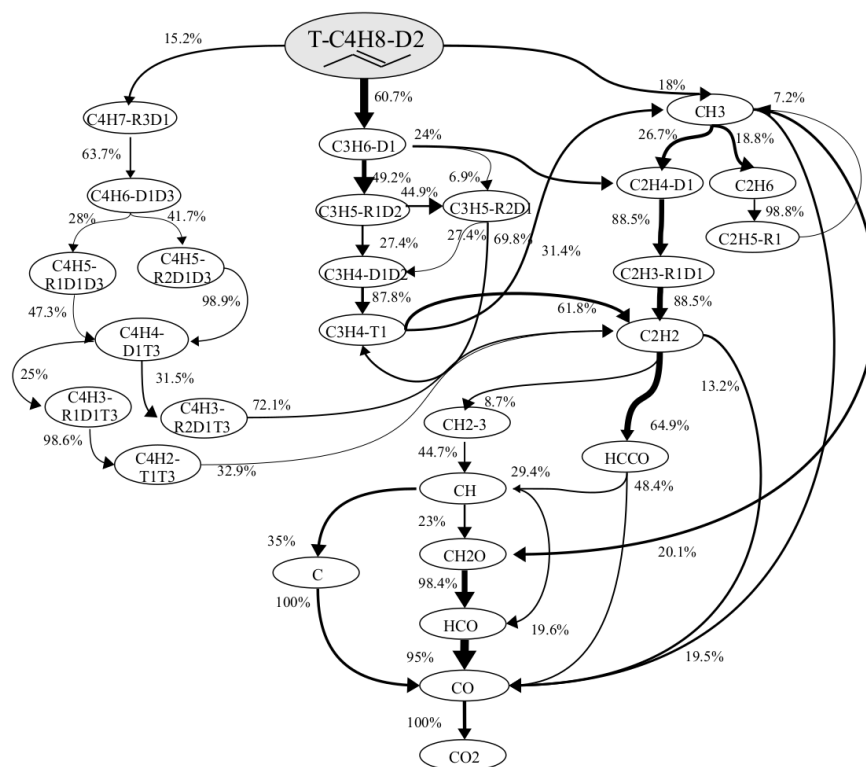


Figure 5.3: *Integrated flow analysis of trans-2-butene ($T-C_4H_8-D_2$) consumption. The thickness of the arrows indicates the contribution of the respective pathway to the total flux of C-atoms (contributions of the destruction of the individual molecule are indicated by percentages next to the arrows) [8].*

2-methyl-1-butene ($C_5H_{10}\text{-D1Me}_2$) is formed from 2-methyl allyl radical with methyl recombination. 2-methyl-1-butene opens a C_4 route that has low relevance for this flame. Consumption of the C_3 species pool is similar to the other isomers and occurs via C_1 and C_2 compounds.

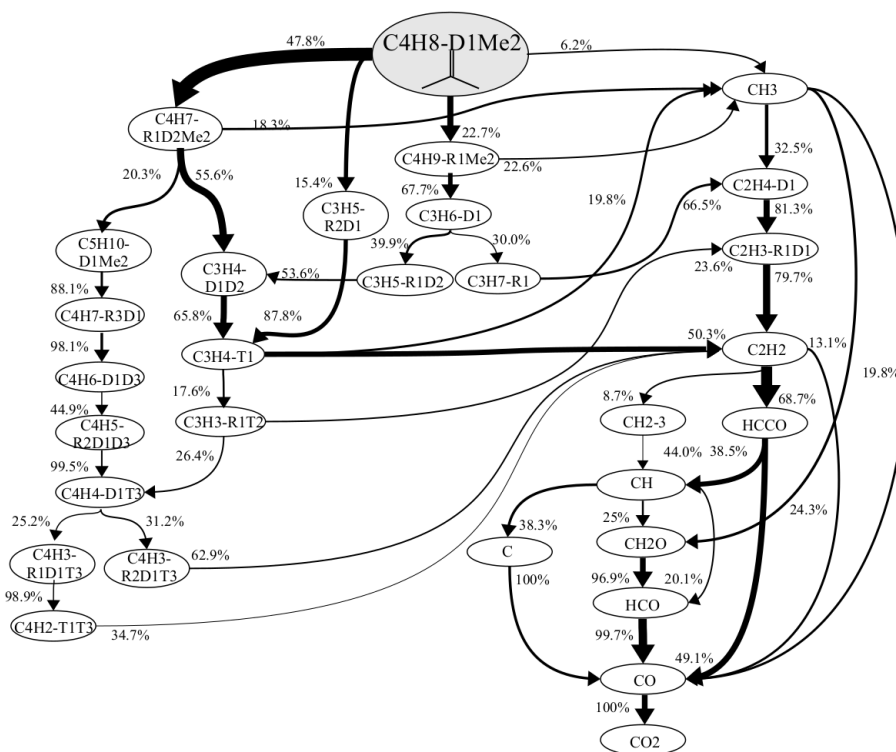


Figure 5.4: Integrated flow analysis of *iso*-butene ($C_4H_8\text{-D1Me}_2$) consumption. The thickness of the arrows indicates the contribution of the respective pathway to the total flux of C-atoms (contributions of the destruction of the individual molecule are indicated by percentages next to the arrows) [8].

The next section includes the discussion of major species together with temperature profiles and most important intermediate species profiles following the reaction pathways explained before.

5.3.1 Major Species

Figure 5.5 shows major species profiles (butene, O_2 , Ar, CO, CO_2 , H_2 , and H_2O) for the three flames together with the perturbed temperature profiles that were used as input parameters for the calculations. Global combustion behavior is similar for three isomers. Nevertheless, a difference around 150 K less is observed for the *iso*-butene flame. This temperature difference can be explained by a lower heat of combustion ($C_4H_8\text{-D1}$: $\Delta H_c^\circ = 2716 \text{ kJ/mol}$, T- $C_4H_8\text{-D2}$: $\Delta H_c^\circ = 2707 \text{ kJ/mol}$, $C_4H_8\text{-D1Me}_2$: $\Delta H_c^\circ = 2699 \text{ kJ/mol}$ [117]) together with an increment in the flux against the burner surface, given that

the reaction zone of the *iso*-butene flame is located slightly closer to the burner surface [8].

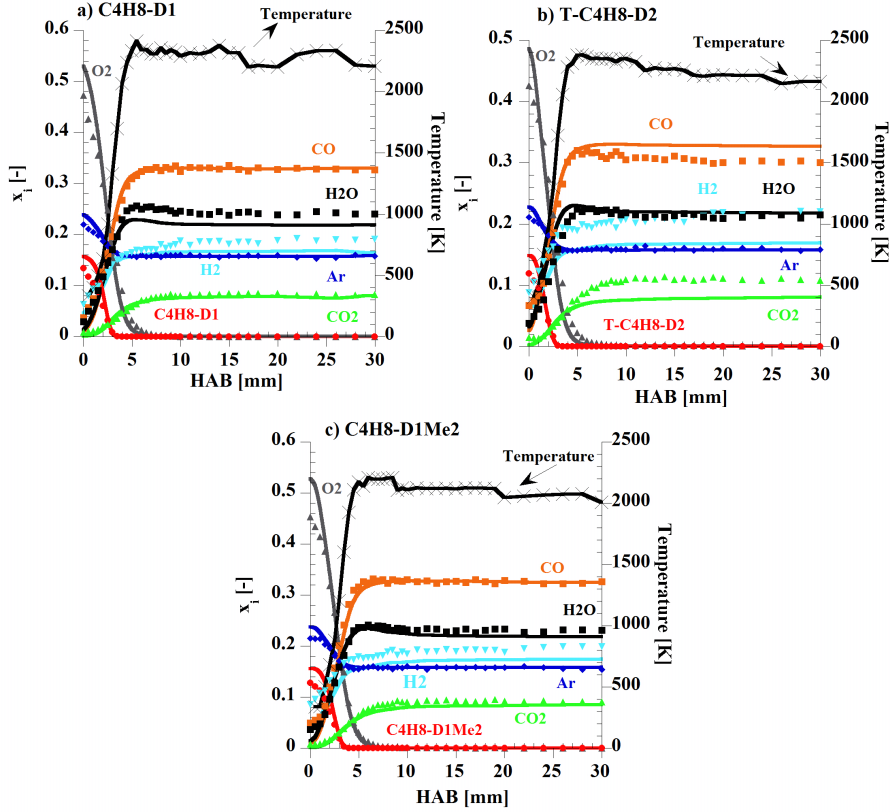


Figure 5.5: Major species mole fractions vs. height above the burner (HAB); a) 1-butene (C₄H₈-D1), b) *trans*-2-butene (T-C₄H₈-D2), and c) *iso*-butene (C₄H₈-D1Me₂); the symbols are from the EI-MBMS experiment from Schenk et al. [8], and the lines are taken from simulations with the model.

Major species are well predicted by the model for all butene isomers. A deviation between simulation and experiment is observed for the *trans*-2-butene flame, which could be explained by the lower pumping efficiency for H₂ [8]. Results are within the experimental error and no additional shift was applied for comparison, neither to the modeling results nor to the perturbed temperature profile. Note that the experimental species profiles may be affected by the perturbation of the flow field by the nozzle. This effect is most distinct for small burner-to-cone distances. Measured data points at heights of $h=1$ mm from the burner surface are therefore less reliable.

5.3.2 Intermediate species

C₃ chemistry plays an important role in the decomposition of butene fuels. Ex-

perimental and modeling profiles for propene (C3H6-D1) are shown in Figure 5.6 c). A slight over-prediction of the model was observed for *trans*-2-butene, while a closer agreement for 1-butene and *iso*-butene was observed. The *iso*-butene profile shape and peak position are very good considering that the H-induced propene channel for *iso*-butene is not included in the model (Dias et al. [95] describe the direct H-induced formation of propene as an important reaction pathway for an *iso*-butene lean flame). Flow analysis shows how 1-butene and *trans*-2-butene flames form propene directly. For *trans*-2-butene, propene represents the major destruction pathway of the fuel. Propene is formed by β -scission of the *iso*-butyl radical (C4H9-R1Me2), which results from reaction R597: C4H9-R1Me2 = C4H8-D1Me2 + H (see Figure 5.4).

The mole fraction of C₃H₅ isomers, namely allyl radical (C3H5-R1D2) and propen-2-yl radical (C3H5-R2D1) is shown in Figure 5.6 b). A good agreement for all the butene isomers is observed. Profile shapes show a good correspondence, with the exception of the peak position in the *iso*-butene flame where a small shift (lower than 0.5 mm) was observed. In all flames, the allyl radical is mainly formed by H-atom abstraction from propene via the reverse reaction R303 (H + C3H5-R1D2 \rightleftharpoons H₂ + C3H6-D1). For the *iso*-butene flame, the propen-2-yl radical C3H5-R2D1, a radical formation is favored.

The allyl radical undergoes an isomerization to propen-2-yl radical (C3H5-R2D1) and via β -scission of the central C-H bond to form allene (C3H4-D1D2). Allene and its isomer propyne (C3H4-T1) are not distinguishable in the EI-MBMS experiment but may be separated in the GC mode [8]. Profiles corresponding to the total C₃H₄ mole fraction (model and experiment) are presented in Figure 5.6 a). Mole fractions are slightly under-predicted for all flames but within the experimental error. Allene isomerizes to form most of the propyne in all flames. The *iso*-butene flame has a dominant pathway via C3H5-R2D1 that forms propyne directly.

C₃H₄ species further dehydrogenation may produce propargyl radicals (C3H3-R1T2), which are known as important benzene and soot precursor species in most flames. Figure 5.7 a) shows propargyl radicals (C3H3-R1T2) mole predictions compared to experimental data where the model slightly under-predicts the experimental measurements. Figure 5.7 b) shows C₆H₆ isomers mole fractions where the highest concentrations were detected in *iso*-butene flames, followed by those in the 1- and *trans*-2-butene flames (half of the amount). Benzene (A1) is the dominant molecule. Mole fraction in the three flames correlates directly with the propargyl radical mole fraction detected. Measurements are comparable to those for *iso*-butane flame [7], while the amount observed in the saturated linear *n*-butane flame is, again, a factor of 2 lower than the one for the branched isomer [8]. Toluene (A1CH3) is another important soot precursor. Mole fractions are shown in Figure 5.7 c), where a good agreement between experiments and model predictions is observed. Toluene is formed in the linear flames mainly from R1150: C4H7-R3D1 + C3H4-T1 \rightarrow A1CH3 + H₂ + H and branched from R1146: C4H7-R1D2Me2 + C3H4-T1 \rightarrow A1CH3 + H₂ + H. Both rates were taken from the work of Wang et al. [105].

Hydrogen abstraction from the fuel produces C₄H₇ radicals. Figure 5.8 a) shows

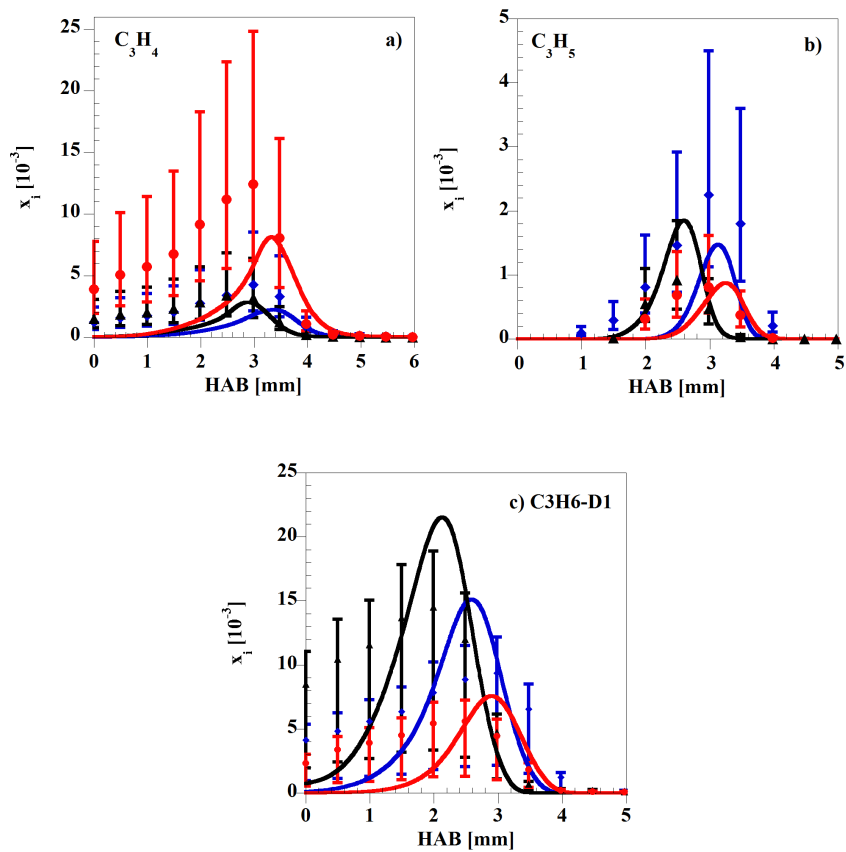


Figure 5.6: Mole fraction profiles of a) C_3H_4 isomers: allene (C_3H_4 -D1D2) and propyne (C_3H_4 -T1), b) C_3H_5 -R1D2 isomers: allyl radical (C_3H_5 -R1D2) and propen-2-yl radical (C_3H_5 -R2D1), and c) propene (C_3H_6 -D1). The symbols represent experimental data and the lines represent modeling results in a 1-butene (C_4H_8 -D1) (\blacklozenge), trans-2-butene (T - C_4H_8 -D2) (\blacktriangle), and iso-butene (C_4H_8 -D1Me2) (\bullet) flame. The corresponding bars show the experimental error.

a comparison between the model prediction (sum of all C₄H₇ isomers) and experimental measurements. C₄H₇ isomers are: secondary radical but-3-en-2-yl (C₄H₇-R3D1), primary radical but-3-en-1-yl (C₄H₇-R1D3), and 2-methyl allyl radical (C₄H₇-R1D2Me2). For the *1*-butene flame, the model predicts 22 % more C₄H₇-R3D1 compared to C₄H₇-R1D3. It shows that resonant stabilization of C₄H₇-R3D1 is more important than the path following the primary radical. The *trans*-2-butene flame only forms C₄H₇-R3D1 radical by abstraction of the H-atom in the methyl group. Finally, for the *iso*-butene flame, C₄H₇-R1D2Me2 is primarily formed by the abstraction of a methyl-H from the fuel. The highest C₄H₇ experimental concentration is observed in the *iso*-butene flame, followed by the *trans*-2-butene and finally the *1*-butene flame. The model predictions are within the experimental error for all the flames showing a good shape and peak position.

C₄H₇ linear radicals can decompose via further H-atom abstraction to C₄H₆ species. The model includes two isomers 1,3-butadiene (C₄H₆-D1D3) and 1,2-butadiene (C₄H₆-D1-D2). 1,3-butadiene (C₄H₆-D1D3) is the dominant isomer, which is formed from C₄H₇-R3D1 and C₄H₇-R1D3 by β -scission of the respective C-H bond. This is not possible in the *iso*-butene flame because the C₄H₇-R1D2Me2 radical cannot directly form any linear C₄H₆ isomer, which explains why the flame has the lowest molar fraction compared to the linear butenes (see Figure 5.8 b). Quantitative model prediction is within experimental error and the profile shape is quite well captured. The *1*-butene flame shows a slight over-prediction of the C₄H₆ mole fraction. The *trans*-2-butene and the *iso*-butene flames are nonetheless under-predicted. Experimentally, 1,3-Butadiene was identified as the dominant isomer in all flames, whereas only minor contributions of 1,2-butadiene, 1-, and 2-butyne were detected [8]. In all butene flames, 1,3-Butadiene is the dominant C₄H₆ isomer making the C₄ destruction pathway similar in all flames. Looking at Figures 5.2 to 5.4, it is seen that butadiene may be destroyed via subsequent dehydrogenation until the C₄ chain breaks apart to contribute to C₂ species pool. Figure 5.9 shows mole fraction profiles for a) vinylacetylene (C₄H₄-D1T3), b) diacetylene (C₄H₂-T1T3), and c) acetylene (C₂H₂).

1,3-butadiene (C₄H₆-D1D3) may form 1,3-butadiene-1-yl radical (C₄H₅-R1D1D3) by H-abstraction in the primary carbon (R954: H + C₄H₆-D1D3 \rightleftharpoons C₄H₅-R2D1D3 + H₂) and 1,3-Butadiene-2-yl radical (C₄H₅-R2D1D3) by H-atom abstraction on the allylic carbon (R943: H + C₄H₆-D1D3 \rightleftharpoons C₄H₅-R1D1D3 + H₂). Both radicals react to form vinylacetylene. Furthermore, the fission of the C-C bond in 1,3-butadiene forms two vinyl radicals, which contribute to the C₂ route. Both the experimental result and the model prediction show a good agreement for *iso*- and *1*-butene and under predictions for *2*-butene.

In analogy to C₄H₅ isomers, H-atom abstraction from vinylacetylene contributes to the C₄H₃ isomers formation (C₄H₃-R1D1T3 and/or C₄H₃-R2D1T3) via the following reactions:

- R885: H + C₄H₄-D1T3 \rightleftharpoons C₄H₃-R2D1T3 + H₂, and
- R884: H + C₄H₄-D1T3 \rightleftharpoons C₄H₃-R1D1T3 + H₂

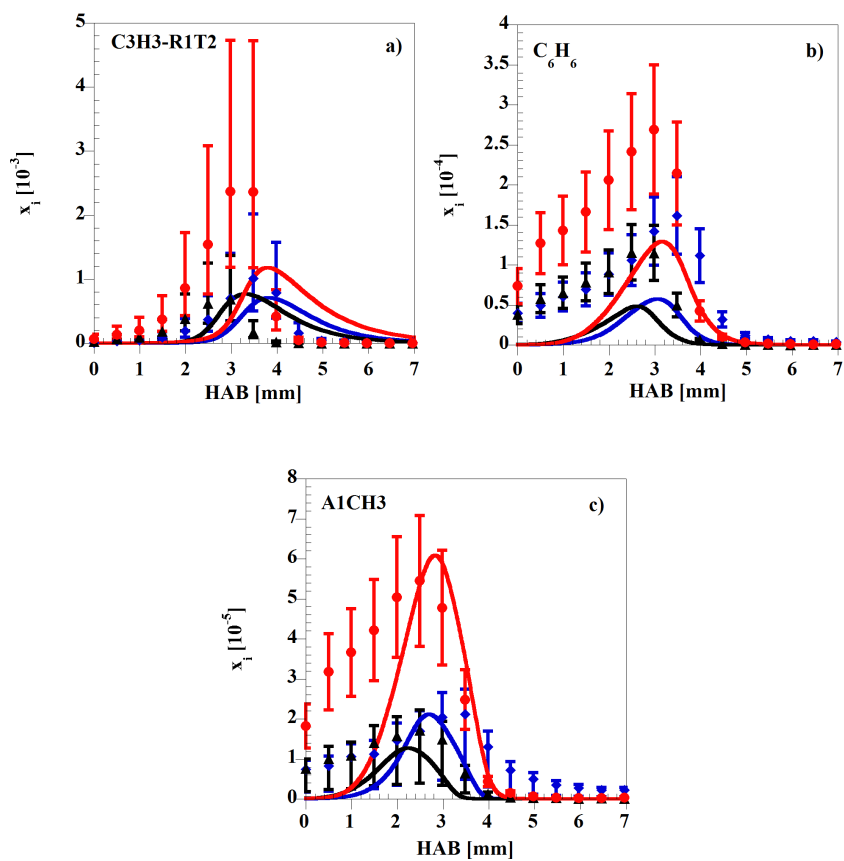


Figure 5.7: Mole fraction profiles of selected soot precursor species: a) propargyl (C_3H_3-R1T2), b) C_6H_6 isomers: fulvene (FC_6H_6) and benzene ($A1$), and c) toluene ($A1CH_3$). The symbols represent experimental data and the lines represent modeling results in a 1-butene (C_4H_8-D1) (\blacklozenge), trans-2-butene ($T-C_4H_8-D2$) (\blacktriangle), and iso-butene ($C_4H_8-D1Me_2$) (\bullet) flame. The corresponding bars show the experimental error.

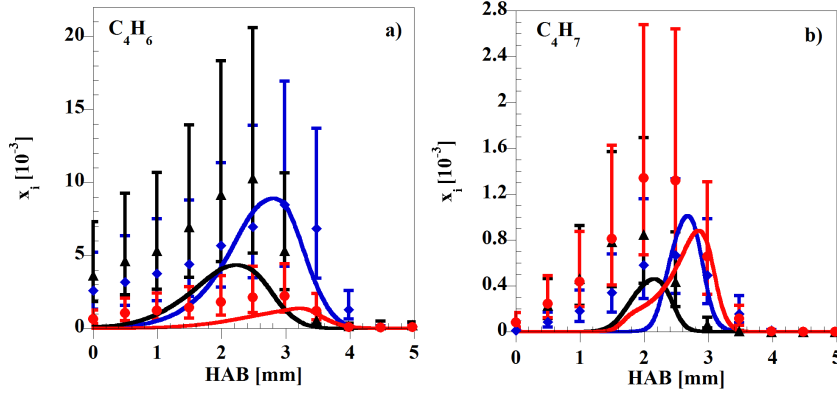


Figure 5.8: Mole fraction profiles of: a) C_4H_7 isomers: but-3-en-2-yl (C_4H_7 -R3D1), but-3-en-1-yl (C_4H_7 -R1D3), and 2-methyl allyl radical (C_4H_7 -R1D2Me2). b) C_4H_6 isomers: 1,3-butadiene (C_4H_6 -D1D3) and 1,2-butadiene (C_4H_6 -D1-D2). The symbols represent experimental data and the lines represent modeling result in a 1-butene (C_4H_8 -D1) (\blacklozenge), *trans*-2-butene (*T*- C_4H_8 -D2) (\blacktriangle), and *iso*-butene (C_4H_8 -D1Me2) (\bullet) flame. The corresponding bars show the experimental error.

C_4H_3 -R1D1T3 radical decomposes via a C-H bond scission to form diacetylene (C_4H_2 -T1T3) (R853: $H + C_4H_2$ -T1T3 \rightleftharpoons C_4H_3 -R1D1T3), while C_4H_3 -R2D1T3 tends to decompose via a C-C bond scission to form acetylene (R869: $H + C_4H_3$ -R2D1T3 \rightleftharpoons $2 C_2H_2$), which is the termination of this reaction chain. A good agreement between experiment and model is observed in Fig. 5.9 c). Acetylene concentrations do not show a dependence on the respective fuel structure.

Methyl radical (CH_3), methane (CH_4), ethane (C_2H_6), and ethene (C_2H_4 -D1) are shown in Figure 5.10. Model prediction and profile shapes are in good agreement with experimental results for all C_1 and C_2 compounds. Methyl is over-predicted for all the flames while methane matches very well all the different butene isomers. Together with acetylene, ethane and ethene represent the C_2 reaction chain. Experimental concentrations for ethane (See Figure 5.10) are very similar for 1-butene and 2-butene, and lower for the *iso*-butene flame. The model can reproduce well this behaviour. Finally, ethane mole fractions show a shape similar to the experimental results, where *trans*-2-butene reaches a maximum concentration earlier than the other two isomers. Concentrations are slightly over-predicted by the model.

Some oxygenated products are presented in Figure 5.11 where formaldehyde profiles (see Figure 5.11 a)) show a slight under-prediction for 2-butene and *iso*-butene. Methanol (see Figure 5.11 b)) shows a good prediction of the experimental profiles compared to the modeling results, while under-predictions

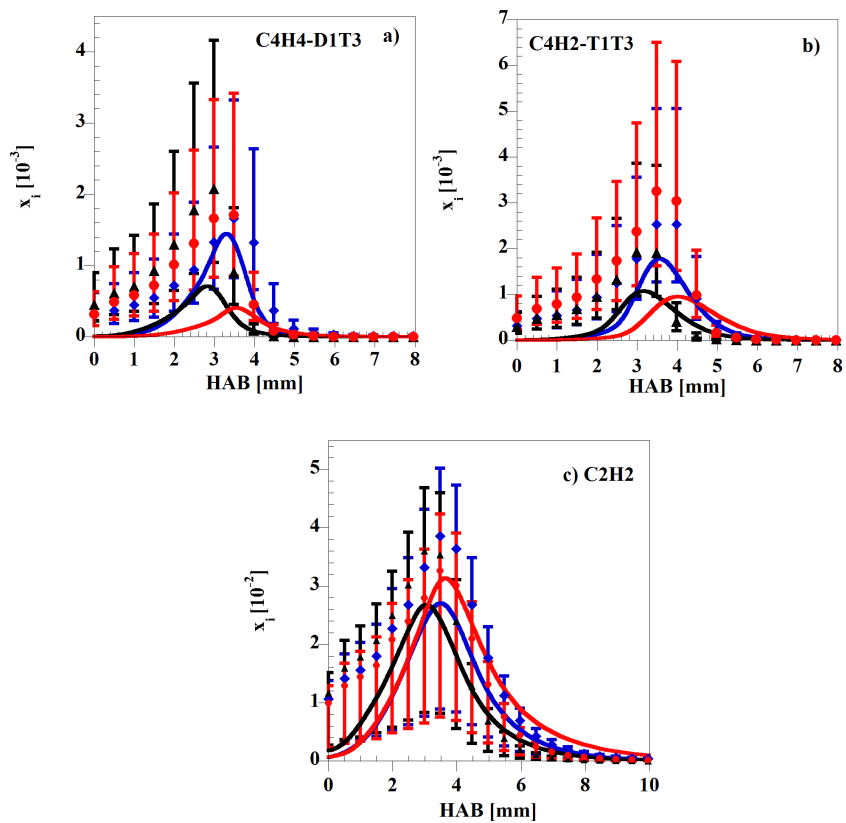


Figure 5.9: Mole fraction profiles of some C_4 fuel decomposition products: a) vinylacetylene (C_4H_4 -D1T3), b) diacetylene (C_4H_2 -T1T3), and c) acetylene (C_2H_2). The symbols represent experimental data and the lines represent modeling results in a 1-butene (C_4H_8 -D1) (\blacklozenge), trans-2-butene (T- C_4H_8 -D2) (\blacktriangle), and iso-butene (C_4H_8 -D1Me2) (\bullet) flame. The corresponding bars show the experimental error.

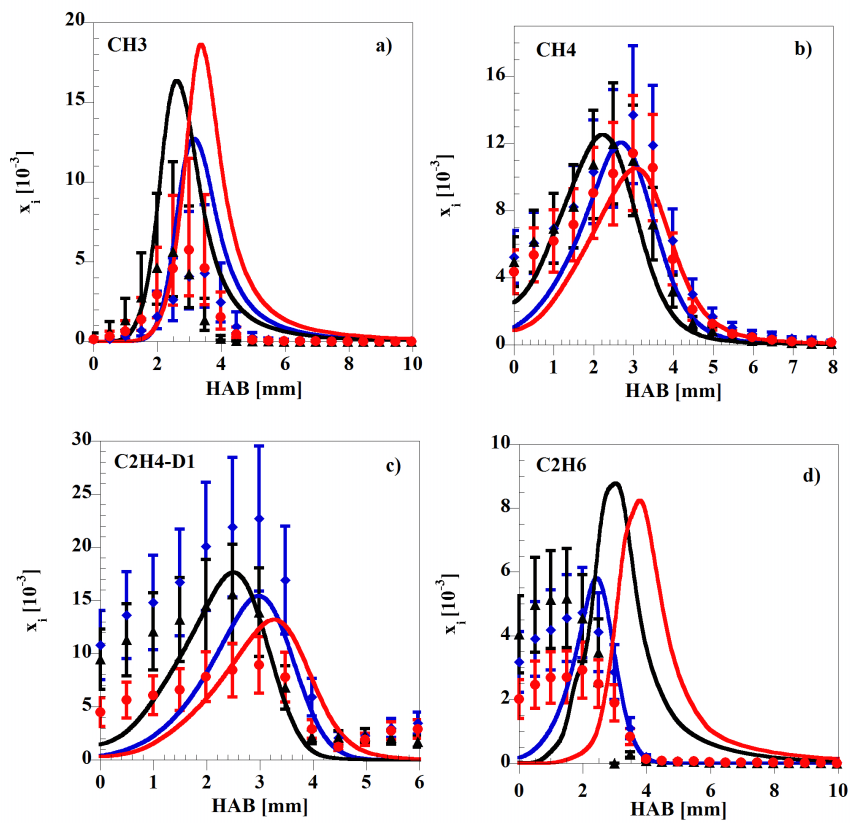


Figure 5.10: Mole fraction profiles of some C_1 and C_2 fuel decomposition products: a) methyl (CH_3), b) methane (CH_4), c) ethene (C_2H_4-D1), and d) ethane (C_2H_6). The symbols represent experimental data and the lines represent modeling results in a 1-butene (C_4H_8-D1) (\blacklozenge), trans-2-butene ($T-C_4H_8-D2$) (\blacktriangle), and iso-butene ($C_4H_8-D1Me_2$) (\bullet) flame. The corresponding bars show the experimental error.

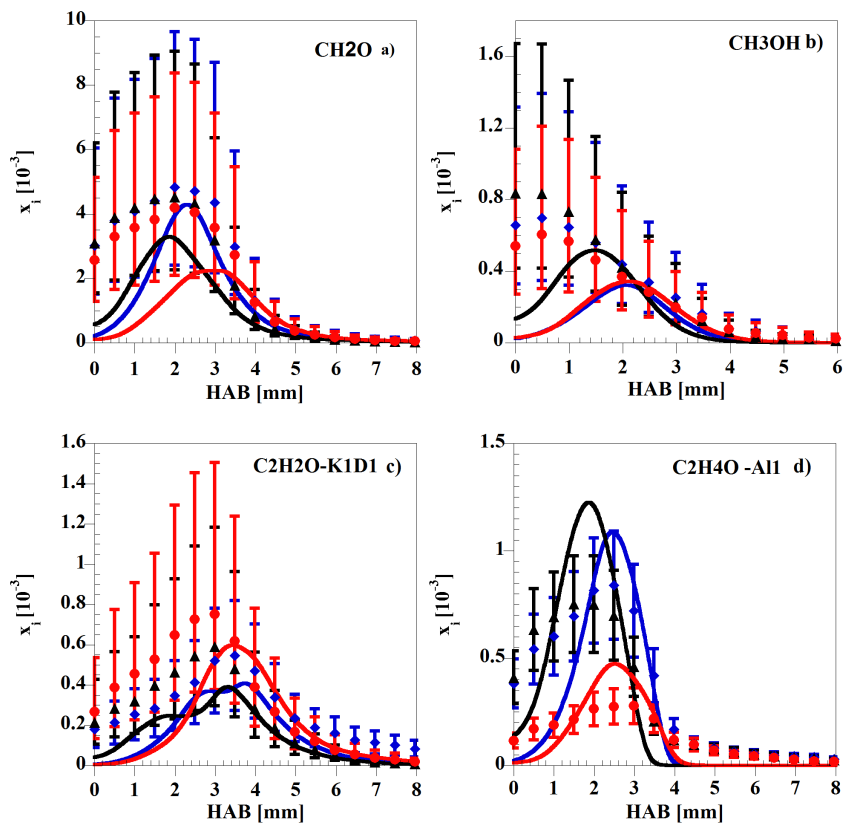


Figure 5.11: Mole fraction profiles of some oxygenated products: a) formaldehyde (CH_2O), b) methanol (CH_3OH), c) ketene ($\text{C}_2\text{H}_2\text{O-K1D1}$) and d) acetaldehyde ($\text{C}_2\text{H}_4\text{O-A11}$). The symbols represent experimental data and the lines represent modeling results in a 1-butene ($\text{C}_4\text{H}_8\text{-D1}$) (\blacklozenge), trans-2-butene ($\text{T-C}_4\text{H}_8\text{-D2}$) (\blacktriangle), and iso-butene ($\text{C}_4\text{H}_8\text{-D1Me2}$) (\bullet) flame. The corresponding bars show the experimental error.

are observed for *1*-butene and *iso*-butene. Ketene results are shown in Figure 5.11 c). The model shows that *iso*-butene is producing its highest concentration while lower concentrations are observed for *1*-butene and *2*-butene. Finally, acetaldehyde shows a concentration dependent on the fuel structure as it was shown in other two studies, where molecules that have high soot precursors mole fractions show a small amount of acetaldehyde and vice versa. Acetaldehyde and its isomer ethenol are not separated in this study. Numerical simulations correspond mostly to acetaldehyde concentration.

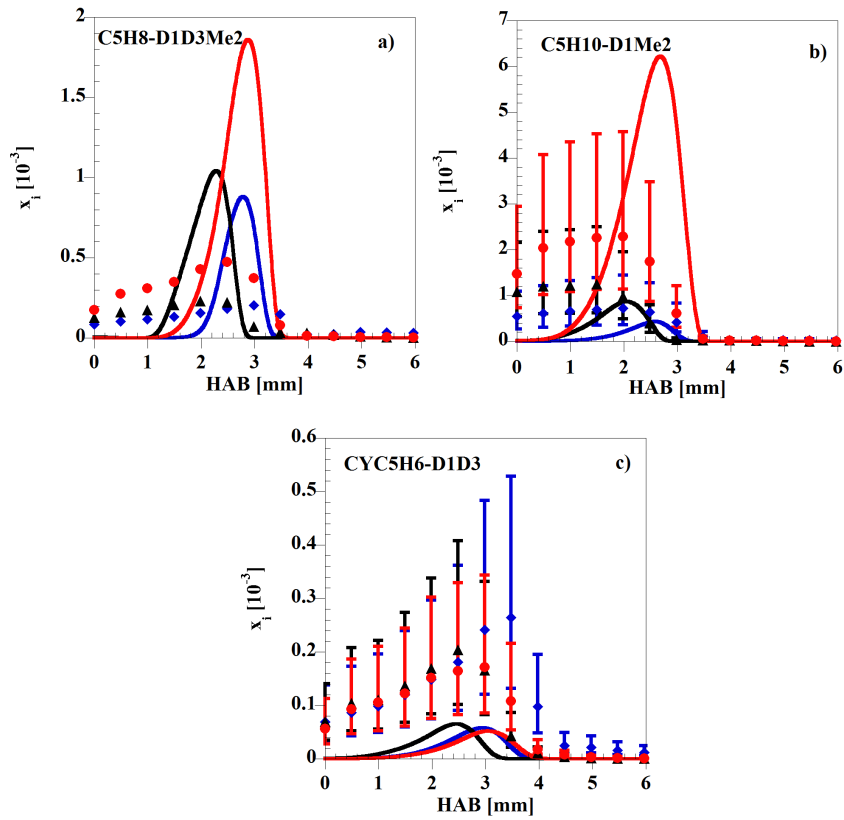


Figure 5.12: Mole fraction profiles of some C_5 fuel decomposition products: a) *iso*-prene ($C_5H_8-D1D3Me_2$), b) *2*-methyl-*1*-butene ($C_5H_{10}-D1Me_2$), and c) cyclopentadiene ($CYC_5H_6-D1D_3$). The symbols represent experimental data and the lines represent modeling results in a *1*-butene (C_4H_8-D1) (\blacklozenge), *trans*-*2*-butene ($T-C_4H_8-D_2$) (\blacktriangle), and *iso*-butene ($C_4H_8-D1Me_2$) (\bullet) flame. The corresponding bars show the experimental error.

Figure 5.12 presents predicted and experimental mole fraction profiles for different C_5 species. In the experimental *1*-butene and *2*-butene flame, *trans*-*2*-

pentene was identified as the main isomer. Other possible isomers are 2-methyl-1-butene, *n*-pentene, and *cis*-2-pentene. In the *iso*-butene flame, the ratio of the isomers is clearly different; here, a minor contribution from *trans*-2-pentene is seen. The second isomer in this flame can most probably be assigned to be 2-methyl-1-butene.

The model includes isoprene (C5H8-D1D3Me2), 2-methyl-1-butene (C5H10-D1Me2), and cyclopentadiene (CYC5H6-D1D3). The concentration of 2-methyl-1-butene in 1-butene and *trans*-2-butene flames is under-predicted by the model and over-predicted for *iso*-butene flame, 2-methyl-1-butene (C5H10-D1Me2) may be formed by recombination of C4H7-R1D2Me2 and methyl radicals (see 5.4) and is involved in the butadiene formation from *iso*-butene. According to the present modeling approach, 2-methyl-1-butene may react over different C₅H₉ radicals to form isoprene (C5H8-D1D3Me2). Isoprene concentration is over-predicted for 1-, 2- and *iso*-butene. Finally, CYC5H6-D1D3 is mainly formed by recombination of C3H5-R1D2 and C2H2 and is underpredicted in all the flames. This experimental observation gives an insight of the importance to better understand the C₅ chemistry. However, development of a full C₅ sub-mechanism is beyond the scope of this chapter.

5.4 Ignition delay time and laminar flame speed validation for butene (C₄H₈) isomers.

The mechanism with the updated chemistry has been further validated against several shock tubes and laminar flame speed experiments. Experimental and modeling results measured by Curran et al. [96] for autoignition of 1.2% *iso*-butene (C4H8-D1Me2) at different equivalence ratios and 2 atm are shown in Fig. 5.13, where the model reproduces the trend and matches the experimental measurements very well.

Another *iso*-butene (C4H8-D1Me2) autoignition experiment was performed by Yasunaga et al. [98] at 1.94 atm, at different equivalence ratios and oxygen concentrations (see Figure 5.14). The ignition delay time in the experiment is defined as the elapsed time between the reflected shock arrival and the onset of the rapid infrared emission increase for CO₂. Figure 5.14 a) shows that mixtures B and C have equivalence ratios of 2.0 and 1.0, respectively. Mixture C has a higher reactivity compared to B. Mixture D has a $\phi=1.0$ and a lower concentration of *iso*-butene and O₂, and shows a reactivity similar to mixture B. The model can reproduce the trend of the experimental results for these mixtures and predict slightly faster ignition delay times. Figure 5.14 b) shows experimental results for mixtures E, F and G with an equivalence ratio of 0.5. Longer ignition delay times are observed for mixture F, which has the lowest concentration of O₂. The model can capture the trend for each mixture, and ignition delay times are shorter at the highest temperatures and longer as the temperature decreases.

Bauge et al. [97] performed autoignition experiments to study the influence of different concentration and equivalence ratios on *iso*-butene/Ar/O₂ mixtures.

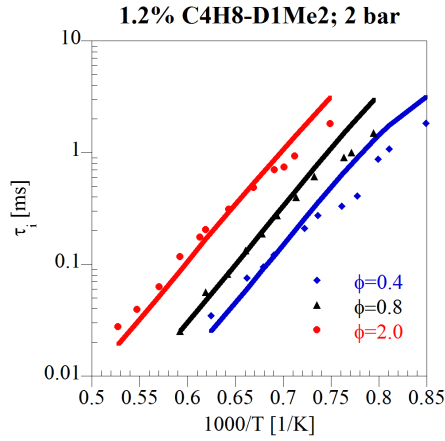


Figure 5.13: Ignition delay times of 1.2% $C_4H_8-D1Me_2/O_2/Ar$ mixtures at 2 atm and $\phi=0.4, 0.8,$ and 2.0 . The symbols correspond to experimental data from Curran et al. [96] and the lines correspond to simulations.

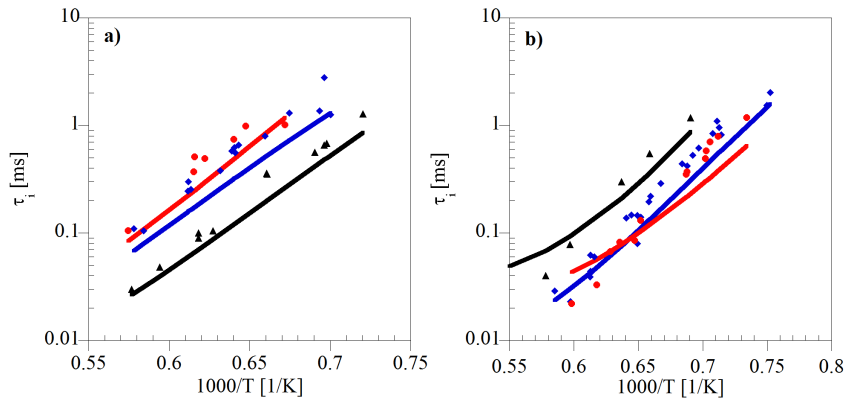


Figure 5.14: a) Ignition delay times for mixtures of: \blacklozenge (B: 1.0% $C_4H_8-D1Me_2, 3.0\%$ O_2 in Ar), \blacktriangle (C: 1.0% $C_4H_8-D1Me_2, 6.0\%$ O_2 in Ar), and \bullet (D: 0.5% $C_4H_8-D1Me_2, 1.5\%$ O_2 in Ar). b) Ignition delay times for mixtures of: \blacktriangle (F: 0.1% $C_4H_8-D1Me_2, 1.2\%$ O_2 in Ar), \blacklozenge (E: 0.5% $C_4H_8-D1Me_2, 6.0\%$ O_2 in Ar), and \bullet (G: 0.1% $C_4H_8-D1Me_2, 4.8\%$ O_2 in Ar). The symbols correspond to experimental data from Yasunaga et al. [98] and the lines correspond to simulations.

Influence on equivalence ratios ($\phi= 1.0-3.0$) are shown in figure 5.15 a), where all mixtures have the same *iso*-butene concentration and oxygen is increased by decreasing the equivalence ratio. Experimental results show that increasing oxygen in the mixture makes ignition faster; modeling results show similar trend to the experiment and slightly faster ignition delay times. Increasing the concentration of *iso*-butene (5.15 b)) and maintaining the equivalence ratio constant ($\phi= 3.0$), shows that there is a faster ignition when the concentration of the fuel is higher. Modeling results show trends similar to the experimental ones. For all mixtures, ignition delay times are shorter with the increase of the temperature.

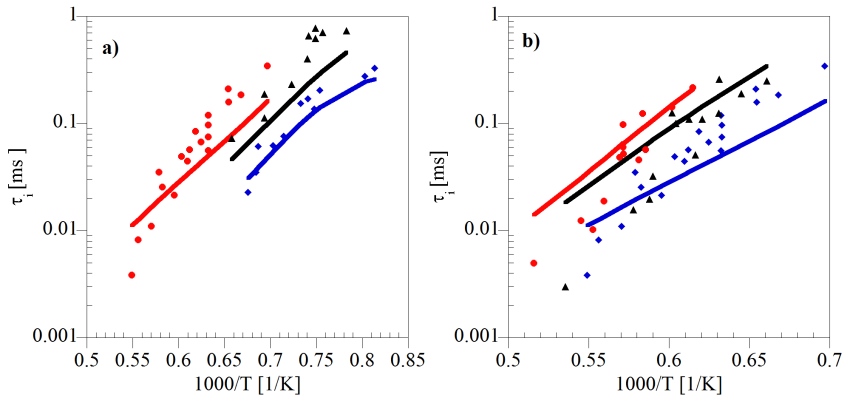


Figure 5.15: a) Ignition delay times with 3.65% of $C_4H_8-D_1Me_2$ for different equivalence ratios (\blacklozenge : $\phi=1.0$, \blacktriangle : $\phi=2.0$, \bullet : $\phi=3.0$) and b) Ignition delay times with $\phi=3$ and for different $C_4H_8-D_1Me_2$ percentages (\bullet : 0.5%, \blacktriangle : 1.0%, \blacklozenge : 3.65%). The symbols correspond to experimental data from Bauge et al. [97] and the lines correspond to simulations.

Heyberger et al. [99] performed experimental measurements for different equivalence ratios for 1% of *1*-butene and for different concentrations of *1*-butene (see Fig. 5.16). Modeling results presented in Figure 5.16 a) show in general a closer agreement to the ignition delay time experimental data at highest temperatures. Figure 5.16 b) compares two different *1*-butene concentrations where the reactivity of the fuel is increased with the concentration. A general good agreement is observed for experimental and modeling results.

Pan et al. [100] performed *1*-butene autoignition experiments for different equivalence ratios and pressures (see Figures 5.17a)-c)). Increasing pressure also implies that the absolute concentration of reactants increase, resulting in shorter ignition delay times. The model predicts this effect over the different pressures and equivalence ratios. Nevertheless, predicted ignition delay times are shorter than measured ones for higher pressures and low equivalence ratio (see Fig. 5.17 a) 4.11 and 16.3 atm). Increasing the equivalence ratio decreases this pressure effect. Li et al. [115] performed high temperature shock tube experiments for

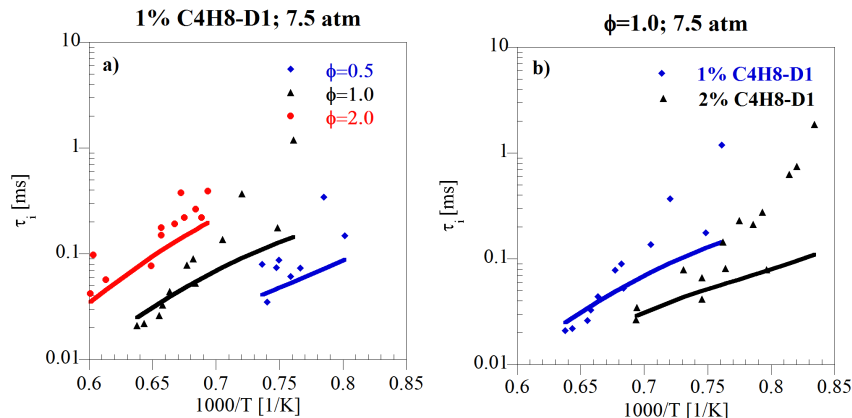


Figure 5.16: a) Ignition delays in a shock tube of the oxidation of 1-butene for different equivalence ratios (\blacklozenge : $\phi=0.5$, \blacktriangle : $\phi=1.0$, \bullet : $\phi=2.0$) and b) Ignition delays in a shock tube for different concentrations of 1-butene (\blacklozenge : 1% C₄H₈-D1, \blacktriangle : 2% C₄H₈-D1). The symbols correspond to experimental data from Heyberger et al. [99] and the lines correspond to simulation results.

1-butene at equivalent ratios of 0.5, 1.0 and 2.0 and high pressures (10, 30, and 50 atm). The influence of pressure on ignition delay times is shown in Figures 5.18 a) to c). Experimental results show that reactivity increases with increasing pressure at all equivalence ratios [100]. The reaction mechanism is able to predict this effect, but higher deviations are observed as the pressure increases, resulting in longer ignition delay times compared to the measured ones.

Ignition delay times of *trans*-2-butene were studied by Li et al. [114]. Similar experimental conditions to 1-butene were investigated (see Figure 5.19 a) to c)). Experimental results show that reactivity increases with increasing pressure at all equivalence ratios. Modeling results predict well the ignition at 30 atm and $\phi=0.5$ -2.0. Autoignition model predictions for 10 atm are in good agreement with experimental measurements for $\phi=0.5$ and 1.0, but higher deviations are observed for $\phi=2.0$. Model predictions for 50 atm result in longer ignition delay times in comparison to the measured ones for $\phi=0.5$, while a closer prediction is observed for $\phi=1.0$ and 2.0.

The laminar flame speed for *iso*-butene as fuel was calculated with the present model at 1 bar and 298 K (See figure 5.20 a)). Experimental measurements from Davis et al. 1998 [42], Zhang et al. 2015 [103], and Zhou et al. [118] are used for comparison. The model follows the trend of the experimental measurements and slightly over-predicts the maximum flame speed at an equivalence ratio of 1.1. The rich side of the flame is following the measurement predictions of Davis et al. 1998 [42] and Zhou et al. [118]. Zhang et al. 2015 [103] (see figure 5.20 b)) studies the pressure dependency with respect to the flame

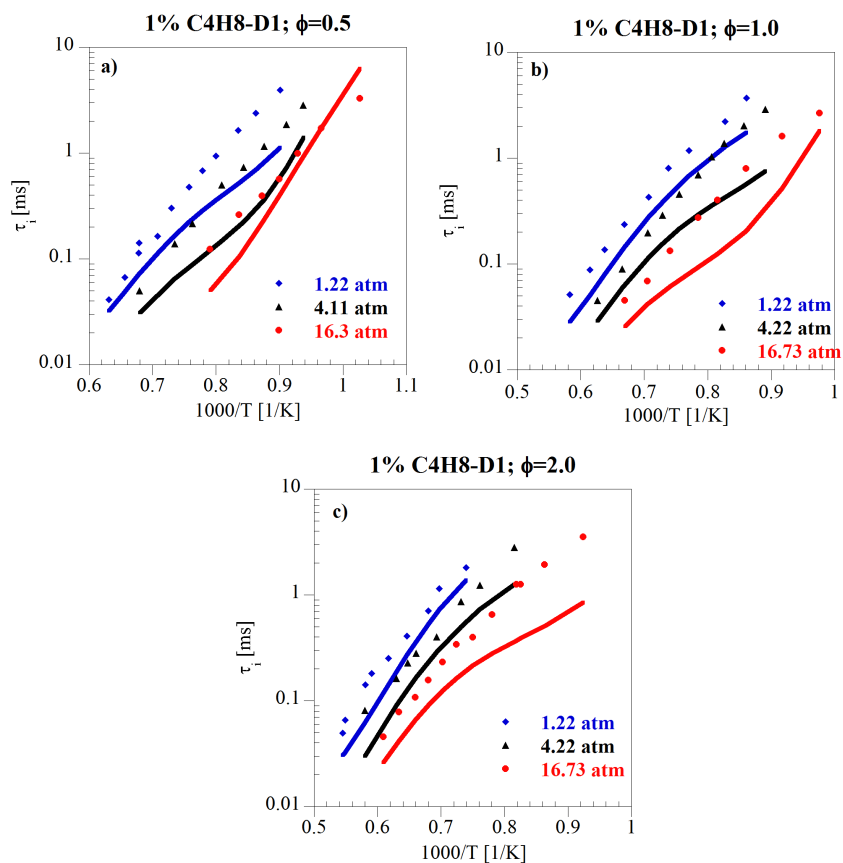


Figure 5.17: Prediction for 1-butene ignition under various conditions: a) 1% of C₄H₈-D1, $\phi=0.5$ at \blacklozenge :1.22 atm, \blacktriangle :4.11 atm, and \bullet :16.3 atm.; b) 1% of C₄H₈-D1, $\phi=1.0$ at \blacklozenge :1.22 atm, \blacktriangle :4.22 atm, and \bullet :16.73 atm.; c) 1% of C₄H₈-D1, $\phi=2.0$ at \blacklozenge :1.22 atm, \blacktriangle :4.22 atm, and \bullet :16.73 atm. The symbols correspond to experimental data from Pan et al. [100] and the lines correspond to simulation results.

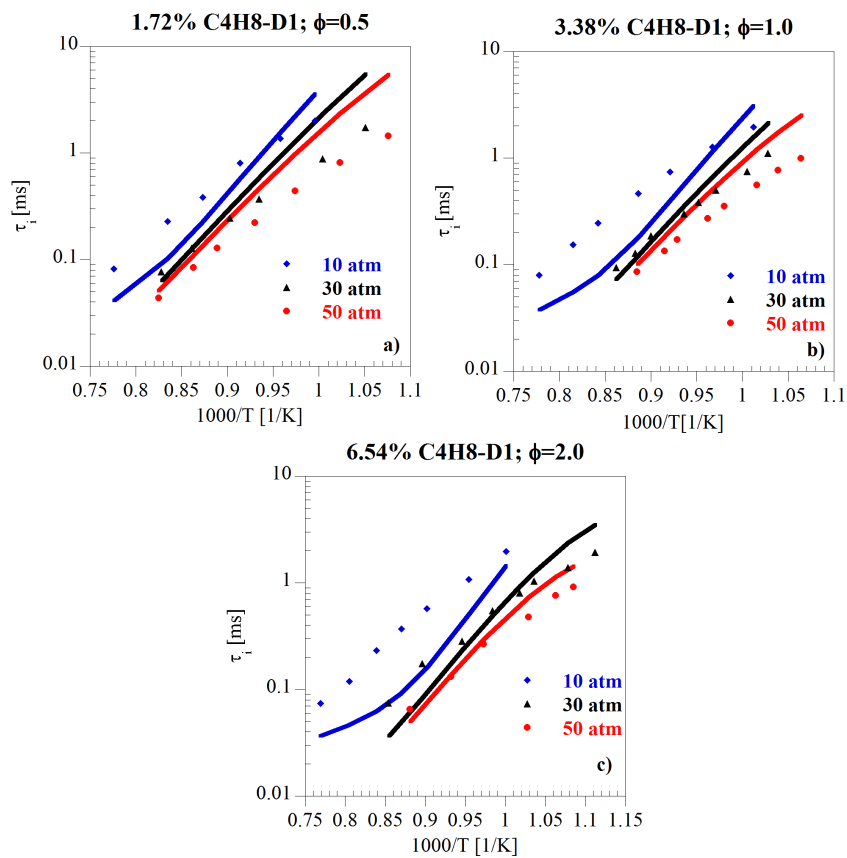


Figure 5.18: Influence of pressure on 1-butene ignition delay time: a) 1.72% of C_4H_8-D1 , $\phi = 0.5$ at \blacklozenge :10 atm, \blacktriangle :30 atm, and \bullet :50 atm, b) 3.38% of C_4H_8-D1 , $\phi = 1.0$ at \blacklozenge :10 atm, \blacktriangle :30 atm, and \bullet :50 atm, c) 6.54% of C_4H_8-D1 , $\phi = 2.0$ at \blacklozenge :10 atm, \blacktriangle :30 atm, and \bullet :50 atm. The symbols correspond to experimental data from Li et al. [115] and the lines correspond to simulation results.

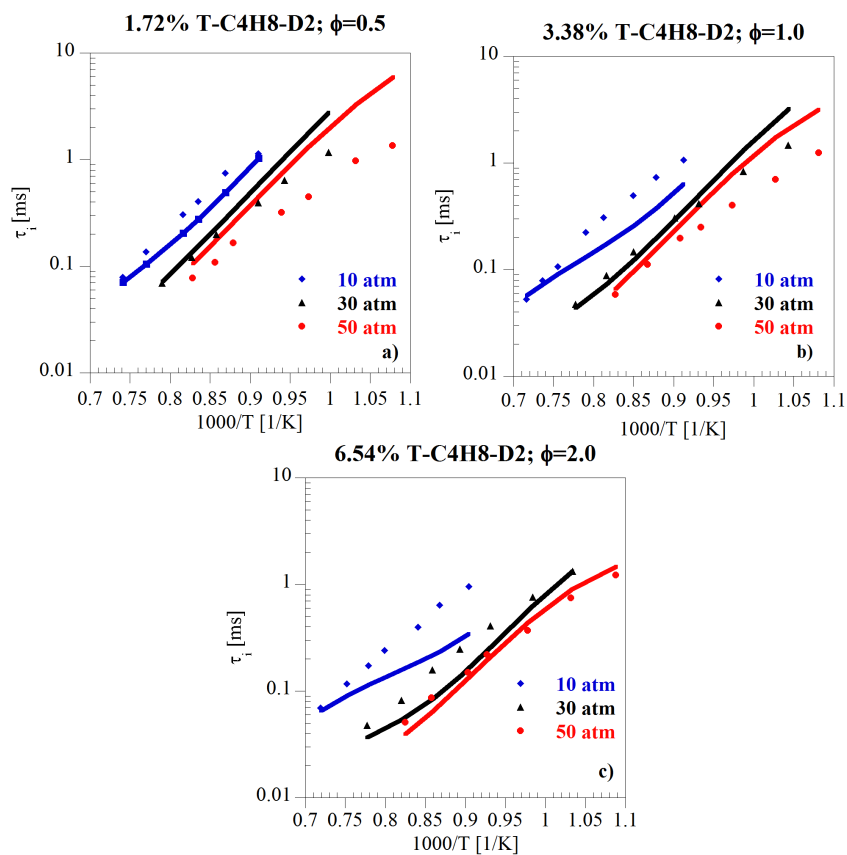


Figure 5.19: Influence of pressure on 2-butene ignition delay time: a) 1.72% of T-C₄H₈-D₂, $\phi = 0.5$ at \blacklozenge :10 atm, \blacktriangle :30 atm, and \bullet :50 atm, b) 3.38% of T-C₄H₈-D₂, $\phi = 1.0$ at \blacklozenge :10 atm, \blacktriangle :30 atm, and \bullet :50 atm, c) 6.54% of T-C₄H₈-D₂, $\phi = 2.0$ at \blacklozenge :10 atm, \blacktriangle :30 atm, and \bullet :50 atm. The symbols correspond to experimental data from Li et al. [114] and the lines correspond to simulation results.

velocity. As expected, the laminar flame speed decreases with the increment of the pressure. Modeling results can capture this behavior but the laminar flame velocity measured experimentally ends up being over-predicted.

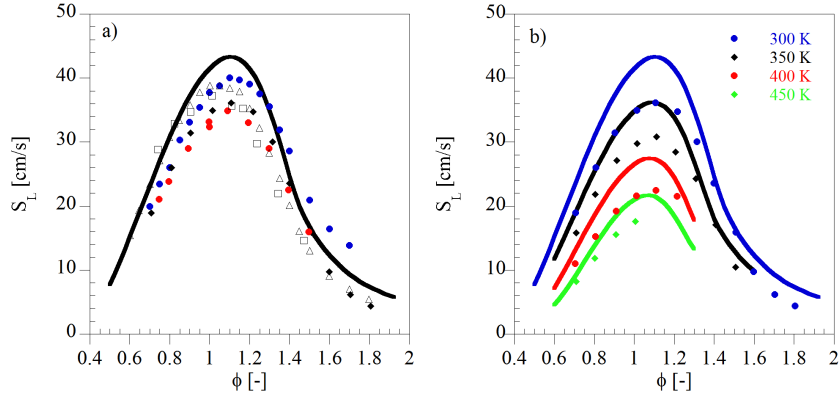


Figure 5.20: a) Numerically determined laminar flame speeds as a function of the equivalence ratio for an iso-butene/air mixture at $T_u = 298\text{ K}$ and $p = 1\text{ atm}$. The black line represents the simulation result in this study. Experiments by: \bullet Davis et al. 1998 [42], \blacklozenge Zhang et al. 2015 [103], \bullet (TAMU), \triangle (LRPG), \square (PU) Zhou et al. [118]. b) Numerically determined laminar flame speeds as a function of the equivalence ratio for iso-butene/air mixture at $T_u = 300\text{ K}$ and $p =$ \bullet : 1 atm, \blacklozenge : 2 atm, \bullet : 5 atm, and \bullet : 10 atm by Zhang et al. 2015 [103]. The lines show the corresponding simulation results.

The laminar flame speed for 1-butene as fuel was calculated with the present model at 1 bar and 298 K (See Figure 5.21 a). For comparison purposes, the experimental measurements from Davis et al. 1998 [42], Zhang et al. 2015 [103] were used. The model follows the trend of the experimental measurements from Davis et al. 1998 [42]. Zhang et al. 2015 [103] (see Figure 5.21 b)) studied the pressure dependency with respect to the flame velocity for this isomer as well. As expected, the laminar flame speed decreases with increasing the pressure. Modeling results can capture this behavior, but the measured laminar flame velocity remains over-predicted.

Figure 5.22 shows the temperature dependency for 1-butene at 1 atm where the model predictions have a similar trend as the experimental measurements. Slightly over-predictions are observed in the maximum of the flame approximately at $\phi = 1.1$.

Laminar flame speeds for 2-butene as fuel were calculated with the present model at 1 bar and 298 K (See figure 5.23 a)). For comparison purposes, the experimental measurements from Zhang et al. 2015 [103] are used. The model

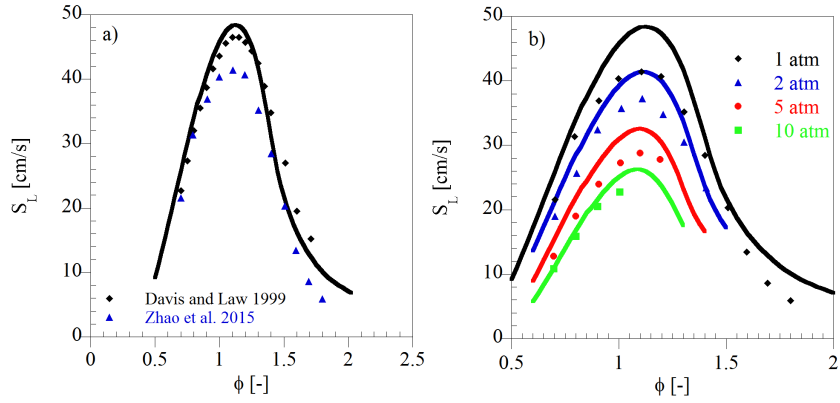


Figure 5.21: a) Numerically determined laminar flame speeds as a function of the equivalence ratio for a 1-butene/air mixture at $T_u = 298$ K and $p = 1$ atm. The black line represents the simulation result in this study. Experiments by: \bullet Davis et al. 1998 [42], \blacklozenge Zhang et al. 2015 [103]. b) Numerically determined laminar flame speeds as a function of the equivalence ratio for 1-butene/air mixture at $T_u = 300$ K and $p =$ \blacklozenge : 1 atm, \blacktriangle : 2 atm, \bullet : 5 atm, and \blacksquare : 10 atm by Zhang et al. 2015 [103]. The lines show the corresponding simulation results.

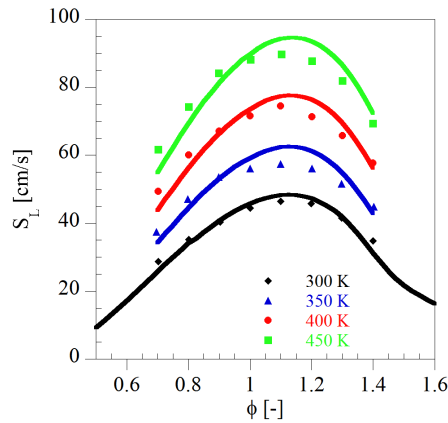


Figure 5.22: Numerically determined laminar flame speeds as a function of the equivalence ratio for 1-butene/air mixture at $p = 1$ atm and $T_u =$ \blacklozenge 300 K, \blacktriangle 350 K, \bullet 400 K, and \blacksquare 450 K. The symbols are experimental points by Fernand et al. [102] and the lines are simulation results.

follows the trend of the experimental measurements but slightly over-predicts the maximum at an equivalence ratio of 1.1. Zhang et al. 2015 [103] (see Figure 5.23 b)) studied the pressure dependency with respect to the flame velocity for this isomer too. As expected, the laminar flame speed decreases with increasing pressure. Modeling results can capture this behavior and the value corresponding to the flame velocity experimentally measured.

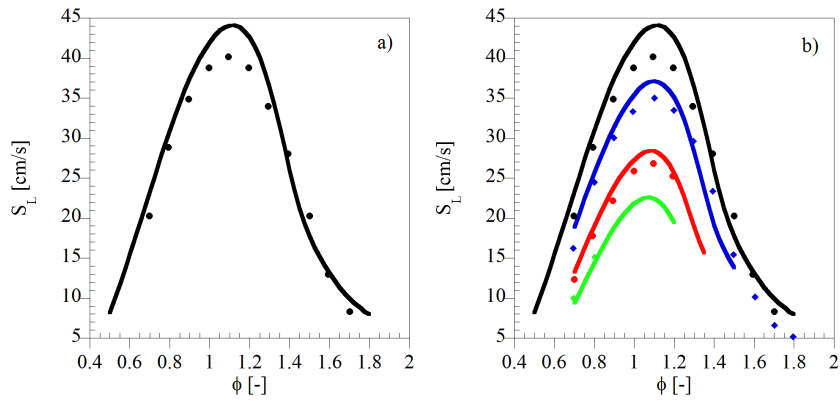


Figure 5.23: a) Numerically determined laminar flame speeds as a function of the equivalence ratio for a 2-butene/air mixture at $T_u = 298$ K and $p = 1$ atm. The black line represents the simulation result in this study. Experiments by: \blacklozenge Zhang et al. 2015 [103]. b) Numerically determined laminar flame speeds as a function of the equivalence ratio for 2-butene/air mixture at $T_u = 300$ K and $p = \bullet$: 1 atm, \blacklozenge : 2 atm, \bullet : 5 atm, and \blacklozenge : 10 atm by Zhang et al. 2015 [103]. The lines show the corresponding simulation results.

Chapter 6

Combustion chemistry of C₅ linear and branched species

In the previous chapter, the chemistry of the butene isomers was analyzed, therefore finding that C₅ chemistry may be an important reaction growth pathway. After that a new publication where a burner stabilized flame for 2-Methyl-2-butene (C₅H₁₀-D2Me2) was measured (Ruwe et al.2018 [11]) showed the importance of C₅ species as possible first ring aromatic precursor. In conversation with the university of Bielefeld (Prof. Kohse-Höinghaus and Lena ruwe), Sandia Laboratory (Nils Hansen), PTB Braunschweig (Kai Moshhammer) and University of Cottbus, we agreed to make a cooperation where they delivered a new experiment for a n-Pentane (C₅H₁₂) burner stabilized flame and in Cottbus, I was responsible for the development of a complete C₅H₁₀ sub-mechanism (2-Methyl-1-butene (C₅H₁₀-D1Me2), 2-Methyl-2-butene (C₅H₁₀-D2Me2), 3-Methyl-1-butene (C₅H₁₀-D1Me3), n-Pentene (C₅H₁₀-D1), and cis-2-Pentene (C₅H₁₀-D2)) reaction mechanism. N-Pentane (C₅H₁₂) chemistry was in the model and was revised and updated in order to make the hierarchically-constructed kinetic model more comprehensive. Thermodynamic data for newly introduced species and their C₅ degradation products were updated using the database of Goos et al. (2013) [9].

Over the past years, several studies have been conducted regarding the C₅H₁₀ isomers, for example: premixed low pressure flames [13], [119], counter-flow flames [11], autoignition experiments for high and low temperature [120], [121], [122], [123], [124]), jet-stirred reactor [120], laminar flame velocity [125], [126], [127], and a plug flow reactor [128]. For n-Pentane, experimental studies can also be found mainly for the autoignition: [129], [33], [130], [131], [132], [133], [124], [134], [135], [136], [123], and some for jet-stirred reactor, flow reactor, opposed-flow diffusion flame and laminar flame speeds: [137], [138], [139], [140], [141], [11], [125], [142], [143], and [144].

2-Methyl-2-butene (C₅H₁₀-D2Me2) as fuel will be analyzed in detail due to its interesting chemical structure with 9 C-H bonds in the allylic position, while n-Pentane (C₅H₁₂) will be studied as an example of a linear alkane molecule. The validation for burner-stabilized flames, laminar flame speeds and ignition

delay times for these two fuels are shown.

Structures of the different C_5H_{10} isomers and n-Pentane (C_5H_{12}), along with their possible consumption pathways are presented in Figures 6.1 to 6.6.

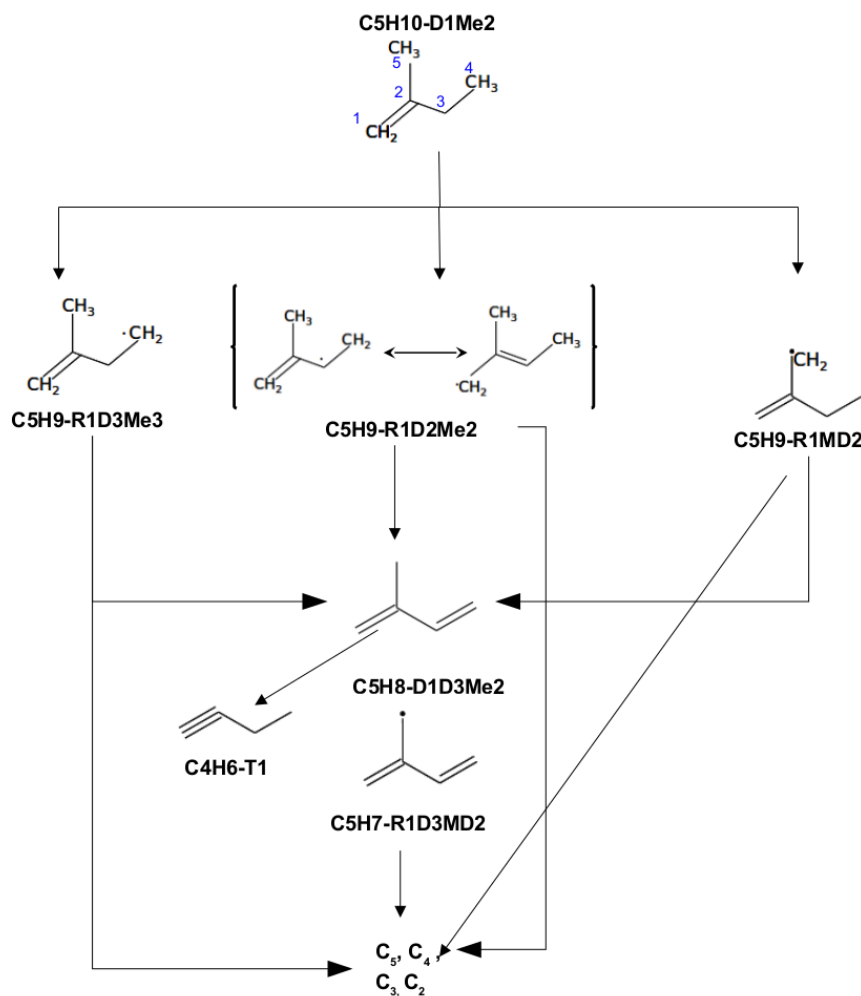


Figure 6.1: 2-Methyl-1-butene ($C_5H_{10}-D1Me2$), their considered alkenyl radicals and further possible decomposition channels added to the model.

2-Methyl-1-butene (see Figure 6.1) is a branched alkene with a C=C double bond in the first carbon, 5 allylic C-H bonds, 2 allylic C-H bonds and 3 C-H primary bonds. H-atom abstraction can take place at one of the allylic (3,5) carbon atoms forming two different radicals, namely 2-Methyl-But-1-en-4-yl ($C_5H_9-R1D3Me3$) and 2-Methyl-But-1-en ($C_5H_9-R1MD2$), or it can take place at the primary (4) carbon atom forming the resonantly stabilized radical 2-Methyl-But-2-en-1-yl ($C_5H_9-R1D2Me2$). In reality, each resonance-stabilized species

has an equivalent mesomeric form. For the development of this model, it is assumed that each pair is one species. Westbrook et al. (2015) [120] implemented a similar methodology for the development of a 2-Methyl-2-butene high and low temperature mechanism.

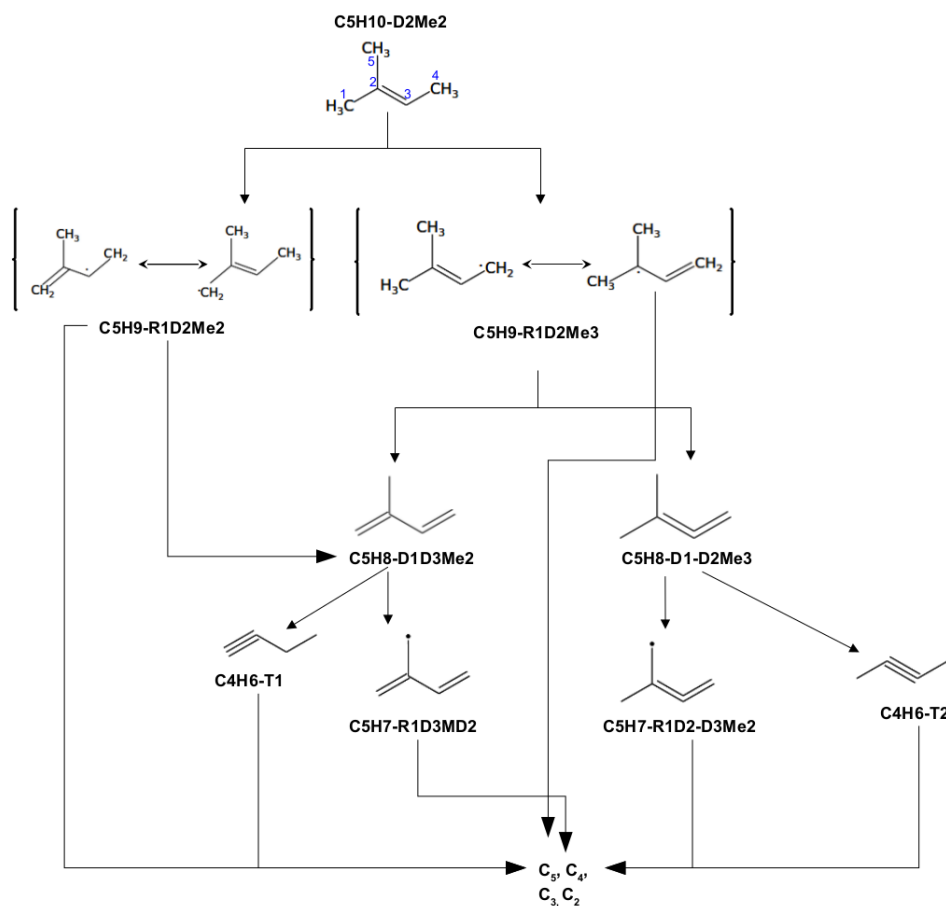


Figure 6.2: 2-Methyl-2-butene ($C_5H_{10}-D_2Me_2$), their considered alkenyl radicals and further possible decomposition channels added to the model.

For 2-Methyl-2-butene (see Figure 6.2), a branched alkene with a C=C double bond in the second carbon, 9 allylic C-H bonds, and one allylic C-H bond. H-atom abstraction can take place at one of the allylic (1,4,5) carbon atoms where resonant stabilized species, $C_5H_9-R_1D_2Me_2$ and 2-Methyl-But-2-en-4-yl ($C_5H_9-R_1D_2Me_3$), may be formed. 3-Methyl-1-butene (see Figure 6.3) has a C=C double bond in the first carbon, a C-H allylic bond, 3 C-H vinylic bonds, and 6 C-H primary bonds. Two different radicals via H-atom abstraction can be formed, namely 3-Methyl-But-1-en-4-yl ($C_5H_9-R_1D_3Me_2$) and ($C_5H_9-R_1D_2Me_3$). C_5H_9 radicals via another H-atom abstraction may form branched dienes such as 2-Methyl-1,3-diene ($C_5H_8-D_1D_3Me_2$) and/ or 2-Methyl-2,3-diene

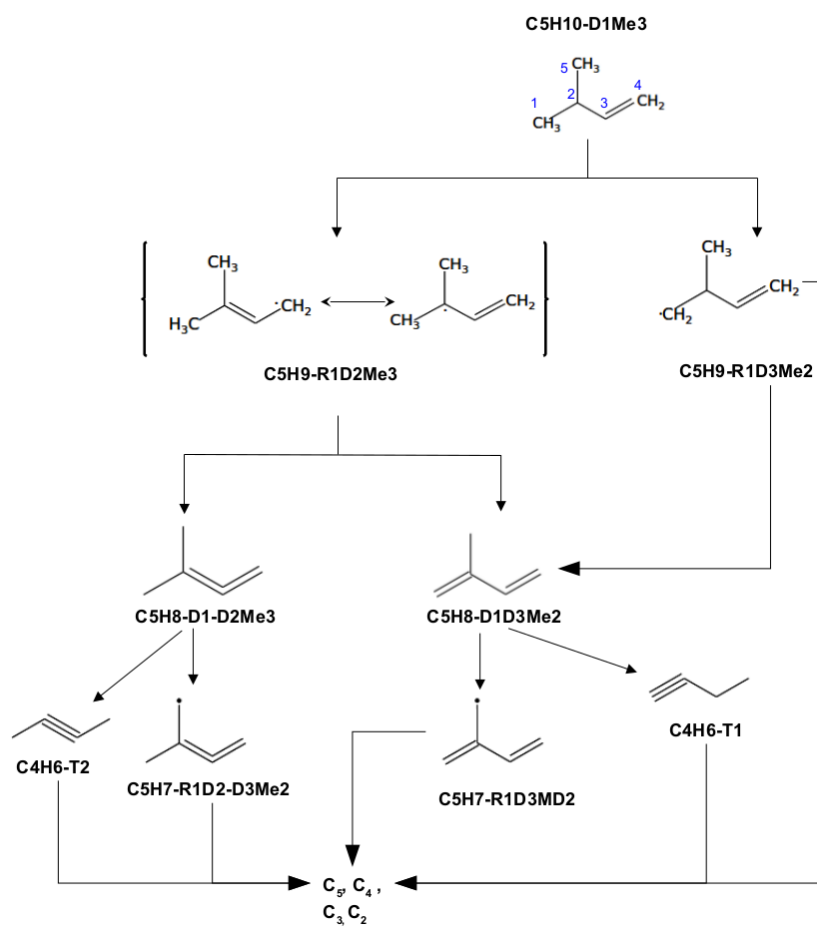


Figure 6.3: *3-Methyl-1-butene (C₅H₁₀-D₁Me₃), their considered alkenyl radicals and further possible decomposition channels added to the model.*

(C5H8-D1-D2Me3). C₅H₈ branched dienes via another H-atom abstraction may form different isomers for branched C₅H₇ radicals (C5H7-R1D3MD2 and C5H7-R1D2-D3Me2).

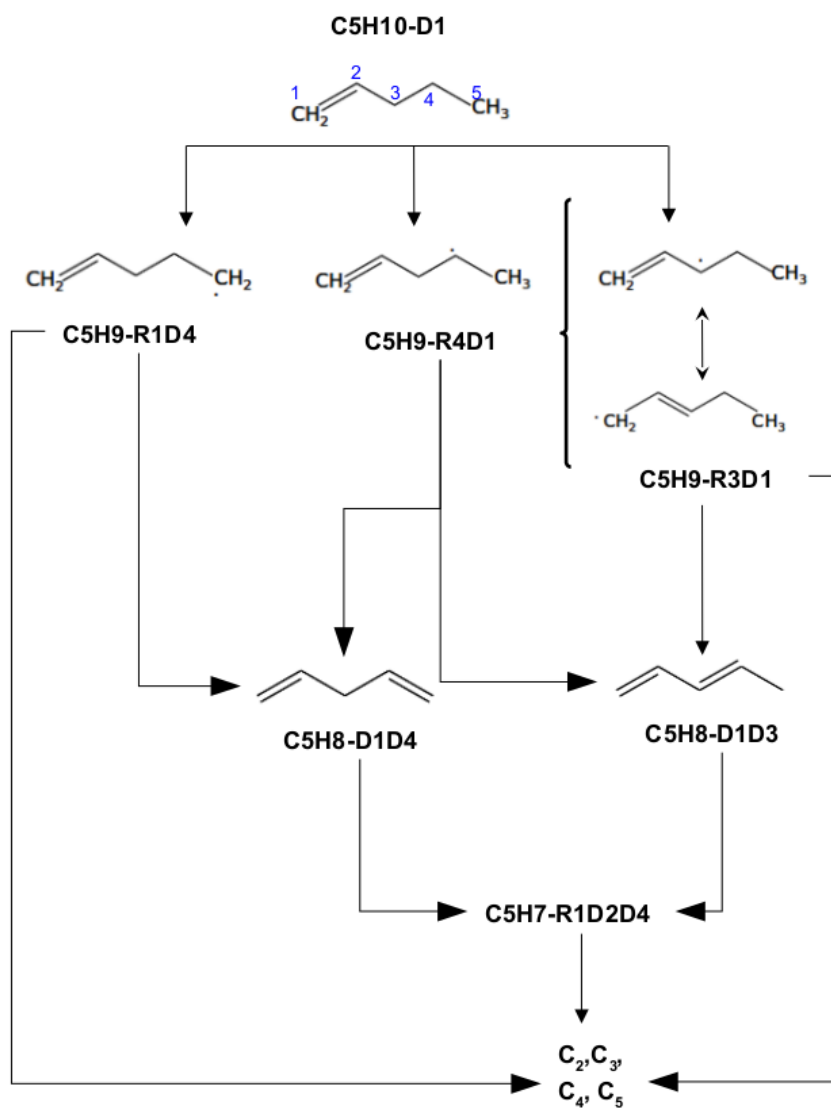


Figure 6.4: *n*-Pentene (C₅H₁₀-D1), their considered alkenyl radicals and further possible decomposition channels added to the model.

Structures regarding linear isomers, n-pentene (C₅H₁₀-D1) and cis-2-pentene (C₅H₁₀-D2), their alkenyl radicals, and C₅H₈ dienes are shown in Figure 6.4 and 6.5. n-pentene may form three different radicals: 1-Penten-3-yl (C₅H₉-R3D1), 1-Penten-4-yl (C₅H₉-R4D1), and 1-Penten-5-yl (C₅H₉-R1D4). H-atom

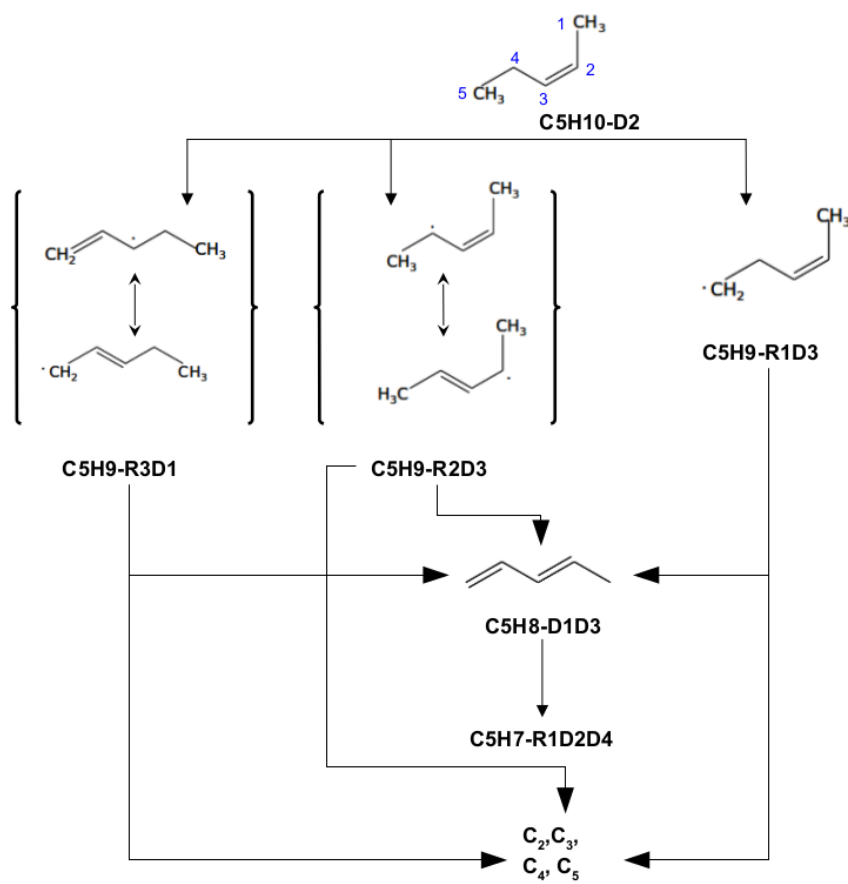


Figure 6.5: *cis*-2-Pentene (C_5H_{10} -D2), their considered alkenyl radicals initiated by H-atom abstraction and further possible decomposition channels added to the model.

abstraction may occur at one allylic (3) carbon, two secondary (4) carbon atoms and 3 primary (5) carbon atoms. C₅H₉-R3D1 resonant stabilized radical may also be produced via H-abstraction from cis-2-pentene along with two other radicals: 2-Penten-4-yl (C₅H₉-R2D3), and 2-Penten-5-yl (C₅H₉-R1D3). C₅H₉ radicals via another H-atom abstraction may result in linear di-enes such as 1,3-Pentadiene (C₅H₈-D1D3) and 1,4-Pentadiene (C₅H₈-D1D4). C₅H₇-R1D2D4 radical may be formed via another H-atom abstraction from the C₅H₈ linear species.

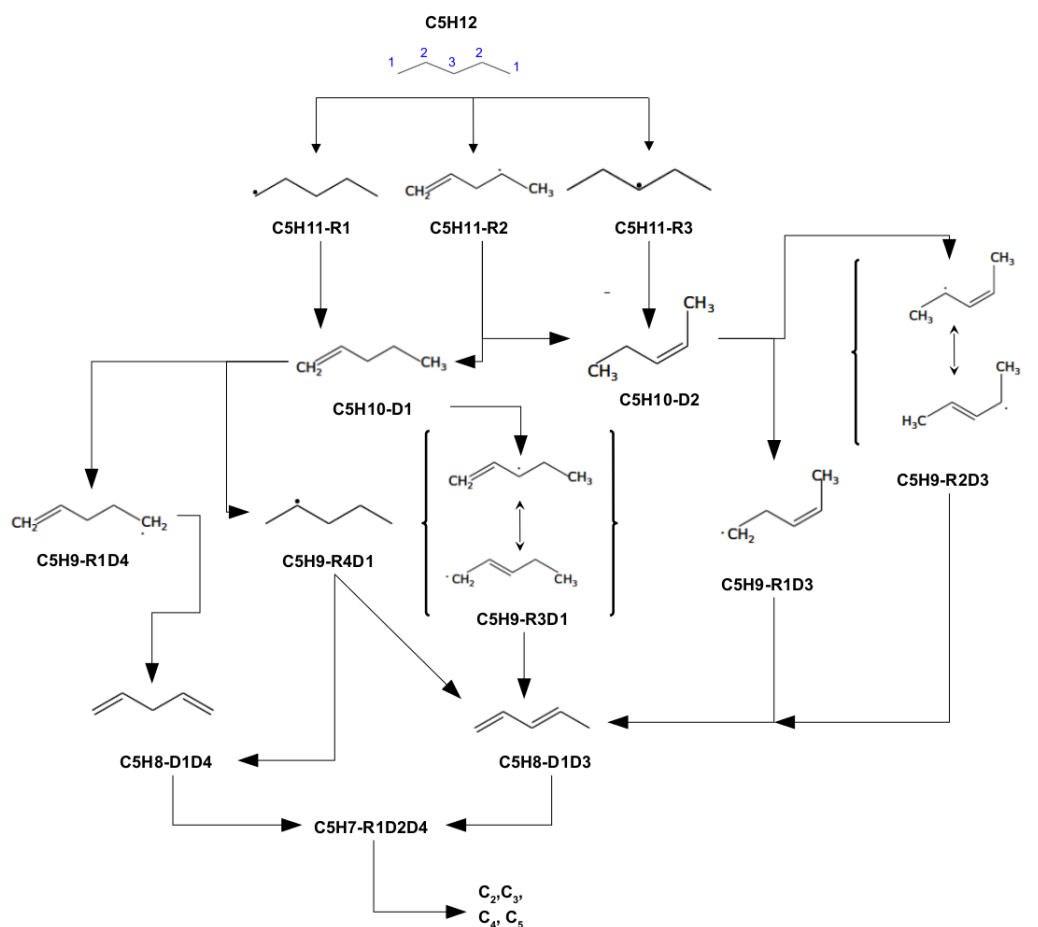


Figure 6.6: *n*-Pentane (C₅H₁₂), their considered alkyl radicals and further possible decomposition channels added to the model.

Figure 6.6 shows the decomposition pathways for *n*-Pentane. The H-atom abstraction can take place in carbon 1, 2 or 3, which leads to the formation of 1-Pentanyl (C₅H₁₁-R1), 2-Pentanyl (C₅H₁₁-R2) or/and 3-Pentanyl (C₅H₁₁-R3). 1-Pentanyl (C₅H₁₁-R1) may form *n*-pentene (C₅H₁₀-D1). 3-Pentanyl (C₅H₁₁-R3) may form *cis*-2-pentene (C₅H₁₀-D2) while 2-Pentanyl (C₅H₁₁-R2) may form both isomers. C₅H₁₀ radicals form five different linear C₅H₉

species (4-Penten-1-yl (C5H9-R1D4), 1-Penten-4-yl (C5H9-R4D1), 1-Penten-3-yl (C5H9-R3D1), 3-Penten-1-yl (C5H9-R1D3) and 3-penten-2-yl (C5H9-R2D3) via subsequent H-atom abstraction. Subsequent decomposition pathways are similar to those discussed for n-pentene (C5H10-D1) and cis-2-pentene (C5H10-D2).

6.1 High temperature chemistry for n-Pentane (C5H12) and C₅H₁₀ isomers

Oxidation reactions were added following the well-established classes introduced by Curran et al. (1998) [104] with modifications as described in the chemical model section. Rate constants are expressed in the Arrhenius form (see eq. 2.19) with the units cm^3, mol, s, cal ; \Rightarrow indicates that only forward reaction is considered; \Leftrightarrow indicates that also the reverse reaction is considered, as well as the data to calculate the pressure dependency. f and b stand for forward and backward reactions.

Main consumption of the fuel may prefer the allylic abstraction route since the vinylic $C-H$ bond (110.7 kcal/mol) has an energy of 22 kcal/mol stronger than the allylic $C-H$ bond (88.8 kcal/mol) (see Blanksby et al. [145]). In this work, vinylic abstraction was not considered.

6.1.1 Class 1: Unimolecular fuel decomposition

For unimolecular fuel decomposition, the suggested rates from Mehl et al. (2008) [107] and Ahmed et al. (2007) [81] were applied with exceptions for reactions: C5H10-D2Me2 \Leftrightarrow CH3 + C4H7-R1D1Me2 and C5H10-D1 \Leftrightarrow C3H6-D1 + C2H4-D1, where the rates from the works of Cheng et al. 2017 [125] and Tsang 1987 [146] were implemented. Tables 6.1 and 6.2 show reaction rates corresponding to the linear and branched isomers while table 6.3 shows the rates corresponding to n-Pentane.

Reactions	A	n	E_a	Ref
C5H10-D1 \Leftrightarrow C2H3-R1D1 + C3H7-R1	5.012E+16	0.00	8.200E+04	[107]
C5H10-D1 \Leftrightarrow C3H5-R1D2 + C2H5-R1	1.000E+16	0.00	7.100E+04	[107]
C5H10-D1 \Leftrightarrow C3H6-D1 + C2H4-D1	3.160E+12	0.00	5.740E+04	[146]
C5H10-D1 \Leftrightarrow C4H7-R1D3 + CH3	2.580E+16	0.00	8.450E+04	[107], ^a
C5H10-D2 \Leftrightarrow C4H7-R2D2 + CH3	5.012E+16	0.00	8.400E+04	[107]
C5H10-D2 \Leftrightarrow C3H6-D1 + C2H4-D1	1.000E+16	0.00	7.100E+04	[107]
C5H10-D1 \Leftrightarrow H + C5H9-R3D1	1.995E+15	0.00	8.200E+04	[107]
C5H10-D1 \Leftrightarrow H + C5H9-R4D1	2.500E+27	-3.80	9.710E+04	[81]
C5H10-D1 \Leftrightarrow H + C5H9-R1D4	2.500E+27	-3.80	9.710E+04	[81]
C5H10-D2 \Leftrightarrow H + C5H9-R1D3	2.500E+27	-3.80	9.710E+04	[81]
C5H10-D2 \Leftrightarrow H + C5H9-R2D3	1.995E+15	0.00	8.200E+04	[107]
C5H10-D2 \Leftrightarrow H + C5H9-R3D1	1.995E+15	0.00	8.400E+04	[107]

Table 6.1: Unimolecular fuel decomposition for n-Pentene (C5H10-D1), and cis-2-Pentene (C5H10-D2) oxidation. ^a: the pre-exponential factor was decreased by factor 2.

Reactions	A	n	E_a	Ref
C5H10-D1Me2 \rightleftharpoons CH3 + C4H7-R1D2Me2	5.012E+16	0.00	8.100E+04	[107]
C5H10-D1Me2 \rightleftharpoons C2H5-R1 + C3H5-R2D1	5.012E+16	0.00	8.200E+04	[107]
C5H10-D2Me2 \rightleftharpoons CH3 + C4H7-R1D1Me2	7.100E+91	-22.8	1.340E+05	[125]
PLOG/ 1.00E-01	6.30E+93	-23.0	134000.0 /	
PLOG/ 1.00E+00	3.38E+93	-22.5	138000.0 /	
PLOG/ 3.50E+00	1.57E+90	-21.4	138000.0 /	
PLOG/ 1.00E+01	4.60E+85	-19.9	136000.0 /	
PLOG/ 3.50E+01	3.03E+78	-17.8	133000.0 /	
PLOG/ 1.00E+02	2.44E+71	-15.7	130000.0 /	
C5H10-D2Me2 \rightleftharpoons CH3 + C4H7-R2D2	1.024E+17	0.00	8.450E+04	[107], ^a
C5H10-D1Me3 \rightleftharpoons CH3 + C4H7-R2D2	1.000E+16	0.00	7.300E+04	[107]
C5H10-D1Me3 \rightleftharpoons C2H3-R1D1 + C3H7-R2	5.012E+16	0.00	8.200E+04	[107]
C5H10-D1Me2 \rightleftharpoons H + C5H9-R1D3Me3	2.500E+27	-3.80	9.708E+04	[81]
C5H10-D1Me2 \rightleftharpoons H + C5H9-R1D2Me2	1.995E+15	0.00	8.200E+04	[107]
C5H10-D1Me2 \rightleftharpoons H + C5H9-R1MD2	1.995E+15	0.00	8.400E+04	[107]
C5H10-D2Me2 \rightleftharpoons H + C5H9-R1D2Me3	1.995E+15	0.00	8.400E+04	[107]
C5H10-D2Me2 \rightleftharpoons H + C5H9-R1D2Me2	1.995E+15	0.00	8.400E+04	[107], ^a
C5H10-D1Me3 \rightleftharpoons H + C5H9-R1D3Me2	2.500E+27	-3.80	9.708E+04	[81]
C5H10-D1Me3 \rightleftharpoons H + C5H9-R1D2Me3	2.500E+27	-3.80	9.708E+04	[81]

Table 6.2: Unimolecular fuel decomposition for 2-Methyl-1-butene (C5H10-D1Me2), 2-Methyl-2-butene (C5H10-D2Me2), and 3-Methyl-1-butene (C5H10-D1Me3). ^a: pre-exponential factor increased by factor 2.

C5H12=C2H5-R1+C3H7-R1	1.000E+28	-3.80	9.011E+04	[81]
C5H12=CH3+C4H9-R1	1.000E+28	-3.80	9.011E+04	[81]
C5H12=H+C5H11-R1	2.500E+27	-3.80	9.708E+04	^a
C5H12=H+C5H11-R2	2.500E+27	-3.80	9.708E+04	^b
C5H12=H+C5H11-R3	2.500E+27	-3.80	9.708E+04	^c

Table 6.3: Unimolecular fuel decomposition for n-Pentane (C5H12). ^a: the pre-exponential factor [81] was multiplied by 6, ^b: the pre-exponential factor [81] was multiplied by 4, ^c: the pre-exponential factor [81] was multiplied by 2.

6.1.2 Class 2: H-atom abstraction from fuel

Reaction rates for linear and branched C₅H₁₀ species are presented in tables 6.4 to 6.8 and for n-Pentane in 6.9. For H-atom abstraction from the fuel molecule in primary and secondary positions, the rates from Ahmed et al. (2007) [81] were applied. For H-atom abstraction from the fuel molecule in tertiary position, the rates from Curran et al. 2002 [77] were applied. A correction for the allylic position has been taken into account as discussed in the previous chapter. The correction is based on the work of Mehl et al. 2008 [107]. For the allylic site, the activation energy applied was 2000 *cal/mol* lower than the one used for the secondary radical formation. A similar analogy is followed for the abstraction in the primary position. A table containing primary, secondary, and allylic reaction rates for this type of reactions can be found in table A.1 from the appendix as a reference. The pre-exponential factor has been multiplied by the number of H-atoms that can be abstracted from each carbon.

Reactions	A	n	E_a	Ref
C5H10-D1 + H \rightleftharpoons H2 + C5H9-R1D4	1.689E+08	2.00	7.713E+03	[81]
C5H10-D1 + H \rightleftharpoons H2 + C5H9-R4D1	4.900E+07	2.00	5.007E+03	[81]
C5H10-D1 + H \rightleftharpoons H2 + C5H9-R3D1	4.900E+07	2.00	3.007E+03	[81], ^a
C5H10-D1 + OH \rightleftharpoons H2O + C5H9-R1D4	5.250E+09	0.97	1.578E+03	[81]
C5H10-D1 + OH \rightleftharpoons H2O + C5H9-R4D1	4.680E+07	1.61	-3.589E+01	[81]
C5H10-D1 + OH \rightleftharpoons H2O + C5H9-R3D1	4.680E+07	1.61	-2.036E+03	[81], ^a
C5H10-D1 + O \rightleftharpoons OH + C5H9-R1D4	1.980E+06	2.40	5.512E+03	[81]
C5H10-D1 + O \rightleftharpoons OH + C5H9-R4D1	2.360E+05	2.50	2.203E+03	[81]
C5H10-D1 + O \rightleftharpoons OH + C5H9-R3D1	2.360E+05	2.50	2.033E+02	[81], ^a
C5H10-D1 + CH3 \rightleftharpoons CH4 + C5H9-R1D4	8.130E+11	0.00	1.162E+04	[81]
C5H10-D1 + CH3 \rightleftharpoons CH4 + C5H9-R4D1	4.000E+11	0.00	9.514E+03	[81]
C5H10-D1 + CH3 \rightleftharpoons CH4 + C5H9-R3D1	4.000E+11	0.00	7.514E+03	[81], ^a
C5H10-D1 + O2 \rightleftharpoons C5H9-R1D4 + HO2	1.251E+13	0.00	4.903E+04	[81]
C5H10-D1 + O2 \rightleftharpoons C5H9-R4D1 + HO2	2.000E+13	0.00	4.768E+04	[81]
C5H10-D1 + O2 \rightleftharpoons C5H9-R3D1 + HO2	2.000E+13	0.00	4.568E+04	[81], ^a
C5H10-D1 + HO2 \rightleftharpoons C5H9-R1D4 + H2O2	8.040E+12	0.00	1.941E+04	[81]
C5H10-D1 + HO2 \rightleftharpoons C5H9-R4D1 + H2O2	4.880E+12	0.00	1.703E+04	[81]
C5H10-D1 + HO2 \rightleftharpoons C5H9-R3D1 + H2O2	4.880E+12	0.00	1.503E+04	[81], ^a
C5H10-D1 + CH3O2 \rightleftharpoons C5H9-R1D4 + CH3O2H	6.060E+12	0.00	2.046E+04	[81]
C5H10-D1 + CH3O2 \rightleftharpoons C5H9-R4D1 + CH3O2H	4.040E+12	0.00	1.773E+04	[81]
C5H10-D1 + CH3O2 \rightleftharpoons C5H9-R3D1 + CH3O2H	4.040E+12	0.00	1.573E+04	[81], ^a
C5H10-D1 + CH3O \rightleftharpoons C5H9-R1D4 + CH3OH	1.581E+11	0.00	7.005E+03	[81]
C5H10-D1 + CH3O \rightleftharpoons C5H9-R4D1 + CH3OH	1.096E+11	0.00	5.007E+03	[81]
C5H10-D1 + CH3O \rightleftharpoons C5H9-R3D1 + CH3OH	1.096E+11	0.00	3.007E+03	[81], ^a

Table 6.4: *H*-atom abstraction for *n*-Pentene (C5H10-D1). ^a: allyl correction for activation energy.

Reactions	A	n	E_a	Ref
C5H10-D2 + H \rightleftharpoons H2 + C5H9-R1D3	1.689E+08	2.00	7.713E+03	[81]
C5H10-D2 + H \rightleftharpoons H2 + C5H9-R2D3	4.900E+07	2.00	3.007E+03	[81], ^a
C5H10-D2 + H \rightleftharpoons H2 + C5H9-R3D1	1.689E+08	2.00	5.713E+03	[81], ^a
C5H10-D2 + OH \rightleftharpoons H2O + C5H9-R1D3	5.270E+09	0.97	1.586E+03	[81]
C5H10-D2 + OH \rightleftharpoons H2O + C5H9-R2D3	4.680E+07	1.61	-2.036E+03	[81], ^a
C5H10-D2 + OH \rightleftharpoons H2O + C5H9-R3D1	5.270E+09	1.61	-4.14E+02	[81], ^a
C5H10-D2 + O \rightleftharpoons OH + C5H9-R1D3	1.980E+06	2.40	5.512E+03	[81]
C5H10-D2 + O \rightleftharpoons OH + C5H9-R2D3	2.360E+05	2.50	2.033E-01	[81], ^a
C5H10-D2 + O \rightleftharpoons OH + C5H9-R3D1	1.980E+06	2.50	3.512E+03	[81], ^a
C5H10-D2 + CH3 \rightleftharpoons CH4 + C5H9-R1D3	8.130E+11	0.00	1.162E+04	[81]
C5H10-D2 + CH3 \rightleftharpoons CH4 + C5H9-R2D3	4.000E+11	0.00	7.514E+03	[81], ^a
C5H10-D2 + CH3 \rightleftharpoons CH4 + C5H9-R3D1	8.130E+11	0.00	9.620E+04	[81]
C5H10-D2 + O2 \rightleftharpoons C5H9-R1D3 + HO2	1.251E+13	0.00	4.903E+04	[81]
C5H10-D2 + O2 \rightleftharpoons C5H9-R2D3 + HO2	2.000E+13	0.00	4.568E+04	[81], ^a
C5H10-D2 + O2 \rightleftharpoons C5H9-R3D1 + HO2	1.251E+13	0.00	4.703E+04	[81], ^a
C5H10-D2 + HO2 \rightleftharpoons C5H9-R1D3 + H2O2	8.040E+12	0.00	1.941E+04	[81]
C5H10-D2 + HO2 \rightleftharpoons C5H9-R2D3 + H2O2	4.880E+12	0.00	1.503E+04	[81], ^a
C5H10-D2 + HO2 \rightleftharpoons C5H9-R3D1 + H2O2	8.040E+12	0.00	1.741E+04	[81], ^a
C5H10-D2 + CH3O2 \rightleftharpoons C5H9-R1D3 + CH3O2H	6.060E+12	0.00	2.046E+04	[81]
C5H10-D2 + CH3O2 \rightleftharpoons C5H9-R2D3 + CH3O2H	4.040E+12	0.00	1.573E+04	[81], ^a
C5H10-D2 + CH3O2 \rightleftharpoons C5H9-R3D1 + CH3O2H	6.060E+12	0.00	1.846E+04	[81], ^a
C5H10-D2 + CH3O \rightleftharpoons C5H9-R1D3 + CH3OH	1.581E+11	0.00	7.005E+03	[81]
C5H10-D2 + CH3O \rightleftharpoons C5H9-R2D3 + CH3OH	1.096E+11	0.00	3.007E+03	[81], ^a
C5H10-D2 + CH3O \rightleftharpoons C5H9-R3D1 + CH3OH	1.581E+11	0.00	5.005E+03	[81], ^a

Table 6.5: *H*-atom abstraction for *cis*-2-Pentene (C5H10-D2). ^a: allyl correction for activation energy.

Reactions	A	n	E_a	Ref
C5H10-D1Me2 + H <=> C5H9-R1D3Me3 + H2	1.689E+08	2.00	7.713E+03	[81]
C5H10-D1Me2 + H <=> C5H9-R1D2Me2 + H2	4.900E+07	2.00	3.007E+03	[81], ^a
C5H10-D1Me2 + H <=> C5H9-R1MD2 + H2	1.689E+08	2.00	5.713E+03	[81], ^a
C5H10-D1Me2 + OH <=> C5H9-R1D3Me3 + H2O	5.250E+09	0.97	1.578E+03	[81]
C5H10-D1Me2 + OH <=> C5H9-R1D2Me2 + H2O	4.680E+07	1.61	-2.036E+03	[81], ^a
C5H10-D1Me2 + OH <=> C5H9-R1MD2 + H2O	5.250E+09	0.97	-4.220E+02	[81], ^a
C5H10-D1Me2 + O <=> C5H9-R1D3Me3 + OH	1.980E+06	2.40	5.512E+03	[81]
C5H10-D1Me2 + O <=> C5H9-R1D2Me2 + OH	2.360E+05	2.50	2.033E-01	[81], ^a
C5H10-D1Me2 + O <=> C5H9-R1MD2 + OH	1.980E+06	2.40	3.512E+03	[81], ^a
C5H10-D1Me2 + CH3 <=> C5H9-R1D3Me3 + CH4	8.130E+11	0.00	1.162E+04	[81]
C5H10-D1Me2 + CH3 <=> C5H9-R1D2Me2 + CH4	4.000E+11	0.00	7.514E+03	[81], ^a
C5H10-D1Me2 + CH3 <=> C5H9-R1MD2 + CH4	8.130E+11	0.00	9.620E+03	[81], ^a
C5H10-D1Me2 + O2 <=> C5H9-R1D3Me3 + HO2	1.251E+13	0.00	4.908E+04	[81]
C5H10-D1Me2 + O2 <=> C5H9-R1D2Me2 + HO2	2.000E+13	0.00	4.568E+04	[81], ^a
C5H10-D1Me2 + O2 <=> C5H9-R1MD2 + HO2	1.251E+13	0.00	4.708E+04	[81], ^a
C5H10-D1Me2 + HO2 <=> C5H9-R1D3Me3 + H2O2	8.040E+12	0.00	1.162E+04	[81]
C5H10-D1Me2 + HO2 <=> C5H9-R1D2Me2 + H2O2	4.880E+12	0.00	1.503E+04	[81], ^a
C5H10-D1Me2 + HO2 <=> C5H9-R1MD2 + H2O2	8.040E+12	0.00	9.620E+03	[81], ^a
C5H10-D1Me2 + CH3O2 <=> C5H9-R1D3Me3 + CH3O2H	6.060E+12	0.00	2.046E+04	[81]
C5H10-D1Me2 + CH3O2 <=> C5H9-R1D2Me2 + CH3O2H	4.040E+12	0.00	1.573E+04	[81], ^a
C5H10-D1Me2 + CH3O2 <=> C5H9-R1MD2 + CH3O2H	6.060E+12	0.00	1.846E+04	[81], ^a
C5H10-D1Me2 + CH3O <=> C5H9-R1D3Me3 + CH3OH	1.581E+11	0.00	7.012E+03	[81]
C5H10-D1Me2 + CH3O <=> C5H9-R1D2Me2 + CH3OH	2.000E+13	0.00	4.568E+04	[81], ^a
C5H10-D1Me2 + CH3O <=> C5H9-R1D2Me2 + CH3OH	1.581E+11	0.00	5.012E+03	[81], ^a

Table 6.6: *H*-atom abstraction for 2-Methyl-1-butene (C5H10-D1Me2).^a: allyl correction for activation energy.

Reactions	A	n	E_a	Ref
C5H10-D2Me2 + H <=> C5H9-R1D2Me3 + H2	1.689E+08	2.00	5.713E+03	[81], ^a
C5H10-D2Me2 + H <=> C5H9-R1D2Me2 + H2	3.378E+08	2.00	5.713E+03	[81], ^a
C5H10-D2Me2 + OH <=> C5H9-R1D2Me3 + H2O	5.250E+09	0.97	-4.220E+02	[81], ^a
C5H10-D2Me2 + OH <=> C5H9-R1D2Me2 + H2O	1.050E+10	0.97	-4.220E+02	[81], ^a
C5H10-D2Me2 + O <=> C5H9-R1D2Me3 + OH	1.980E+06	2.40	3.512E+03	[81], ^a
C5H10-D2Me2 + O <=> C5H9-R1D2Me2 + OH	3.960E+06	2.40	3.512E+03	[81], ^a
C5H10-D2Me2 + CH3 <=> C5H9-R1D2Me3 + CH4	8.130E+11	0.00	9.620E+03	[81], ^a
C5H10-D2Me2 + CH3 <=> C5H9-R1D2Me2 + CH4	1.626E+12	0.00	9.620E+03	[81], ^a
C5H10-D2Me2 + O2 <=> C5H9-R1D2Me3 + HO2	1.251E+13	0.00	4.708E+04	[81], ^a
C5H10-D2Me2 + O2 <=> C5H9-R1D2Me2 + HO2	2.502E+13	0.00	4.708E+04	[81], ^a
C5H10-D2Me2 + HO2 <=> C5H9-R1D2Me3 + H2O2	8.040E+12	0.00	9.620E+03	[81], ^a
C5H10-D2Me2 + HO2 <=> C5H9-R1D2Me2 + H2O2	1.608E+13	0.00	9.620E+03	[81], ^a
C5H10-D2Me2 + CH3O2 <=> C5H9-R1D2Me3 + CH3O2H	6.060E+12	0.00	1.846E+04	[81], ^a
C5H10-D2Me2 + CH3O2 <=> C5H9-R1D2Me2 + CH3O2H	6.060E+12	0.00	1.846E+04	[81], ^a
C5H10-D2Me2 + CH3O <=> C5H9-R1D2Me3 + CH3OH	1.581E+11	0.00	5.012E+03	[81], ^a
C5H10-D2Me2 + CH3O <=> C5H9-R1D2Me2 + CH3OH	3.162E+11	0.00	5.012E+03	[81], ^a

Table 6.7: *H*-atom abstraction for 2-Methyl-2-butene (C5H10-D2Me2). ^a: allyl correction for activation energy.

Reactions	A	n	E_a	Ref
C5H10-D1Me3 + H <=> C5H9-R1D3Me2 + H2	1.689E+08	2.00	7.713E+03	[81]
C5H10-D1Me3 + H <=> C5H9-R1D2Me3 + H2	6.020E+05	2.40	0.583E+03	[77], ^a
C5H10-D1Me3 + OH <=> C5H9-R1D3Me2 + H2O	5.250E+09	0.97	1.578E+03	[81]
C5H10-D1Me3 + OH <=> C5H9-R1D2Me3 + H2O	1.700E+06	1.90	-3.451E+02	[77], ^a
C5H10-D1Me3 + O <=> C5H9-R1D3Me2 + OH	1.980E+06	2.40	5.512E+03	[81]
C5H10-D1Me3 + O <=> C5H9-R1D2Me3 + OH	3.830E+05	2.41	-1.107E+03	[77], ^a
C5H10-D1Me3 + CH3 <=> C5H9-R1D3Me2 + CH4	8.130E+11	0.00	1.162E+04	[81]
C5H10-D1Me3 + CH3 <=> C5H9-R1D2Me3 + CH4	8.960E+03	2.33	4.147E+03	[77], ^a
C5H10-D1Me3 + O2 <=> C5H9-R1D3Me2 + HO2	1.251E+13	0.00	4.908E+04	[81]
C5H10-D1Me3 + O2 <=> C5H9-R1D2Me3 + HO2	7.000E+12	0.00	4.406E+04	[77], ^a
C5H10-D1Me3 + HO2 <=> C5H9-R1D3Me2 + H2O2	8.040E+12	0.00	1.162E+04	[81]
C5H10-D1Me3 + HO2 <=> C5H9-R1D2Me3 + H2O2	2.800E+12	0.00	1.401E+04	[77], ^a
C5H10-D1Me3 + CH3O2 <=> C5H9-R1D3Me2 + CH3O2H	6.060E+12	0.00	2.046E+04	[81]
C5H10-D1Me3 + CH3O2 <=> C5H9-R1D2Me3 + CH3O2H	2.800E+12	0.00	1.401E+04	[77], ^a
C5H10-D1Me3 + CH3O <=> C5H9-R1D3Me2 + CH3OH	1.581E+11	0.00	7.012E+03	[81]
C5H10-D1Me3 + CH3O <=> C5H9-R1D2Me3 + CH3OH	1.900E+10	0.00	8.000E+02	[77], ^a

Table 6.8: *H*-atom abstraction for 3-Methyl-1-butene (C5H10-D1Me3). ^a: allyl correction for activation energy.

Reactions	A	n	E_a	Ref
C2H3-R1D1+C5H12=C5H11-R1+C2H4-D1	1.002E+12	0.00	1.802E+04	^a
C2H3-R1D1+C5H12=C5H11-R2+C2H4-D1	8.000E+11	0.00	1.681E+04	^b
C2H3-R1D1+C5H12=C5H11-R3+C2H4-D1	4.000E+11	0.00	1.682E+04	^c
C2H5-R1+C5H12=C5H11-R1+C2H6	1.002E+11	0.00	1.342E+04	^a
C2H5-R1+C5H12=C5H11-R2+C2H6	1.000E+11	0.00	1.042E+04	^b
C2H5-R1+C5H12=C5H11-R3+C2H6	5.000E+10	0.00	1.042E+04	^c
CH3+C5H12=C5H11-R1+CH4	1.302E+12	0.00	1.161E+04	^a
CH3+C5H12=C5H11-R2+CH4	8.000E+11	0.00	9.505E+03	^b
CH3+C5H12=C5H11-R3+CH4	4.000E+11	0.00	9.505E+03	^c
CH3O+C5H12=C5H11-R1+CH3OH	3.162E+11	0.00	7.005E+03	^a
CH3O+C5H12=C5H11-R2+CH3OH	2.192E+12	0.00	5.002E+03	^b
CH3O+C5H12=C5H11-R3+CH3OH	1.096E+12	0.00	5.002E+03	^c
CH3O2+C5H12=C5H11-R1+CH3O2H	1.212E+13	0.00	2.044E+04	^a
CH3O2+C5H12=C5H11-R2+CH3O2H	8.080E+12	0.00	1.771E+04	^b
CH3O2+C5H12=C5H11-R3+CH3O2H	4.040E+12	0.00	1.771E+04	^c
H+C5H12=C5H11-R1+H2	3.378E+08	2.00	7.710E+03	^a
H+C5H12=C5H11-R2+H2	9.800E+07	2.00	5.005E+03	!4*AHM0
H+C5H12=C5H11-R3+H2	4.900E+07	2.00	5.002E+03	^c
HO2+C5H12=C5H11-R1+H2O2	1.608E+13	0.00	1.966E+04	^a
HO2+C5H12=C5H11-R2+H2O2	9.760E+12	0.00	1.702E+04	^b
HO2+C5H12=C5H11-R3+H2O2	4.880E+12	0.00	1.702E+04	^c
O+C5H12=C5H11-R1+OH	2.196E+06	2.40	5.507E+03	^a
O+C5H12=C5H11-R2+OH	4.720E+05	2.50	2.201E+03	^b
O+C5H12=C5H11-R3+OH	2.360E+05	2.50	2.201E+03	^c
O2+C5H12=C5H11-R1+HO2	2.502E+13	0.00	4.905E+04	^a
O2+C5H12=C5H11-R2+HO2	4.000E+13	0.00	4.761E+04	^b
O2+C5H12=C5H11-R3+HO2	2.000E+13	0.00	4.764E+04	^c
OH+C5H12=C5H11-R1+H2O	1.050E+10	0.97	1.592E+03	^a
OH+C5H12=C5H11-R2+H2O	9.360E+07	1.61	-3.585E+01	^b
OH+C5H12=C5H11-R3+H2O	4.680E+07	1.61	-3.585E+01	^c

Table 6.9: *H*-atom abstraction for *n*-Pentane (C5H12). ^a: the pre-exponential factor [81] was multiplied by 6, ^b: the pre-exponential factor [81] was multiplied by 4, ^c: the pre-exponential factor [81] was multiplied by 2.

6.1.3 Class 3: Alkyl and alkenyl radical decomposition

For alkenyl decomposition, the rates of Mehl et al. (2008) [107] were applied (see tables 6.10 and 6.11). Branched alkyl radicals follow the recommendation of Ahmed et al. (2007) [81] and the linear alkyl radicals: pent-1-yl (C5H11-R1), pent-2-yl (C5H11-R2), and pent-3-yl (C5H11-R3) follow the recommendation of Comandini et al. (2012) [147] presented in tables 6.12 and 6.13, respectively.

Reactions	A	n	E_a	Ref
C5H9-R1D4 \rightleftharpoons C2H4-D1 + C3H5-R1D2	3.162E+13	0.00	3.500E+04	[107]
C5H9-R4D1 \rightleftharpoons C2H3-R1D1 + C3H6-D1	1.000E+14	0.00	3.100E+04	[107]
C5H9-R3D1 \rightleftharpoons C4H6-D1D3 + CH3	1.000E+13	0.00	3.750E+04	[107]
C5H9-R1D3 \rightleftharpoons C2H4-D1 + C3H5-R1D2	1.000E+14	0.00	3.000E+04	[107]
C5H9-R1D3 \rightleftharpoons C4H6-D1D3 + CH3	1.000E+14	0.00	3.250E+04	[107]
C5H9-R2D3 \rightleftharpoons C4H6-D1D3 + CH3	1.000E+13	0.00	3.750E+04	[107]
H + C5H8-D1D4 \rightleftharpoons C5H9-R1D4	3.160E+10	0.00	1.500E+03	[107]
H + C5H8-D1D3 \rightleftharpoons C5H9-R4D1	3.160E+10	0.00	1.500E+03	[107]
H + C5H8-D1D4 \rightleftharpoons C5H9-R4D1	3.160E+10	0.00	1.500E+03	[107]
H + C5H8-D1D3 \rightleftharpoons C5H9-R3D1	3.160E+10	0.00	1.500E+03	[107]
H + C5H8-D1D3 \rightleftharpoons C5H9-R1D3	3.160E+10	0.00	1.500E+03	[107]
H + C5H8-D1D3 \rightleftharpoons C5H9-R2D3	3.160E+10	0.00	1.500E+03	[107]

Table 6.10: Reaction rates for linear C_5H_9 alkenyl radical decomposition.

Reactions	A	n	E_a	Ref
C5H8-D1D3Me2 + H \rightleftharpoons C5H9-R1D2Me2	3.160E+10	0.00	1.500E+03	[107]
C5H8-D1D3Me2 + H \rightleftharpoons C5H9-R1D3Me3	3.160E+10	0.00	1.500E+03	[107]
C5H8-D1D3Me2 + H \rightleftharpoons C5H9-R1D2Me3	3.160E+10	0.00	1.500E+03	[107]
C5H8-D1D3Me2 + H \rightleftharpoons C5H9-R1D3Me2	3.160E+10	0.00	1.500E+03	[107]
C5H8-D1-D2Me3 + H \rightleftharpoons C5H9-R1D2Me3	6.320E+10	0.00	1.500E+03	[107]
C5H9-R1D3Me3 \rightleftharpoons C3H5-R2D1 + C2H4-D1	1.000E+14	0.00	2.850E+04	[107]
C5H9-R1D2Me2 \rightleftharpoons CH3 + C4H6-D1-D2	1.000E+13	0.00	3.750E+04	[107]
C5H9-R1MD2 \rightleftharpoons C2H5-R1 + C3H4-D1D2	1.000E+13	0.00	3.50E+04	[107]
C5H9-R1D3Me2 \rightleftharpoons CH3 + C4H6-D1D3	1.000E+14	0.00	3.000E+04	[107]
C5H9-R1D3Me2 \rightleftharpoons C2H3-R1D1 + C3H6-D1	1.000E+14	0.00	3.500E+04	[107]

Table 6.11: Reaction rates for branched C_5H_9 alkenyl radical decomposition.

Reactions	A	n	E_a	Ref
C5H11-R1Me3 \rightleftharpoons C2H4-D1 + C3H7-R2	8.500E+10	0.00	1.060E+04	[81]
C5H11-R2Me3 \rightleftharpoons CH3 + T-C4H8-D2	8.500E+10	0.00	7.800E+03	[81]
C5H11-R2Me2 \rightleftharpoons CH3 + C4H8-D1Me2	2.650E+10	1.19	3.020E+04	[88]
C5H11-R1Me2 \rightleftharpoons C2H5-R1 + C3H6-D1	4.250E+10	0.00	1.060E+04	[81]
C5H11-R1Me2 \rightleftharpoons C4H8-D1 + CH3	8.500E+10	0.00	7.800E+03	[81]
C5H10-D1Me2 + H \rightleftharpoons C5H11-R1Me2	1.000E+13	0.00	4.900E+03	[81]
C5H10-D1Me2 + H \rightleftharpoons C5H11-R2Me2	1.000E+13	0.00	1.200E+03	[81]
C5H10-D2Me2 + H \rightleftharpoons C5H11-R2Me2	2.500E+13	0.00	2.900E+03	[81]
C5H10-D2Me2 + H \rightleftharpoons C5H11-R2Me3	1.000E+13	0.00	4.900E+03	[81]
C5H10-D1Me3 + H \rightleftharpoons C5H11-R2Me3	1.000E+13	0.00	1.200E+03	[81]
C5H10-D1Me3 + H \rightleftharpoons C5H11-R1Me3	1.000E+13	0.00	2.900E+03	[81]

Table 6.12: Branched alkyl radical decomposition for branched C_5H_{11} radicals.

Reactions	A	n	E_a	Ref
C5H11-R1 \rightleftharpoons C2H4-D1 + C3H7-R1				[147]
PLOG/0.1	4.410E+03	2.192	1.883E+04	
PLOG/1.0	8.060E+20	-2.628	2.923E+04	
PLOG/10.0	2.170E+28	-4.578	3.486E+04	
PLOG/100.0	6.470E+24	-3.383	3.439E+04	
PLOG/ 1000.0	2.340E+17	-1.123	3.1176E+04	
C5H11-R1 \rightleftharpoons H + C5H10-D1				[147]
PLOG/0.1	3.240E-14	7.022	1.5354E+04	
PLOG/1.0	5.100E+12	-0.402	2.9991E+04	
PLOG/10.0	4.070E+27	-4.483	3.9814E+04	
PLOG/100.0	1.020E+26	-3.794	4.0806E+04	
PLOG/ 1000.0	6.520E+16	-0.987	3.6957E+04	
C5H11-R2 \rightleftharpoons C3H6-D1 + C2H5-R1				[147]
PLOG/0.1	8.540E+25	-4.241	3.1303E+04	
PLOG/1.0	2.340E+31	-5.581	3.5992E+04	
PLOG/10.0	4.630E+28	-4.592	3.6186E+04	
PLOG/100.0	3.770E+20	-2.108	3.2927E+04	
PLOG/ 1000.0	3.560E+14	-0.301	3.0124E+04	
C5H11-R2 \rightleftharpoons C5H10-D1 + H				[147]
PLOG/0.1	8.260E+10	-0.118	2.9715E+04	
PLOG/1.0	6.920E+26	-4.456	3.9997E+04	
PLOG/10.0	3.810E+29	-4.969	4.3662E+04	
PLOG/100.0	4.220E+20	-2.160	4.0523E+04	
PLOG/ 1000.0	5.050E+11	0.526	3.6461E+04	
C5H11-R2 \rightleftharpoons C5H10-D2 + H				[147]
PLOG/0.1	2.797E+13	-0.833	3.04227E+04	
PLOG/1.0	9.922E+27	-4.775	3.9987E+04	
PLOG/10.0	8.504E+29	-5.063	4.31506E+04	
PLOG/100.0	1.026E+21	-2.275	3.99532E+04	
PLOG/ 1000.0	3.141E+12	0.287	3.60682E+04	
C5H11-R3 \rightleftharpoons C4H8-D1 + CH3				[147]
PLOG/0.1	1.310E+16	-1.137	2.9671E+04	
PLOG/1.0	1.850E+25	-3.643	3.5787E+04	
PLOG/10.0	1.010E+24	-3.130	3.6363E+04	
PLOG/100.0	1.980E+16	-0.793	3.3017E+04	
PLOG/ 1000.0	2.100E+11	0.685	3.0583E+04	
C5H11-R3 \rightleftharpoons C5H10-D2 + H				[147]
PLOG/0.1	5.119E+06	1.511	2.91387E+04	
PLOG/1.0	4.068E+22	-2.949	3.87655E+04	
PLOG/10.0	2.298E+25	-3.569	4.177E+04	
PLOG/100.0	8.104E+16	-0.983	3.8322E+04	
PLOG/ 1000.0	1.214E+10	1.047	3.50087E+04	

Table 6.13: Alkyl radical decomposition for linear C_5H_{11} radicals.

6.1.4 Class 4: Alkenyl radical + O2 direct formation of di-olefin and HO2

This type of reaction results in direct formation of olefin and HO2. The reaction rates from Chakir et al. (1989) [106] were implemented in the model and are shown on tables 6.14 and 6.15 .

Reactions	A	n	E_a	Ref
C5H9-R1D2Me2 + O2 <=> C5H8-D1D3Me2 + HO2	2.500E+12	0.00	4.251E+03	^a
C5H9-R1D2Me3 + O2 <=> C5H8-D1-D2Me3 + HO2	2.500E+12	0.00	4.251E+03	^a
C5H9-R1D3Me2 + O2 <=> C5H8-D1D3Me2 + HO2	5.000E+12	0.00	4.251E+03	^a
C5H9-R1D3Me3 + O2 <=> C5H8-D1D3Me2 + HO2	5.000E+12	0.00	4.251E+03	^a
C5H9-R1D4 + O2 <=> C5H8-D1D4 + HO2	2.500E+12	0.00	4.251E+03	^a
C5H9-R4D1 + O2 <=> C5H8-D1D3 + HO2	2.500E+12	0.00	4.251E+03	^a
C5H9-R4D1 + O2 <=> C5H8-D1D4 + HO2	2.500E+12	0.00	4.251E+03	^a
C5H9-R3D1 + O2 <=> C5H8-D1D3 + HO2	1.000E+12	0.00	4.251E+03	^a
C5H9-R1D3 + O2 <=> C5H8-D1D3 + HO2	2.500E+12	0.00	4.251E+03	^a
C5H9-R2D3 + O2 <=> C5H8-D1D3 + HO2	1.000E+12	0.00	4.251E+03	^a

Table 6.14: Alkenyl radical + O2 direct formation of olefin and HO2. ^a: analogy to Chakir et al. (1989) [106].

Reactions	A	n	E_a	Ref
C5H11-R1+O2=C5H10-D1+HO2	1.000E+12	0.00	2.060E+03	^a
C5H11-R2+O2=C5H10-D1+HO2	2.000E+12	0.00	4.251E+03	^a
C5H11-R2+O2=C5H10-D2+HO2	2.000E+12	0.00	4.251E+03	^a
C5H11-R3+O2=C5H10-D2+HO2	2.000E+12	0.00	4.251E+03	^a

Table 6.15: Alkyl radical + O2 direct formation of olefin and HO2. ^a: analogy to Chakir et al. (1989) [106].

6.1.5 Class 5: Alkyl and alkenyl radical isomerization

The reaction rates implemented in the model for alkenyl and alkyl radicals are shown on tables 6.16 and 6.17. Alkenyl reaction rates are applied following the recommendations from Ahmed et al. (2007) [81] while alkyl reaction rates are taken from the work of Comandini et al. 2012 [147].

Reactions	A	n	E_a	Ref
C5H9-R1D4 <=> C5H9-R4D1	5.480E+08	1.62	3.876E+04	[81]
C5H9-R1D4 <=> C5H9-R3D1	1.390E+09	0.98	3.376E+04	[81]
C5H9-R1D3 <=> C5H9-R2D3	5.480E+08	1.62	3.876E+04	[81]
C5H9-R1D3Me2 <=> C5H9-R1D2Me3	2.740E+08	1.62	3.876E+04	[81]
REV	8.700E+06	2.01	4.124E+04	
C5H9-R1D3Me3 <=> C5H9-R1D2Me2	2.740E+08	1.62	3.876E+04	[81]
REV	8.700E+06	2.01	4.124E+04	
C5H9-R1D2Me3 <=> C5H9-R1D2Me2	1.250E+09	0.35	1.976E+04	[81]
REV	1.610E+08	0.74	2.226E+04	

Table 6.16: Reaction rates for isomerization of alkenyl radicals.

Reactions	A	n	E_a	Ref
C5H11-R1 \rightleftharpoons C5H11-R2				[147]
PLOG/0.1	1.610E+10	-0.128	1.6305E+04	
PLOG/1.0	2.880E+17	-2.073	2.1414E+04	
PLOG/10.0	5.090E+18	-2.284	2.3337E+04	
PLOG/100.0	1.380E+14	-0.838	2.1871E+04	
PLOG/ 1000.0	1.600E+08	0.954	19221.0	
C5H11-R1 \rightleftharpoons C5H11-R3				[147]
PLOG/0.1	6.080E-15	6.876	1.1901E+04	
PLOG/1.0	7.680E+07	0.667	2.5012E+04	
PLOG/10.0	1.260E+19	-2.350	3.2938E+04	
PLOG/100.0	1.160E+16	-1.256	3.3072E+04	
PLOG/ 1000.0	6.060E+06	1.570	2.9120E+04	
C5H11-R2 \rightleftharpoons C5H11-R3				[147]
PLOG/0.1	4.800E-04	3.725	28298.0	
PLOG/1.0	3.410E+22	-3.517	42976.0	
PLOG/10.0	1.570E+32	-6.005	50425.0	
PLOG/100.0	3.120E+24	-3.514	48305.0	
PLOG/ 1000.0	1.590E+14	-0.404	43709.0	

Table 6.17: Reaction rates for isomerization of Alkyl radicals.

6.1.6 Class 6: Abstraction reactions from bi-olefin

The reaction rates applied in this study to the resulting C_5H_8 branched and linear isomers are presented in table 6.18. Recommendations from Ahmed et al. 2007 [81] with a correction for the allylic H-atom abstraction have been followed.

Reactions	A	n	E_a	Ref
H + C5H8-D1D3 <=> H2 + C5H7-R1D2D4	8.445E+07	2.00	5.713E+03	^a
OH + C5H8-D1D3 <=> H2O + C5H7-R1D2D4	5.250E+09	0.97	-4.220E+02	^a
O + C5H8-D1D3 <=> OH + C5H7-R1D2D4	1.980E+06	2.40	3.512E+03	^a
CH3 + C5H8-D1D3 <=> CH4 + C5H7-R1D2D4	8.130E+11	0.00	9.620E+03	^a
HO2 + C5H8-D1D3 <=> H2O2 + C5H7-R1D2D4	8.040E+12	0.00	1.741E+04	^a
CH3O + C5H8-D1D3 <=> CH3OH + C5H7-R1D2D4	1.581E+11	0.00	5.005E+03	^a
O2 + C5H8-D1D3 <=> HO2 + C5H7-R1D2D4	1.251E+13	0.00	4.703E+04	^a
CH3O2 + C5H8-D1D3 <=> CH3O2H + C5H7-R1D2D4	6.060E+12	0.00	1.846E+04	^a
H + C5H8-D1D4 <=> H2 + C5H7-R1D2D4	2.450E+07	2.00	3.007E+03	^a
OH + C5H8-D1D4 <=> H2O + C5H7-R1D2D4	4.680E+07	1.61	-2.036E+03	^a
O + C5H8-D1D4 <=> OH + C5H7-R1D2D4	2.360E+05	2.50	2.033E-01	^a
CH3 + C5H8-D1D4 <=> CH4 + C5H7-R1D2D4	4.000E+11	0.00	7.514E+03	^a
O2 + C5H8-D1D4 <=> HO2 + C5H7-R1D2D4	2.000E+13	0.00	4.568E+04	^a
HO2 + C5H8-D1D4 <=> H2O2 + C5H7-R1D2D4	4.880E+12	0.00	1.503E+04	^a
CH3O + C5H8-D1D4 <=> CH3OH + C5H7-R1D2D4	1.096E+11	0.00	3.007E+03	^a
CH3O2 + C5H8-D1D4 <=> CH3O2H + C5H7-R1D2D4	4.040E+12	0.00	1.573E+04	^a
H + C5H8-D1D3Me2 <=> H2 + C5H7-R1D3MD2	8.445E+07	2.00	5.706E+03	^a
OH + C5H8-D1D3Me2 <=> H2O + C5H7-R1D3MD2	5.250E+09	0.97	-4.100E+02	^a
O + C5H8-D1D3Me2 <=> OH + C5H7-R1D3MD2	1.099E+06	2.40	3.507E+03	^a
CH3 + C5H8-D1D3Me2 <=> CH4 + C5H7-R1D3MD2	6.510E+11	0.00	9.620E+03	^a
HO2 + C5H8-D1D3Me2 <=> H2O2 + C5H7-R1D3MD2	8.040E+12	0.00	1.741E+04	^a
CH3O + C5H8-D1D3Me2 <=> CH3OH + C5H7-R1D3MD2	5.267E+10	0.00	5.005E+03	^a
O2 + C5H8-D1D3Me2 <=> HO2 + C5H7-R1D3MD2	1.581E+11	0.00	4.703E+04	^a
CH3O2 + C5H8-D1D3Me2 <=> CH3O2H + C5H7-R1D3MD2	6.060E+12	0.00	1.846E+04	^a
H + C5H8-D1-D2Me3 <=> H2 + C5H7-R1D2-D3Me2	1.680E+08	2.00	5.713E+03	^a
OH + C5H8-D1-D2Me3 <=> H2O + C5H7-R1D2-D3Me2	1.050E+10	0.97	-4.220E+02	^a
O + C5H8-D1-D2Me3 <=> OH + C5H7-R1D2-D3Me2	2.196E+06	2.40	3.512E+03	^a
CH3 + C5H8-D1-D2Me3 <=> CH4 + C5H7-R1D2-D3Me2	1.302E+12	0.00	9.620E+03	^a
HO2 + C5H8-D1-D2Me3 <=> H2O2 + C5H7-R1D2-D3Me2	1.608E+13	0.00	1.741E+04	^a
CH3O + C5H8-D1-D2Me3 <=> CH3OH + C5H7-R1D2-D3Me2	3.162E+11	0.00	5.005E+03	^a
O2 + C5H8-D1-D2Me3 <=> HO2 + C5H7-R1D2-D3Me2	2.502E+13	0.00	4.703E+04	^a
CH3O2 + C5H8-D1-D2Me3 <=> CH3O2H + C5H7-R1D2-D3Me2	1.212E+13	0.00	1.846E+04	^a

Table 6.18: Abstraction reactions from linear and branched C_5H_8 species. ^a: Ahmed et al. 2007 [81] reactions rates with allyl correction.

6.1.7 Class 7: Addition of radical species to Olefin

The addition of OH and O to the double bond of C_5H_{10} branched and linear species may result in small C_1 to C_4 alkanes, alkenes, radicals and oxygenated species. The resulting products were chosen looking at the more feasible structure (see Curran et al. [77]). Reaction rates have been applied following the recommendations of Ahmed et al. 2007 [81] and are presented in table 6.19.

Reactions	A	n	E_a	Ref
O + C5H10-D1 \rightleftharpoons C3H7-R1 + C2H3O-R1A12	2.000E+10	0.00	-1.052E+03	[81]
O + C5H10-D2 \rightleftharpoons C2H4-D1 + C3H6O-A11	2.000E+10	0.00	-1.052E+03	[81]
OH + C5H10-D1 \rightleftharpoons C4H9-R1 + CH2O	2.000E+10	0.00	-4.003E+03	[81]
OH + C5H10-D2 \rightleftharpoons C3H7-R1 + C2H4O-A11	2.000E+10	0.00	-4.003E+03	[81]
O + C5H10-D1 \rightarrow C2H3O-R1K1 + C3H7-R1	2.000E+10	0.00	-1.050E+03	[81]
O + C5H10-D2 \rightarrow C2H4O-A11 + C3H6-D1	2.000E+10	0.00	-1.050E+03	[81]
OH + C5H10-D2 \rightarrow C3H6O-A11 + C2H5-R1	2.000E+10	0.00	-4.000E+03	[81]
O + C5H10-D1Me2 \rightleftharpoons CH3 + C4H7O-O1D2Me2	2.000E+10	0.00	-1.050E+03	[81]
OH + C5H10-D2Me2 \rightleftharpoons CH2O + C4H9-R2	2.000E+10	0.00	-4.000E+03	[81]
O + C5H10-D2Me2 \rightleftharpoons C3H6O-K2 + C2H4-D1	2.000E+10	0.00	-1.050E+03	[81]
OH + C5H10-D2Me2 \rightleftharpoons C2H4O-A11 + C3H7-R2	2.000E+10	0.00	-4.000E+03	[81]
O + C5H10-D1Me3 \rightleftharpoons C2H3O-R1A12 + C3H7-R2	2.000E+10	0.00	-1.050E+03	[81]
OH + C5H10-D1Me3 \rightleftharpoons CH2O + C4H9-R1Me2	2.000E+10	0.00	-4.000E+03	[81]

Table 6.19: Addition of OH and O radical species to C_5H_{10} isomers.

6.1.8 Class 8: Radical decomposition

Resulting C_5H_7 radicals are resonant stabilized species. Reasonable products were chosen for C5H7-R1D2D4, C5H7-R1D3MD2, and C5H7-R1D2-D3Me2. Reaction rates following the recommendations from Mehl et al. 2008 [107] were applied for the reactions:

- C5H7-R1D2D4 \rightleftharpoons CyC5H6-D1D3 + H,
- C5H7-R1D3MD2 \rightleftharpoons C3H4-D1D2 + C2H3-R1D1, and
- C5H7-R1D3MD2 \rightleftharpoons C3H4-T1 + C2H3-R1D1.

The reaction rate proposed by Weissmann et al. 1984 [148] was applied for C2H3-R1D1 + C3H4-D1D2 \rightleftharpoons C5H7-R1D2D4.

6.1.9 Class 9: Di-olefin decomposition

Reaction rates for di-olefin decomposition are presented in table 6.20. Reaction rates were taken mostly from the works of Mehl et al. 2008 [107], Ranzi et al. 2015 [149], Gonzales Alatorre et al. 2001 [119], with an exception for reaction H + C5H8-D1D3 \rightleftharpoons C3H5-R1D2 + C2H4-D1, which follows Marinov et al. 1997 [150] and for reaction C2H3-R1D1 + C3H6-D1 \rightleftharpoons C5H8-D1D3 + H, following the recommendation from Tsang 1989 [85].

Reactions	A	n	E_a	Ref
C5H8-D1D3 \rightleftharpoons C4H5-R1D1D3 + CH3	1.000E+28	-3.80	9.100E+04	[107]
C5H8-D1D4 \rightleftharpoons C3H5-R1D2 + C2H3-R1D1	2.000E+28	-3.80	9.100E+04	[107]
H + C5H8-D1D3 \rightleftharpoons C3H5-R1D2 + C2H4-D1	3.335E+08	1.50	2.000E+03	[150]
C2H3-R1D1 + C3H6-D1 \rightleftharpoons C5H8-D1D3 + H	7.230E+11	0.00	6.439E+03	[85]
C5H8-D1D3 \rightarrow CyC5H6-D1D3 + H + H	1.000E+16	0.00	8.000E+04	[149]
C5H8-D1D4 \rightarrow CyC5H6-D1D3 + H + H	1.000E+16	0.00	8.000E+04	[149]
C2H3-R1D1 + C5H8-D1D3 \rightarrow CyC5H6-D1D3 + C2H5-R1	1.000E+12	0.00	3.000E+03	[149]
C4H7-R2D2 + C4H8-D1Me2 \rightleftharpoons C3H7-R2 + C5H8-D1D3	3.000E+12	0.00	6.000E+03	[149]
C5H8-D1D3 \rightleftharpoons H + C5H7-R1D2D4	1.995E+15	0.00	8.200E+04	[149]
C5H8-D1D4 \rightleftharpoons H + C5H7-R1D2D4	1.995E+15	0.00	8.200E+04	[149]
C5H8-D1D3Me2 \rightleftharpoons C3H5-R2D1 + C2H3-R1D1	1.000E+16	0.00	8.100E+04	^a
C5H8-D1D3Me2 \rightleftharpoons CH3 + C4H5-R2D1D3	5.010E+16	0.00	8.450E+04	[107]
C3H6-D1 + C2H3-R1D1 \rightleftharpoons H + C5H8-D1D3Me2	1.400E+12	0.00	1.000E+04	^b
H + C5H8-D1D3Me2 \rightleftharpoons C4H6-T1 + CH3	1.130E+13	0.00	1.860E+03	[119]
C5H8-D1D3Me2 \rightleftharpoons H + C5H7-R1D3MD2	1.995E+15	0.00	8.400E+04	[107]
H + C5H8-D1-D2Me3 \rightleftharpoons C4H6-T2 + CH3	3.160E+10	0.00	1.500E+03	[119]
C5H8-D1-D2Me3 \rightleftharpoons CH3 + C4H5-R1T2	5.010E+16	0.00	8.400E+04	[107]
C5H8-D1-D2Me3 \rightleftharpoons H + C5H7-D2D3MR2	1.995E+15	0.00	8.400E+04	[107]

Table 6.20: *Di-olefin decomposition.*^a: Mehl et al. 2008 [107], A factor was decreased by 2.5; ^b: reaction rates were applied in analogy to C3H4-T1 + C3H5-R1D2 \rightleftharpoons H + C6H8-D1T5.

Recognizing the importance of allylic bonds (C-H or C-C bonds that are next to a C=C bond) makes 2-Methyl-2-butene (C5H10-D2Me2) an attractive molecule to study. 2-Methyl-2-butene has 9 of its 10 H-atom in allylic position and they result in two C₅H₉ resonance-stabilized species. At the same time, n-Pentane (C5H12) is taken as an example of a linear molecule, which allows to understand the differences between both fuels. Predictions for experimental measurements in two burner-stabilized flames from Ruwe et al. 2017 [13] and Leon et al. [5], shock tube measurements by Westbrook et al. 2015 [120] and laminar flame speeds using 2-Methyl-2-butene (C5H10-D2Me2) and n-Pentane (C5H12) as fuels measured by Cheng et al. 2017 [125], Ji et al. [142], Kelley et al. [143], Dirrenberger et al. [144], and Zhong et al. 2018 [126] will be discussed in this chapter.

6.2 Reaction pathways for aromatic formation

In the work of Ruwe et al. 2017 [13], different reaction pathways that may lead to aromatic formation coming from the fuel structure (2-Methyl-2-butene) were discussed. Radical 3-methylen-1-buten-4-yl (C5H7-R1D3MD2) and 3-methylen-2-buten-4-yl (C5H7-R1D2-D3Me2) are two of the main products formed from fuel consumption via H-atom abstraction. Both radicals have structures similar to C4H5-R1D1D3 and C4H5-R2D1D3 radicals. Recombination of 3-methylen-2-buten-4-yl (C5H7-R1D2-D3Me2) with acetylene (C2H2) resulting in a methyl-substituted fulvene (CH3FC6H6) (C5H7-R1D2-D3Me2 + C2H2 \rightleftharpoons CH3FC6H6) has been proposed by Ruwe et al. 2017 and implemented in this model using an analogy to the reaction rates suggested by Senossian et al. 2007 [151] for the reaction C4H5-R2D1D3 + C2H2 \rightleftharpoons FC6H6 + H. A similar analogy for the reaction C4H5-R2D1D3 + C4H4-D1T3 \rightleftharpoons C2H3FC6H6 + H forming an ethyl-substituted fulvene has been implemented in the model. Direct and H-

atom assisted isomerization reactions that lead to toluene and styrene have been taken into account. Reaction rates follow the recommendation of Melius et al. 1992 [152] and Marinov et al. 1997 [150] ((see table 6.21). The reaction rate for the recombination of C4H5-R1T2 that leads to o-xylene (C8H10-A1M1M2) follows the recommendations of Hoyermann et al. 2004 [6].

In the model, 3-methylen-1-buten-4-yl radical (C5H7-R1D3MD2) reactions that lead directly to fulvene, benzene and toluene, have been implemented following the recommendation of Senossian et al. 2007 [151] based on previously described analogies (see table 6.21).

Reactions	A	n	E_a	Ref
Reaction pathways proposed by Ruwe et al. 2017				
C5H7-R1D2-D3Me2 + C2H2 \rightleftharpoons CH3FC6H6	5.22E+41	-7.94	3.96E+04	[151]
CH3FC6H6 \rightleftharpoons A1CH3	7.590E+13	0.00	7.385E+04	[152]
CH3FC6H6 + H \rightleftharpoons A1CH3 + H	3.000E+12	0.50	2.00E-03	[150]
C3H3-R1T2 + C4H5-R1T2 \rightleftharpoons A1CH3	2.500E+27	-3.80	9.708E+04	[153]
2C4H5-R1T2 \rightleftharpoons C8H10-A1M1M2	5.000E+12	0.00	0.000E+00	[6].
C4H5-R2D1D3 + C4H4-D1T3 \rightleftharpoons C2H3FC6H6 + H	5.22E+41	-7.94	3.96E+04	[151]
C2H3FC6H6 \rightleftharpoons A1C2H3	7.590E+13	0.00	7.385E+04	[152]
C2H3FC6H6 + H \rightleftharpoons A1C2H3 + H	3.000E+12	0.50	2.00E-03	[150]
This work				
C5H7-R1D2-D3Me2 + C2H2 \rightleftharpoons FC6H6 + CH3	5.22E+41	-7.94	3.96E+04	[151]
C5H7-R1D3MD2 + C2H2 \rightleftharpoons A1CH3 + H	1.65E+16	-1.01	9.49E+03	[151]
C5H7-R1D3MD2 + C2H2 \rightleftharpoons A1 + CH3	1.65E+16	-1.01	9.49E+03	[151]

Table 6.21: Aromatic formation reaction pathways proposed by Ruwe et al. [13] and in this work.

6.3 Thermodynamic data

Thermodynamic data for newly introduced species and their C₅ degradation products were updated using the database of Goos et al. (2013) [9]. Species that were not available in the database were calculated using additivity rules from Gao et al. (2016) [12].

Only 1,3-butadiene (C4H6-D1D3) was detected experimentally. The work from Ruwe et al. [13] states that a fast isomerization from C4H6-D1-D2 to C4H6-D1D3 may occur. Model prediction shows similar concentrations of 1,3-butadiene (C4H6-D1D3) and 1,2-butadiene (C4H6-D1-D2) (dashed line in Figure 6.7). Based on these observations, the sub-mechanism for C₄H₆ isomers was revised. 1-butyne (C4H6-T1), 2-butyne and their corresponding C₄H₅ radicals were implemented in the model following the work of Belmekki *et al.* 2002 [154]. These changes did not show a real impact in the concentrations for the two aforementioned species.

For example, the model predicted maximum mole fractions of $4.35 \cdot 10^{-3}$ and $5.53 \cdot 10^{-3}$ respectively for 1,3-butadiene (C4H6-D1D3) and 1,2-butadiene (C4H6-D1D2), respectively, suggesting 1,2-butadiene to be formed as the main C₄H₆ isomer in the combustion of 2-methyl-2-butene. The flow analysis showed that the decomposition of 2-methyl-2-butene was dominated by H-atom abstraction

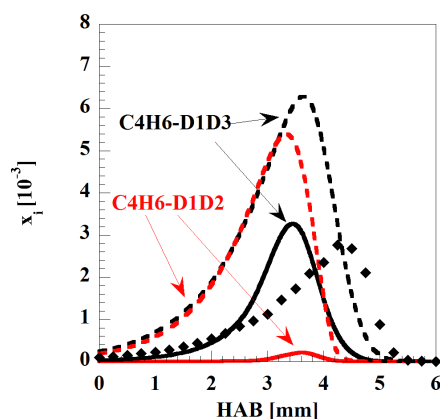


Figure 6.7: Mole fraction profiles of 1,3-butadiene (C_4H_6-D1D3) and 1,2-butadiene (C_4H_6-D1D2). The symbols represent experimental data; the dash lines represent simulation results using original thermodata and the solid lines represent modeling results using MOPAC thermodata.

forming the fuel radical 2-methyl-2-buten-1-yl ($C_5H_9-R1D2Me_2$), which further decomposes by abstraction of a methyl radical into 1,2-butadiene (C_4H_6-D1D2). However, the experimental results of [16] showed that 1,2-butadiene was not detectable in the experiments. Probable reasons are a concentration of the 1,2-butadiene at the detection limit and experimental limitations resulting from difficulties separating the 1,2- and 1,3-butadiene isomers. However, measurements obtained in a jet-stirred reactor by Westbrook et al. [40] also showed only very low concentrations of 1,2-butadiene (5 times lower than that of 1,3-butadiene).

Finally, due to the big uncertainty arising from using thermodynamic data from different sources (different calculation methods), a new set of thermodata using the program MOPAC 2016 [14] were calculated and implemented for all the related C_5 species (see 6.22). The change of the thermodata resulted in a change of the fuel decomposition flow (see Figure 6.8).

After the change on thermodata of C_5 related species, the isomerization of $C_5H_9-R1D2Me_2$ via

R1241: $C_5H_9-R1D2Me_2 = C_5H_9-R1D3Me_3$ becomes more important than the radical decomposition via the reaction

R1233: $C_5H_9-R1D3Me_3 = C_4H_6-D1-D2 + CH_3$, making the decomposition of $C_5H_9-R1D3Me_3$ the dominant reaction pathway (see Figure 6.8 b)).

The complete mechanism consists of 330 species and 3791 forward and backward reactions and is available in the supplementary material.

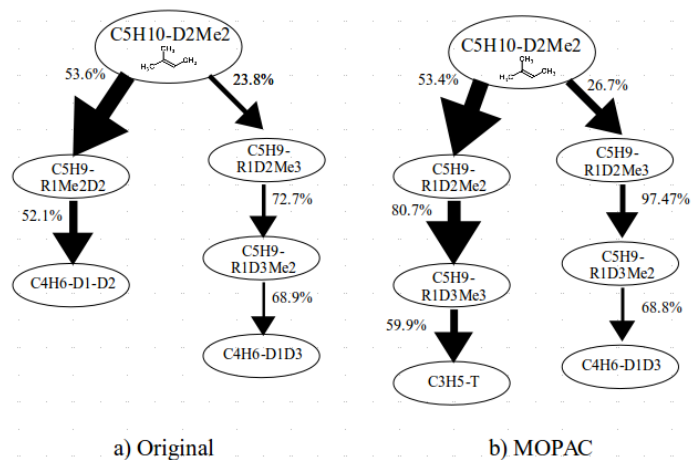


Figure 6.8: Integrated flow analysis of 2-Methyl-2-butene ($C_5H_{10}-D_2Me_2$) consumption using a) Original and b) MOPAC thermodata.

Name	Name in mechanism	$\Delta H_{f,298}^\circ$ (kJ/mol)
pentane	C5H12	-139.270
iso-pentane	C5H12-M2	-140.006
Pent-1-yl	C5H11-R1	4.010
pent-2-yl	C5H11-R2	-23.382
pent-3-yl	C5H11-R3	-21.295
2-methylbut-1-yl	C5H11-M2R1	5.909
2-methylbut-2-yl	C5H11-M2R2	-45.017
2-methylbut-3-yl	C5H11-M2R3	-23.051
2-methylbut-4-yl	C5H11-M2R4	2.175
2-methyl-1-butene	C5H10-M2D1	-41.583
3-methyl-1-butene	C5H10-M3D1	-25.438
2-methyl-2-butene	C5H10-M2D2	-57.050
1-pentene	C5H10-D1	-22.615
2-pentene	C5H10-D2	-40.867
2-methyl-but-1-en-4-yl	C5H9-M2D1R4	102.287
2-methyl-but-1-en	C5H9-M2RD1	74.538
2-methyl-but-2-en-1-yl	C5H9-M2D2R1	51.029
2-methyl-but-2-en-4-yl	C5H9-M2D2R4	45.045
3-methyl-but-1-en-4-yl	C5H9-M3D1R4	121.831
1-penten-3-yl	C5H9-D1R3	65.932
1-penten-4-yl	C5H9-D1R4	93.410
1-penten-5-yl	C5H9-D1R5	120.186
2-penten-4-yl	C5H9-D2R4	41.342
2-penten-5-yl	C5H9-D2R5	103.214
2-methyl-1,3-butadiene	C5H8-M2D1D3	75.390
3-methyl-1,2-butadiene	C5H8-M2D2D3	85.383
1,3-pentadiene	C5H8-D1D3	72.276
1,4-pentadiene	C5H8-D1D4	93.647
3-methylen-1-buten-4-yl	C5H7-D1D3MR2	192.201
3-methylen-2-buten-4-yl	C5H7-D2D3MR2	200.692
1,3-pentadiene-5-yl	C5H7-D1D3R5	166.694

Table 6.22: Thermodynamic data for the C_5 molecules calculated using the semi-empirical quantum chemistry program MOPAC 2016 [14].

6.4 Validation of burner-stabilized flame experiments: 2-Methyl-2-butene (C₅H₁₀-D₂Me₂) and n-Pentane (C₅H₁₂).

The results of fuel consumption pathways for a 2-Methyl-2-butene and an n-Pentane burner-stabilized flame measured in the publication of Ruwe et al. (2017) [13] and Leon et al. (2019) [5], respectively, will be analyzed (equivalence ratio (ϕ) of 1.8, at 40 mbar, and $T_i=340$ K). Simulations were performed using the Freely propagating module of LOGEresearch [26].

Figure 6.9 shows the decomposition of 2-methyl-2-butene (C₅H₁₀-D₂Me₂). The breakdown of the fuel molecule is mainly dominated by H-atom abstraction to form 53.6% of (C₅H₉-R₁D₂Me₂) and 26.7% of C₅H₉-R₁D₂Me₃ radicals. 80.7% of C₅H₉-R₁D₂Me₂ isomerizes to form C₅H₉-R₁D₃Me₃, whose decomposition contributes to C₃ and C₂ routes. 4.38% of C₅H₉-R₁D₂Me₂ forms 2-methyl-1,3-butadiene (C₅H₈-D₁D₃Me₂) via β -scission of a C-H bond. C₅H₈-D₁D₃Me₂ is also resulting from recombination of C₃H₅-R₂D₁ with vinyl radical (C₂H₃-R₁D₁) (R1250b: C₅H₈-D₁D₃Me₂ \rightleftharpoons C₃H₅-R₂D₁ + C₂H₃-R₁D₁). C₃H₅-R₂D₁ via H-atom abstraction forms allyl (C₃H₄-D₁D₂), which isomerizes to propyne (C₃H₄-T₁). 48% of C₅H₇-R₁D₃MD₂ radical contributes to C₃H₄-T₁ formation.

97.4 % of C₅H₉-R₁D₂Me₃ isomerizes towards C₅H₉-R₁D₃Me₂ and 2.6% forms 2-methyl-2,3-butadiene (C₅H₈-D₁-D₂Me₃) via β -scission of a C-H bond. 38.2% of C₅H₈-D₁D₃Me₂ via H-atom abstraction results in C₅H₇-R₁D₃MD₂ radical which via C-C bond break contributes to C₃ and C₂ routes. C₅H₈-D₁-D₂Me₃ via H-atom abstraction forms C₅H₇-R₁D₂-D₃Me₂ radical, which contributes to the C₄ route.

Finally, the H-atom addition to the fuel in the C=C double bond forms different C₅H₁₁ allyl radicals (R1147: C₅H₁₀-D₂Me₂ + H \rightleftharpoons C₅H₁₁-R₂Me₂). C₅H₁₁-R₂Me₂ is the most dominant radical and its decomposition is dominated by β -scission of the C-C bond breaking, which will form 80% of *iso*-butene (C₄H₈-D₁Me₂) (R1147: C₅H₁₀-D₂Me₂ + H \rightleftharpoons C₅H₁₁-R₂Me₂). C₄H₈-D₁Me₂ via H-atom abstraction forms C₄H₇-R₁D₂Me₂ which via C-C bond break contributes to the C₃ and C₂ routes.

Final oxidation is achieved through C₂ and C₁ reaction sequences. The C₂ route starts from ethyl radical (C₂H₅-R₁) via ethene (C₂H₄-D₁) by H-atom abstraction. Ethene (C₂H₄-D₁) via further dehydrogenation forms the vinyl radical (C₂H₃-R₁D₁) and finally acetylene (C₂H₂). Acetylene mainly forms the ketyl radical (HCCO) towards CO and CO₂.

For *n*-pentane (C₅H₁₂), the predicted fuel decomposition is presented in Fig. 6.10. Its breakdown is dominated by an H-atom abstraction at the primary carbon atom forming 42% of 1-pentyl radical (C₅H₁₁-R₁), followed by H-atom abstractions at the two secondary carbon atoms 2 and 3 that are leading to the formation of the 2-pentyl radical (C₅H₁₁-R₂, 38%) and the 3-pentyl radical (C₅H₁₁-R₃, 19%), respectively. The 1-pentyl radical, which is the primary

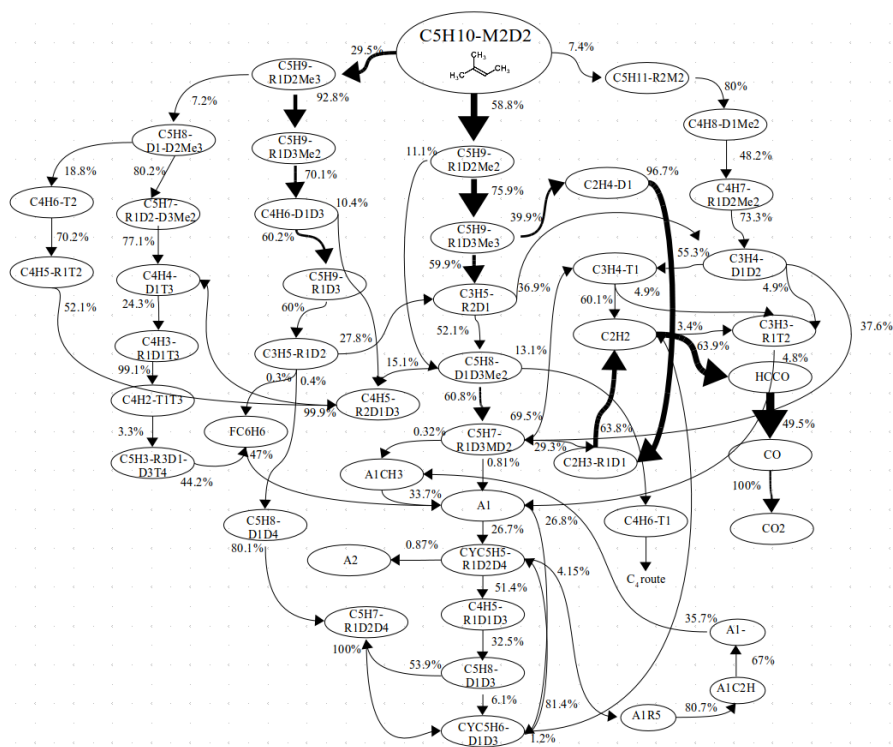


Figure 6.9: Integrated flow analysis of 2-Methyl-2-butene ($C_5H_{10}-D_2Me_2$) consumption. The thickness of the arrows indicates the contribution of the respective pathway to the total flux of C-atoms (contributions of the destruction of the individual molecule are indicated by percentages next to the arrows) [5].

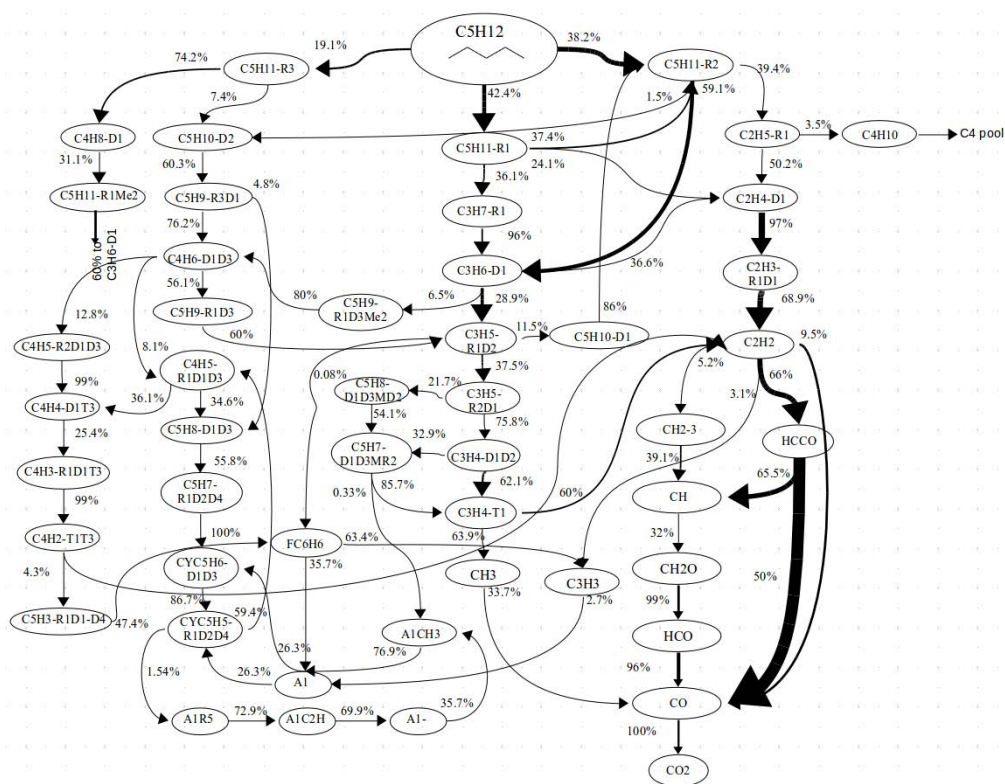


Figure 6.10: Integrated flow analysis of *n*-pentane (C_5H_{12}) consumption. The thickness of the arrows indicates the contribution of the respective pathway to the total flux of C-atoms (contributions of the destruction of the individual molecule are indicated by percentages next to the arrows) [5].

decomposition product in the combustion process of *n*-pentane, can form *cis*-2-pentene (C5H10-D2, 1.11%) *via* an H-atom abstraction or further decompose to ethene (C2H4-D1, 24%) and to the *n*-propyl radical (C3H7-R1, 36%) (see R1299: C5H11-R1 \rightleftharpoons C2H4-D1 + C3H7-R1) by a C-C β -scission. *n*-Propyl radicals can form propene by H-atom abstraction and therefore contribute to the C₃ destruction pathway. Additionally, an isomerization reaction of the 1-pentyl radical that leads to the formation of the 2-pentyl radical (C5H11-R2) contributes with 37.88% to its consumption.

The 2-pentyl radical can further decompose *via* C-C β -scission to the ethyl radical (C2H5-R1, 39.55%) and propene (C3H6-D1, 59%). The ethyl radical (C2H5-R1) contributes to the C₂ reaction pathway, because it mainly decomposes with 49.9% to ethene (C2H4-D1), which subsequently forms the vinyl radical (C2H3-R1D1, 97%), acetylene (C2H2, 67.4%) and the ketyl radical (HCCO, 66%). The decomposition of the 3-pentyl radical, which is the most unlikely fuel radical, is dominated by a C-C β -scission (76.45%) leading to 1-butene (C4H8-D1) and the methyl radical (CH3, 18.97%), as well as by an H-atom abstraction leading to *cis*-2-pentene (C5H10-D2, 4.58%).

6.4.1 Major Species

Experimental and modeling results of major species mole fractions for both flames are presented in Figure 6.11. A good agreement between experiments and model results is observed for most of the species. Small deviations for fuel and oxygen (1 *mm* shift) are observed. The shift also appears for the intermediates. This deviation can be due to uncertainties of the flame temperature due to steeper gradients and might also be related to probe perturbations (see discussions in [13]). No position shift has been applied between the experiment and the model.

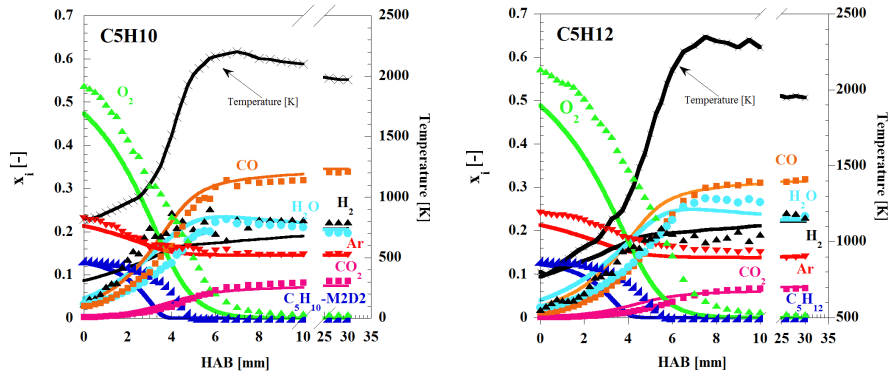


Figure 6.11: Major species mole fractions vs. height above the burner (HAB) for 2-methyl-2-butene ($C_5H_{10}\text{-D2Me2}$) and *n*-pentane (C_5H_{12}) flames. The symbols are from the EI-MBMS experiment by Ruwe et al. (2017) [13] and Leon et al. [5], respectively; the lines are from simulations with the model. Equilibrium mole fractions are given in the exhaust. Black lines represent the perturbed temperature profiles for 2-methyl-2-butene and *n*-Pentane, respectively.

6.4.2 Intermediate species

Experimental and simulated mole fraction profiles of some $C_1\text{-}C_4$ intermediate species are shown with the purpose of discussing the global predictive capability of the model.

Mole fraction profiles of methyl (CH_3), methane (CH_4), ethene ($C_2H_4\text{-D1}$), ethane (C_2H_6), and propene ($C_3H_6\text{-D1}$) are a good representation of C_1 to C_3 small intermediate species. Looking at Figure 6.12, a good agreement regarding the peak mole fractions and the profile shapes is observed, and the model predictions are within experimental error for all the species. Important reactions for the formation of of ethane (C_2H_6) and ethene ($C_2H_4\text{-D1}$) in the 2-methyl-2-butene flame are:

- R67b: $C_2H_6(+M) \rightleftharpoons 2CH_3(+M)$,
- R1398f: $C_5H_9\text{-R1D3} \rightleftharpoons C_2H_4\text{-D1} + C_3H_5\text{-R1D2}$,
- R1232f: $C_5H_9\text{-R1D3M3} \rightleftharpoons C_3H_5\text{-R2D1} + C_2H_4\text{-D1}$,
- R338f: $C_3H_6\text{-D1} \rightleftharpoons C_2H_4\text{-D1} + CH_3$,
- R339f: $C_3H_6\text{-D1} \rightleftharpoons C_2H_4\text{-D1} + CH_3$, and
- R347f: $O + C_3H_6\text{-D1} \rightleftharpoons CH_2O + C_2H_4\text{-D1}$.

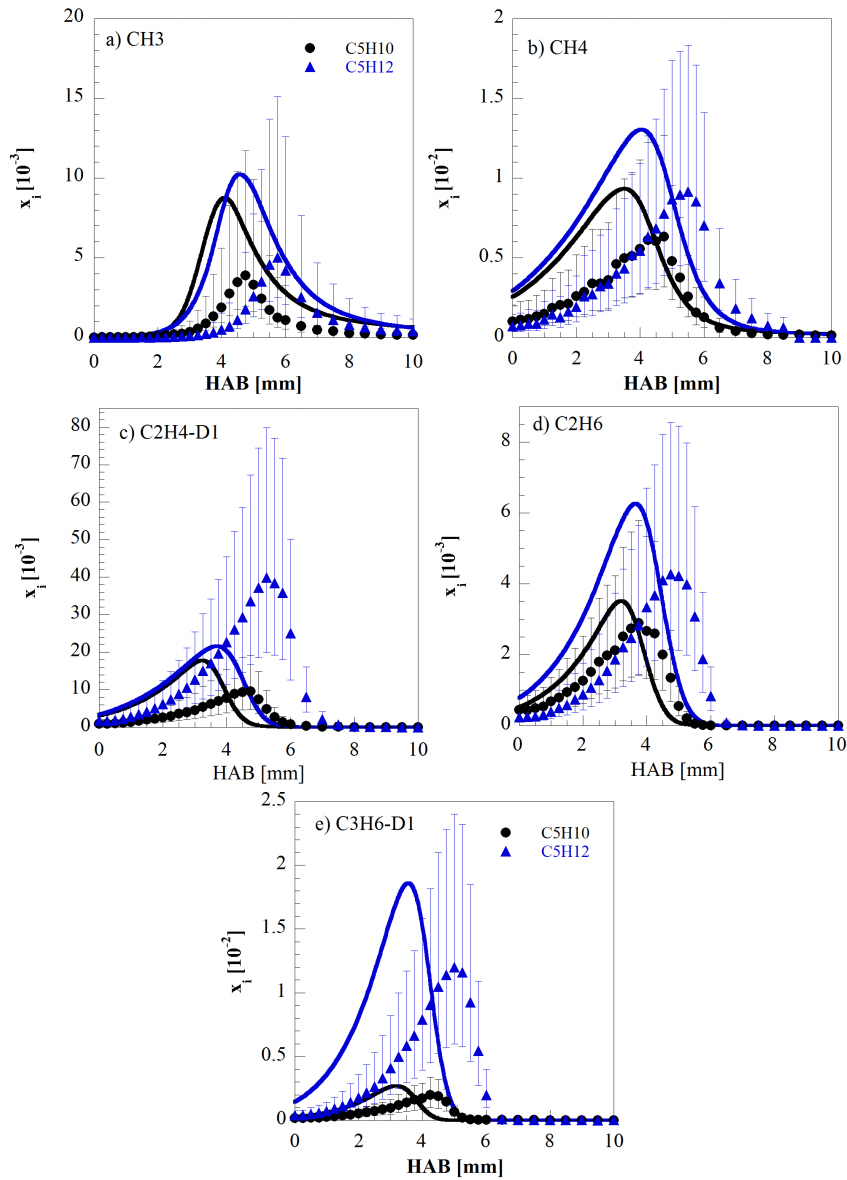


Figure 6.12: Mole fraction profiles of: a) methyl (CH_3), b) methane (CH_4), c) ethene (C_2H_4 -D1), d) ethane (C_2H_6), and e) propene (C_3H_6 -D1). The symbols represent experimental data for (●) 2-methyl-2-butene, (▲) n-Pentane and the lines represent modeling results. The corresponding error bars show the experimental error.

In the case of n-Pentane flame, there are similar reaction pathways as for 2-methyl-2-butene (R67b, R338f, R339f and R347f) and others, which depend on

the fuel structure like R1317f: $C_5H_{11}-R_1 \rightleftharpoons C_2H_4-D_1 + C_3H_7-R_1$, as it may be observed in Figures 6.9 and 6.10. Propene ($C_3H_6-D_1$) is an important C_3 intermediate. Looking at the 2-methyl-2-butene flame, it is mainly formed from C_5H_9 and C_5H_8 radicals, via reactions

- R1235f: $C_5H_9-R_1D_3Me_2 \rightleftharpoons C_3H_6-D_1 + C_2H_3-R_1D_1$
- R1253b: $C_3H_6-D_1 + C_2H_3-R_1D_1 \rightleftharpoons H + C_5H_8-D_1D_3Me_2$.

In the case of n-Pentane flame, this specie is formed from C_5H_{11} and C_3H_7 radicals, specifically

- R1322f: $C_5H_{11}-R_2 \rightleftharpoons C_3H_6-D_1 + C_2H_5-R_1$ and
- R360b: $H + C_3H_6-D_1 \rightleftharpoons C_3H_7-R_1$.

The n-Pentane flame has a higher concentration of C_2 species ($C_2H_4-D_1$ and C_2H_6) and propene (C_3H_6), because the linear structure of the molecule favors their formation.

Other important small intermediate species are 1-butene ($C_4H_8-D_1$), 2-butene (T- $C_4H_8-D_2$), *iso*-butene ($C_4H_8-D_1Me_2$), 1,3-butadiene ($C_4H_6-D_1D_3$), 1,2-butadiene ($C_4H_6-D_1D_2$), 1-butyne ($C_4H_6-T_1$) and 2-butyne ($C_4H_6-T_2$), diacetylene ($C_4H_2-T_1T_3$) and vinylacetylene ($C_4H_4-D_1T_3$) (see Figures 6.13- 6.15)

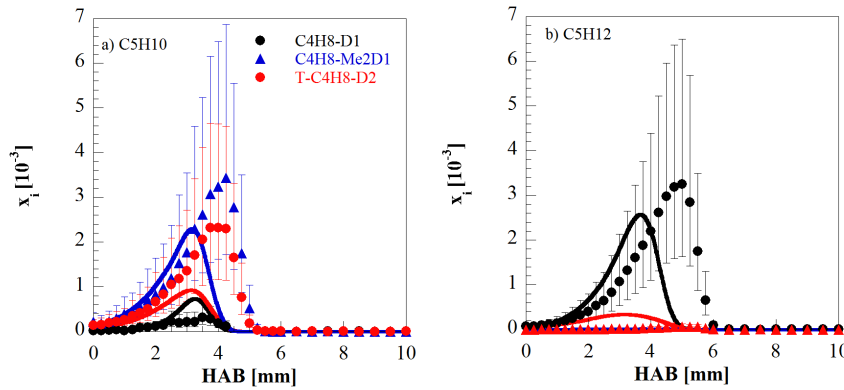


Figure 6.13: Mole fraction profiles of: 1-butene ($C_4H_8-D_1$), 2-butene (T- $C_4H_8-D_2$), and *iso*-butene ($C_4H_8-D_1Me_2$) for a) 2-methyl-2-butene and b) n-Pentane flames. The symbols represent experimental data and the lines represent modeling results. The corresponding bars show the experimental error.

Experimental and modeling profiles for the different C_4H_8 isomers are shown in Figure 6.13 a) for 2-methyl-2-butene and Figure 6.13 b) for n-Pentane. Slight under-predictions regarding the peak mole fractions are observed in all isomers,

while the profile shape represents the experimental behaviour. In the 2-methyl-2-butene flame, *iso*-butene (C4H8-D1Me2) has been mostly formed, followed by 2-butene (T-C4H8-D2) and 1-butene (C4H8-D1) while in the n-Pentane flame the dominant isomer is 1-butene. The C5H11-R2Me2 radical decomposition R1444f: C5H11-R2Me2 \rightleftharpoons C4H8-D1Me2 + CH3 is the major formation pathway to produce *iso*-butene, while 1-butene (C4H8-D1) and 2-butene (T-C4H8-D2) are mainly resulting from

- R1146f: C5H11-R1Me2 \rightleftharpoons C4H8-D1 + CH3 and
- R1143f: C5H11-R2Me3 \rightleftharpoons T-C4H8-D2 + CH3 respectively.

In the n-Pentane flame, 1-butene (C4H8-D1) is mainly formed from R1325f: C5H11-R3 \rightleftharpoons C4H8-D1 + CH3. H-atom addition to the double bond in the 2-methyl-2-butene molecule results in the formation of C₅H₁₁ allyl radicals, which explains the fact that the total concentration of the C₄H₈ isomers is almost twice when compared to the n-Pentane flame.

C₄H₆ isomers: 1,3-butadiene (C4H6-D1D3), 1,2-butadiene (C4H6-D1D2), 1-butyne (C4H6-T1) and 2-butyne (C4H6-T2) are shown in Figure 6.14a-d). Experimental results show that 1,3-butadiene is dominant C₄H₆ isomer in both flames followed by 1-butyne. A very good agreement between experimental and modeling results has been found for all the profiles except for Figure 6.14 d). The model underpredicts the experimental measurements. C₄H₆ isomer has a low concentration in the flame. Its validation will need validation against other experimental data, which is out of the scope of this study.

1,3-butadiene in the 2-methyl-2-butene flame results mainly from the C5H9-R1D3Me2 radical decomposition via C-C bond breaking R1234: C5H9-R1D3Me2 \rightleftharpoons C4H6-D1D3 + CH3. The other two radicals are formed in lower concentration in the flame via reactions

- R1254: H + C5H8-D1D3Me2 \rightleftharpoons C4H6-T1 + CH3 and
- R1255: H + C5H8-D1-D2Me3 \rightleftharpoons C4H6-T2 + CH3.

For n-Pentane flame, 1,3-butadiene and 1-butyne are formed via reactions

- R1234: C5H9-R1D3Me2 \rightleftharpoons C4H6-D1D3 + CH3
- R474f: CH2-3 + C3H5-R1 \rightleftharpoons C4H6-D1D3 + H and
- R508b: C4H6-T1 \rightleftharpoons C3H3-R1T2 + CH3

1-butyne (C4H6-T1) and 2-butyne (C4H6-T2) have similar reaction time to C₅H₈ isomers in the 2-methyl-2-butene flame (see discussion related to Figure 6.23).

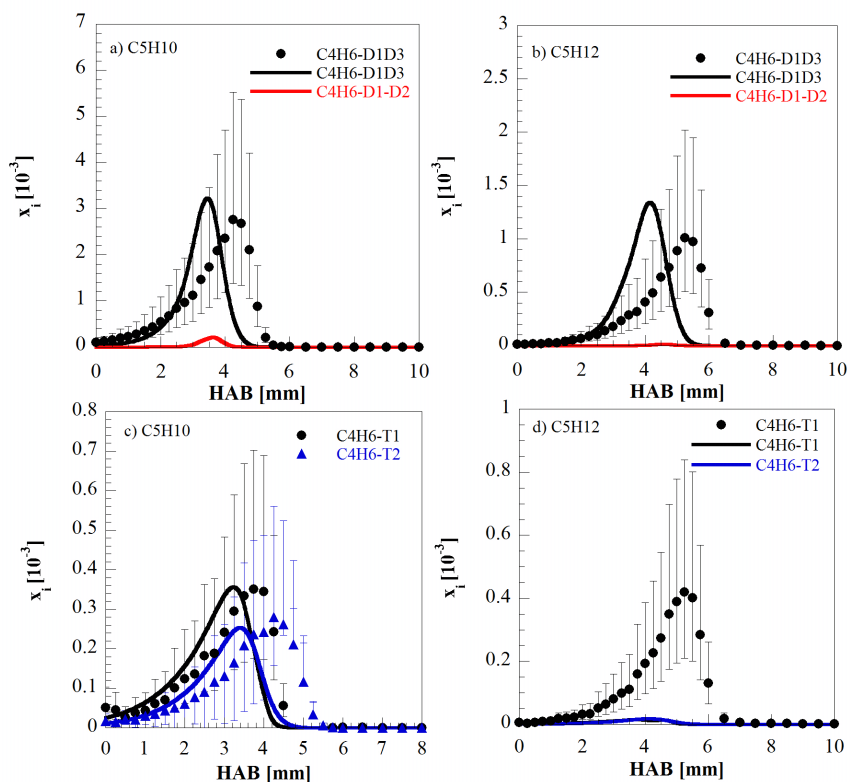


Figure 6.14: Mole fraction profiles of: 1,3-butadiene (C_4H_6-D1D3), 1,2-butadiene (C_4H_6-D1D2), 1-butyne (C_4H_6-T1) and 2-butyne (C_4H_6-T2) (C_4H_6-T2). The symbols represent experimental data and the lines represent modeling results. The corresponding bars show the experimental error.

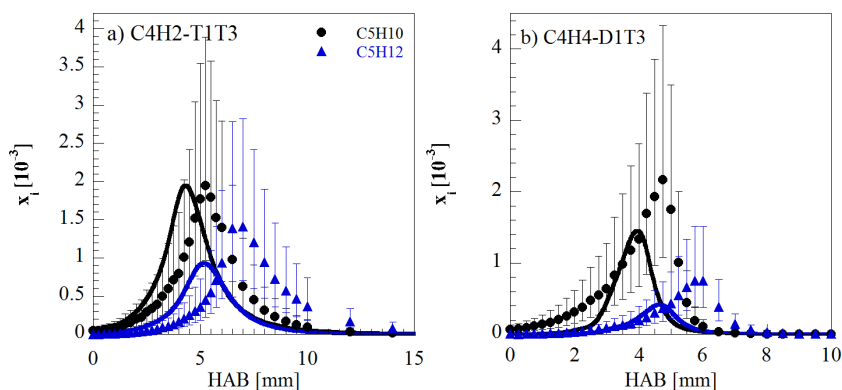


Figure 6.15: Mole fraction profiles of: a) diacetylene (C_4H_2-T1T3) and b) vinylacetylene (C_4H_4-D1T3). The symbols represent experimental data and the lines represent modeling results. The corresponding bars show the experimental error.

Figures 6.15 a) and b) show mole fraction concentrations of vinylacetylene (C_4H_4-D1T3) and diacetylene (C_4H_2-T1T3), respectively. Diacetylene (C_4H_2-T1T3) has a maximum calculated concentration of $1.93E-3$ and $0.93E-3$, and experimental concentrations of $1.9E-3$ and $1.41E-3$ for 2-methyl-2butene and n-Pentane flames. In the same way, Vinylacetylene (C_4H_4-D1T3) has a maximum calculated concentration of $1.44E-3$ and $0.414E-3$, and an experimental concentration of $2.16E-3$ and $0.757E-3$. Modeling results and experimental measurements are in good agreement and within the experimental error. C_4H_4-D1T3 and C_4H_2-T1T3 are formed in the 2-methyl-2-butene flame mainly from reactions:

- R1043: $C_4H_5-R2D1D3 \rightleftharpoons C_4H_4-D1T3 + H$
- R1041: $H + C_4H_4-D1T3 \rightleftharpoons C_4H_5-R1D1D3$
- R1033: $H + C_4H_3-R2D1T3 \rightleftharpoons C_4H_2-T1T3 + H_2$ and
- R1013: $C_4H_2-T1T3 + H \rightleftharpoons C_4H_3-R1D1T3$

6.4.3 Aromatic ring formation and precursors

Comparing the experimental toluene and Benzene concentrations in the 2-methyl-2-butene and n-Pentane flames (see Figure 6.16), a tendency to form more aromatics in the 2-methyl-2-butene flame is observed (see discussion in Ruwe et al. [13]). The maximum peak concentration for Toluene ($A1CH_3$) in the 2-methyl-2-butene flame is $1.8E-4$ and $1.1E-5$ in the n-Pentane flame; in the case of benzene ($A1$) the maximum concentrations are $4.3E-4$ and $1.8E-4$, respectively.

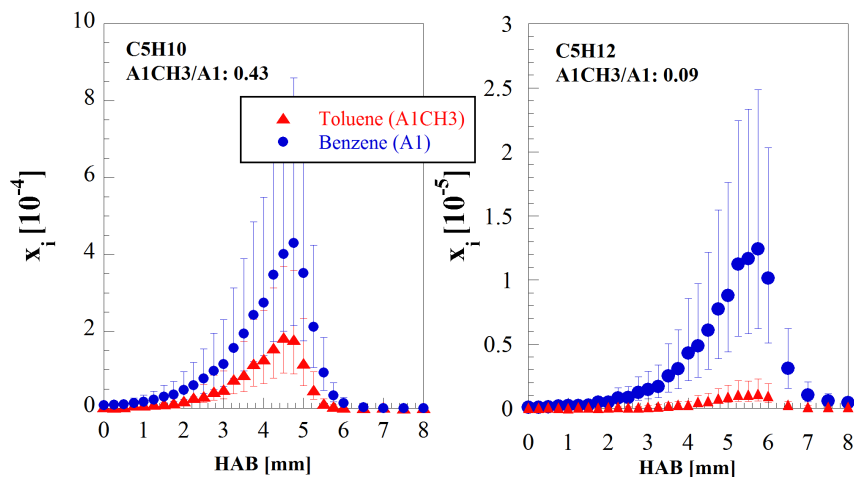


Figure 6.16: Experimental mole fraction profiles of Toluene (A1CH3)/Benzene (A1) ratio for a) 2-Methyl-2-Butene and b) n-Pentane flames. The symbols represent experimental data and the lines represent modeling results. The corresponding bars show the experimental error.

In this way, the ratio between A1CH3/A1 is 0.43 for the branched molecule and 0.09 for the linear one. The investigation of Ruwe et al. [13] presented the values corresponding to the same correlation for other fuels (alkanes, alkenes, branched), which values vary between 0.1 and 0.2 (see Table 6.23), putting the ratio of n-Pentane in agreement with those from the referential literature. At this point, does the methyl-2-butene flame produce more Toluene because of its structure?.

Fuel	A1	A1CH3	A1CH3/A1	Ref.
1-butene	1.6E-4	2.1E-5	0.13	[8]
2-butene	1.2E-4	1.7E-5	0.14	[8]
iso-butene	2.7E-4	5.4E-5	0.20	[8]
n-butane	5.2E-5	5.7E-6	0.11	[7]
iso-butane	1.1E-4	1.4E-5	0.13	[7]
n-heptane	7.9E-5	8.6E-6	0.11	[155]
2-MF	4.5E-4	1.0E-4	0.23	[156]
2M2B	4.3E-4	1.8E-4	0.43	[13]

Table 6.23: Peak mole fraction values of benzene (A1) and toluene (A1CH3) along with their ratios (A1CH3/A1) for different fuels. 2-Methyl furan is abbreviated as 2-MF and 2-methyl-2-butene as 2M2B [13].

To answer this question, we will discuss in detail the simulation results for Benzene and Toluene. Figure 6.18 shows the results for C₆H₆ isomers. Experi-

mental peak molar fractions for benzene (A1) and fulvene (FC6H6) are 4.29E-4 and 2.5E-5, and simulated fractions are 2.7E-4 and 1.6E-5, respectively. Model shape is in good agreement with the experimental measurements while peak concentrations are slightly under-predicted.

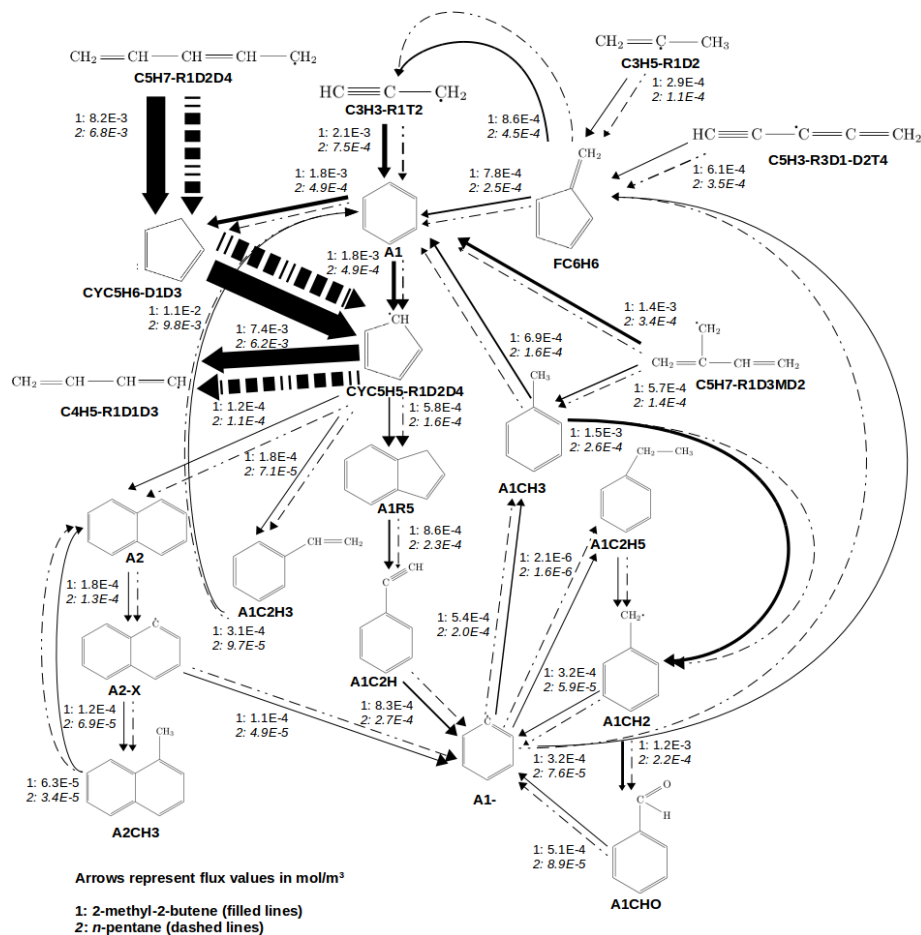


Figure 6.17: Integrated flow analysis of major reaction pathways for the aromatic species formation in the 2-methyl-2-butene and n-Pentane flames. The arrows represent the integrated flux values in mol/m³ [5].

Looking at the flow analysis for the aromatic formation in Figure 6.17, most important reactions for benzene and fulvene formation are similar in both flames and listed below:

- R948f: $2C_3H_3-R1T2 \rightleftharpoons A1 + H$
- R957f: $FC6H6 + H \rightleftharpoons A1 + H$
- R969f: $C_5H_7-R1M3MD2 + C_2H_2 \rightleftharpoons A1 + CH_3$
- R1685f: $H + A1CH_3 \rightleftharpoons CH_3 + A1$

- R959f: $2\text{C}_3\text{H}_3\text{-R1T2} \rightleftharpoons \text{FC6H6}$
- R958f: $\text{C}_3\text{H}_3\text{-R1T2} + \text{C}_3\text{H}_5\text{-R1D2} \rightleftharpoons \text{FC6H6} + 2\text{H}$ and
- R964f: $\text{C}_5\text{H}_3\text{-R3D1-D2T4} + \text{CH}_3 = \text{FC6H6}$

The difference in the concentration of the benzene and fulvene prediction is the amount of precursors; for example: the flow of propargyl ($\text{C}_3\text{H}_3\text{-R1T2}$) in the 2-methyl-2-butene flame is almost 3 times higher than in the n-Pentane flame. Another interesting observation is that

R969f: $\text{C}_5\text{H}_7\text{-R1M3MD2} + \text{C}_2\text{H}_2 \rightleftharpoons \text{A1} + \text{CH}_3$, implemented in this work (see table 6.21), resulted to be relevant for the C_5H_{12} flame, which is in accordance to the $\text{C}_5\text{H}_8\text{-D1D3Me}_2$ prediction in the flame.

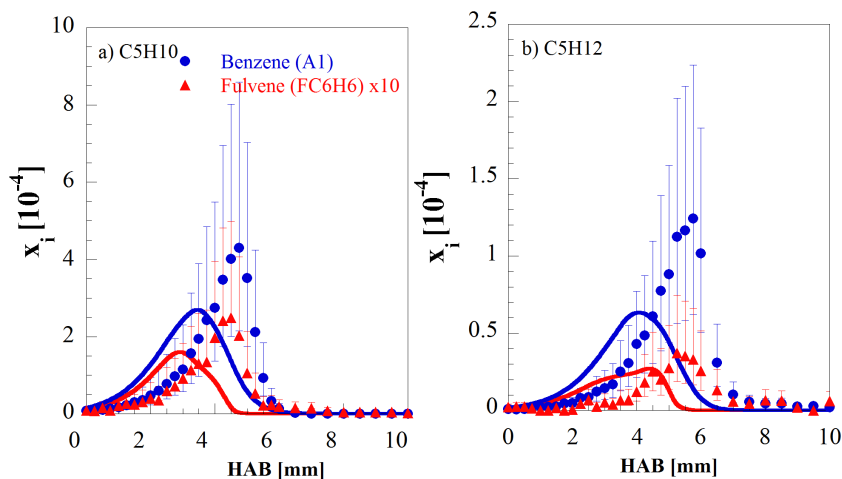


Figure 6.18: Mole fraction profiles of C_6H_6 isomers: benzene (A1) and fulvene (FC6H6) for a) 2-Methyl-2-Butene and b) n-Pentane flames. The symbols represent experimental data and the lines represent modeling results. The corresponding bars show the experimental error.

Experimental and modeling toluene (A1CH_3) profiles (see Figure 6.19) show that the profiles are well captured by the model. The difference in the concentration in both flames is of a magnitude order and in the 2-methyl-2-butene flame the maximum is underpredicted by the model ($1.84\text{E-}4$, $1.08\text{E-}4$), while in the n-Pentane flame ($1.1\text{E-}5$, $2.1\text{E-}5$) the model is over-predicted in both cases by a factor of 2. The reactions discussed on Table 6.21 were implemented in the model to see if toluene could be used as a reference point for PAH formation in the 2-methyl-2-butene flame. Looking at Figure 6.17, toluene is formed in both flames from similar reactions like the recombination of methyl and benzyl

R1665b: $\text{A1CH}_3 \rightleftharpoons \text{CH}_3 + \text{A1}$ -, and R968f: $\text{C}_5\text{H}_7\text{-R1D3MD2} + \text{C}_2\text{H}_2 \rightleftharpoons \text{A1CH}_3 + \text{H}$. In this case, the n-Pentane flame's low concentration is traced back

to the low number of reactants A1- and C5H7-R1D3MD2.

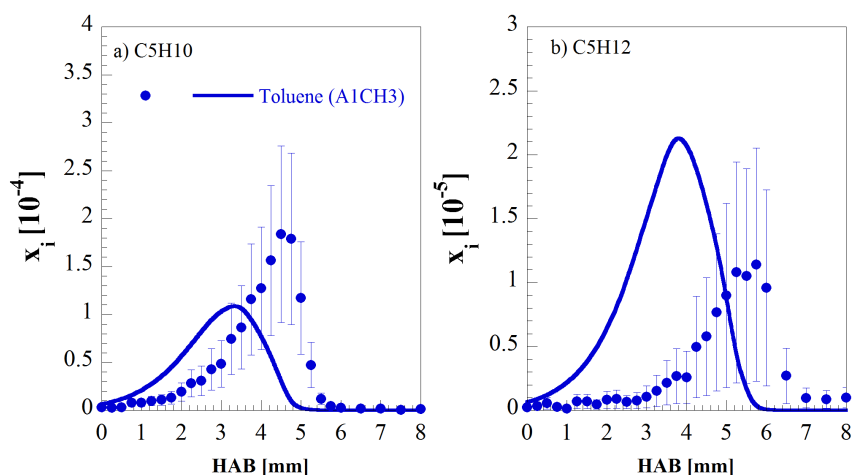


Figure 6.19: Mole fraction profiles of toluene ($A1CH3$) for a) 2-Methyl-2-Butene and b) *n*-Pentane flames. The symbols represent experimental data and the lines represent modeling results. The corresponding bars show the experimental error.

Following the discussion on benzene and toluene with the finding that formation pathways are similar in both flames but that the concentration differences rely in the precursors concentrations, the formation of some aromatic species like styrene ($A1C2H3$), indene ($A1R5$), and naphthalene ($A2$) will be discussed.

Figure 6.20 shows experimental and simulation results for 2-methyl-2-butene flame and only simulation results for *n*-Pentane flame, since these species were not detected while performing the experiment (see [5] for more details).

Experimentally, the maximum concentration of benzene was detected at a height above the burner of 4.75 *mm*, while styrene was detected at 4.25 *mm*. This means that styrene is formed at earlier reaction steps. Styrene ($A1C2H3$) (see Figure 6.20 a)) has experimental and simulated peak concentrations of 5.17E-5 and 1.6E-5, respectively, for 2-methyl-2-butene and a simulated peak concentration of 4.2E-6 for *n*-Pentane. In both flames, it is mainly formed from reaction R978b: $C3H3-R1T2 + CyC5H5-R1D2D4 \rightleftharpoons A1C2H3$. Implemented reactions proposed by Ruwe et al. 2017 [13] (see table 6.21) do not show a big influence on this specie.

Other aromatic species such as indene ($A1R5$) and naphthalene ($A2$) are shown in Figure 6.20b) and c). Calculated (1.6E-5) and measured (2.56E-5) peak mole fractions of indene are in satisfactory agreement. Indene ($A1R5$) is mainly

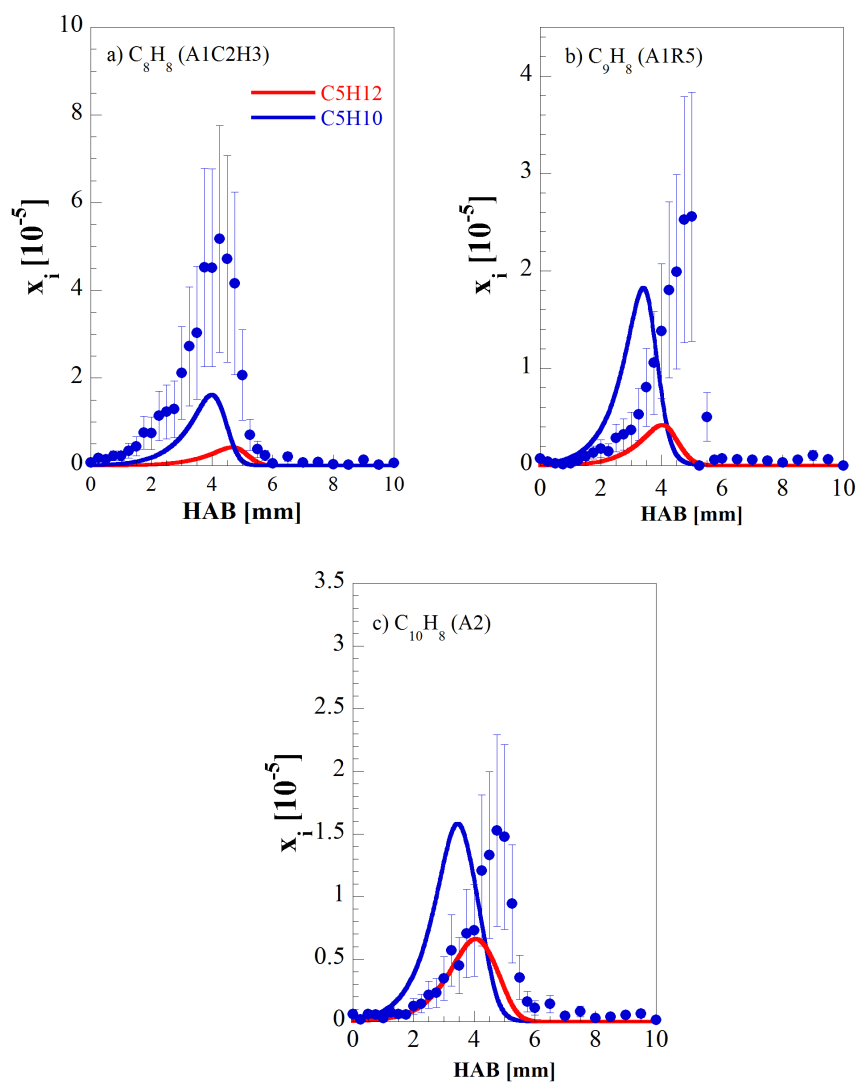


Figure 6.20: Mole fraction profiles of: styrene (A1C2H3), indene (A1R5), and naphthalene (A2). Line 2: The symbols represent experimental data and the lines represent modeling results. The corresponding bars show the experimental error.

formed via

R1512f: $\text{CyC5H5-R1D2D4} + \text{CyC5H6-D1D3} \Rightarrow \text{A1R5} + \text{CH3}$ and

R1513: $\text{CyC5H5-R1D2D4} + \text{C4H4-D1T3} \Rightarrow \text{A1R5} + \text{H}$ while reactions

R1521f: $\text{C7H7-D1D4D6} + \text{C2H2} = \text{A1R5}$ and

R1515f: $\text{A1-} + \text{C3H3-R1T2} = \text{A1R5}$ are of minor importance.

Naphthalene (A2) has a maximum peak concentration of 1.53E-5 for the experiment and 1.8E-5 for the simulation of 2-methyl-2-butene. It is mainly formed via recombination of cyclo-pentadienyl radical

R1507f: $2\text{CyC5H5-R1D2D4} \Rightarrow \text{A2} + 2\text{H}$, and ring expansion of indene (A1R5)

R1501f: $\text{A1R5} + \text{CH3} \Rightarrow \text{A2} + \text{H} + \text{H2}$. Other minor contributing reactions are

- R1533b: $\text{A2} + \text{CH2-3} \rightleftharpoons \text{A2CH3}$
- R1546f: $\text{A2CH3} + \text{H} \rightleftharpoons \text{A2} + \text{CH3}$ and
- R1534b: $\text{A2} + \text{CH2-1} \rightleftharpoons \text{A2CH3}$.

As it can be observed in Figure 6.17, the major aromatic formation pathways are independent of the molecular fuel structure and share the same growth steps.

In the following paragraphs, we will discuss the formation pathways and how the fuel structure impacts the formation of the precursors in both flames.

Figure 6.21 shows the mole fraction profiles of acetylene (C2H2), propargyl (C3H3-R1T2), and cyclopentadiene (CYC5H6-D1D3). The latter was chosen because it was the closest stable species to cyclopentadienyl radical (CyC5H5-R1D2D4). On the left side of the plots are all the experimental and simulation results corresponding to the 2-methyl-2-butene flame and on the right side those corresponding to n-Pentane flame. Acetylene experimental concentrations are very similar for both flames but propargyl and cyclopentadiene are roughly 4 times higher for the 2-methyl-2-butene flame.

The shape of the curve is in good agreement with the experiments. Peak concentrations for both fuels are over-predicted by the model but within the experimental error. Important reactions for the formation of C2H2 are

- R143: $\text{C2H3-R1D1(+M6)} \rightleftharpoons \text{C2H2} + \text{H(+M6)}$
- R265: $\text{CH} + \text{C2H2} \rightleftharpoons \text{C3H3-R1T2}$
- R266: $\text{CH2-1} + \text{C2H2} \rightleftharpoons \text{C3H3-R1T2} + \text{H}$ and
- R267: $\text{CH} + \text{C2H2} \rightleftharpoons \text{C3H3-R1T2}$.

Propargyl is mainly formed in the flame by acetylene with 34.86% in 2-methyl-2-butene and 42.09% in C5H12 (see Figure 6.22), but also C₃H₄ isomers (C3H4-D1D2: 13.97%, 10.80% and C3H4-T1: 24.35%). This reaction formation pathways will be discussed later in this work.

Cyclopentadienyl radical is formed mainly from cyclopentadiene decomposition R1746f: $\text{H} + \text{CyC5H6-D1D3} \rightleftharpoons \text{CyC5H5-R1D2D4} + \text{H2}$ and cyclopentadiene (CyC5H6-D1D3) from the following recombination and decomposition reactions:

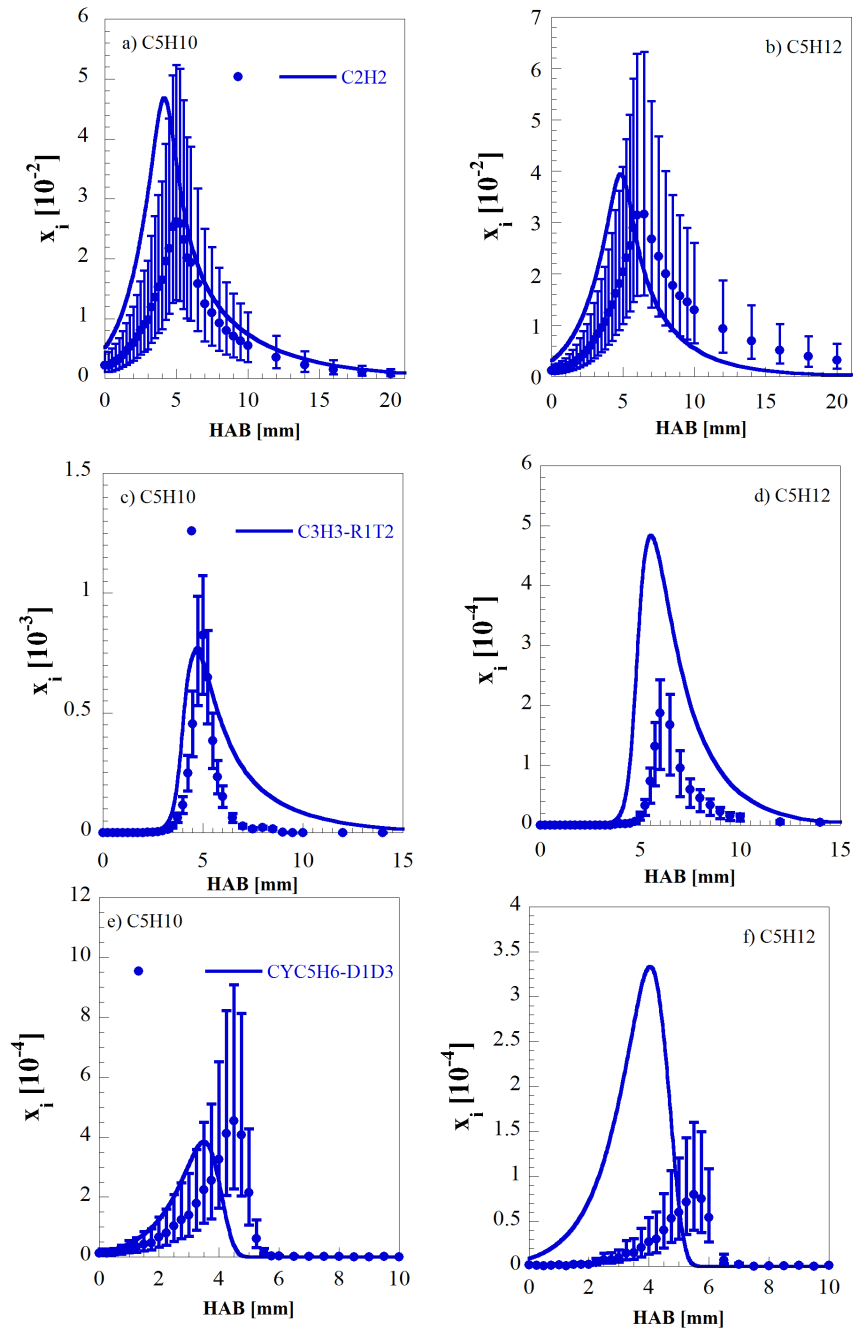


Figure 6.21: Mole fraction profiles of a) acetylene (C_2H_2), (b) propargyl (C_3H_3-R1T2), and (c) cyclopentadienyl ($CYC5H_6-D1D3$) for a) 2-Methyl-2-Butene (left) and b) n-Pentane (right) flames. The symbols represent experimental data and the lines represent modeling results. The corresponding bars show the experimental error.

R1447f: $C_2H_2 + C_3H_5-R1D2 \rightleftharpoons CyC_5H_6-D1D3 + H$,
 R1445f: $C_5H_7-R1D2D4 \rightleftharpoons CyC_5H_6-D1D3 + H$, and R1433f: $C_5H_8-D1D3 \rightleftharpoons CyC_5H_6-D1D3 + 2H$. Overprediction in cyclopentadiene may explain the overprediction for naphthalene concentration in the n-Pentane flame.

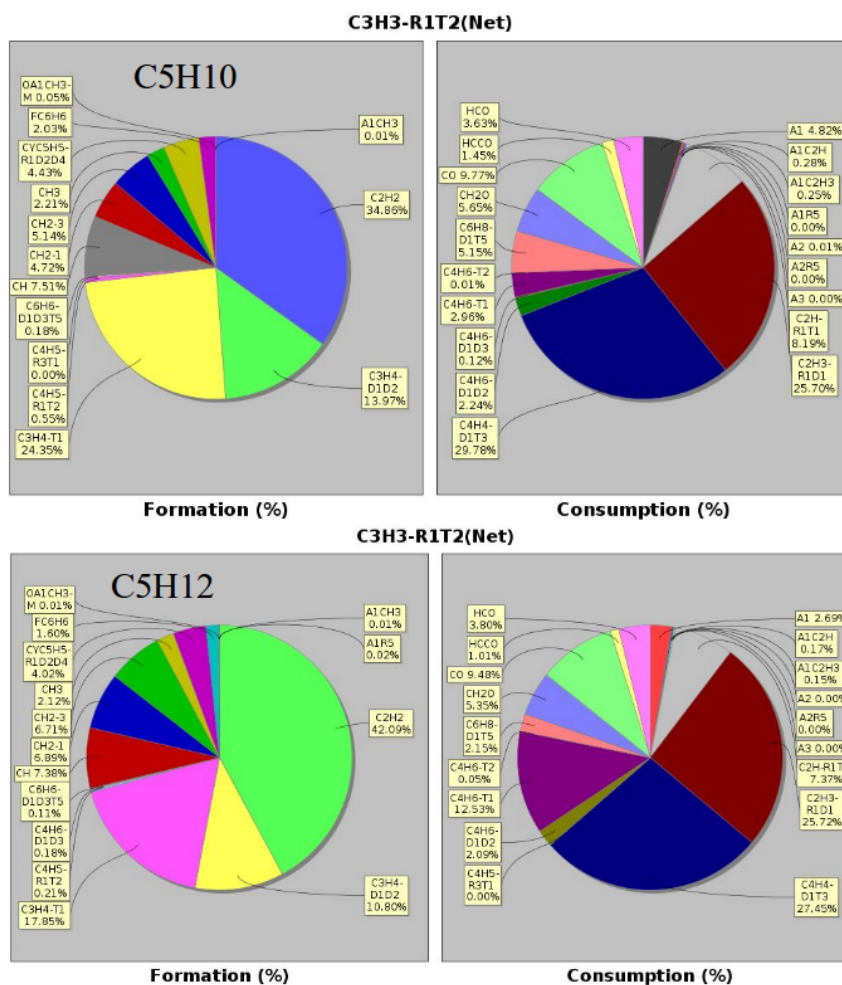


Figure 6.22: Net contribution of different species to the formation and consumption (top: 2-methyl-2-butene and bottom: n-Pentane) of propargyl (C3H3-R1T2) based on an integrated atom flow from $h = 0$ mm to 30 mm.

Figure 6.23 shows other C_3H_4 and C_5H_8 species that are fundamental for understanding the formation of the precursor in both flames. In each flame, measurements were made for two C_5H_8 molecules for 2-methyl-2-butene: two branched species C5H8-D1D3Me2 (2-methyl-1,3-butadiene) and C5H8-D1-D2Me3 (3-methyl-1,2-butadiene), for n-Pentane: two linear species C5H8-D1D4 (1,4-pentadiene), and C5H8-D1D3 (1,3-pentadiene). The model represents well both branched species and the linear specie 1-4-butadiene. Deviations with the other lin-

ear specie 1-3-butadiene are observed. A very high concentration of C5H8-D1D3Me2 can be observed for 2-methyl-2-butene, which leads to the radical C5H7-R1M3MD2 and explains the high concentration of toluene in the flame via the sequence C5H8-D1D3Me2 => C5H7-R1D3MD2 => A1CH3. Another way will be via Allene (C3H4-D1D2) with the sequence C3H4-D1D2 => C5H7-R1D3MD2 => A1CH3.

The experimental results reveal that the maximum mole fraction of propyne (C3H4-T1) is with 2.81E-3 around a factor of 1.5 larger compared to the maximum mole fraction of allene (C3H4-D1D2, 1.79E-3) at the same height above the burner. The mole fractions predicted by the model are with 1.53E-3 and 4.2E-3 for allene and propyne, respectively, within the experimental uncertainties. In the model, allene (C3H4-D1D2) is mainly formed from the propen-2-yl radical (C3H5-R2D1) via the reaction R308f: C3H5-R2D1 <=> C3H4-D1D2 + H and from the 2-methyl allyl radical (C4H7-R1D2Me2) via the reaction R700f: C4H7-R1D2Me2 <=> C3H4-D1D2 + CH3. Propyne is mainly produced from the isomerization of allene as well as from the 3-methylen-1-buten-4-yl radical (C5H7-R1D3MD2) via a C-C beta-scission (see R1270f: C5H7-R1D3MD2 <=> C3H4-T1 + C2H3-R1D1). The latter reaction of the 3-methylen-1-buten-4-yl radical (C5H7-R1D3MD2) was newly implemented in our model, since in the previous version of the model the low of allene that isomerizes to propyne was not enough to capture the intense formation of propyne.

In the new model, the aforementioned reaction significantly contributes to the propyne formation and its implementation leads to a proper prediction of the C₃H₄ isomers formation during the combustion process of 2-methyl-2-butene. Also for the n-Pentane flame, the experimentally derived concentration of propyne (C3H4-T1) is with 1.00E-3, again with a factor of 1.5 large than the peak concentration of allene (C3H4-D1D2, 0.7E-3) and the mole fraction profiles of both C3H4 isomers are well predicted by the model (C3H4-D1D2: 1.37E-3 and C3H4-T1: 0.70E-3). In the model, allene (C3H4-D1D2) is mainly formed via H-atom abstraction from the propen-2-yl radical (C3H5-R2D1) (see R308: C3H5-R2D1 <=> C3H4-D1D2 + H), as well as from the allyl radical (C3H5-R1D2) (see R297: H + C3H5-R1D2 <=> C3H4-D1D2 + H2). In the n-Pentane flame, propyne is formed via the same reactions that were discussed before for the combustion process of 2-methyl-2-butene, namely via the isomerization of allene as well as by a C-C beta-scission of the 3-methylen-1-buten-4-yl radical (C5H7-R1D3MD2).

Analyzing the formation of C3H5-R2D1 in Figure 6.24, the radical is mainly formed via the sequence C5H9-R3D1=>C3H5-R1D2=>C3H5-R2D1 for the n-Pentane flame while in the 2-methyl-2-butene flame this is a secondary route and the principal route is via reaction R1232f: C5H9-R1D3Me3 <=> C3H5-R2D1 + C2H4-D1, meaning that this radical is directly formed from a fuel molecule radical, explaining its big contribution to the formation of aromatic rings following the route C3H5-R2D1 => C5H8-D1D3Me2 => C5H7-R1D3MD2 => A1/A1CH3. Finally, the difference in the amount of one and two aromatic rings found in each flame cannot be attributed to different reactions pathways but to

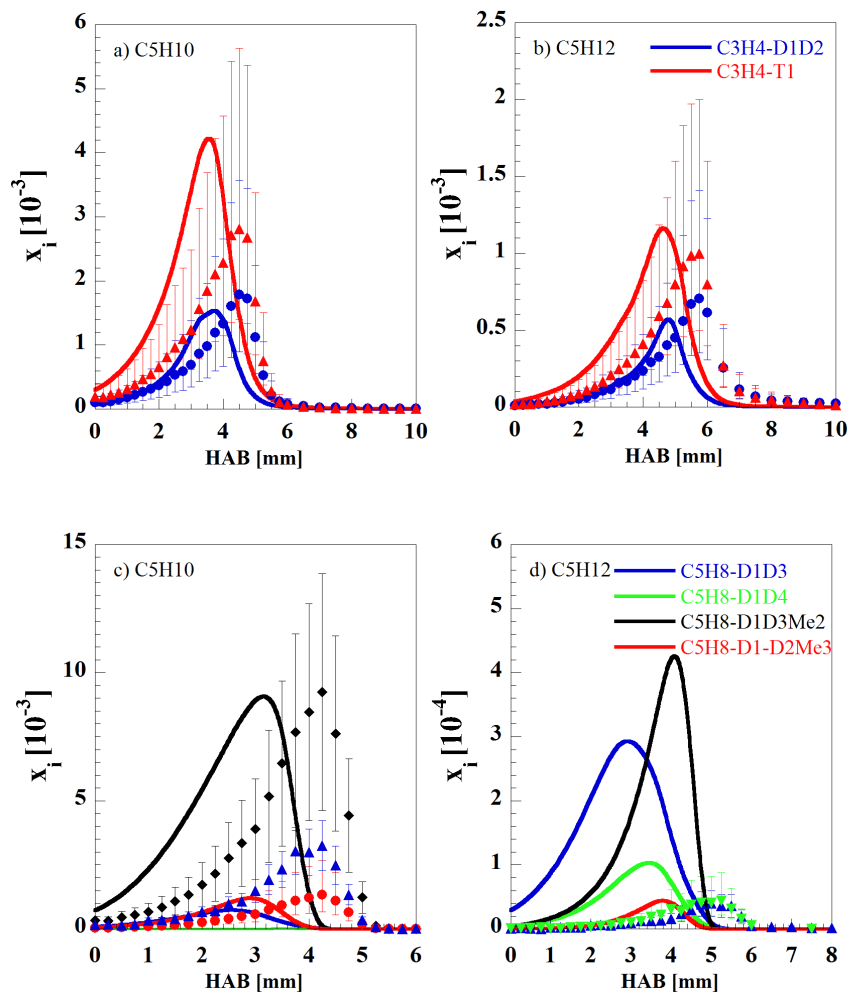


Figure 6.23: Mole fraction profiles of a-b) C_3H_4 ($C3H4-D1D2$ and $C3H4-T1$) as well as c-d) C_5H_8 ($C5H8-D1D3Me2$, $C5H8-D1-D2Me3$, $C5H8-D1D4$, and $C5H8-D1D3$) for a) 2-Methyl-2-Butene and b) *n*-Pentane flames. The symbols represent experimental data and the lines represent modeling results. The corresponding bars show the experimental error.

6.4.4 Influence of C₅ chemistry on premixed butene flames

After the implementation of a complete C₅H₁₀ high temperature chemistry in the model, simulations of the butene isomers burner-stabilized flames measured by Schenk et al. 2013 [8] were repeated. In general, predictions for the major and minor decomposition pathways similar to the ones presented in chapter 4 have been observed. Figure 6.25 a) shows experimental and predicted molar fractions for C₅H₁₀ isomers in the *iso*-butene flame. The main contribution to the C₅H₁₀ total comes from the species C5H10-D1Me2 via R1151: C5H10-D1Me2 \rightleftharpoons C4H7-R1D2Me2 + CH₃, followed by C5H10-D2Me2 via R1142: C5H10-D2Me2 + H \rightleftharpoons C5H11-R2Me2. The model slightly under-predicts the maximum peak concentration with a concentration of 1.407E-03 compared to the experimental value 2.28E-3.

C₅H₁₀ isomers in *1*-butene (C4H8-D1) flame (Figure 6.25 b)) show that total concentration is resulting from the contribution of C5H10-D2 via R1328: C5H11-R2 + O₂ \rightleftharpoons C5H10-D2 + HO₂, C5H10-D1 via R1407: C5H10-D1 \rightleftharpoons C3H5-R1D2 + C2H5-R1. Minor contributions are from C5H10-D1Me3 and C5H10-D1Me2 species. The model captures well the experimental profile shape and slightly over-predicts the maximum peak with a concentration of 1.8E-3 compared to the experimental of 7.2E-3.

Finally, for *trans-2*-butene (T-C4H8-D2) (see Figure 6.25 c)), the major contribution is coming from C5H10-D2 via R1410b: C5H10-D2 \rightleftharpoons C4H7-R2D2 + CH₃ and C5H10-D1Me3 via R1155b: C5H10-D1Me3 \rightleftharpoons C4H7-R2D2 + CH₃. Both isomers have been formed according to the modeling result at different heights. The total concentration underestimates the experimental prediction. Nevertheless, modeling results are within experimental uncertainty.

Figures 6.26 a) to c) show the total C₄H₈ and C₅H₈ isomers contribution for each butene. *iso*-butene flame predicts isoprene (C5H8-D1D3Me2) as major contributor to the total concentration. Minor contributions from C5H8-D1D3Me2 and C5H8-D1D3 are also observed. Maximum experimental and predicted concentrations are 0.47E-3 and 1.87E-3, respectively. Most important reactions are R1250b: C5H8-D1D3Me2 \rightleftharpoons C3H5-R2D1 + CH₃, R1255: C5H8-D1-D2Me3 \rightleftharpoons CH₃ + C4H5-R1T2, and R1427: C5H8-D1D3 \rightleftharpoons C4H5-R1D1D3 + CH₃.

The *1*-butene (C4H8-D1) flame shows isoprene (C5H8-D1D3Me2) and 1,3-pentadiene (C5H8-D1D3) as major contributors and the other two isomers as minor contributors. The maximum model concentration is over-predicting the experimental results. More important reactions are R1250: C5H8-D1D3Me2 \rightleftharpoons C3H5-R2D1 + CH₃, R1331f: C5H9-R4D1 + O₂ \rightleftharpoons C5H8-D1D3 + HO₂, R1332f: C5H9-R4D1 + O₂ \rightleftharpoons C5H8-D1D4 + HO₂, R1402f: H + C5H8-D1D3 \rightleftharpoons C5H9-R4D1 and R1401f: H + C5H8-D1D4 \rightleftharpoons C5H9-R4D1.

trans-2-butene (T-C4H8-D2) shows C5H8-D1D3 as major contributor followed

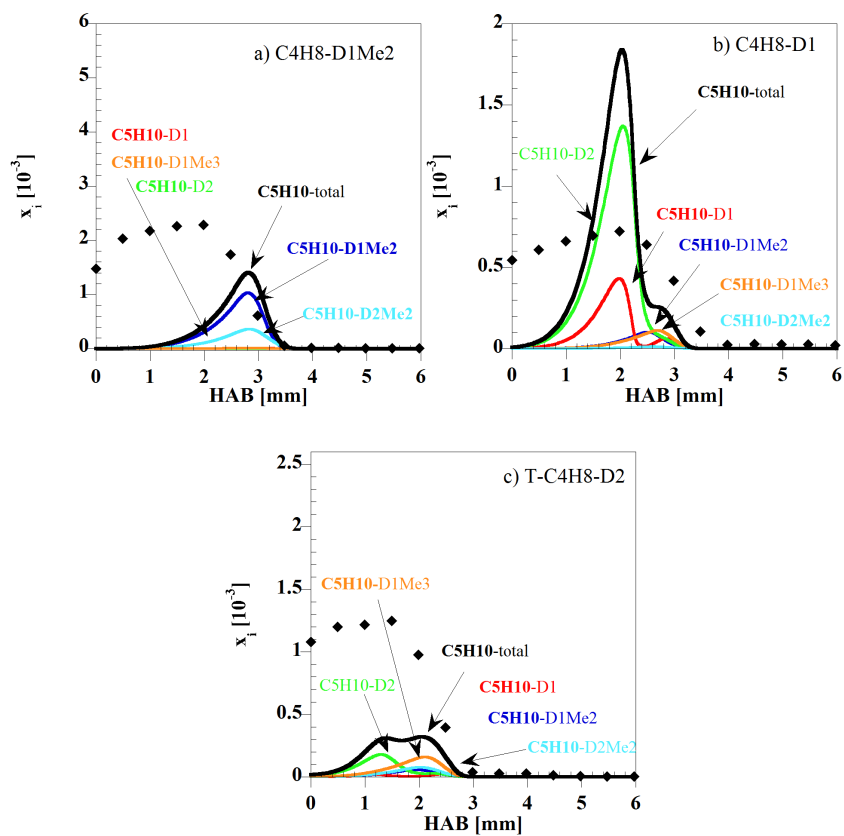


Figure 6.25: Mole fraction profiles of C_5H_{10} isomers: 2-Methyl-1-butene (C_5H_{10} -D1Me2), 2-Methyl-2-butene (C_5H_{10} -D2Me2), 3-Methyl-1-butene (C_5H_{10} -D1Me3), *n*-Pentene (C_5H_{10} -D1), and *cis*-2-Pentene (C_5H_{10} -D2). The symbols represent experimental data and the lines represent modeling results in a) \blacklozenge : *iso*-butene (C_4H_8 -D1Me2), b) \blacklozenge : 1-butene (C_4H_8 -D1) and c) \blacklozenge : *trans*-2-butene (T - C_4H_8 -D2).

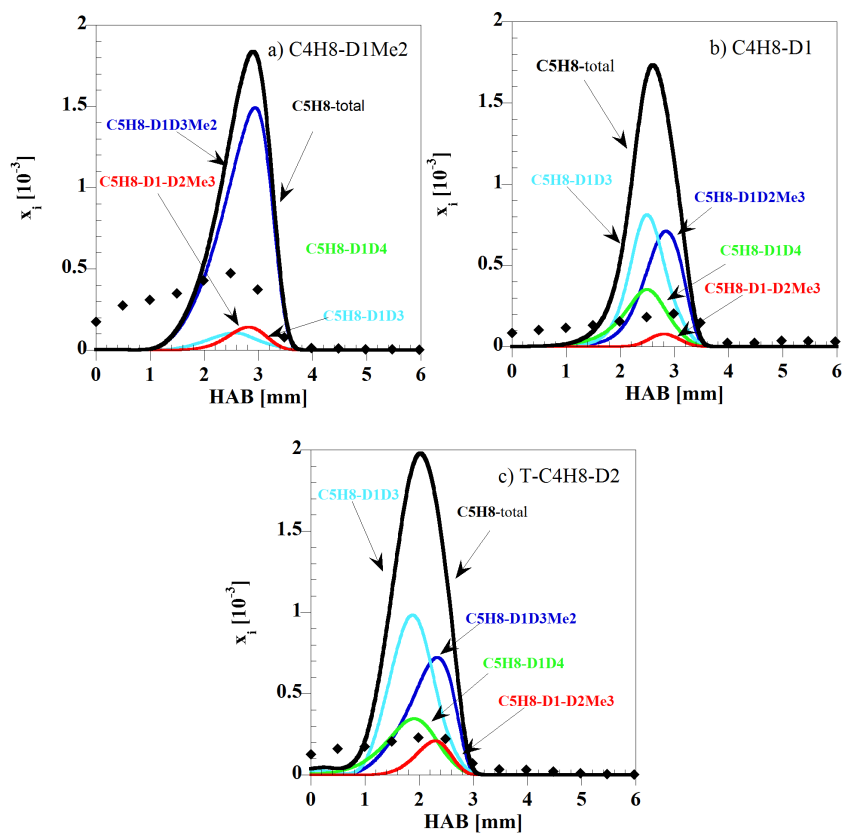


Figure 6.26: Mole fraction profiles of C_5H_8 isomers: 2-Methyl-1,3-diene (C_5H_8 -M2D1D3), 2-Methyl-2,3-diene (C_5H_8 -M2D2D3), 1,3-pentadiene (C_5H_8 -D1D3), and 1,4-pentadiene (C_5H_8 -D1D4). The symbols represent experimental data, and the lines represent modeling results in a) \blacklozenge : iso-butene (C_4H_8 -D1Me2), b) \blacklozenge : 1-butene (C_4H_8 -D1) and c) \blacklozenge : trans-2-butene (T - C_4H_8 -D2).

by C5H8-D1D3Me2, C5H8-D1D4, and C5H8-D1-D2Me3. Most important reactions are similar to *1*-butene flame (R1331f, R1402f, R1250b).

Figure 6.27 compares the experimental and simulation results for the CyC5H6-D1D3 species profile. Profile shapes are well captured and the maximum concentration is over-predicted for *1*-, and *iso*-butene. Predicted profiles lie within the experimental error. The main contribution to the formation of CyC5H6-D1D3 comes from the following reactions: R1446f: C5H7-R1D2D4 \rightleftharpoons CyC5H6-D1D3 + H, R1433f: C5H8-D1D3 \rightarrow CyC5H6-D1D3 + 2H, and R1434f: C5H8-D1D4 \rightarrow CyC5H6-D1D3 + 2H.

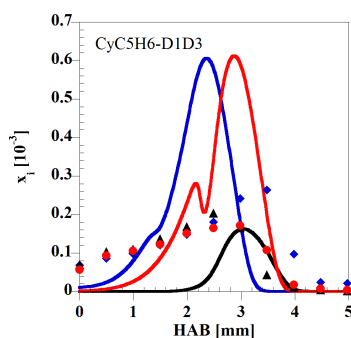


Figure 6.27: Mole fraction profiles of cyclopentadiene (CyC5H6-D1D3). The symbols represent experimental data and the lines represent modeling results in a *1*-butene (C₄H₈-D1) (◆), *trans*-2-butene (T-C₄H₈-D2) (▲), and *iso*-butene (C₄H₈-D1Me2) (●) flame.

The updated model with additional chemistry for C₅ species resulted in an increase in C₅ mole fraction compared with the results shown in chapter 4. The contribution of the different isomers was analyzed showing that C₅ species are mainly formed by build-up reactions in the three butene flames.

6.5 Validation of shock tube and Laminar flame speed experiments for 2-Methyl-2-butene and n-Pentane

Westbrook et al. 2015 [120] performed 2-methyl-2-butene autoignition experiments for different equivalence ratios ($\phi=0.5, 1.0,$ and 2.0) and pressures ($1.7 atm, 11 atm, 31 atm$), shown on Figures 6.28 a) and c). Increasing the pressure also implies that the absolute concentration of reactants increases, which results in shorter ignition delay times. The model predicts this effect over the different pressures and equivalence ratios. Predicted ignition delay times are in very good agreement with the measurements except for $\phi=0.5$ at $1666 K$, where the predicted ignition delay times are longer compared to the experimental measurements.

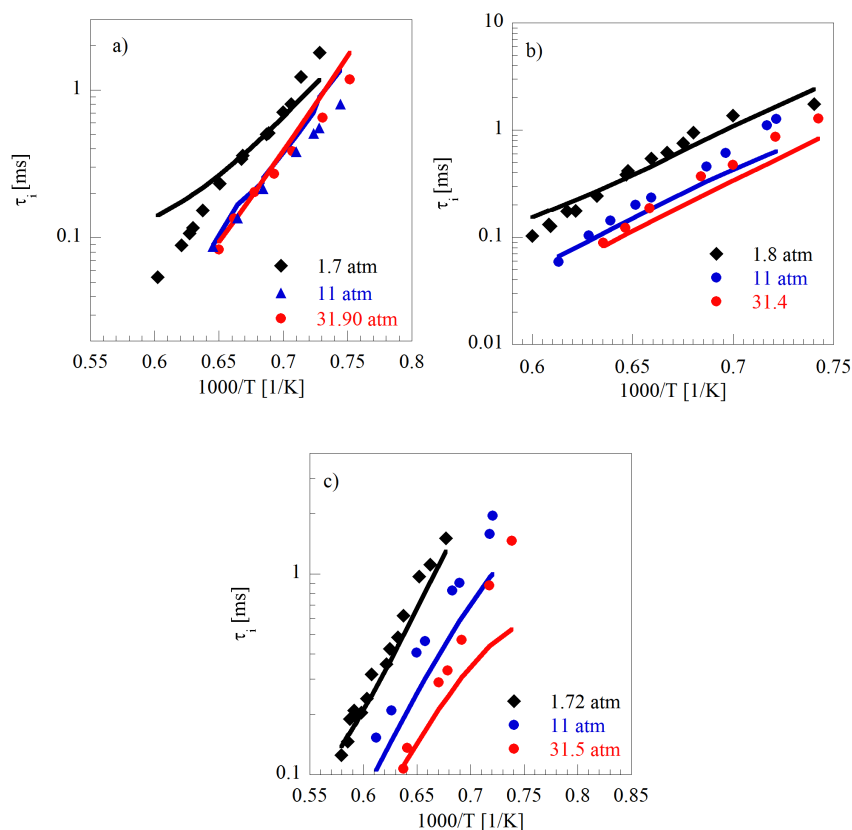


Figure 6.28: *Effect of the pressure on the ignition delay time of 2-methyl-2-butene in 99% Ar at a) $\phi=0.5$, b) $\phi=1.0$, and c) $\phi=2.0$. The lines are simulation results and the symbols are experiments by Westbrook et al. 2015 [120]; \blacklozenge 1.7 atm, \bullet 11 atm, and \blacktriangle at 31 atm.*

Figure 6.29 shows the experimental measurements performed by Bugler et al. 2016 [129] and simulation results for n-Pentane autoignition for different equivalence ratios ($\phi=0.5$, 1.0, and 2.0) and pressures (1.1 atm, 9.5 atm, 22.5 atm). The model can predict the trend of the different ignition delay times and the pressure dependency well but the times are longer compared to the experimental measurements.

Laminar flame speeds for 2-Methyl-2-butene and n-Pentane are depicted in Figures 6.30-6.33. n-Pentane laminar flame speeds are very well predicted by the model while for 2-Methyl-2-butene deviations are observed, specifically for low equivalence ratios (lower than 1.3). Nevertheless, for the experimental condition of the burner-stabilized flames as described in the previous chapter ($\phi=1.8$), an acceptable agreement is observed.

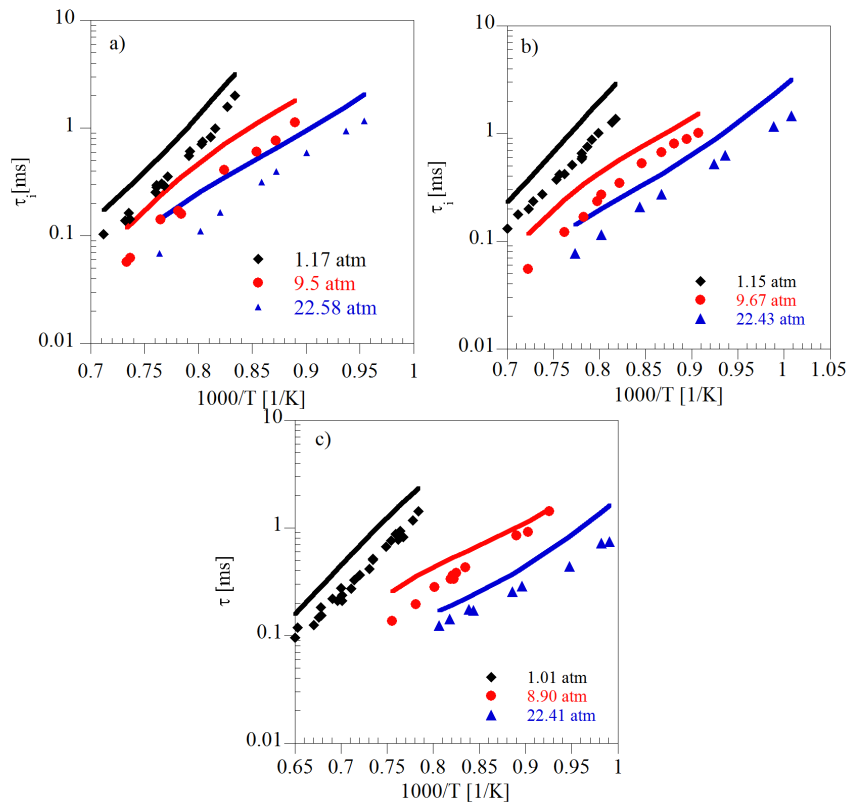


Figure 6.29: Effect of the pressure variation on the ignition delay time of *n*-Pentane in air at a) $\phi=0.5$, b) $\phi=1.0$, and c) $\phi=2.0$. The lines are simulation results and the symbols are experiments by Bugler et al. 2016 [129]; \blacklozenge 1.1 atm, \bullet 9.5 atm, and \blacktriangle at 22.5 atm.

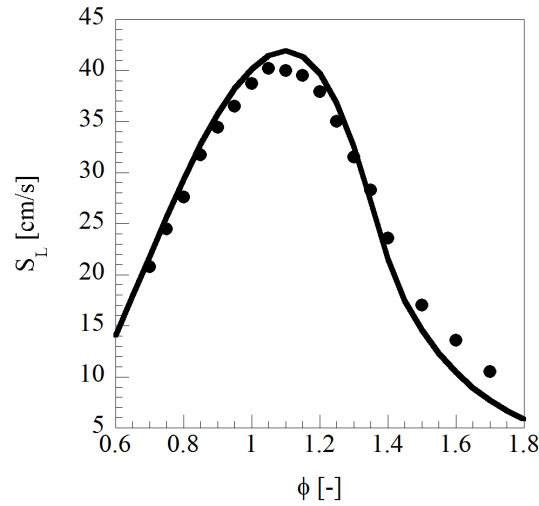


Figure 6.30: a) Numerically determined laminar flame speeds as a function of the equivalence ratio for an *n*-Pentane/air mixture at $T_u = 298$ K and $p = 1$ atm. Experiments: • by Davis et al. 1998 [42]. The black line represents the simulation results.

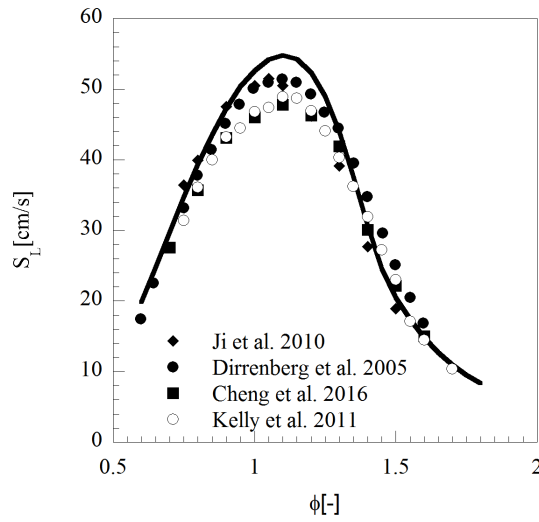


Figure 6.31: a) Numerically determined laminar flame speeds as a function of the equivalence ratio for an *n*-Pentane/air mixture at $T_u = 353\text{K}-358\text{K}$ K and $p = 1$ atm. Experiments: • by Cheng et al. [125], Ji et al. [142], Kelly et al. [143], and Dirrenberger et al. [144]. The black line represents the simulation results.

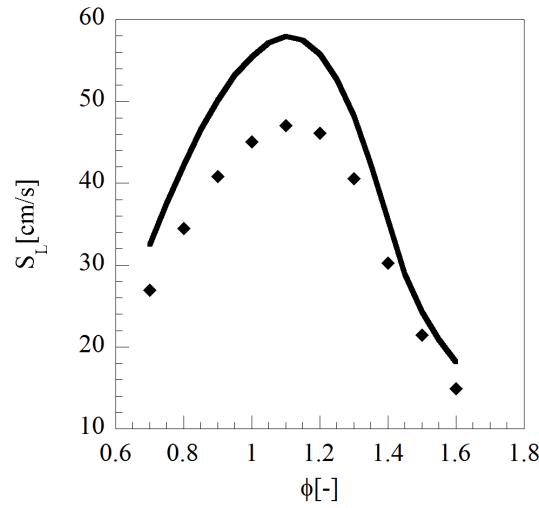


Figure 6.32: a) Numerically determined laminar flame speeds as a function of the equivalence ratio for a 2-methyl-2-butene/air mixture at $T_u = 353$ K and $p = 1$ atm. The black line represents the simulation result in this study. Experiments: \bullet by Cheng et al. 2017 [125]. The lines show the corresponding simulation results.

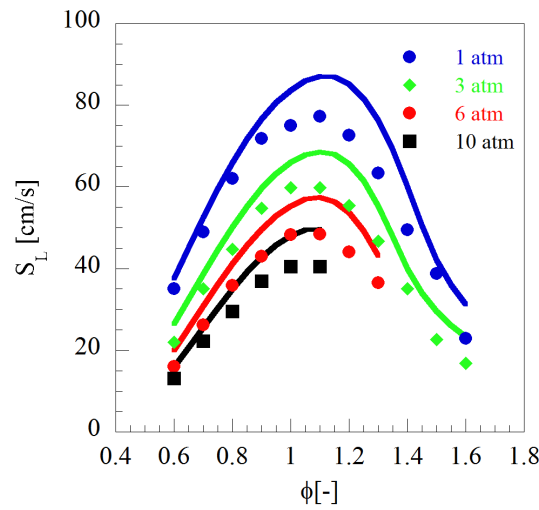


Figure 6.33: a) Numerically determined laminar flame speeds as a function of the equivalence ratio for an n-Pentane/air mixture at $T_u = 450$ K and pressures from \bullet : 1 atm, \blacklozenge : 3 atm, \bullet : 6 atm, and \blacksquare : 10 atm. The black line represents the simulation result in this study. Experiments by Zhong et al. 2018 [126]. The lines show the corresponding simulation results.

Chapter 7

Conclusion

In this work, a nomenclature and a hierarchically detailed chemical reaction mechanism have been developed. The mechanism is able to represent the oxidation pathways from C_3 to C_5 hydrocarbons and their connections under different experimental conditions.

Chapter 3 presented two strategies to determine sensitive parameters in a reaction mechanism. Sensitive species have been determined with the help of enthalpy and reaction rates sensitivity analysis for propane and propene as fuel. Thermodynamic data for C3H6-D1, C3H5-R1D2, C3H3-R1T2, and C2H5-R1 are available [9] and have been included in the reaction mechanism. Change of the thermo-data has direct influences on the reactions sensitivities, which results in a change in the ignition delays time under these operating conditions. Ignition delay times calculations and burner-stabilized flame profiles are sensitive to thermo-data changes, and only a marginal influence of the thermo-data on the calculated laminar flame speed was found. These results indicate that critical inspection of C_2 and C_3 thermo-data can help to improve hydrocarbon oxidation schemes as discussed. This strategy can be applied to burner stabilized flames, Jet stirred reactors, rapid compression machine experiments with the aim to identify sensitive intermediates whose thermodynamic data can be sensitive with respect to the target. This molecule can be further study and more reliable thermodynamic data can be calculated.

The high temperature chemistry of *n*-butane (C_4H_{10}) and *iso*-butane (C_4H_{10} -Me2) was discussed in chapter 4. The sub-mechanisms have been updated and used to study two flat flames in identical experimental conditions and their intermediates. The difference in the chemical pathways for both isomers were discussed. Major species mole fractions are well predicted by the model. Most intermediate species mole fractions agree within the experimental uncertainty. Flow analysis for *n*-butane shows that the decomposition pathways have a high contribution to the C_2 species pool, while the flow analysis for *iso*-butane shows that this fuel decomposes via the C_3 hydrocarbon species pool. This favors soot precursors production such as propargyl. The branched flame shows a concentration two times higher than for linear butane. Laminar flame speed for butane (C_4H_{10}) isomers were simulated and a good agreement was found between experimental and modeling results. Ignition delay time for each isomer and their

mixtures have been calculated and a good representation of the model has been observed except for *iso*-butane experiments at 35 atm, where predicted ignition delay times are shorter than the measured ones.

Butene (C₄H₈) isomers chemistry was discussed in chapter 5. Major features included in the C₄H₈ sub-mechanisms are a correction for the H-atom allyl abstraction and updates of the reaction rates that were presented in the literature. The sub-mechanisms have been validated for burner-stabilized flames of the three butene isomers. Major and minor intermediates species show a good agreement with the experimental measurements. The majority of intermediates are predicted under the experimental error. The fuel destruction follows mainly the C₃ and C₄ routes for the linear isomers, while for *iso*-butene (C₄H₈-D1Me₂) it mainly follows the C₃ route. C₅ intermediates species are poorly represented by the model. As in the butane isomers, *iso*-butene (C₄H₈-D1Me₂) is producing the highest benzene and toluene concentrations. Laminar flame speeds for the three isomers were simulated. 1-butene and *iso*-butene are slightly over-predicted by the model at 1 atm and 298 K. This behavior is accentuated at pressures up to 10 atm. For 2-butene a good agreement is observed from 1 to 10 atm. Ignition delay times were validated for all isomers and a good agreement was found for almost all the experimental conditions. Discrepancies were observed at pressures ranging from 10 atm to 50 atm. These deviations suggest that other pressure dependent reactions may be included in the model to successfully describe this experimental condition.

In chapter 6, the model was extended to C₅ chemistry, where a complete C₅H₁₀ sub-mechanism for *n*-Pentene (C₅H₁₀-D1), *cis*-2-Pentene (C₅H₁₀-D2), 2-Methyl-1-butene (C₅H₁₀-D1Me₂), 2-Methyl-2-butene (C₅H₁₀-D2Me₂), and 3-Methyl-1-butene (C₅H₁₀-D1Me₃) has been developed. The mechanism was validated against the experimental data from Ruwe et al. (2017) [13] where a 2-Methyl-2-butene (C₅H₁₀-D2Me₂) burner-stabilized flat flame was measured. Next, a sensitivity analysis of thermodynamic data for maximum concentration profiles was performed and concentration profiles that may be affected by the change of C₅H₉-R1D2Me₂ thermodynamic data have been determined. This is why a new set of thermo-data for C₅ species calculated with MOPAC method has been used. In general, major and minor species mole fractions are well predicted by the model. The fuel destruction follows mainly the C₅ and C₄ routes. In addition, reaction pathways leading to soot precursors such as toluene and styrene, ethyl benzene and α -methyl naphthalene have been updated and included in the model in order to describe the formation pathways of PAH in more detail. A good representation for most of these species has been observed.

Furthermore, the influence and impact of new reaction pathways in the C₄H₈ chemistry was discussed. The contribution of the different isomers and their importance was analyzed showing that C₅ species are mainly formed by build-up reactions in the three-butene flames. Some deviations from the model prediction in comparison with the experimental data were found and a rearrangement for some reaction rates was needed in order to predict the concentration within the experimental uncertainty.

Finally, the kinetic model gives a reasonable description of the global 2-Methyl-

2-butene combustion chemistry and its intermediates. The model results confirm that reaction formation pathways for one and two ring aromatic species are similar for C₅H₁₀ and C₅H₁₂ flame, but the amount of smaller precursors (propargyl, C₃H₄ and C₃H₅, C₅H₈ isomers) are dependent on the structure of each fuel. Further experimental and theoretical investigation on C₅ fuels (iso-pentane, 1-pentene and 2-pentene) should be performed to gain a more comprehensive understanding of C₅ fuel decomposition and aromatic formation.

As a result, the starting model have been expanded to predict the oxidation from C₃ to C₅ hydrocarbon species. This detailed model can be used to generate compact models for practical applications and to aid in the creation of efficient industrial processes with low emissions [2]. The models can be expanded for the prediction of low temperature regime and their validation can be extended to another combustion conditions that could be of interest.

Bibliography

- [1] Turns S. R. *An introduction to Combustion: Concepts and applications*. McGraw Hill Book Co, 2012.
- [2] Kohse-Höinghaus K. Clean combustion: Chemistry and diagnostics for a systems approach in transportation and energy conversion. *Progress in Energy and Combustion Science*, 65:1–5, 2018.
- [3] Boden et al. (2016), UNFCCC (2016), and BP (2016). The numbers reproduced from the global carbon atlas (www.globalcarbonatlas.org). Accessed at 18.07.18.
- [4] Online AGVES Meeting. Euro 7 ldv, <https://circabc.europa.eu/sd/a/06f34a81-4184-45c3-8b98-b7515d60592f/ec2021>.
- [5] Leon L., Ruwe L., Moshhammer K., Seidel L., Shrestha K. P., Mauss F., Wang X., Kohse-Höinghaus K., and Hansen N. Chemical insights into the larger sooting tendency of 2-methyl-2-butene compared to n-pentane. *Combustion and Flame*, pages 182–197, 2019.
- [6] Hoyermann K., Mauß F., and Zeuch T. A detailed chemical reaction mechanism for the oxidation of hydrocarbons and its application to the analysis of benzene formation in fuel-rich premixed laminar acetylene and propene flames. *Physical Chemistry Chemical Physics*, 6:3824–3835, 2004.
- [7] Osswald P., Kohse-Höinghaus K., Struckmeier U., Zeuch T., Seidel L., Leon L., and Mauss F. Combustion chemistry of the butane isomers in premixed low-pressure flames. *Zeitschrift für Physikalische Chemie*, 225:1029–1054, 2011.
- [8] Schenk M., Leon L., Moshhammer K., Osswald P., Zeuch T., Seidel L., Mauss F., and Kohse-Höinghaus K. Detailed mass spectrometric and modeling study of isomeric butene flames. *Combustion and Flame*, 160(3):487–503, 2013.
- [9] Goos E., Burcat A., and Ruscic B. Extended third millennium thermodynamic database for combustion and air-pollution use with updates from active thermochemical tables available via <http://burcat.technion.ac.il/dir/>, 2013.
- [10] Nawdiyal A. *The influence of allylic site abstraction reactions of olefin on cyclo-paraffin formation*. PhD thesis, Brandenburg University of Technology Cottbus–Senftenberg, 2018.

- [11] Ruwe L., Moshhammer K., Hansen N., and Kohse-Höinghaus K. Influences of the molecular fuel structure on combustion reactions towards soot precursors in selected alkane and alkene flames. *Physical Chemistry Chemical Physics*, 20(16):10780–10795, 2018.
- [12] Gao C. W., Allen J. W., Green W. H., and West R. H. Reaction Mechanism Generator: Automatic construction of chemical kinetic mechanisms. *Computer Physics Communications*, 203:212–225, 2016.
- [13] Ruwe L., Moshhammer K., Hansen N., and Kohse-Hoinghaus K. Consumption and hydrocarbon growth processes in a 2-methyl-2-butene flame. *Combustion and Flame*, 175:34–46, 2017.
- [14] Stewart J.J.P. MOPAC2016. Stewart Computational Chemistry, Colorado Springs, CO, USA, 2016.
- [15] Glassman I. and Yetter R. A. *Combustion*. Elsevier, 4th edition, 2008.
- [16] Warnatz J., Maas U., and Dibble R.W. *Combustion. Physical and chemical fundamentals, modeling and simulation, experiments, pollutant formation*. Springer, 4th edition, 2006.
- [17] McNaught A. D. and Wilkinson A. Compendium of chemical terminology, 2nd ed. (the "gold book"). Blackwell Scientific Publications, 2006.
- [18] Lindemann F. A. Discussion on "the radiation theory of chemical action". *Transactions of the Faraday Society*, 17:598–606, 1922.
- [19] Goos E. and Burcat A. *Handbook of Combustion-Thermochemistry*. Wiley-VCH, 2010.
- [20] Kuo K. K. Principles of combustion, Second Edition. *Combustion and Flame*, 73(3):337, 1986.
- [21] March J. *Advanced Organic Chemistry: Reactions, Mechanisms, and Structure*. Wile, New York, 3rd edition, 1985.
- [22] Bellanca R. *BlueBellMouse A Tool for Kinetic Model Development*. PhD thesis, Lund University, 2004.
- [23] LOGE SOFT version 1.06. *Manual - Book 2 - Homogeneous Reactor Models*, 2015.
- [24] Law C. K. *Combustion Physics*. Cambridge University Press, Cambridge-England, 2006.
- [25] LOGE SOFT version 1.06. *Manual - Book 4 - Flames*, 2015.
- [26] LOGEresearchv1.10-000. Loge lund combustion engineering. www.logesoft.com/de/logesoft, 2018.
- [27] Atakan B., Hartlieb A. T., Brand J., and Kohse-Höinghaus K. An experimental investigation of preixed fuel-rich low-pressure propene/oxygen/argon flames by laser spectroscopy and molecular-beam mass spectrometry. *Proc. Combust. Inst*, 27:435, 1998.

- [28] Hughes K. J., Griffiths J. F., Fairweather M., and Tomlin A. S. Evaluation of models for the low temperature combustion of alkanes through interpretation of pressure-temperature ignition diagrams. *Physical chemistry chemical physics : PCCP*, 8(27):3197–3210, 2006.
- [29] Goos E., Sickfeld C., Mauß F., Seidel L., Ruscic B., Burcat A., and Zeuch T. Prompt NO formation in flames: The influence of NCN thermochemistry. *Proceedings of the Combustion Institute*, 34(1):657–666, 2013.
- [30] Burcat A., Scheller K., and Lifshitz A. Shock-tube investigation of comparative ignition delay times for C₁-C₅ alkanes. *Combustion and Flame*, 16:29–33, 1971.
- [31] Brown C. J. and Thomas G. O. Experimental studies of shock-induced ignition and transition to detonation in ethylene and propane mixtures. *Combustion and Flame*, 117(4):861–870, 1999.
- [32] Herzler J., Jerig L., and Roth P. Shock-tube study of the ignition of propane at intermediate temperatures and high pressures. In *Combustion Science and Technology*, volume 176, pages 1627–1637, 2004.
- [33] Zhukov V. P., Sechenov V. A., and Starikovskii A. Yu. Autoignition of a lean propane-air mixture at high pressures. *Kinetics and Catalysis*, 46(3):319–327, 2005.
- [34] Lam K. Y., Hong Z., Davidson D. F., and Hanson R. K. Shock tube ignition delay time measurements in propane/O₂/argon mixtures at near-constant-volume conditions. *Proceedings of the Combustion Institute*, 33(1):251–258, 2011.
- [35] Burcat A. and Radhakrishnan K. High temperature oxidation of propene. *Combustion and Flame*, 60(2):157–169, 1985.
- [36] Qin Z., Yang H., and Gardiner W. C. Measurement and modeling of shock-tube ignition delay for propene. *Combustion and Flame*, 124(1-2):246–254, 2001.
- [37] Burke S. M., Burke U., Mc Donagh R., Mathieu O., Osorio I., Keesee C., Morones A., Petersen E. L., Wang W., DeVerter T. A., Oehlschlaeger M. A., Rhodes B., Hanson R. K., Davidson D. F., Weber B. W., Sung C. J., Santner J., Ju Y., Haas F. M., Dryer F. L., Volkov E. N., Nilsson E. J.K., Konnov A. A., Alrefae M., Khaled F., Farooq A., Dirrenberger P., Glaude P. A., Battin-Leclerc F., and Curran H. J. An experimental and modeling study of propene oxidation. Part 2: Ignition delay time and flame speed measurements. *Combustion and Flame*, 162(2):296–314, 2015.
- [38] Metghalchi M. and Keck J. C. Laminar burning velocity of propane-air mixtures at high temperature and pressure. *Combustion and Flame*, 38(C):143–154, 1980.
- [39] Egolfopoulos F. N., Zhu D. L., and Law C. K. Experimental and numerical determination of laminar flame speeds: Mixtures of C₂-hydrocarbons with oxygen and nitrogen. *Symposium (International) on Combustion*, 23(1):471–478, 1991.

- [40] Vagelopoulos C. M., Egolfopoulos F. N., and Law C. K. Further considerations on the determination of laminar flame speeds with the counterflow twin-flame technique. *Symposium (International) on Combustion*, 25(1):1341–1347, 1994.
- [41] Vagelopoulos C. N. and Egolfopoulos F. N. Direct experimental determination of laminar flame speeds. *Proc. combust. Inst.*, 27:513, 1998.
- [42] Davis S. G. and Law C. K. Determination of and fuel structure effects on laminar flame speeds of C₁ to C₈ hydrocarbons. *Combustion Science and Technology*, 140:427, 1998.
- [43] Hassan M. I., Aung K. T., Kwon O. C., and Faeth G. M. Properties of laminar premixed hydrocarbon/air flames at various pressures. *J. Propul. Power*, 14:479–488, 1998.
- [44] Bosschaart K. J. and de Goey L. P. H. The laminar burning velocity of flames propagating in mixtures of hydrocarbons and air measured with the heat flux method. *Combustion and Flame*, 136:261–269, 2004.
- [45] Jomaas G., Zheng X. L., Zhu D. L., and Law C. K. Experimental determination of counterflow ignition temperatures and laminar flame speeds of C₂-C₃ hydrocarbons at atmospheric and elevated pressures. *Proceedings of the Combustion Institute*, 30(1):193–200, 2005.
- [46] Huzayyin A. S., Moneib H. A., Shehatta M. S., and Attia A. M.A. Laminar burning velocity and explosion index of LPG-air and propane-air mixtures. *Fuel*, 87(1):39–57, 2008.
- [47] Wu F., Kelley A. P., Tang C., Zhu D., and Law C. K. Measurement and correlation of laminar flame speeds of CO and C₂ hydrocarbons with hydrogen addition at atmospheric and elevated pressures. *International Journal of Hydrogen Energy*, 36(20):13171–13180, 2011.
- [48] Lowry W., de Vries J., Krejci M., Petersen E., Serinyel Z., Metcalfe W., Curran H., and Bourque G. Laminar Flame Speed Measurements and Modeling of Pure Alkanes and Alkane Blends at Elevated Pressures. *Journal of Engineering for Gas Turbines and Power*, 2011.
- [49] Dirrenberger P., Le Gall H., Bounaceur R., Herbinet O., Glaude P.A., Konnov A., and Battin-Leclerc F. Measurements of laminar flame velocity for components of natural gas. *Energy and fuels*, 25:3875–3884, 2011.
- [50] Davis S. G., Law C. K, and Wang H. Propene pyrolysis and oxidation kinetics in a flow reactor and laminar flames. *Combustion and Flame*, 119:375–399, 1999.
- [51] Burcat A. *Combustion Chemistry. Chapter 8, Thermochemical Data for Combustion Calculations*. Springer-Verlag, New York, 1984.
- [52] National Center for Biotechnology Information. Pubchem compound database. CID=7843, <https://pubchem.ncbi.nlm.nih.gov/compound/7843>, (accessed July 7, 2015).

- [53] National Center for Biotechnology Information. Pubchem compound database. CID=6360, <https://pubchem.ncbi.nlm.nih.gov/compound/6360>, (accessed July 7, 2015).
- [54] Morganti K. J., Foong T. M., Brear M. J., da Silva G., Yang Y., and Dryer F. L. The Research and Motor octane numbers of Liquefied Petroleum Gas (LPG). *Fuel*, 108:797–811, 2013.
- [55] Tran L. S., Pieper J., Zeng M., Li Y., Zhang X., Li W., Graf I., Qi F., and Kohse-Höinghaus K. Influence of the biofuel isomers diethyl ether and n-butanol on flame structure and pollutant formation in premixed n-butane flames. *Combustion and Flame*, 175:47–59, 2017.
- [56] Marinov N. M., Pitz W.J., Westbrook C.K., Castaldi M.J., Senkan S.M., and Melius C.F. Aromatic and polycyclic aromatic hydrocarbon formation in a laminar premixed n-butane flame. *Combustion and Flame*, 114:192–213, 1998.
- [57] Hirasawa T., Law C. K., Sung C. J., Wang H., and Yang Z. Determination of laminar flame speeds of ethylene/n-butane/air flames using digital particle image velocimetry. *2nd Joint Meeting of the U.S.A Section of the Combustion Institute*, 2001. Oakland.
- [58] Tang C. L., Huang Z. H., and Law C. K. Determination, correlation, and mechanistic interpretation of effects of hydrogen addition on laminar flame speeds of hydrocarbon-air mixtures. *Proceedings of the Combustion Institute*, 33(1):921–928, 2011.
- [59] Wu H., Hu E., Yu H., Li Q., Zhang Z., Chen Y., and Huang Z. Experimental and Numerical Study on the Laminar Flame Speed of n-Butane/Dimethyl Ether-Air Mixtures. *Energy & Fuels*, 28(5):3412–3419, 2014.
- [60] Veloo P. S., Wang Y. L., Egolfopoulos F. N., and C. K. Westbrook. A comparative experimental and computational study of methanol, ethanol, and n-butanol flames. *Combustion and Flame*, 157:1989–2004, 2010.
- [61] Wang Y. L., Feng Q., Egolfopoulos F. N., and Tsotsis T. T. Studies of C₄ and C₁₀ methyl ester flames. *Combustion and Flame*, 158(8):1507–1519, 2011.
- [62] Herbinet O., Battin-Leclerc F., Bax S., Le Gall H., Glaude P.A., Fournet R., Zhou Z., Deng L., Guo H., Xie M., and Qi F. Detailed product analysis during the low temperature oxidation of n-butane. *Physical Chemistry Chemical Physics*, 13:296–308, 2011.
- [63] Dagaut P., Luche J., and Cathonnet M. Reduction of NO by n-butane in a jsr: Experiments and kinetic modeling. *Energy and Fuels*, 14(3):712–719, 2000.
- [64] Cathonnet M., Boettner J.C., and James H. Experimental study and numerical modeling of high temperature oxidation of propane and n-butane. *Symposium (International) on Combustion*, 18(1):903–913, 1981.

- [65] Chakir A., Cathonnet M., Boettner J. C., and Gaillard F. Kinetic study of n-butane oxidation. *Combustion Science and Technology*, 65(4-6):207–230, 1989.
- [66] Dagaut P., Luche J., and Cathonnet M. Experimental and kinetic modeling of the reduction of NO by isobutane in a jsr at 1 atm. *International Journal of Chemical Kinetics*, 32(6):365–377, 2000.
- [67] Horning D.C., Davidson D.F., and Hanson R.K. Study of the high-temperature autoignition of n-alkane/O₂/ar mixtures. *Journal of Propulsion and Power*, 18:363–371, 2002.
- [68] Healy D., Donato N.S., Aul C.J. and Petersen E.L., Zinner C.M., Bourque G., and Curran H.J. n-butane: Ignition delay measurements at high pressure and detailed chemical kinetic simulations. *Combustion and Flame*, 157:1526–1539, 2010.
- [69] Oehlschlaeger M.F., Davidson D.F., Herbon J.T., and Hanson R.K. Shock tube measurements of branched alkane ignition times and OH concentration time histories. *International Journal of Chemical Kinetics*, 36:67–78, 2004.
- [70] Healy D., Donato N. S., Aul C. J., Petersen E. L., Zinner C. M., Bourque G., and Curran H. J. Isobutane ignition delay time measurements at high pressure and detailed chemical kinetic simulations. *Combustion and Flame*, 157:1540–1551, 2010.
- [71] Ogura T., Nagumo Y., Miyoshi A., and Koshi M. Chemical kinetic mechanism for high temperature oxidation of butane isomers. *Energy and Fuels*, 21:130–135, 2007.
- [72] Donato N., Aul C., Petersen E., Zinner C., Curran H., and Bourque G. Ignition and oxidation of 50/50 n-butane/iso-butane blend. *Proceedings of ASME Turbo Expo 2009: Power for Land, Sea and Air*, GT2009-59673, 2009.
- [73] Gersen S., Mokhov A.V., Darmeveil J.H., and Levinsky H.B. Ignition properties of n-butane and iso-butane in a rapid compression machine. *Comb. and Flame*, 157:240–245, 2010.
- [74] Oehlschlaeger M. A., Davidson D. F., and Hanson R. K. High-temperature thermal decomposition of isobutane and n-butane behind shock waves. *The Journal of Physical Chemistry A*, 108(19):4247–4253, 2004.
- [75] Griffiths J.F. and Barnard J.A. *Flame and Combustion*. CRC Press, 3rd edition, 1995.
- [76] Dean A. M. Predictions of pressure and temperature effects upon radical addition and recombination reactions. *The Journal of Physical Chemistry*, 89:4600–4608, 1985.
- [77] Curran H. J., Gaffuri P., Pitz W. J., and Westbrook C. K. A comprehensive modeling study of iso-octane oxidation. *Combustion and Flame*, 129:253–280, 2002.

- [78] Aguilera-Ipaguirre J., Curran H. J., Klopper W., and Simmie J. M. Accurate benchmark calculation of the reaction barrier height for hydrogen abstraction by the hydroperoxyl radical from methane. implications for C_nH_{2n+2} where $n=2-4$. *Journal of Physical Chemistry A*, 112:7047–7054, 2008.
- [79] Westbrook C. K., Warnatz J., and Pitz W. J. A detailed chemical kinetic reaction mechanism for the oxidation of iso-octane and n-heptane over an extended temperature range and its application to analysis of engine knock. *Symposium (International) on Combustion*, 22(1):893–901, 1989.
- [80] Carstensen H-H, Dean A. M., and Deutschmann O. Rate constants for the H abstraction from alkanes (R–H) by RO_2 radicals: A systematic study on the impact of R and R. *Proceedings of the combustion Institute*, 31:149–157, 2007.
- [81] Ahmed S. S., Mauss F., Moréac G., and Zeuch T. A comprehensive and compact n-heptane oxidation model derived using chemical lumping. *Physical Chemistry Chemical Physics*, 9(9):1107–1126, 2007.
- [82] Allara D. L. and Shaw R. A compilation of kinetic parameters for the thermal degradation of n-alkane molecules. *Journal of Physical and Chemical Reference Data*, 9:523–559, 1980.
- [83] Baldwin R. R. and Walker R. W. Rate constants for hydrogen + oxygen system, and for H atoms and OH radicals + alkanes. *Journal of the Chemical Society, Faraday Transactions 1*, 75(0):140–154, 1979.
- [84] Atkinson R. Estimations of OH radical rate constants from H-atom abstraction from C-H and O-H bonds over the temperature range 250-1000 K. *International Journal of Chemical Kinetics*, 18(5):555–568, 1986.
- [85] Tsang W. Chemical kinetic data base for combustion chemistry part 4. isobutane. *Journal Physical Chemistry Reference Data*, 19(1):1–68, 1990.
- [86] Cohen N. Are reaction rate coefficients additive? Revised transition state theory calculations for OH + alkane reactions. *International Journal of Chemical Kinetics*, 23(5):397–417, 1991.
- [87] Blurock E. and Battin-Leclerc F. *Modeling Combustion with Detailed Kinetic Mechanisms*, pages 17–57. Springer London, London, 2013.
- [88] Curran H. J. Rate constant estimation for C_1 to C_4 alkyl and alkoxy radical decomposition. *International Journal of Chemical Kinetics*, (4):250–275, 2006.
- [89] Matheu D. M., Green W. H., and Grenda J. M. Capturing pressure-dependence in automated mechanism generation: Reactions through cycloalkyl intermediates. *International Journal of Chemical Kinetics*, 35(3):95–119, 2003.
- [90] Hirasawa T., Sung C.J., Joshi A., Yang Z., Wang H., and Law C.K. Determination of laminar flame speeds using digital particle image velocimetry: Binary fuel blends of ethylene, n-butane, and toluene. *Proceedings of the Combustion Institute*, 29(2):1427–1434, 2002.

- [91] National Center for Biotechnology Information. Pubchem compound database. CID=7844, <https://pubchem.ncbi.nlm.nih.gov/compound/7844>, (accessed July 8, 2015).
- [92] National Center for Biotechnology Information. Pubchem compound database. CID=8255, <https://pubchem.ncbi.nlm.nih.gov/compound/8255>, (accessed July 8, 2015).
- [93] National Center for Biotechnology Information. Pubchem compound database. CID=5287573, <https://pubchem.ncbi.nlm.nih.gov/compound/5287573>, (accessed July 8, 2015).
- [94] National Center for Biotechnology Information. Pubchem compound database. CID=62695, <https://pubchem.ncbi.nlm.nih.gov/compound/62695>, (accessed July 8, 2015).
- [95] Dias V. and Vandooren J. Experimental and modeling study of a lean pre-mixed iso-butene/hydrogen/oxygen/argon flame. *Fuel*, 89(9):2633–2639, 2010.
- [96] Curran H. J., Dunphy M.P., and Simmie J. M. Shock tube ignition of ethanol, isobutene and mtbe: experiments and modeling. *Twenty-fourth Symposium (International) on Combustion/The Combustion Institute*, (24):769–776, 1992.
- [97] Bauge J. C., Battin-Leclerc F., and Baronnet F. Experimental and modeling study of the oxidation of isobutene. *International Journal of Chemical Kinetics*, 30(9):629–640, 1998.
- [98] Yasunaga K., Kuraguchi Y., Ikeuchi R. Masaoka H., Takahashi O., Koike T., and Hidaka Y. Shock tube and modeling study of isobutene pyrolysis and oxidation. *Proceedings of the combustion institute*, (32):453–460, 2009.
- [99] Heyberger B., Belmekki N., Conraud V., Glaude P.-A., Fournet R., and Battin-Leclerc F. Oxidation of small alkenes at high temperature. *International Journal of Chemical Kinetics*, 34(12):666–677, 2002.
- [100] Pan L., Hu E., Zhang J., Tian Z., Li X., and Huang Z. A high pressure shock tube study of 1-butene oxidation and its comparison with n-butane and alkenes. *Fuel*, 157:21–27, 2015.
- [101] Dagaut P. and Cathonnet M. Isobutene oxidation and ignition: Experimental and detailed kinetic modeling study. *Combustion Science and Technology*, (137):237–275, 1998.
- [102] Fenard Y., Dayma G., Halter F., Foucher F., Serinyel Z., and Dagaut P. Experimental and modeling study of the oxidation of 1-butene and cis -2-butene in a jet-stirred reactor and a combustion vessel. *Energy and Fuels*, 29(2):1107–1118, 2015.

- [103] Zhao P., Yuan W., Sun H., Li Y., Kelley A. P., Zheng X., and Law C. K. Laminar flame speeds, counterflow ignition, and kinetic modeling of the butene isomers. *Proceedings of the Combustion Institute*, 35(1):309–316, 2015.
- [104] Curran H. J., Gaffuri P., Pitz W. J., and Westbrook C. K. A comprehensive modeling study of n-heptane oxidation. *Combustion and Flame*, 114(1-2):149–177, 1998.
- [105] Wang H., You X., Joshi A.V., Davis S.G., Laskin A., Egolfopoulos F., and Law C.K. High-temperature combustion reaction model of H₂/CO/C₁-C₄ compounds. <http://ignis.usc.edu/Mechanisms/USC-Mech>(accessed July 8, 2015).
- [106] Chakir A., Cathonnet M., Boettner J. C., and Gaillard F. Kinetic study of 1-butene oxidation in a jet-stirred flow reactor. *Symposium (International) on Combustion*, 22(1):873–881, 1989.
- [107] Mehl M., Vanhove G., Pitz W. J., and Ranzi E. Oxidation and combustion of the n-hexene isomers: A wide range kinetic modeling study. *Combustion and Flame*, 155(4):756–772, 2008.
- [108] Huynh L. K., Barriger K., and Violi A. Kinetics Study of the OH + Alkene \longrightarrow H₂O + Alkenyl Reaction Class. *The Journal of Physical Chemistry A*, 112(7):1436–1444, 2008.
- [109] Goldsmith C. F., Ismail H., and Green W. H. Pressure and Temperature Dependence of the Reaction of Vinyl Radical with Alkenes III: Measured Rates and Predicted Product Distributions for Vinyl + Butene. *The Journal of Physical Chemistry A*, 113(47):13357–13371, 2009.
- [110] Sun H. and Law C. K. Kinetics of hydrogen abstraction reactions of butene isomers by oh radical. *The Journal of Physical Chemistry A*, 114(45):12088–12098, 2010. PMID: 20977273.
- [111] Zador J., Klippenstein S. J., and Miller J. A. Pressure-dependent oh yields in alkene + HO₂ reactions: A theoretical study. *The Journal of Physical Chemistry A*, 115(36):10218–10225, 2011. PMID: 21819062.
- [112] Chen C. and Bozzelli J. W. Thermochemical property, pathway and kinetic analysis on the reactions of allylic isobutenyl radical with O₂: an elementary reaction mechanism for isobutene oxidation. *The Journal of Physical Chemistry A*, 104(43):9715–9732, 2000.
- [113] Zheng X. L., Sun H. Y., and Law C. K. Thermochemical and Kinetic Analyses on Oxidation of Isobutenyl Radical and 2-Hydroperoxymethyl-2-propenyl Radical. *The Journal of Physical Chemistry A*, 109(40):9044–9053, 2005.
- [114] Li Y., Zhou C. W., Somers K. P., Zhang K., and Curran H. J. The oxidation of 2-butene: A high pressure ignition delay, kinetic modeling study and reactivity comparison with isobutene and 1-butene. *Proceedings of the Combustion Institute*, 36(1):403–411, 2017.

- [115] Li Y., Zhou C. W., and Curran H. J. An extensive experimental and modeling study of 1-butene oxidation. *Combustion and Flame*, 181:198–213, 2017.
- [116] Fenard Y., Dagaut P., Dayma G., Halter F., and Foucher F. Experimental and kinetic modeling study of trans-2-butene oxidation in a jet-stirred reactor and a combustion bomb. *Proceedings of the Combustion Institute*, 35(1):317–324, 2015.
- [117] *NIST Chemistry WebBook, NIST Standard Reference Database Number 69*. <http://webbook.nist.gov>, 2018.
- [118] Zhou C. W., Li Y., O’Connor E., Somers K. P., S. Thion, Keesee C., Mathieu O., Petersen E. L., DeVerter T. A., Oehlschlaeger M. A., Kukkadapu G., Sung C. J., Alrefae M., Khaled F., Farooq A., Dirrenberger P., Glaude P. A., Battin-Leclerc F., Santner J., Ju Y., Held T., Haas F. M., Dryer F. L., and Curran H. J. A comprehensive experimental and modeling study of isobutene oxidation. *Combustion and Flame*, 167:353–379, 2016.
- [119] González Alatorre G., Böhm H., Atakan B., and Kohse-Höinghaus K. Experimental and Modelling Study of 1-Pentene Combustion at Fuel-Rich Conditions. *Zeitschrift für Physikalische Chemie*, 215(8):981, 2001.
- [120] Westbrook C. K., Pitz W. J., Mehl M., Glaude P. A., Herbinet O., Bax S., Battin-Leclerc F., Mathieu O., Petersen E. L., Bugler J., and Curran H. J. Experimental and Kinetic Modeling Study of 2-Methyl-2-Butene: Allylic Hydrocarbon Kinetics. *Journal of Physical Chemistry A*, 119(28):7462–7480, 2015.
- [121] Mehl M., Pitz W. J., Westbrook C. K., Yasunaga K., Conroy C., and Curran H. J. Autoignition behavior of unsaturated hydrocarbons in the low and high temperature regions. *Proceedings of the Combustion Institute*, 33(1):201–208, 2011.
- [122] Touchard S., Buda F., Dayma G., Glaude P. A., Fournet R., and Battin-Leclerc F. Experimental and modeling study of the oxidation of 1-pentene at high temperature. *International Journal of Chemical Kinetics*, 37(8):451–463, 8 2005.
- [123] Ribaucour M., Minetti R., and Sochet L.R. Autoignition of n-pentane and 1-pentene: Experimental data and kinetic modeling. *Proc. Combust. Inst.*, 27(1):345–351, 1 1998.
- [124] Minetti R., Roubaud A., Therssen E., Ribaucour M., and Sochet L.R. The Chemistry of Pre-ignition of n-Pentane and 1-Pentene. *Combustion and Flame*, 118(1-2):213–220, 7 1999.
- [125] Cheng Y., Hu E., Lu X., Li X., Gong J., Li Q., and Huang Z. Experimental and kinetic study of pentene isomers and n-pentane in laminar flames. *Proceedings of the Combustion Institute*, 36:1279–1286, 2017.

- [126] Zhong B.-J., Zeng Z.-M., and Peng H.-S. The pressure dependence of laminar flame speed of 2-methyl-2-butene/air flames in the 0.1-1.0 MPa range. *Combustion Science and Technology*, pages 1–14, 5 2018.
- [127] Zhong B.-J. and Peng H.-S. Measurement of Laminar Flame Speed and Chemical Kinetic Model of 1-Pentene/Air Mixtures. *Combustion Science and Technology*, 189(10):1698–1712, 10 2017.
- [128] Prabhu S. K., Bhat R. K., Miller D. L., and Cernansky N. P. 1-Pentene Oxidation and Its Interaction with Nitric Oxide in the Low and Negative Temperature Coefficient Regions. *Combustion and Flame*, 104:377–390, 1996.
- [129] Bugler J., Marks B., Mathieu O., Archuleta R., Camou A., Grégoire C., Heufer K.A., Petersen E. L., and Curran H.J. An ignition delay time and chemical kinetic modeling study of the pentane isomers. *Combustion and Flame*, 163:138–156, 2016.
- [130] Cheng Y., Hu E., Deng F., Yang F., Zhang Y., Tang C., and Huang Z. Experimental and kinetic comparative study on ignition characteristics of 1-pentene and n-pentane. *Fuel*, 172:263–272, 2016.
- [131] Marks B., Mathieu O., Archuleta R., Petersen E., Metcalfe W., Curran H., and Bourque G. Ignition Delay Time Measurements and Modeling of n-Pentane and iso-Pentane at Elevated Pressures. In *51st AIAA Aerospace Sciences Meeting including the New Horizons Forum and Aerospace Exposition*, pages AIAA 2013–0160, 2013.
- [132] Westbrook C.K., Curran H.J., Pitz W.J., Griffiths J.F., Mohamed C., and Wo S.K. The effects of pressure, temperature, and concentration on the reactivity of alkanes: Experiments and modeling in a rapid compression machine. *Symposium (International) on Combustion*, 27(1):371–378, 1998.
- [133] Ribaucour M., Minetti R., Sochet L.R., Curran H.J., Pitz W.J., and Westbrook C.K. Ignition of isomers of pentane: An experimental and kinetic modeling study. *Proceedings of the Combustion Institute*, 28(2):1671–1678, 2000.
- [134] Griffiths J.F., Halford-Maw P.A., and Rose D.J. Fundamental features of hydrocarbon autoignition in a rapid compression machine. *Combustion and Flame*, 95(3):291–306, 1993.
- [135] Minetti R., Ribaucour M., Carlier M., and Sochet L R. Autoignition Delays of a Series of Linear and Branched Chain Alkanes in the Intermediate Range of Temperature. *Combustion Science and Technology*, 113(1):179–192, 1996.
- [136] Griffiths J. F., Halford-Maw P. A., and Mohamed C. Spontaneous ignition delays as a diagnostic of the propensity of alkanes to cause engine knock. *Combustion and Flame*, 111(4):327–337, 1997.
- [137] Rodriguez A., Herbinet O., Wang Z., Qi F., Fittschen C., Westmoreland P. R., and Battin-Leclerc F. Measuring hydroperoxide chain-branching agents during n-pentane low-temperature oxidation. *Proc. Combust. Inst.*, 36:333–342, 2017.

- [138] Bugler J., Rodriguez A., Herbinet O., Battin-Leclerc F., Togbé C., Dayma G., Dagaut P., and Curran H. J. An experimental and modelling study of n-pentane oxidation in two jet-stirred reactors: The importance of pressure-dependent kinetics and new reaction pathways. *Proceedings of the Combustion Institute*, 36(1):441–448, 2017.
- [139] Simon V., Simon Y., Scacchi G., and Baronnet F. Experimental study and modeling of the oxidation reactions of n-pentane and cyclopentane. *Canadian Journal of Chemistry*, 75(5):575–584, 1997.
- [140] Chakir A., Belumam M., Boettner J. C., and Cathonnet M. Kinetic Study of N-Pentane Oxidation. *Combustion Science and Technology*, 77(4-6):239–260, 1991.
- [141] Jin H., Pieper J., Hemken C., Bräuer E., Ruwe L., and Kohse-Höinghaus K. Chemical interaction of dual-fuel mixtures in low-temperature oxidation, comparing n-pentane/dimethyl ether and n-pentane/ethanol. *Combust. Flame*, 193:36–53, 2018.
- [142] Ji C., Dames E., Wang Y. L., Wang H., and Egolfopoulos F. N. Propagation and extinction of premixed C₅-C₁₂ n-alkane flames. *Combustion and Flame*, 157(2):277–287, 2010.
- [143] Kelley A.P., Smallbone A.J., Zhu D.L., and Law C.K. Laminar flame speeds of C₅ to C₈ n-alkanes at elevated pressures: Experimental determination, fuel similarity, and stretch sensitivity. *Proceedings of the Combustion Institute*, 33(1):963–970, 2011.
- [144] Dirrenberger P., Le Gall H., Bounaceur R., Glaude P., and Battin-Leclerc F. Measurements of laminar burning velocities above atmospheric pressure using the heat flux method-application to the case of n-pentane. *Energy & Fuels*, 29(1):398–404, 2015.
- [145] Blanksby S.J. and Ellison G.B. Bond dissociation energies of organic molecules. *Acc. Chem. Res.*, 36(4):255–263, 2003.
- [146] Tsang W. Chemical Kinetic Data Base for Combustion Chemistry. Part 2. Methanol. *Journal of Physical and Chemical Reference Data*, 16(3):471–508, 1987.
- [147] Comandini A., Awan I. A., and Manion J. A. Thermal decomposition of 1-pentyl radicals at high pressures and temperatures. *Chemical Physics Letters*, 552:20–26, 2012.
- [148] Weissman M. and Benson S. W. Pyrolysis of methyl chloride, a pathway in the chlorine-catalyzed polymerization of methane. *International Journal of Chemical Kinetics*, 16(4):307–333, 1984.
- [149] Ranzi E., Cavallotti C., Cuoci A., Frassoldati A., Pelucchi M., and Faravelli T. New reaction classes in the kinetic modeling of low temperature oxidation of n-alkanes. *Combustion and Flame*, 162(5):1679–1691, 2015.
- [150] Marinov N. M., Castaldi M. J., Melius C. F., and Tsang W. Aromatic and Polycyclic Aromatic Hydrocarbon Formation in a Premixed Propane Flame. *Combustion Science and Technology*, 128(1-6):295–342, 1997.

- [151] Senosiain J. P. and Miller J. A. The reaction of n- and I-C₄H₅ radicals with acetylene. *Journal of Physical Chemistry A*, 111:3740–3747, 2007.
- [152] Melius C. F., Miller J. A., and Evleth E. M. Unimolecular reaction mechanisms involving C₃H₄, C₄H₄, and C₆H₆ hydrocarbon species. *Symposium (International) on Combustion*, 24(1):621–628, 1992.
- [153] Ahmed S., Mauß F., and Zeuch T. The generation of a compact n-heptane/toluene reaction mechanism using the chemistry guided reduction (cgr) technique. *Zeitschrift für Physikalische Chemie*, 223:551–563, 2009.
- [154] Belmekki N., Glaude P. A., Da Costa I., Fournet R., and Battin-Leclerc F. Experimental and modeling study of the oxidation of 1-butyne and 2-butyne. *International Journal of Chemical Kinetics*, 34(3):172–183, 2002.
- [155] Seidel L., Moshhammer K., Wang X., Zeuch T., Kohse-Höinghaus K., and Mauss F. Comprehensive kinetic modeling and experimental study of a fuel-rich, premixed n-heptane flame. *Combustion and Flame*, 162(5):2045–2058, 2015.
- [156] Moshhammer K., Lucassen A., Togbé C., and Kohse-Höinghaus K. Hansen N. Formation of oxygenated and hydrocarbon intermediates in premixed combustion of 2-methylfuran. *Zeitschrift für Physikalische Chemie*, 229:507–528, 2014.

Appendix A

Appendix - Class 2: H-atom abstraction from fuel

The H-atom abstraction can take place at primary, secondary, tertiary, and allylic sites. The values are summarised in tables A.1 and A.2.

Reactions	A	n	E_a	Ref
$C_nH_m + H=C_nH_{m-1} + H_2$				
Primary	5.630E+07	2.00	7.713E+03	[81]
Primary allyl	5.630E+07	2.00	5.713E+03	[81], ^a
Secondary	2.450E+07	2.00	5.007E+03	[81]
Secondary allyl	2.450E+07	3.007	3.00E+03	[81], ^a
Tertiary	6.020E+05	2.40	2.583E+03	[77]
Tertiary allyl	6.020E+05	2.40	5.83E+02	[77], ^a
$C_nH_m + OH=C_nH_{m-1} + H_2O$				
Primary	1.750E+09	0.97	1.578E+03	[81]
Primary allyl	1.750E+09	0.97	-4.220E+02	[81], ^a
Secondary	2.340E+07	1.61	-3.589E+01	[81]
Secondary allyl	2.340E+07	1.61	-2.036E+03	[81], ^a
Tertiary	1.700E+06	1.90	-1.451E+03	[77]
Tertiary allyl	1.700E+06	1.90	-3.451E+03	[77], ^a
$C_nH_m + O=C_nH_{m-1} + OH$				
Primary	3.660E+05	2.40	5.512E+03	[81]
Primary allyl	3.660E+05	2.40	3.512E+03	[81], ^a
Secondary	1.180E+05	2.50	2.203E+03	[81]
Secondary allyl	1.180E+05	2.50	2.030E+02	[81], ^a
Tertiary	3.830E+05	2.41	8.930E+02	[77]
Tertiary allyl	3.830E+05	2.41	-1.107E+03	[77], ^a
$C_nH_m + CH_3=C_nH_{m-1} + CH_4$				
Primary	2.700E+11	0.00	1.162E+04	[81]
Primary allyl	2.700E+11	0.00	9.620E+04	[81], ^a
Secondary	2.000E+11	0.00	9.514E+03	[81]
Secondary allyl	2.000E+11	0.00	7.514E+03	[81], ^a
Tertiary	8.960E+03	2.33	6.147E+03	[77]
Tertiary allyl	8.960E+03	2.33	4.147E+03	[77], ^a
$C_nH_m + HO_2=C_nH_{m-1} + H_2O_2$				
Primary	2.680E+12	0.00	1.941E+04	[81]
Primary allyl	2.680E+12	0.00	1.741E+04	[81], ^a
Secondary	2.440E+12	0.00	1.703E+04	[81]
Secondary allyl	2.440E+12	0.00	1.503E+04	[81], ^a
Tertiary	2.800E+12	0.00	1.601E+04	[77]
Tertiary allyl	2.800E+12	0.00	1.401E+04	[77], ^a

Table A.1: Reaction rates for H-atom abstraction at primary, secondary, tertiary, and allylic sites.

Reactions	A	n	E_a	Ref
$C_nH_m + CH_3O=C_nH_{m-1} + CH_3OH$				
Primary	5.270E+10	0.00	7.005E+03	[81]
Primary allyl	5.270E+10	0.00	5.005E+03	[81], ^a
Secondary	5.480E+11	0.00	5.007E+03	[81]
Secondary allyl	5.480E+11	0.00	3.007E+03	[81], ^a
Tertiary	1.900E+10	0.00	2.80E+03	[77]
Tertiary allyl	1.900E+10	0.00	8.00E+02	[77], ^a
$C_nH_m + O_2=C_nH_{m-} + HO_2$				
Primary	4.170E+12	0.00	4.903E+04	[81]
Primary allyl	4.170E+12	0.00	4.703E+04	[81], ^a
Secondary	1.000E+13	0.00	4.768E+04	[81]
Secondary allyl	1.000E+13	0.00	4.568E+04	[81], ^a
Tertiary	7.000E+12	0.00	4.606E+04	[77]
Tertiary allyl	7.000E+12	0.00	4.406E+04	[77], ^a
$C_nH_m + C_2H_5=C_nH_{m-1} + C_2H_6$				
Primary	1.670E+10	0.00	1.340E+04	[81]
Primary allyl	1.670E+10	0.00	1.140E+04	[81], ^a
Secondary	2.500E+10	0.00	1.040E+04	[81]
Secondary allyl	2.500E+10	0.00	8.400E+03	[81], ^a
Tertiary	1.000E+11	0.00	7.900E+03	[77]
Tertiary allyl	1.000E+11	0.00	5.900E+03	[77], ^a
$C_nH_m + C_2H_3=C_nH_{m-1} + C_2H_4$				
Primary	1.670E+11	0.00	1.800E+04	[81]
Primary allyl	1.670E+11	0.00	1.600E+04	[81], ^a
Secondary	2.000E+11	0.00	1.680E+04	[81]
Secondary allyl	2.000E+11	0.00	1.480E+04	[81], ^a
Tertiary	2.000E+11	0.0	1.430E+04	[77]
Tertiary allyl	2.000E+11	0.00	1.230E+04	[77], ^a
$C_nH_m + CH_3O_2=C_nH_{m-1} + CH_3O_2H$				
Primary	2.020E+12	0.00	2.046E+04	[81]
Primary allyl	2.020E+12	0.00	1.846E+04	[81], ^a
Secondary	2.000E+12	0.00	1.773E+04	[81]
Secondary allyl	2.000E+12	0.00	1.573E+04	[81], ^a
Tertiary	2.800E+12	0.00	1.601E+04	[77]
Tertiary allyl	2.800E+12	0.00	1.401E+04	[77], ^a

Table A.2: Reaction rates for H-atom abstraction at primary, secondary, tertiary, and allylic sites. ^a: allyl correction for activation energy.

Appendix B

Appendix - Nomenclature

B.1 Species containing no carbon

N₂

- Name in mechanism: N₂
- Molecular formula: N₂
- Structure: N = N
- IUPAC-name: nitrogen
- Other names (eng): molecular nitrogen
- Other names (ger): Stickstoff

Ar

- Name in mechanism: Ar
- Molecular formula: Ar
- Structure: Ar
- IUPAC-name: argon
- Other names (eng): argon
- Other names (ger): Argon

O

- Name in mechanism: O
- Molecular formula: O
- Structure: $\dot{\text{O}}$
- IUPAC-name: oxidanylidene
- Other names (eng): oxygen, atomic
- Other names (ger): Sauerstoff-Atom

O₂

- Name in mechanism: O₂
- Molecular formula: O₂
- Structure: O = O
- IUPAC-name: 1,2-dioxidanediyl
- Other names (eng): oxygen
- Other names (ger): Sauerstoff

H

- Name in mechanism: H
- Molecular formula: H
- Structure: $\dot{\text{H}}$
- IUPAC-name: hydrogen atom
- Other names (eng): hydrogen atom
- Other names (ger): Wasserstoff-Atom

H₂

- Name in mechanism: H₂
- Molecular formula: H₂
- Structure: H — H
- IUPAC-name: molecular hydrogen
- Other names (eng): hydrogen, dihydrogen
- Other names (ger): Wasserstoff

OH

- Name in mechanism: OH
- Molecular formula: OH
- Structure: $\dot{\text{O}} - \text{H}$
- IUPAC-name: hydroxide
- Other names (eng): hydroxyl radical
- Other names (ger): Hydroxyl-Radikal, OH-Radikal

HO₂

- Name in mechanism: HO₂
- Molecular formula: HO₂
- Structure: H — O — $\dot{\text{O}}$
- IUPAC-name: hydroperoxyl
- Other names (eng): hydroperoxyl radical, perhydroxyl radical
- Other names (ger): Hydroperoxid-Radikal

H2O2

- Name in mechanism: H2O2
- Molecular formula: H₂O₂
- Structure: H — O — O — H
- IUPAC-name: hydrogen peroxide
- Other names (eng): hydrogen peroxide, dioxidane
- Other names (ger): Wasserstoffperoxid

H2O

- Name in mechanism: H2O
- Molecular formula: H₂O
- Structure: H — O — H
- IUPAC-name: dihydrogen monoxide
- Other names (eng): water
- Other names (ger): Wasser, Diwasserstoffmonoxid, Wasserstoffhydroxid, Dihydrogeniumoxid, Hydrogeniumoxid, Hydrogeniumhydroxid

B.2 C₁ species

C

- Name in mechanism: C
- Molecular formula: C
- Structure: \dot{C}
- IUPAC-name: carbon
- Other names (eng): carbon
- Other names (ger): Kohlenstoff

CO

- Name in mechanism: CO
- Molecular formula: CO
- Structure: $\dot{C} \equiv \dot{O}$
- IUPAC-name: carbon monoxide
- Other names (eng): carbon monoxide
- Other names (ger): Kohlenstoffmonoxid

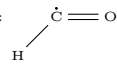
CO2

- Name in mechanism: CO2
- Molecular formula: CO₂
- Structure: O = C = O
- IUPAC-name: carbon dioxide
- Other names (eng): carbon dioxide
- Other names (ger): Kohlenstoffdioxid

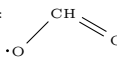
CH

- Name in mechanism: CH
- Molecular formula: CH
- Structure: $\dot{C} - H$
- IUPAC-name: carbon(1-) monohydride

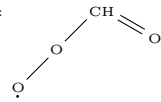
HCO

- Name in mechanism: HCO
- Molecular formula: CHO
- Structure: 
- IUPAC-name: formyl radical
- Other names (eng): formyl radical
- Other names (ger): Formyl-Radikal

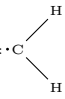
OCHO

- Name in mechanism: OCHO
- Molecular formula: CHO₂
- Structure: 
- IUPAC-name: formate
- Other names (eng): formate


O2CHO

- Name in mechanism: O2CHO
- Molecular formula: CHO₃
- Structure: 
- IUPAC-name: formyldioxidanyl
- Other names (eng): formyldioxidanyl

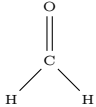
CH2-3

- Name in mechanism: CH2-3
- Molecular formula: CH₂
- Structure: 
- IUPAC-name: Triplet Carbene
- Other names (eng): methylene radical (Triplet)
- Old name: CH2-P

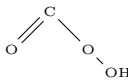
CH2-1

- Name in mechanism: CH2-1
- Molecular formula: CH₂
- Structure: 
- IUPAC-name: Singlet Carbene
- Other names (eng): methylene radical (singlet)
- Old name: CH2-S

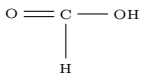
CH2O

- Name in mechanism: CH2O
- Molecular formula: CH₂O
- Structure: 
- IUPAC-name: formaldehyde
- Other names (eng): Methanal, formol, Methyl aldehyde, Methylene oxide
- Other names (ger): Methanal, Methylaldehyd, Formol

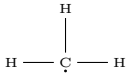
HO2CHO

- Name in mechanism: HO2CHO
- Molecular formula: CH₂O₃
- Structure: 
- IUPAC-name: peroxyformic acid
- Other names (eng): performic acid, methaneperoxic acid

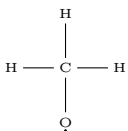
HOCHO

- Name in mechanism: HOCHO
- Molecular formula: CH₂O₂
- Structure: 
- IUPAC-name: formic acid
- Other names (eng): formic acid, hydrogen carboxylic acid
- Other names (ger): Ameisensäure

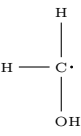
CH3

- Name in mechanism: CH3
- Molecular formula: CH₃
- Structure: 
- IUPAC-name: methyl radical
- Other names (eng): methyl radical
- Other names (ger): Methyl-Radikal

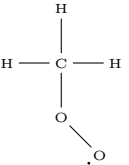
CH3O

- Name in mechanism: CH3O
- Molecular formula: CH₃O
- Structure: 
- IUPAC-name: methoxy radical
- Other names (eng): methoxy radical, methoxydanyl
- Other names (ger): Methoxy-Radikal

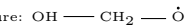
CH2OH

- Name in mechanism: CH2OH
- Molecular formula: CH₃O
- Structure: 
- IUPAC-name: hydroxymethyl
- Other names (eng): hydroxymethyl radical
- Other names (ger): Hydroxymethyl-Radikal

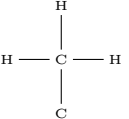
CH3O2

- Name in mechanism: CH3O2
- Molecular formula: CH₃O₂
- Structure: 
- IUPAC-name: methylperoxydanyl
- Other names (eng): Methylperoxy, Methylperoxy radical
- Other names (ger): Methylperoxydanyl-Radikal

HOCH2O

- Name in mechanism: HOCH2O
- Molecular formula: CH₃O₂
- Structure: 
- IUPAC-name: hydroxymethanolate
- Other names (eng): hydroxymethanolate
- Other names (ger): Hydroxymethanolat

CH4

- Name in mechanism: CH4
- Molecular formula: CH₄
- Structure: 
- IUPAC-name: methane
- Other names (eng): methane, carbon tetrahydride
- Other names (ger): Methan

CH3OH

- Name in mechanism: CH3OH
- Molecular formula: CH₄O
- Structure:
$$\begin{array}{c} \text{H} \\ | \\ \text{H} - \text{C} - \text{H} \\ | \\ \text{OH} \end{array}$$
- IUPAC-name: methanol
- Other names (eng): Carbinol, Hydroxymethane, Methyl alcohol, Methyl hydrate, Methyl hydroxide, Methyl alcohol, Methylol
- Other names (ger): Methylalkohol, Carbinol

CH3O2H

- Name in mechanism: CH3O2H
- Molecular formula: CH₄O₂
- Structure:
$$\begin{array}{c} \text{H} \\ | \\ \text{H} - \text{C} - \text{H} \\ | \\ \text{O} \\ | \\ \text{OH} \end{array}$$
- IUPAC-name: methyl hydroperoxide
- Other names (eng): methyl hydroperoxide
- Other names (ger): Methylhydroperoxid

B.3 C₂ species

C2H-R1T1

- Name in mechanism: C2H-R1T1
- Molecular formula: C₂H
- Structure:
$$\text{H} - \text{C} \equiv \dot{\text{C}}$$
- IUPAC-name: ethynyl radical
- Other names (eng): ethynyl radical
- Other names (ger): Ethinyl-Radikal
- Old name in mechanism: C2H

C2O-E12T1

- Name in mechanism: C2O-R1K1D1
- Molecular formula: C₂O
- Structure:
$$\begin{array}{c} \text{C} \\ ||| \\ \text{C} \end{array} \begin{array}{c} \diagup \\ \text{O} \\ \diagdown \end{array}$$
- IUPAC-name: 1-oxacycloprop-2-yne
- Other names (eng): epoxy acetylene
- Old name in mechanism: C2O

HCCO

- Name in mechanism: HCCO
- Molecular formula: C₂HO
- Structure:
$$\text{H} - \text{C} \equiv \text{C} - \dot{\text{O}}$$
- IUPAC-name: ethynyloxidanyl radical
- Other names (eng): ethynyloxidanyl radical
- Other names (ger): Ethynyloxidanyl-Radikal

C2H2

- Name in mechanism: C2H2
- Molecular formula: C₂H₂
- Structure:
$$\text{H} - \text{C} \equiv \text{C} - \text{H}$$
- IUPAC-name: acetylene
- Other names (eng): ethyne, acetylene
- Other names (ger): Ethin, Acetylen

C2H2O-K1D1

- Name in mechanism: C2H2O-K1D1
- Molecular formula: C₂H₂O
- Structure:
$$\text{H}_2\text{C} = \text{C} = \text{O}$$
- IUPAC-name: Ethenone
- Other names (eng): Ethenone, Ketene
- Other names (ger): Ethenon, Keten
- Old name in mechanism: CH2CO

C2H3O-R1OH2D1

- Name in mechanism: C2H3O-R1OH2D1
- Molecular formula: C₂H₃O
- Structure:
$$\begin{array}{c} \text{H} \dot{\text{C}} \\ \diagdown \\ \text{C} = \text{C} - \text{O} - \text{H} \\ \diagup \\ \text{H} \end{array}$$
- IUPAC-name: 1-ethen-2-ol
- Other names (eng): 1-ethen-2-ol
- Old name in mechanism: C2H2OH

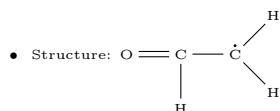
C2H3-R1D1

- Name in mechanism: C2H3-R1D1
- Molecular formula: C₂H₃
- Structure:
$$\text{H}_2\text{C} = \dot{\text{C}} - \text{H}$$
- IUPAC-name: vinyl radical
- Other names (eng): vinyl radical, ethenyl radical
- Other names (ger): Vinyl-Radikal
- Old name in mechanism: C2H3

C2H3O-R1A12

- Name in mechanism: C2H3O-R1A12

- Molecular formula: C₂H₃O

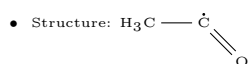


- IUPAC-name: ethanal radical
- Other names (eng): ethanal radical
- Old name in mechanism: CH₂CHO

C2H3O-R1K1

- Name in mechanism: C2H3O-R1K1

- Molecular formula: C₂H₃O

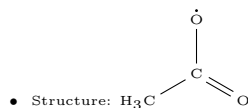


- IUPAC-name: ethanoyl
- Other names (eng): acetyl radical
- Other names (ger): Acetyl-Radikal
- Old name in mechanism: CH₃CO

C2H3O2-K1O1

- Name in mechanism: C2H3O2-K1O1

- Molecular formula: C₂H₃O₂

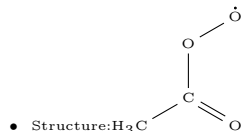


- IUPAC-name: acetate
- Other names (eng): acetate
- Other names (ger): Acetat-Radikal
- Old name in mechanism: CH₃CO₂

C2H3O3-OO1K1

- Name in mechanism: C2H3O3-OO1K1

- Molecular formula: C₂H₃O₃



- IUPAC-name: acetyldioxidanyl
- Other names (eng): acetyldioxidanyl
- Other names (ger): Acetyldioxidanyl
- Old name in mechanism: CH₃CO₃

C2H4-D1

- Name in mechanism: C2H4-D1

- Molecular formula: C₂H₄

- Structure: H₂C = CH₂

- IUPAC-name: ethene

- Other names (eng): ethylene

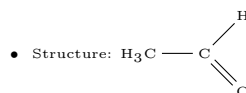
- Other names (ger): Ethen, Ethylen, Äthen, Äthylen, Elaylgas, Vinylwasserstoff, Acetan

- Old name in mechanism: C₂H₄

C2H4O-A11

- Name in mechanism: C2H4O-A11

- Molecular formula: C₂H₄O



- IUPAC-name: ethanal

- Other names (eng): Acetic Aldehyde, Ethyl Aldehyde

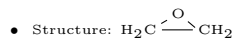
- Other names (ger): Acetaldehyd, Acetylaldehyd

- Old name in mechanism: CH₃CHO

C2H4O-E12

- Name in mechanism: C2H4O-E12

- Molecular formula: C₂H₄O



- IUPAC-name: oxirane

- Other names (eng): ethylene oxide

- Other names (ger): Ethylenoxid

- Old name in mechanism: C₂H₄O-2

C2H4O-OH1D1

- Name in mechanism: C2H4O-OH1D1

- Molecular formula: C₂H₄O

- Structure: H₂C = CH — OH

- IUPAC-name: Ethenol

- Other names (eng): Vinyl Alcohol, formyl-methyl

- Other names (ger): Ethenol

- Old name in mechanism: CH₂CHOH

C2H4O2-HP1D1

- Name in mechanism: C2H4O2-HP1D1

- Molecular formula: C₂H₄O₂

- Structure: CH₂ = CH — O — OH

- IUPAC-name: vinyl hydroperoxide

- Other names (eng): vinyl hydroperoxide

- Other names (ger): Vinylhydroperoxid

- Old name in mechanism: C₂H₃OOH

C2H4O3-K1HP1

- Name in mechanism: C2H4O3-K1HP1
- Molecular formula: C₂H₄O₃
- Structure:
- IUPAC-name: ethaneperoxy acid
- Other names (eng): Parectic acid, Peroxyacetic acid
- Other names (ger): Peroxyessigsäure, Ethanperoxosäure, Peressigsäure
- Old name in mechanism: CH3CO3H

C2H4O3-OO1OH2

- Name in mechanism: C2H4O3-OO1OH2
- Molecular formula: C₂H₄O₃
- Structure:
- IUPAC-name: 1-ethaneperoxide radical 2-ol
- Other names (eng): 1-ethaneperoxide radical 2-ol
- Old name in mechanism: CH3CO3H

C2H4O4-A11E1HP2

- Name in mechanism: C2H4O4-A11E1HP2
- Molecular formula: C₂H₄O₄
- Structure:
- IUPAC-name: 1-formyl-,1-ether-, 2-hydroperoxide
- Old name in mechanism: HO2CH2OCHO

C2H5-R1

- Name in mechanism: C2H5-R1
- Molecular formula: C₂H₅
- Structure:
- IUPAC-name: ethyl radical
- Other names (eng): ethyl radical
- Other names (ger): Ethyl-Radikal
- Old name in mechanism: C2H5

C2H5O-R1OH2

- Name in mechanism: C2H5O-R1OH2
- Molecular formula: C₂H₅O
- Structure:
- IUPAC-name: 2-Hydroxyethyl
- Other names (eng): 2-Hydroxyethyl
- Other names (ger): 2-Hydroxyethyl
- Old name in mechanism: CH2CH2OH

C2H5O-R1OH1

- Name in mechanism: C2H5O-R1OH1
- Molecular formula: C₂H₅O
- Structure:
- IUPAC-name: 1-Hydroxyethyl
- Other names (eng): 1-Hydroxyethyl radical
- Other names (ger): 1-Hydroxyethyl-Radikal
- Old name in mechanism: CH3CHO

C2H5O-O1

- Name in mechanism: C2H5O-O1
- Molecular formula: C₂H₅O
- Structure:
- IUPAC-name: Ethyloxidanyl
- Other names (eng): ethoxy radical, ethyloxidanyl
- Other names (ger): Ethyloxidanyl
- Old name in mechanism: C2H5O

C2H5O-R1E1

- Name in mechanism: C2H5O-R1E1
- Molecular formula: C₂H₅O
- Structure:
- IUPAC-name: methoxymethyl
- Other names (eng): methoxymethyl
- Other names (ger): Methoxymethyl
- Old name in mechanism: CH3OCH2

C2H5O2-OO1

- Name in mechanism: C2H5O2-OO1
- Molecular formula: C₂H₅O₂
- Structure:
- IUPAC-name: ethyldioxy radical
- Other names (eng): ethyldioxy radical, Ethyldioxy, peroxyethyl radical
- Other names (ger): Ethyldioxy radical
- Old name in mechanism: C2H5O2

C2H5O2-R1HP2

- Name in mechanism: C2H5O2-R1HP2
- Molecular formula: C₂H₅O₂
- Structure: H₂ $\overset{\cdot}{\text{C}}$ — CH₂ — O — OH
- IUPAC-name: 2-hydroperoxy,1-ethyl radical
- Other names (eng): 2-hydroperoxy,1-ethyl radical
- Old name in mechanism: C2H4O2H

C2H5O3-OO1E1

- Name in mechanism: C2H5O3-OO1E1
- Molecular formula: C₂H₅O₃
- Structure: CH₃ — O — CH₂ — O — $\overset{\cdot}{\text{O}}$
- IUPAC-name: (methoxymethyl) dioxidanyl
- Other names (eng): Methylidioxo, methoxy-
- Other names (ger): (Methoxymethyl) dioxidanyl
- Old name in mechanism: CH3OCH2O2

C2H5O3-R1E1HP2

- Name in mechanism: C2H5O3-R1E1HP2
- Molecular formula: C₂H₅O₃
- Structure: $\overset{\cdot}{\text{C}}\text{H}_2$ — O — CH₂ — O — OH
- IUPAC-name: 1-Methylene, 1-ether, 2-hydroperoxide
- Old name in mechanism: CH2OCH2OOH

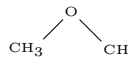
C2H6

- Name in mechanism: C2H6
- Molecular formula: C₂H₆
- Structure: H₃C — CH₃
- IUPAC-name: ethane
- Other names (eng): ethane
- Other names (ger): Ethan

C2H6O-OH1

- Name in mechanism: C2H6O-OH1
- Molecular formula: C₂H₆O
- Structure: H₃C — CH₂ — OH
- IUPAC-name: ethanol
- Other names (eng): ethyl alcohol, ethyl hydrate, ethyl hydroxide, ethylic alcohol, ethylol
- Other names (ger): Ethanol, Ethylalkohol
- Old name in mechanism: C2H5OH

C2H6O-E1

- Name in mechanism: C2H6O-E1
- Molecular formula: C₂H₆O
- Structure: 
- IUPAC-name: methoxymethane
- Other names (eng): dimethylether
- Other names (ger): Methoxymethan
- Old name in mechanism: CH3OCH3-DME

C2H6O2-HP1

- Name in mechanism: C2H6O2-HP1
- Molecular formula: C₂H₆O₂
- Structure: H₃C — CH₂ — O — OH
- IUPAC-name: 1-ethyl hydroperoxide
- Other names (eng): Peroxyethane
- Other names (ger): Peroxyethan
- Old name in mechanism: C2H5O2H

B.4 C₃ species

C3H2-2R1T2

- Name in mechanism: C3H2-R1R3D1D2
- Molecular formula: C₃H₂
- Structure: HC ≡ C — $\overset{\cdot}{\text{C}}$ — H
- IUPAC-name: propynylidene
- Other names (eng): propynylidene
- Old Name in mechanism: C3H2

C3H3-R1T2

- Name in mechanism: C3H3-R1T2
- Molecular formula: C₃H₃
- Structure: HC ≡ C — $\overset{\cdot}{\text{C}}\text{H}_2$
- IUPAC-name: propargyl radical
- Other names (eng): propargyl radical
- Other names (ger): Propargyl-Radikal
- Old Name in mechanism: C3H3

C3H3O-R1K1D2

- Name in mechanism: C3H3O-R1K1D2
- Molecular formula: C₃H₃O
- Structure: H₂C = CH — $\overset{\cdot}{\text{C}}$ = O
- IUPAC-name: 1-Oxo-2-propen-1-yl
- Other names (eng): 1-Oxoprop-2-enyl
- Old Name in mechanism: C2H3CO

C3H4-D1D2

- Name in mechanism: C3H4-D1D2
- Molecular formula: C₃H₄
- Structure: CH₂ = C = CH₂
- IUPAC-name: Propa-1,2-diene
- Other names (eng): Allene
- Other names (ger): Propadien, Allen, Dimethylenmethan
- Old Name in mechanism: C3H4

C3H4-T1

- Name in mechanism: C3H4-T1
- Molecular formula: C₃H₄
- Structure: CH₃ — C ≡ CH
- IUPAC-name: Prop-1-yne
- Other names (eng): Methylacetylene; 1-Propyne, Allylen
- Other names (ger): Propin
- Old Name in mechanism: C3H4P

C3H4O-K1D1

- Name in mechanism: C3H4O-K1D1
- Molecular formula: C₃H₄O
- Structure: O = C = CH — CH₃
- IUPAC-name: 1-Propen-1-one
- Other names (eng): methylketene
- Other names (ger): Methylketen
- Old Name in mechanism: CH3CHCO

C3H4O-A1D2

- Name in mechanism: C3H4O-A1D2
- Molecular formula: C₃H₄O
- Structure: H₂C = CH — C $\begin{array}{l} \text{H} \\ \diagup \\ \text{=} \text{O} \end{array}$
- IUPAC-name: 2-Propenal
- Other names (eng): acrolein; acrylaldehyde
- Other names (ger): Acrylaldehyd
- Old Name in mechanism: C2H3CHO

C3H5-R1D2

- Name in mechanism: C3H5-R1D2
- Molecular formula: C₃H₅
- Structure: CH₂ = CH — CH₂ \cdot
- IUPAC-name: prop-2-en-1-yl
- Other names (eng): allyl radical
- Other names (ger): Prop-2-en-1-yl
- Old Name in mechanism: C3H5

C3H5-R2D1

- Name in mechanism: C3H5-R2D1
- Molecular formula: C₃H₅
- Structure: CH₂ = $\dot{\text{C}}$ — CH₃
- IUPAC-name: prop-2-en-2-yl
- Old Name in mechanism: C3H5-T

C3H5O-R1K1

- Name in mechanism: C3H5O-R1K1
- Molecular formula: C₃H₅O
- Structure: H₃C — CH₂ — $\dot{\text{C}}$ = O
- IUPAC-name: propan-1-one
- Other names (eng): propanoyl, 1-Oxopropyl
- Other names (ger): Propionyl-Radikal
- Old Name in mechanism: C2H5CO

C3H5O-O1D2

- Name in mechanism: C3H5O-O1D2
- Molecular formula: C₃H₅O
- Structure: CH₂ = CH — CH₂ \cdot
 $\begin{array}{c} | \\ \text{O} \end{array}$
- IUPAC-name: 2-propene-1-oxy radical
- Other names (eng): Allyloxy radical
- Old Name in mechanism: C3H5O

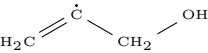
C3H5O-R1A13

- Name in mechanism: C3H5O-R1A13
- Molecular formula: C₃H₅O
- Structure: $\dot{\text{C}}\text{H}_2$ — CH₂ — C $\begin{array}{l} \text{H} \\ | \\ \text{=} \text{O} \end{array}$
- IUPAC-name: 3-formyl-propan-1-yl
- Old Name in mechanism: CH2CH2CHO

C3H5O-R1K2

- Name in mechanism: C3H5O-R1K2
- Molecular formula: C₃H₅O
- Structure: H₃C — C $\begin{array}{l} \text{O} \\ || \\ \text{CH}_2 \end{array}$ \cdot
- IUPAC-name: 2-Oxopropyl radical
- Old Name in mechanism: CH3COCH₂

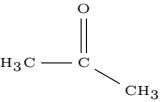
C3H5O-R2OH1D2

- Name in mechanism: C3H5O-R2OH1D2
- Molecular formula: C₃H₅O
- Structure: 
- IUPAC-name: 2-propene-2-yl-1-ol radical
- Old Name in mechanism: CH2CCH2OH

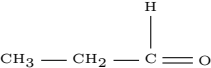
C3H6-D1

- Name in mechanism: C3H6-D1
- Molecular formula: C₃H₆
- Structure: CH₂ = CH — CH₃
- IUPAC-name: prop-1-ene
- Other names (eng): propene, propylene
- Other names (ger): 1-Propen
- Old Name in mechanism: C3H6

C3H6O-K2

- Name in mechanism: C3H6O-K2
- Molecular formula: C₃H₆O
- Structure: 
- IUPAC-name: propan-2-one
- Other names (eng): acetone, propanone
- Other names (ger): Aceton
- Old Name in mechanism: CH3COCH3

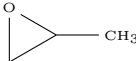
C3H6O-A11

- Name in mechanism: C3H6O-A11
- Molecular formula: C₃H₆O
- Structure: 
- IUPAC-name: 1-Propanal
- Other names (eng): propionaldehyde
- Other names (ger): Propionaldehyd
- Old Name in mechanism: C2H5CHO


C3H6O-OH1D2

- Name in mechanism: C3H6O-OH1D2
- Molecular formula: C₃H₆O
- Structure: CH₂ = CH — CH₂ — OH
- IUPAC-name: 2-Propen-1-ol
- Other names (eng): allyl alcohol
- Other names (ger): 2-Propen-1-ol
- Old name: C3H5OH, C3H5OHZ

C3H6O-E12

- Name in mechanism: C3H6O-E12
- Molecular formula: C₃H₆O
- Structure: 
- IUPAC-name: 2-methyloxirane
- Other names (eng): methyl oxirane; 1,2-Epoxypropane; Propylene oxide
- Other names (ger): 2-Methyloxiran
- Old name: C3H6O1-2

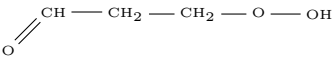
C3H6O-E13

- Name in mechanism: C3H6O-E13
- Molecular formula: C₃H₆O
- Structure: 
- IUPAC-name: Oxetane
- Other names (eng): 1,3-propylene oxide; 1,3-epoxypropane
- Other names (ger): Oxetan
- Old name: C3H6O1-3

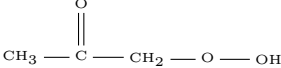
C3H6O2-HP1D2

- Name in mechanism: C3H6O2-HP1D2
- Molecular formula: C₃H₆O₂
- Structure: CH₂ = CH — CH₂ — O — OH
- IUPAC-name: 1-hydroperoxyprop-2-ene
- Other names (eng): Allyl hydroperoxide
- Other names (ger): Allylhydroperoxid
- Old name: C3H5OOH-R2

C3H6O3-A11HP3

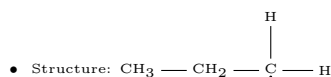
- Name in mechanism: C3H6O3-A11HP3
- Molecular formula: C₃H₆O₃
- Structure: 
- IUPAC-name: 3-hydroperoxy-1-propanal
- Old name: OCHCH2CH2OOH

C3H6O3-K2HP1

- Name in mechanism: C3H6O3-K2HP1
- Molecular formula: C₃H₆O₃
- Structure: 
- IUPAC-name: 1-hydroperoxy-2-propanone
- Old name: CH3COCH2OOH

C3H7-R1

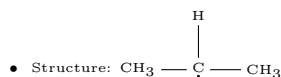
- Name in mechanism: C3H7-R1
- Molecular formula: C₃H₇



- IUPAC-name: prop-1-yl radical
- Other names (eng): n-propyl radical
- Other names (ger): 1-Propyl
- Old name: N-C3H7

C3H7-R2

- Name in mechanism: C3H7-R2
- Molecular formula: C₃H₇



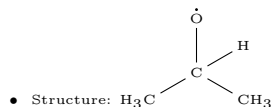
- IUPAC-name: prop-2-yl radical
- Other names (eng): iso-propyl radical
- Other names (ger): 2-Propyl
- Old name: I-C3H7

C3H7O-O1

- Name in mechanism: C3H7O-O1
- Molecular formula: C₃H₇O
- Structure: $\text{CH}_3 - \text{CH}_2 - \overset{\cdot}{\text{O}} - \text{CH}_2$
- IUPAC-name: 1-Propyloxidanyl
- Other names (eng): n-propoxy radical, Propyloxidanyl
- Other names (ger): Propyloxidanyl
- Old name: N-C3H7O

C3H7O-O2

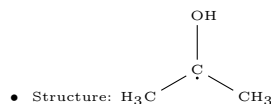
- Name in mechanism: C3H7O-O2
- Molecular formula: C₃H₇O



- IUPAC-name: Isopropyloxidanyl
- Other names (eng): iso-propoxy radical, Iso-propyloxidanyl
- Other names (ger): 1-Propyloxidanyl
- Old name: I-C3H7O

C3H7O-R2OH2

- Name in mechanism: C3H7O-R2OH2
- Molecular formula: C₃H₇O



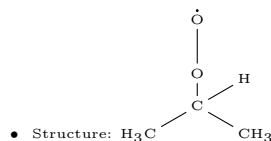
- IUPAC-name: 2-Propyl-2-ol
- Old name: T-C3H6OH

C3H7O2-O01

- Name in mechanism: C3H7O2-O01
- Molecular formula: C₃H₇O₂
- Structure: $\text{CH}_3 - \text{CH}_2 - \overset{\cdot}{\text{O}} - \text{CH}_2 - \overset{\cdot}{\text{O}}$
- IUPAC-name: Propyldioxidanyl
- Other names (eng): Propyldioxy
- Other names (ger): Propyldioxidanyl
- Old name: N-C3H7O2

C3H7O2-O02

- Name in mechanism: C3H7O2-O02
- Molecular formula: C₃H₇O₂



- IUPAC-name: Isopropyldioxidanyl
- Other names (eng): iso-propylperoxy radical, iso-propyldioxidanyl
- Other names (ger): Isopropyldioxidanyl
- Old name: I-C3H7O2

C3H7O2-R1HP1

- Name in mechanism: C3H7O2-R1HP1
- Molecular formula: C₃H₇O₂
- Structure: $\text{CH}_3 - \text{CH}_2 - \overset{\cdot}{\text{C}}\text{H} - \text{O} - \text{OH}$
- IUPAC-name: 1-hydroperoxy-propan-1-yl
- Old name: N-C3H6OOH-R2

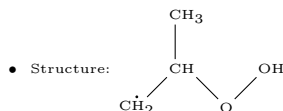
C3H7O2-R1HP3

- Name in mechanism: N-C3H6OOH-R1
- Molecular formula: C₃H₇O₂
- Structure: $\overset{\cdot}{\text{C}}\text{H}_2 - \text{CH}_2 - \text{CH}_2 - \text{O} - \text{OH}$
- IUPAC-name: 3-hydroperoxy-propan-1-yl
- Old name: N-C3H6OOH-R1

C3H7O2-R1HP2

- Name in mechanism: C3H7O2-R1HP2

- Molecular formula: C₃H₇O₂



- IUPAC-name: 2-hydroperoxy-propan-1-yl

- Old name: I-C3H6OOH-R1

C3H7O4-OO2HP1

- Name in mechanism: C3H7O4-OO2HP1

- Molecular formula: C₃H₇O₄



- Structure: CH₃ — CH — CH₂ — O — OH

- IUPAC-name: 1-hydroperoxy-2-propanoxy radical

- Old name: CH3CHOOCH2OOH

C3H7O4-OO1HP3

- Name in mechanism: C3H7O4-HP1P3

- Molecular formula: C₃H₇O₄



- Structure: CH₂ — CH₂ — CH₂ — O — OH

- IUPAC-name: 1-hydroperoxy-3-propanoxy radical

- Old name: O2C3H6OOH-R1

C3H7O4-OO1HP2

- Name in mechanism: C3H7O4-OO1HP2

- Molecular formula: C₃H₇O₄



- Structure: CH₃ — CH — CH₂ — O — O•

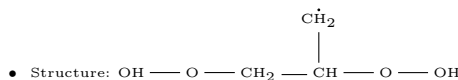
- IUPAC-name: 2-hydroperoxy-1-propanoxy radical

- Old name: CH3CHOOHCH2OO

C3H7O4-R1HP2HP3

- Name in mechanism: C3H7O4-R1HP2HP3

- Molecular formula: C₃H₇O₄



- IUPAC-name: 2-,3-dihydroperoxy-1-propyl radical

- Old name: C3H51-2-3OOH

C3H7O4-R2HP1HP3

- Name in mechanism: C3H7O4-R2HP1HP3

- Molecular formula: C₃H₇O₄

- Structure: OH — O — CH₂ — C• — CH₂ — O — OH

- IUPAC-name: 1-,3-dihydroperoxy-2-propyl radical

- Old name: C3H52-1-3OOH

C3H8

- Name in mechanism: C3H8

- Molecular formula: C₃H₈

- Structure: CH₃ — CH₂ — CH₃

- IUPAC-name: propane

- Other names (ger): Propan

C3H8O-HP1

- Name in mechanism: C3H8O-HP1

- Molecular formula: C₃H₈O₂

- Structure: CH₃ — CH₂ — CH₂ — O — OH

- IUPAC-name: 1-hydroperoxide propane

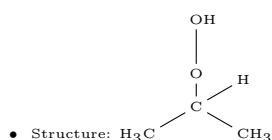
- Other names (eng): n-hydroxyperoxypropane, n-propylhydroperoxide

- Old name: N-C3H7O2H

C3H8O-HP2

- Name in mechanism: C3H8O-HP2

- Molecular formula: C₃H₈O₂



- IUPAC-name: 2-hydroperoxy propane

- Other names (eng): iso-propylhydroperoxide, iso-propyl-hydroxypertoxy

- Old name: I-C3H7O2H

B.5 C₄ species

C4H-R1T1T3

- Name in mechanism: C4H-R1T1T3

- Molecular formula: C₄H

- Structure: CH ≡ C — C ≡ C•

- IUPAC-name: 1,3-Butadiyn-1-yl

- Other names (eng): butadiynyl

- Other names (ger): 1,3-Butadiin-1-yl

- Old name in mechanism : C4H

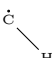
C4H2-T1T3

- Name in mechanism: C4H2-T1T3
- Molecular formula: C₄H₂
- Structure: CH ≡ C — C ≡ CH
- IUPAC-name: buta-1,3-diyne
- Other names (eng): 1,3-Butadiyne, 1,3-butadiyne, biacetylene, butadiyne
- Other names (ger): Diacetylen, Butadiin, 1,3-Butadiin
- Old name in mechanism: C4H2

C4H2O-K1D1-D3

- Name in mechanism: C4H2O-K1D1-D3
- Molecular formula: C₄H₂O
- Structure: H₂C = C = C = C = O
- IUPAC-name: 1-Butatrienone
- Other names (eng): 1,2,3-Butatrien-1-one
- Other names (ger): 1-Butatrienon
- Old name in mechanism: H2C4O

C4H3-R1D1T3

- Name in mechanism: C4H3-R1D1T3
- Molecular formula: C₄H₃
- Structure: CH ≡ C — CH = $\overset{\cdot}{\text{C}}$ 
- IUPAC-name: but-1-en-3-yne-1-yl
- Old name in mechanism: N-C4H3

C4H3-R2D1T3

- Name in mechanism: C4H3-R2D1T3
- Molecular formula: C₄H₃
- Structure: CH₂ = $\overset{\cdot}{\text{C}}$ — C ≡ CH
- IUPAC-name: but-1-en-3-yne-2-yl
- Old name in mechanism: I-C4H3

C4H4-D1T3

- Name in mechanism: C4H4-D1T3
- Molecular formula: C₄H₄
- Structure: CH₂ = CH — C ≡ CH
- IUPAC-name: 1-Buten-3-yne
- Other names (eng): Butenyne, vinylacetylene, Ethynylethene
- Other names (ger): 1-Buten-3-in
- Old name in mechanism: C4H4

C4H5-R1D1D3

- Name in mechanism: C4H5-R1D1D3
- Molecular formula: C₄H₅
- Structure: CH₂ = CH — CH = $\overset{\cdot}{\text{C}}$ H
- IUPAC-name: buta-1,3-diene-1-yl radical
- Other names (eng): 1,3-butadiene-1-yl
- Old name in mechanism: N-C4H5

C4H5-R2D1D3

- Name in mechanism: C4H5-R2D1D3
- Molecular formula: C₄H₅
- Structure: CH₂ = CH — $\overset{\cdot}{\text{C}}$ = CH₂
- IUPAC-name: buta-1,3-diene-2-yl radical
- Other names (eng): 1,3-Butadiene-2-yl
- Old name in mechanism: I-C4H5

C4H5-R3T1

- Name in mechanism: C4H5-R3T1
- Molecular formula: C₄H₅
- Structure: CH₃ — $\overset{\cdot}{\text{C}}$ H — C ≡ CH
- IUPAC-name: 1-Butyn-3-yl radical
- Other names (ger): 1-Butin-3-yl-Radikal
- Old name in mechanism: C4H5-1

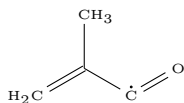
C4H5-R1T3

- Name in mechanism: C4H5-R1T3
- Molecular formula: C₄H₅
- Structure: H₂ $\overset{\cdot}{\text{C}}$ — CH₂ — C ≡ CH
- IUPAC-name: 3-Butyn-1-yl radical
- Other names (ger): 3-Butin-1-yl-Radikal
- Old name in mechanism: C4H5-1N

C4H5-R1T2

- Name in mechanism: C4H5-R1T2
- Molecular formula: C₄H₅
- Structure: H₂ $\overset{\cdot}{\text{C}}$ — C ≡ C — CH₃
- IUPAC-name: 2-Butyn-1-yl
- Other names (ger): 2-Butin-1-yl-Radikal
- Old name in mechanism: C4H5-2

C4H5O-R1K1D2Me2

- Name in mechanism: C4H5O-R1K1D2Me2
- Molecular formula: C₄H₅O
- Structure: 
- IUPAC-name: 2-Methyl-1-oxo-2-propen-1-ylum
- Other names (ger): 2-Methyl-1-oxo-2-propen-1-ylum
- Old name in mechanism: I-C3H5CO

C4H6-D1D3

- Name in mechanism: C4H6-D1D3
- Molecular formula: C₄H₆
- Structure: CH₂ = CH — CH = CH₂
- IUPAC-name: 1,3-Butadiene
- Other names (eng): α,γ-Butadiene; Buta-1,3-diene
- Other names (ger): Bivinyll; Divinyll
- Old name in mechanism: C4H6

C4H6-D1-D2

- Name in mechanism: C4H6-D1-D2
- Molecular formula: C₄H₆
- Structure: CH₂ = C = CH — CH₃
- IUPAC-name: 1,2-Butadiene
- Other names (eng): Methylallene; Buta-1,2-diene
- Old name in mechanism: C4H612

C4H6-T1

- Name in mechanism: C4H6-T1
- Molecular formula: C₄H₆
- Structure: CH ≡ C — CH₂ — CH₃
- IUPAC-name: But-1-yne,
- Other names (eng): 1-Butyne; Ethylacetylene
- Other names (ger): Ethylethyne
- Old name in mechanism: C4H6-1

C4H6-T2

- Name in mechanism: C4H6-T2
- Molecular formula: C₄H₆
- Structure: CH₃ — C ≡ C — CH₃
- IUPAC-name: But-2-yne,
- Other names (eng): 2-Butyne; Dimethyl acetylene
- Other names (ger): 2-Butin
- Old name in mechanism: C4H6-2

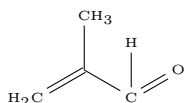
C4H6O-K2D3

- Name in mechanism: C4H6O-K2D3
- Molecular formula: C₄H₆O
- Structure: H₂C = CH — C(=O) — CH₃
- IUPAC-name: But-3-en-2-one
- Other names (eng): Methyl vinyl ketone
- Other names (ger): Vinylmethylketon
- Old name in mechanism: C2H3COCH3

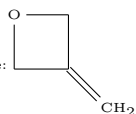
C4H6O-K1D1

- Name in mechanism: C4H6O-K1D1
- Molecular formula: C₄H₆O
- Structure: H₃C — CH₂ — CH = C = O
- IUPAC-name: But-1-en-1-one
- Old name in mechanism: C2H5CHCO

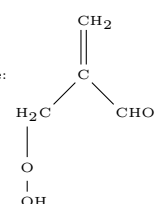
C4H6O-A11D2Me2

- Name in mechanism: C4H6O-A11D2Me2
- Molecular formula: C₄H₆O
- Structure: 
- IUPAC-name: 2-Methyl-2-propen-1-al
- Other names (eng): Methacrolein, Methyl propenal, Methacryladehyde
- Old name in mechanism: I-C3H5CHO


C4H6O-E13MD2

- Name in mechanism: C4H6O-E13MD2
- Molecular formula: C₄H₆O
- Structure: 
- IUPAC-name: 2-methylene-oxetane
- Other names (eng): 2-methylene-oxetane
- Old name in mechanism: I-C4H6O

C4H6O3-A11HP3MD2

- Name in mechanism: C4H6O3-A11HP3MD2
- Molecular formula: C₄H₆O₃
- Structure: 
- IUPAC-name: 2-methylene-3-hydroperoxy-1-propanal
- Old name in mechanism: I-C4H6O3

C4H7O2-OO1D3

- Name in mechanism: C4H7O2-OO1D3
- Molecular formula: C₄H₇O₂
- Structure: H₂C = CH — CH₂ — CH₂ — 
- IUPAC-name: 3-buten-1-peroxy radical
- Old name in the mechanism: C4H7O2-P

C4H7O2-R1HP1D3

- Name in mechanism: C4H7O2-R1HP1D3
- Molecular formula: C₄H₇O₂
- Structure: $\text{H}_2\text{C}=\text{CH}-\text{CH}_2-\overset{\cdot}{\text{C}}\text{H}$
 $\begin{array}{c} | \\ \text{O} \\ | \\ \text{OH} \end{array}$
- IUPAC-name: 3-buten-1-hydroperoxy-1-yl
- Old name in the mechanism: C4H6O2-HP4R3

C4H7O2-OO3D1

- Name in mechanism: C4H7O2-D1P3
- Molecular formula: C₄H₇O₂
- Structure: $\text{CH}_3-\text{CH}-\text{CH}=\text{CH}_2$
 $\begin{array}{c} | \\ \text{O} \\ | \\ \text{O} \end{array}$
- IUPAC-name: 1-buten-3-peroxy radical
- Old name in the mechanism: C4H7O2-S

C4H7O2-R1HP2D3

- Name in mechanism: C4H7O2-R1HP2D3
- Molecular formula: C₄H₇O₂
- Structure: $\text{CH}_2-\text{CH}-\text{CH}=\text{CH}_2$
 $\begin{array}{c} | \\ \text{O} \\ | \\ \text{OH} \end{array}$
- IUPAC-name: 3-buten-2-hydroperoxy-1-yl
- Old name in the mechanism: C4H6O2-HP3R4

C4H8O2-HP1D3

- Name in mechanism: C4H8O2-HP1D3
- Molecular formula: C₄H₈O₂
- Structure: $\text{H}_2\text{C}=\text{CH}-\text{CH}_2-\text{CH}_2$
 $\begin{array}{c} | \\ \text{O} \\ | \\ \text{OH} \end{array}$
- IUPAC-name: 3-buten-1-hydroperoxy
- Old name in the mechanism: C4H8O2-P

C4H8O2-HP3D1

- Name in mechanism: C4H8O2-HP3D1
- Molecular formula: C₄H₈O₂
- Structure: $\text{CH}_3-\text{CH}-\text{CH}=\text{CH}_2$
 $\begin{array}{c} | \\ \text{O} \\ | \\ \text{OH} \end{array}$
- IUPAC-name: 1-buten-3-hydroperoxy
- Old name in the mechanism: C4H8O2-S

C4H6O-E12D3

- Name in mechanism: C4H6O-E12D3
- Molecular formula: C₄H₆O
- Structure: $\text{H}_2\text{C} \begin{array}{c} \text{O} \\ \diagup \quad \diagdown \end{array} \text{CH}-\text{CH}=\text{CH}_2$
- IUPAC-name: (2S)-2-Vinyloxirane
- Other names (ger): (2S)-2-Vinyloxiran
- Old name in the mechanism: C4H6O-E34

C4H7O4-OO2HP1D3

- Name in mechanism: C4H7O4-OO2HP1D3
- Molecular formula: C₄H₇O₄
- Structure: $\text{H}_2\text{C}=\text{CH}-\text{CH}-\text{CH}_2$
 $\begin{array}{c} | \quad | \\ \text{O} \quad \text{O} \\ | \quad | \\ \text{O} \quad \text{OH} \end{array}$
- IUPAC-name: 3-buten-1-hydroperoxy-2-peroxy radical
- Old name in the mechanism: C4H6O4-HP4P3

C4H7O4-OO1HP2D3

- Name in mechanism: C4H7O4-OO1HP2D3
- Molecular formula: C₄H₇O₄
- Structure: $\text{H}_2\text{C}=\text{CH}-\text{CH}-\text{CH}_2$
 $\begin{array}{c} | \quad | \\ \text{O} \quad \text{O} \\ | \quad | \\ \text{OH} \quad \text{O} \end{array}$
- IUPAC-name: 3-buten-2-hydroperoxy-1-peroxy radical
- Old name in the mechanism: C4H6O4-HP3P4

C4H6O3-A11HP2D3

- Name in mechanism: C4H6O3-A11HP2D3
- Molecular formula: C₄H₆O₃
- Structure: $\text{H}_2\text{C}=\text{CH}-\text{CH}-\overset{\text{O}}{\parallel}{\text{C}}-\text{H}$
 $\begin{array}{c} | \\ \text{O} \\ | \\ \text{OH} \end{array}$
- IUPAC-name: 3-buten-2-hydroperoxy-1-al
- Old name in the mechanism: C4H6O3-A4HP3

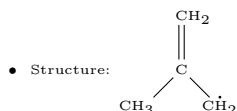
C4H6O3-K2HP1D3

- Name in mechanism: C4H6O3-K2HP1D3
- Molecular formula: C₄H₆O₃
- Structure: $\text{H}_2\text{C}=\text{CH}-\overset{\text{O}}{\parallel}{\text{C}}-\text{CH}_2$
 $\begin{array}{c} | \\ \text{O} \\ | \\ \text{OH} \end{array}$
- IUPAC-name: 3-buten-1-hydroperoxy-2-one
- Old name in the mechanism: C4H6O3-A3HP4

C4H7-R1D2Me2

- Name in mechanism: C4H7-R1D2Me2

- Molecular formula: C₄H₇

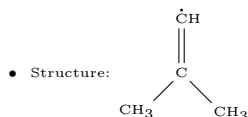


- IUPAC-name: 2-Methyl-2-propen-1-yl
- Other names (eng): 2-Methylallyl radical
- Old name in mechanism: I-C4H7

C4H7-R1D1Me2

- Name in mechanism: C4H7-R1D1Me2

- Molecular formula: C₄H₇

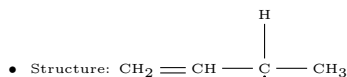


- IUPAC-name: 2-Methyl-1-propen-1-yl
- Other names (eng): vinylic isobuten-1-yl radical
- Old name in mechanism: I1-C4H7

C4H7-R3D1

- Name in mechanism: C4H7-R3D1

- Molecular formula: C₄H₇

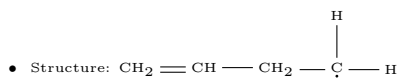


- IUPAC-name: 1-buten-3-yl
- Other names (eng): 1-Methylallyl radical, 1-Buten-3-yl radical; 2-butenyl; But-2-enyl
- Other names (ger): But-2-en-1-yl
- Old name in mechanism: C4H7s-1

C4H7-R1D3

- Name in mechanism: C4H7-R1D3

- Molecular formula: C₄H₇



- IUPAC-name: 3-buten-1-yl
- Other names (eng): But-3-en-1-yl radical; 3-butenyl; But-3-enyl; 1-Buten-4-yl
- Old name in mechanism: C4H7p-1

C4H7-R2D2

- Name in mechanism: C4H7-R2D2

- Molecular formula: C₄H₇

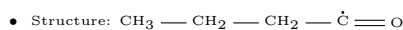


- IUPAC-name: 2-buten-2-yl
- Other names (eng): 2-Buten-2-yl
- Old name in mechanism: C4H7S-2

C4H7O-R1K1

- Name in mechanism: C4H7O-R1K1

- Molecular formula: C₄H₇O

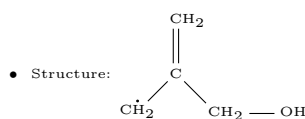


- IUPAC-name: butan-1-one
- Old name in mechanism: N-C3H7CO

C4H7O-R1OH3MD2

- Name in mechanism: C4H7O-R1OH3MD2

- Molecular formula: C₄H₇O

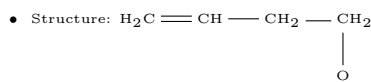


- IUPAC-name: 2-Methylene-3-propanol-1-yl
- Old name in mechanism: I-C4H6OH

C4H7O-O1D3

- Name in mechanism: C4H7O-O1D3

- Molecular formula: C₄H₇O

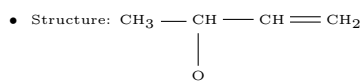


- IUPAC-name: 3-buten-1-oxy radical
- Old name in mechanism: C4H7O-P

C4H7O-O3D1

- Name in mechanism: C4H7O-O3D1

- Molecular formula: C₄H₇O

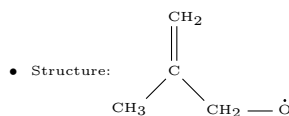


- IUPAC-name: 1-buten-3-oxy radical
- Other names (eng): butyl oxy radical
- Old name in mechanism: C4H7O-S

C4H7O-O1D2Me2

- Name in mechanism: C4H7O-O1D2Me2

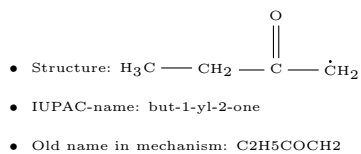
- Molecular formula: C₄H₇O



- IUPAC-name: 2-Methyl-2-propen-1-oxy radical
- Other names (eng): 2-Methyl Allyloxy Radical
- Old name in mechanism: I-C4H7O

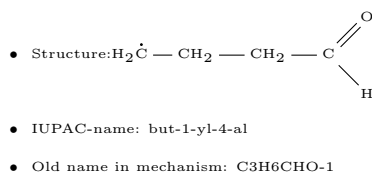
C4H7O-R1K2

- Name in mechanism: C4H7O-R1K2
- Molecular formula: C₄H₇O



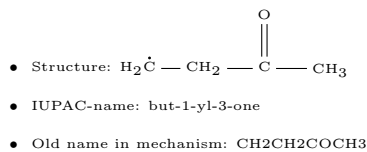
C4H7O-R1A14

- Name in mechanism: C4H7O-R1A14
- Molecular formula: C₄H₇O



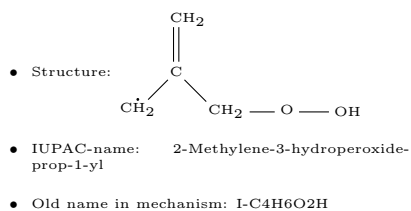
C4H7O-R1K3

- Name in mechanism: C4H7O-R1K3
- Molecular formula: C₄H₇O



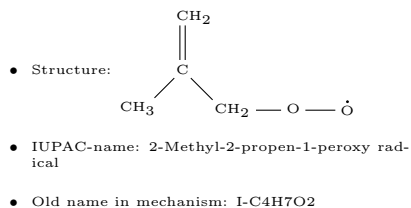
C4H7O2-R1HP3MD2

- Name in mechanism: C4H7O2-R1HP3MD2
- Molecular formula: C₄H₇O₂



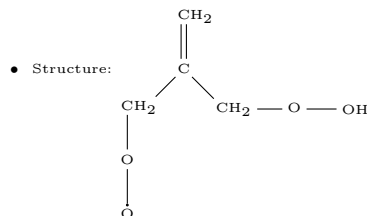
C4H7O2-OO1D2Me2

- Name in mechanism: C4H7O2-OO1D2Me2
- Molecular formula: C₄H₇O₂



C4H7O4-OO1HP3MD2

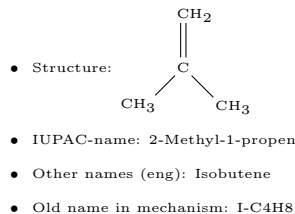
- Name in mechanism: C4H7O4-OO1HP3MD2
- Molecular formula: C₄H₇O₄



- IUPAC-name: 2-Methylene-3-properoxol-1-peroxy radical
- Old name in mechanism: I-C4H7O4

C4H8-D1Me2

- Name in mechanism: C4H8-D1Me2
- Molecular formula: C₄H₈

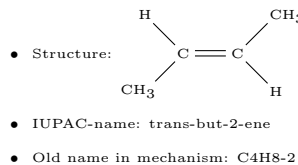


C4H8-D1

- Name in mechanism: C4H8-D1
- Molecular formula: C₄H₈
- Structure:
- IUPAC-name: but-1-ene
- Other names (eng): ethylethylene, 1-butylene, α-butylene
- Old name in mechanism: C4H8-1

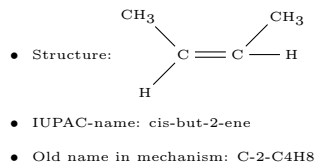
T-C4H8-D2

- Name in mechanism: T-C4H8-D2
- Molecular formula: C₄H₈

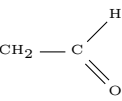


C-C4H8-D2

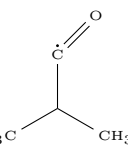
- Name in mechanism: C-C4H8-D2
- Molecular formula: C₄H₈



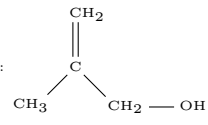
C4H8O-A11

- Name in mechanism: C4H8O-A11
- Molecular formula: C₄H₈O
- Structure: 
- IUPAC-name: butanal
- Other names (eng): Butyraldehyde
- Old name in mechanism: N-C3H7CHO

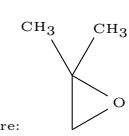
C4H8O-R1K1Me2

- Name in mechanism: C4H8O-R1K1Me2
- Molecular formula: C₄H₈O
- Structure: 
- IUPAC-name: 2-Methylpropanal
- Other names (eng): Isobutyraldehyde
- Other names (ger): 2-Methylpropanal
- Old name in mechanism: I-C3H7CHO

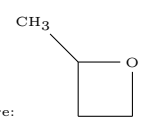
C4H8O-OH1D2Me2

- Name in mechanism: C4H8O-OH1D2Me2
- Molecular formula: C₄H₈O
- Structure: 
- IUPAC-name: 2-Methyl-2-propen-1-ol
- Other names (eng): 2-Methyl-2-propen-1-ol, 2-Methylallyl alcohol
- Old name in mechanism: I-C4H7OH

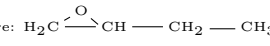
C4H8O-E12Me2

- Name in mechanism: C4H8O-R2O1Me2
- Molecular formula: C₄H₈O
- Structure: 
- IUPAC-name: 2,2-Dimethyloxirane
- Other names (eng): 1,2-Epoxyisobutane
- Other names (ger): 2,2-Dimethyloxiran
- Old name in mechanism: I-C4H8O

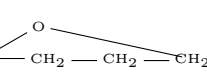
C4H8O-E13

- Name in mechanism: CC4H8O
- Molecular formula: C₄H₈O
- Structure: 
- IUPAC-name: 2-Methyloxetane
- Other names (eng): 1,3-Butylene oxide
- Old name in the mechanism: CC4H8O, C4H8O-E13

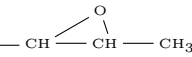
C4H8O-E12

- Name in mechanism: C4H8O-E12
- Molecular formula: C₄H₈O
- Structure: 
- IUPAC-name: 2-Ethyloxirane
- Other names (eng): 2-Ethyloxirane

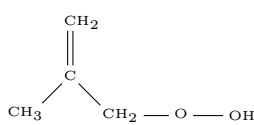
C4H8O-E14

- Name in mechanism: C4H8O-E14
- Molecular formula: C₄H₈O
- Structure: 
- IUPAC-name: Tetrahydrofuran
- Other names (eng): Tetrahydrofuran

C4H8O-E23

- Name in mechanism: C4H8O-E23
- Molecular formula: C₄H₈O
- Structure: 
- IUPAC-name: 2,3-Dimethyloxirane

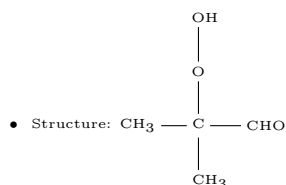
C4H8O2-HP1D2Me2

- Name in mechanism: C4H8O2-HP1D2Me2
- Molecular formula: C₄H₈O₂
- Structure: 
- IUPAC-name: 1-Hydroperoxy-2-Methyl-2-butene
- Old name in mechanism: I-C4H7O2H

C4H8O3-A11HP2Me2

- Name in mechanism: C4H8O3-A11HP2Me2

- Molecular formula: C₄H₈O₃



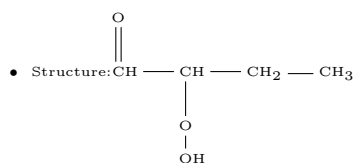
- IUPAC-name: 2-Methyl-2-Hydroperoxy-1-propanal

- Old name in mechanism: I-C4H8O3-T

C4H8O3-A11HP2

- Name in mechanism: C4H8O3-A11HP2

- Molecular formula: C₄H₈O₃



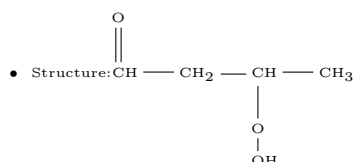
- IUPAC-name: 2-Hydroperoxy-1-butanal

- Old name in the mechanism: C4H8O3-A1HP2

C4H8O3-A11HP3

- Name in mechanism: C4H8O3-A11HP3

- Molecular formula: C₄H₈O₃



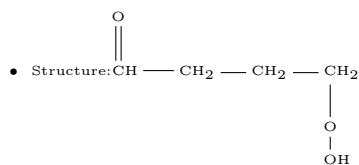
- IUPAC-name: 3-Hydroperoxy-1-butanal

- Old name in the mechanism: C4H8O3-A1HP3

C4H8O3-A11HP4

- Name in mechanism: C4H8O3-A11HP4

- Molecular formula: C₄H₈O₃

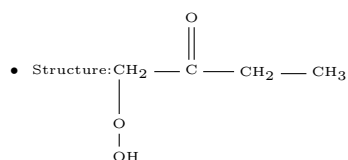


- IUPAC-name: 4-Hydroperoxy-1-butanal

C4H8O3-K2HP1

- Name in mechanism: C4H8O3-K2HP1

- Molecular formula: C₄H₈O₃



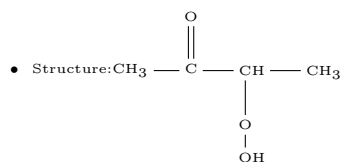
- IUPAC-name: 1-Hydroperoxy-2-butanone

- Old name in the mechanism: C4H8O3-A2HP1

C4H8O3-K2HP3

- Name in mechanism: C4H8O3-K2HP3

- Molecular formula: C₄H₈O₃



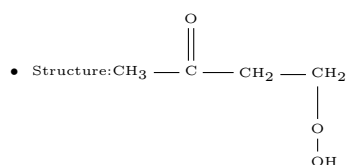
- IUPAC-name: 3-Hydroperoxy-2-butanone

- Old name in the mechanism: C4H8O3-A2HP3

C4H8O3-K3HP1

- Name in mechanism: C4H8O3-K3HP1

- Molecular formula: C₄H₈O₃



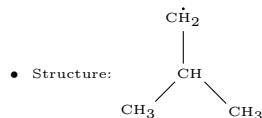
- IUPAC-name: 1-Hydroperoxy-3-butanone

- Old name in the mechanism: C4H8O3-A2HP4

C4H9-R1Me2

- Name in mechanism: C4H9-R1Me2

- Molecular formula: C₄H₉



- IUPAC-name: Isobutyl

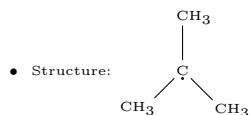
- Other names (eng): iso-Butyl radical

- Old name in the mechanism: I-C4H9

C4H9-R2Me2

- Name in mechanism: C4H9-R2Me2

- Molecular formula: C₄H₉



- IUPAC-name: 2-Methyl-2-propanyl

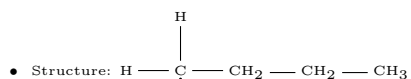
- Other names (eng): t-Butyl radical

- Old name in mechanism: T-C4H9

C4H9-R1

- Name in mechanism: C4H9-R1

- Molecular formula: C₄H₉



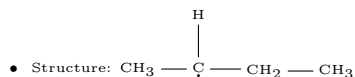
- IUPAC-name: 1-Butyl radical

- Old name in mechanism: C4H9-1

C4H9-R2

- Name in mechanism: C4H9-R2

- Molecular formula: C₄H₉



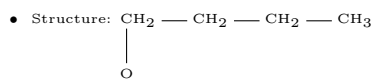
- IUPAC-name: 2-Butyl radical

- Old name in mechanism: C4H9-2

C4H9O-O1

- Name in mechanism: C4H9O-O1

- Molecular formula: C₄H₉O



- IUPAC-name: 1-Butoxy radical

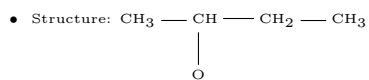
- Other names (eng): Butyloxidanyl

- Other names (ger): Butyloxidanyl

C4H9O-O2

- Name in mechanism: C4H9O-O2

- Molecular formula: C₄H₉O

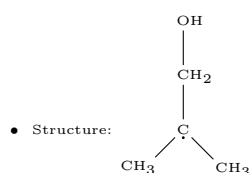


- IUPAC-name: 2-Butoxy radical

C4H9O-R2OH1Me2

- Name in mechanism: C4H9O-R2OH1Me2

- Molecular formula: C₄H₉O



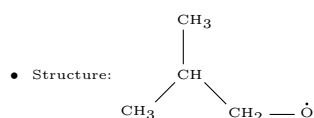
- IUPAC-name: 2-methylpropan-1-ol

- Old name in mechanism: I-C4H8OH

C4H9O-O1Me2

- Name in mechanism: C4H9O-O1Me2

- Molecular formula: C₄H₉O



- IUPAC-name: 2-Methyl-1-propanolate

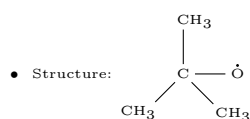
- Other names (eng): isobutoxide

- Old name in mechanism: I-C4H9O

C4H9O-O2Me2

- Name in mechanism: C4H9O-O2Me2

- Molecular formula: C₄H₉O



- IUPAC-name: (2-Methyl-2-propanyl)oxidanyl

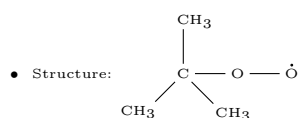
- Other names (eng): t-Butoxy radical

- Old name in mechanism: T-C4H9O

C4H9O2-OO12Me2

- Name in mechanism: C4H9O2-OO12Me2

- Molecular formula: C₄H₉O₂



- IUPAC-name: (2-Methyl-2-propanyl)dioxidanyl

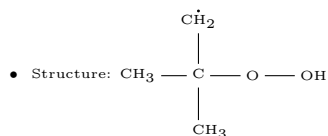
- Other names (eng): tert-butyldioxy

- Old name in mechanism: T-C4H9O2

C4H9O2-R1HP2Me2

- Name in mechanism: C4H9O2-R1HP2Me2

- Molecular formula: C₄H₉O₂



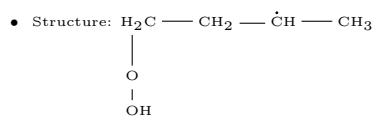
- IUPAC-name: 2-Methyl-2-hydroperoxy-1-propanyl

- Old name in mechanism: T-C4H8O2H-I

C4H9O2-R3HP1

- Name in mechanism: C4H9O2-R3HP1

- Molecular formula: C₄H₉O₂



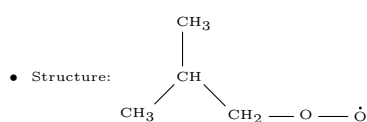
- IUPAC-name: 1-hydroperoxy-3-butanyl radical

- Old name in the mechanism: C4H9O2-HP1R3

C4H9O2-OO1Me2

- Name in mechanism: C4H9O2-OO1Me2

- Molecular formula: C₄H₉O₂



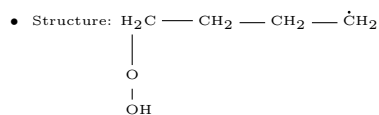
- IUPAC-name: 2-Methyl-1-peroxy-propan radical

- Old name in mechanism: I-C4H9O2

C4H9O2-R1HP4

- Name in mechanism: C4H9O2-R1HP4

- Molecular formula: C₄H₉O₂



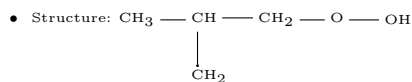
- IUPAC-name: 4-hydroperoxy-1-butanyl radical

- Old name in the mechanism: C4H9O2-HP1R4

C4H9O2-R1HP3Me2

- Name in mechanism: C4H9O2-R1HP3Me2

- Molecular formula: C₄H₉O₂



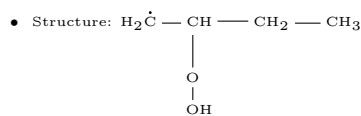
- IUPAC-name: 2-Methyl-3-hydroperoxy-1-propanyl radical

- Old name in mechanism: I-C4H8O2H-I

C4H9O2-R1HP2

- Name in mechanism: C4H9O2-R1HP2

- Molecular formula: C₄H₉O₂



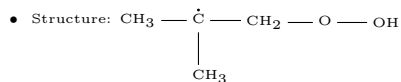
- IUPAC-name: 2-hydroperoxy-1-butanyl radical

- Old name in the mechanism: C4H9O2-HP2R1

C4H9O2-R2HP1Me2

- Name in mechanism: C4H9O2-R2HP1Me2

- Molecular formula: C₄H₉O₂



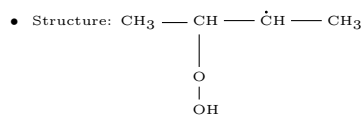
- IUPAC-name: 2-Methyl-1-hydroperoxy-2-propanyl radical

- Old name in mechanism: I-C4H8O2H-T

C4H9O2-R2HP3

- Name in mechanism: C4H9O2-R2HP3

- Molecular formula: C₄H₉O₂



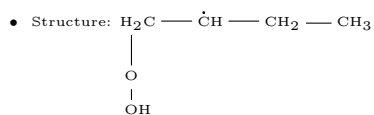
- IUPAC-name: 3-hydroperoxy-2-butanyl radical

- Old name in the mechanism: C4H9O2-HP2R3

C4H9O2-R2HP1

- Name in mechanism: C4H9O2-R2HP1

- Molecular formula: C₄H₉O₂



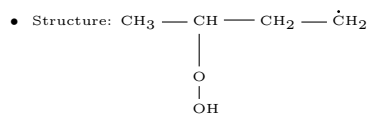
- IUPAC-name: 1-hydroperoxy-2-butanyl radical

- Old name in the mechanism: C4H9O2-HP1R2

C4H9O2-R1HP3

- Name in mechanism: C4H9O2-R1HP3

- Molecular formula: C₄H₉O₂



- IUPAC-name: 3-hydroperoxy-1-butanyl radical

- Old name in the mechanism: C4H9O2-HP2R4

C4H9O2-OO1

- Name in mechanism: C4H9O2-OO1
- Molecular formula: C₄H₉O₂
- Structure: $\text{CH}_2 - \text{CH}_2 - \text{CH}_2 - \text{CH}_3$
 $\begin{array}{c} | \\ \text{O} \\ | \\ \dot{\text{O}} \end{array}$

• IUPAC-name: 1-Butylperoxy

C4H9O2-OO2

- Name in mechanism: C4H9O2-OO2
- Molecular formula: C₄H₉O₂
- Structure: $\text{CH}_3 - \text{CH} - \text{CH}_2 - \text{CH}_3$
 $\begin{array}{c} | \\ \text{O} \\ | \\ \dot{\text{O}} \end{array}$

• IUPAC-name: 2-Butylperoxy

C4H9O3-OO2OH1Me2

- Name in mechanism: C4H9O3-OO2OH1Me2
- Molecular formula: C₄H₉O₃
- Structure: $\begin{array}{c} \text{OH} \\ | \\ \text{CH}_2 \\ | \\ \text{CH}_3 - \text{C} - \text{O} - \dot{\text{O}} \\ | \\ \text{CH}_3 \end{array}$

• IUPAC-name: 2-Methyl-2-peroxy-1-propanol radical

• Old name in mechanism: IO2C4H8OH

C4H9O4-OO2HP1Me2

- Name in mechanism: C4H9O4-OO2HP1Me2
- Molecular formula: C₄H₉O₄
- Structure: $\begin{array}{c} \text{O} - \dot{\text{O}} \\ | \\ \text{CH}_3 - \text{C} - \text{CH}_2 - \text{O} - \text{OH} \\ | \\ \text{CH}_3 \end{array}$

• IUPAC-name: 2-Methyl-2-peroxy-1-properoxol radical

• Old name in mechanism: I-C4H9O4-T

C4H9O4-OO2HP1

- Name in mechanism: C4H9O4-OO2HP1
- Molecular formula: C₄H₉O₄
- Structure: $\begin{array}{c} \dot{\text{O}} \\ | \\ \text{O} \\ | \\ \text{CH}_2 - \text{CH} - \text{CH}_2 - \text{CH}_3 \\ | \\ \text{O} \\ | \\ \text{OH} \end{array}$

• IUPAC-name: 1-hydroperoxy-2-peroxy-butane radical

C4H9O4-OO3HP1

- Name in mechanism: C4H9O4-OO3HP1
- Molecular formula: C₄H₉O₄
- Structure: $\begin{array}{c} \dot{\text{O}} \\ | \\ \text{O} \\ | \\ \text{CH}_2 - \text{CH}_2 - \text{CH} - \text{CH}_3 \\ | \\ \text{O} \\ | \\ \text{OH} \end{array}$

• IUPAC-name: 1-hydroperoxy-3-peroxy-butane radical

C4H9O4-OO1HP4

- Name in mechanism: C4H9O4-OO1HP4
- Molecular formula: C₄H₉O₄
- Structure: $\begin{array}{c} \dot{\text{O}} \\ | \\ \text{O} \\ | \\ \text{CH}_2 - \text{CH}_2 - \text{CH}_2 - \text{CH}_2 \\ | \\ \text{O} \\ | \\ \text{OH} \end{array}$

• IUPAC-name: 1-hydroperoxy-4-peroxy-butane radical

C4H9O4-OO1HP2

- Name in mechanism: C4H9O4-OO1HP2
- Molecular formula: C₄H₉O₄
- Structure: $\begin{array}{c} \dot{\text{O}} \\ | \\ \text{O} \\ | \\ \text{CH}_2 - \text{CH} - \text{CH}_2 - \text{CH}_3 \\ | \\ \text{O} \\ | \\ \text{OH} \end{array}$

• IUPAC-name: 2-hydroperoxy-1-peroxy-butane radical

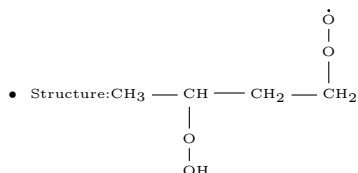
C4H9O4-OO2HP3

- Name in mechanism: C4H9O4-HP2P3
- Molecular formula: C₄H₉O₄
- Structure: $\begin{array}{c} \dot{\text{O}} \\ | \\ \text{O} \\ | \\ \text{CH}_3 - \text{CH} - \text{CH} - \text{CH}_3 \\ | \\ \text{O} \\ | \\ \text{OH} \end{array}$

• IUPAC-name: 3-hydroperoxy-2-peroxy-butane radical

C4H9O4-OO1HP3

- Name in mechanism: C4H9O4-OO1HP3
- Molecular formula: C₄H₉O₄



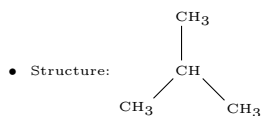
- IUPAC-name: 3-hydroperoxy-1-peroxy-butane radical

C4H10

- Name in mechanism: C4H10
- Molecular formula: C₄H₁₀
- Structure: CH₃ — CH₂ — CH₂ — CH₃
- IUPAC-name: Butane

C4H10-Me2

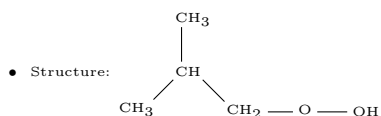
- Name in mechanism: C4H10-Me2
- Molecular formula: C₄H₁₀



- IUPAC-name: Isobutan
- Other names (eng): Iso-butane
- Old name in mechanism: I-C4H10

C4H10O2-HP1Me2

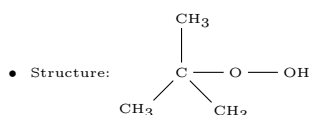
- Name in mechanism: C4H10O2-HP1Me2
- Molecular formula: C₄H₁₀O₂



- IUPAC-name: 2-Methyl-1-properoxol
- Old name in mechanism: I-C4H9O2H

C4H10O2-HP2Me2

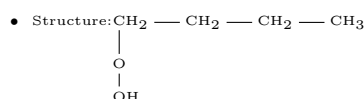
- Name in mechanism: C4H10O2-HP2Me2
- Molecular formula: C₄H₁₀O₂



- IUPAC-name: 2-Methyl-2-properoxol
- Old name in mechanism: T-C4H9O2H

C4H10O2-HP1

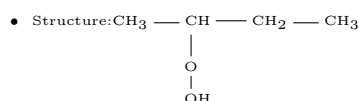
- Name in mechanism: C4H10O2-HP1
- Molecular formula: C₄H₁₀O₂



- IUPAC-name: 1-butanoxol

C4H10O2-HP2

- Name in mechanism: C4H10O2-HP2
- Molecular formula: C₄H₁₀O₂



- IUPAC-name: 2-butanoxol

B.6 C₅ species

C5H2-R1R3D1-D2T4

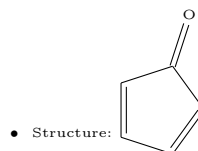
- Name in mechanism: C5H2-R1R3D1-D2T4
- Molecular formula: C₅H₂
- Structure: HC ≡ C — $\dot{\text{C}}$ = C = $\dot{\text{C}}\text{H}$
- IUPAC-name: 1,2-pentadiene-4-yne-1,3-diyl radical
- Old name in mechanism : C5H2

C5H3-R3D1-D2T4

- Name in mechanism: C5H3-R3D1-D2T4
- Molecular formula: C₅H₃
- Structure: HC ≡ C — $\dot{\text{C}}$ = C = CH₂
- IUPAC-name: 1,2-pentadiene-4-yne-1,3-diyl radical
- Old name in mechanism : C5H3

CyC5H4O-K1D2D4

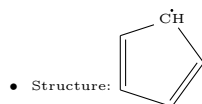
- Name in mechanism: CyC5H4O-K1D2D4
- Molecular formula: C₅H₄O



- IUPAC-name: 2,4-cyclopentadiene-1-one
- Other names (eng): 2,4-cyclopentien-1-one
- Other names (ger): 2,4-Cyclopentadien-1-on
- Old name in mechanism: OCyC5H4, C5H4O

CyC5H5-R1D2D4

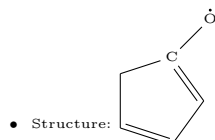
- Name in mechanism: CyC5H5-R1D2D4
- Molecular formula: C₅H₅



- IUPAC-name: 2,4-Cyclopentadien-1-yl
- Other names (eng): Cyclopentadienyl radical
- Old name in mechanism: CyC5H5-, C5H5; CyC5H5

CyC5H5O-O1D1D3

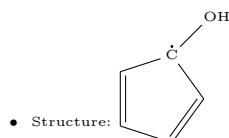
- Name in mechanism: CyC5H5O-O1D1D3
- Molecular formula: C₅H₅O



- IUPAC-name: 1,3-Cyclopentadien-1-olate
- Old name in mechanism: OCYC5H5, C5H5O

CyC5H5O-OH1D2D4

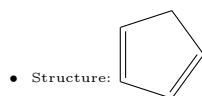
- Name in mechanism: CyC5H5O-OH1D2D4
- Molecular formula: C₅H₅O



- IUPAC-name: 2,4-Cyclopentadien-1-ol,
- Other names (eng): cyclopentadienylradical
- Old name in mechanism: OHCYC5H4-, C5H4O; OHCyC5H4*

CyC5H6-D1D3

- Name in mechanism: CyC5H6-D1D3
- Molecular formula: C₅H₆



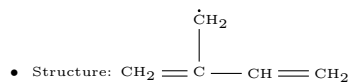
- IUPAC-name: cyclopenta-1,3-diene
- Other names (eng): 1,3-cyclopentadiene
- Old name in mechanism: CYC5H6

C5H7-R1D2D4

- Name in mechanism: C5H7-R1D2D4
- Molecular formula: C₅H₇
- Structure: CH₂ = CH — CH = CH — ĊH₂
- IUPAC-name: 2,4-pentadiene-1-yl
- Old name in mechanism : C5H7-D1D3R5

C5H7-R1D3MD2

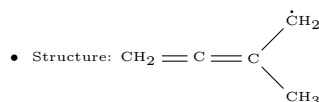
- Name in mechanism: C5H7-R1D3MD2
- Molecular formula: C₅H₇



- IUPAC-name: 2-methylen-3-buten-1-yl
- Old name in mechanism : C5H7-D1D3MR2

C5H7-R1D2-D3Me2

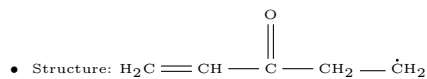
- Name in mechanism: C5H7-R1D2-D3Me2
- Molecular formula: C₅H₇



- IUPAC-name: 2-methyl-2,3-buten-1-yl
- Old name in mechanism: C5H7-D2D3MR2

C5H7O-R1K3D4

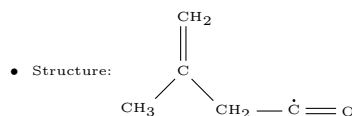
- Name in mechanism: C5H7O-R1K3D4
- Molecular formula: C₅H₇O



- IUPAC-name: penta-4-dien-1-yl-3-one
- Old name in mechanism: C2H4COC2H3-1

C5H7O-R1K1D3Me3

- Name in mechanism: C5H7O-R1K1D3Me3
- Molecular formula: C₅H₇O



- IUPAC-name: 3-Methyl-1-one-3-butene-1-yl
- Old name in mechanism : I-C4H7CO

C5H8-D1D3

- Name in mechanism: C5H8-D1D3
- Molecular formula: C₅H₈
- Structure: CH₂ = CH — CH = CH — CH₃
- IUPAC-name: Penta-1,3-diene
- Other names (eng): Penta-1,3-diene; Piperylene
- old name in the mechanism: C5H8-13

C5H8-D1D4

- Name in mechanism: C5H8-D1D4
- Molecular formula: C₅H₈
- Structure: CH₂ = CH — CH₂ — CH = CH₂
- IUPAC-name: Penta-1,4-diene
- Other names (eng): 1,4-Pentadiene; allylethylene
- old name in the mechanism: C5H8-14

C5H8-D1D3Me2

- Name in mechanism: C5H8-D1D3Me2
- Molecular formula: C₅H₈
- Structure:
$$\begin{array}{c} \text{CH}_3 \\ | \\ \text{CH}_2 = \text{C} - \text{CH} = \text{CH}_2 \end{array}$$
- IUPAC-name: 2-Methyl-1,3-butadiene
- Other names (eng): 2-Methyl-1,3-butadiene; Isoprene
- old name in the mechanism: C5H8-M2D1D3, I-A-C5H8

C5H8-D1-D2Me3

- Name in mechanism: C5H8-D1-D2Me3
- Molecular formula: C₅H₈
- Structure:
$$\begin{array}{c} \text{CH}_3 \\ \diagup \\ \text{CH}_2 = \text{C} = \text{C} \\ \diagdown \\ \text{CH}_3 \end{array}$$
- IUPAC-name: 3-Methyl-1,2-butadiene
- Other names (eng): 2-Methyl-2,3-butadiene; 3-Methylbuta-1,2-diene; 3,3-Dimethylallene; 1,1-Dimethylallene
- Old name in mechanism : C5H8-M2D2D3

C5H8O-K1D1

- Name in mechanism: C5H8O-K1D1
- Molecular formula: C₅H₈O
- Structure: CH₃ — CH₂ — CH₂ — CH = C = O
- IUPAC-name: penta-1-dien-1-one
- Old name in mechanism : N-C3H7CHCO

C5H8O-K3D1

- Name in mechanism: C5H8O-K3D1
- Molecular formula: C₅H₈O
- Structure:
$$\begin{array}{c} \text{O} \\ || \\ \text{H}_3\text{C} - \text{CH}_2 - \text{C} - \text{CH} = \text{CH}_2 \end{array}$$
- IUPAC-name: penta-1-dien-3-one
- Old name in mechanism : C2H5COC2H3

C5H9-R1D3Me3

- Name in mechanism: C5H9-R1D3Me3
- Molecular formula: C₅H₉
- Structure:
$$\begin{array}{c} \text{CH}_3 \\ | \\ \text{CH}_2 = \text{C} - \text{CH}_2 - \dot{\text{C}}\text{H}_2 \end{array}$$
- IUPAC-name: 3-Methyl-3-buten-1-yl
- Old name in the mechanism: C5H9-M2D1R4, I-A-C5H9P

C5H9-R1D2Me2

- Name in mechanism: C5H9-R1D2Me2
- Structure:
$$\begin{array}{c} \text{CH}_3 \\ | \\ \dot{\text{C}}\text{H}_2 - \text{C} = \text{CH} - \text{CH}_3 \end{array}$$
- IUPAC-name: 2-Methyl-2-buten-1-yl
- Other names (eng): 2-methyl-but-2-en-1-yl
- Old name in the mechanism: C5H9-M2D2R1, I-A-C5H9S

C5H9-R1MD2

- Name in mechanism: C5H9-R1MD2
- Molecular formula: C₅H₉
- Structure:
$$\begin{array}{c} \dot{\text{C}}\text{H}_2 \\ | \\ \text{CH}_2 = \text{C} - \text{CH}_2 - \text{CH}_3 \end{array}$$
- IUPAC-name: 2-Methylene-but-1-yl
- Other names (eng): 2-methyl-but-1-en
- Old name in mechanism : C5H9-M2RD1

C5H9-R1D2Me3

- Name in mechanism: C5H9-R1D2Me3
- Molecular formula: C₅H₉
- Structure:
$$\begin{array}{c} \text{CH}_3 \\ | \\ \text{CH}_3 - \text{C} = \text{CH} - \dot{\text{C}}\text{H}_2 \end{array}$$
- IUPAC-name: 3-Methyl-2-buten-1-yl
- Old name in mechanism : C5H9-M2D2R4

C5H9-R1D3Me2

- Name in mechanism: C5H9-R1D3Me2
- Molecular formula: C₅H₉
- Structure:
$$\begin{array}{c} \text{CH}_3 \\ | \\ \dot{\text{C}}\text{H}_2 - \text{CH} - \text{CH} = \text{CH}_2 \end{array}$$
- IUPAC-name: 2-Methyl-3-buten-1-yl
- Other names (eng): 3-methyl-but-1-en-4-yl
- Old name in mechanism : C5H9-M3D1R4

C5H9-R1D4

- Name in mechanism: C5H9-R1D4
- Molecular formula: C₅H₉
- Structure:
$$\begin{array}{c} \text{H} \\ \diagdown \\ \text{C} = \text{CH} - \text{CH}_2 - \text{CH}_2 - \dot{\text{C}}\text{H}_2 \\ \diagup \\ \text{H} \end{array}$$
- IUPAC-name: 4-Penten-1-yl
- Old name in the mechanism: C5H9-D1R5

C5H9-R4D1

- Name in mechanism: C5H9-R4D1
- Molecular formula: C₅H₉
- Structure:
$$\begin{array}{c} \text{H} \\ \diagdown \\ \text{C} = \text{CH} - \text{CH}_2 - \dot{\text{C}}\text{H} - \text{CH}_3 \\ \diagup \\ \text{H} \end{array}$$
- IUPAC-name: 1-Penten-4-yl
- Old name in the mechanism: C5H9-D1R4

C5H9-R3D1

- Name in mechanism: C5H9-R3D1
- Molecular formula: C₅H₉
- Structure:
$$\begin{array}{c} \text{H} \\ \diagdown \\ \text{C} = \text{CH} - \dot{\text{C}}\text{H} - \text{CH}_2 - \text{CH}_3 \\ \diagup \\ \text{H} \end{array}$$
- IUPAC-name: 1-Penten-3-yl
- Old name in the mechanism: C5H9-D1R3

C5H9-R1D3

- Name in mechanism: C5H9-R1D3
- Molecular formula: C₅H₉
- Structure: CH₃ — CH = CH — CH₂ — $\dot{\text{C}}\text{H}_2$
- IUPAC-name: 3-Penten-1-yl
- Old name in the mechanism: C5H9-D2R5

C5H9-R2D3

- Name in mechanism: C5H9-R2D3
- Molecular formula: C₅H₉
- Structure: CH₃ — CH = CH — $\dot{\text{C}}\text{H}$ — CH₃
- IUPAC-name: 3-Penten-2-yl
- Old name in the mechanism: C5H9-D2R4

C5H9O-R1K3

- Name in mechanism: C5H9O-R1K3
- Molecular formula: C₅H₉O
- Structure:
$$\text{H}_3\text{C} - \text{CH}_2 - \overset{\text{O}}{\parallel} \text{C} - \text{CH}_2 - \dot{\text{C}}\text{H}_2$$
- IUPAC-name: penta-1-yl-3-one
- Old name in mechanism : C2H4COC2H5-1

C5H9O-R1K4

- Name in mechanism: C5H9O-R1K4
- Molecular formula: C₅H₉O
- Structure:
$$\text{H}_2\dot{\text{C}} - \text{CH}_2 - \text{CH}_2 - \overset{\text{O}}{\parallel} \text{C} - \text{CH}_3$$
- IUPAC-name: penta-1-yl-4-one
- Old name in the mechanism: C3H6COCH3-1

C5H9O-R1K2

- Name in mechanism: C5H9O-R1K2
- Molecular formula: C₅H₉O
- Structure:
$$\text{CH}_3 - \text{CH}_2 - \text{CH}_2 - \overset{\text{O}}{\parallel} \text{C} - \dot{\text{C}}\text{H}_2$$
- IUPAC-name: penta-1-yl-2-one
- Old name in the mechanism: N-C3H7COCH2

C5H9O-R1K1

- Name in mechanism: C5H9O-R1K1
- Molecular formula: C₅H₉O
- Structure:
$$\text{O} = \dot{\text{C}} - \text{CH}_2 - \text{CH}_2 - \text{CH}_2 - \text{CH}_3$$
- IUPAC-name: penta-1-yl-1-one
- Old name in mechanism : N-C4H9CO

C5H10-D1Me2

- Name in mechanism: C5H10-D1Me2
- Molecular formula: C₅H₁₀
- Structure:
$$\begin{array}{c} \text{CH}_3 \\ | \\ \text{CH}_2 = \text{C} - \text{CH}_2 - \text{CH}_3 \end{array}$$
- IUPAC-name: 2-Methyl-1-butene
- Other names (eng): 1-Butene, 2-methyl, 1-Isoamylene
- Old name in the mechanism: C5H10-M2D1, I-A-C5H10

C5H10-D2Me2

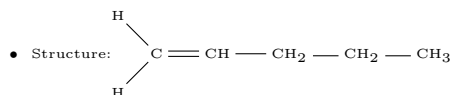
- Name in mechanism: C5H10-D2Me2
- Molecular formula: C₅H₁₀
- Structure:
$$\begin{array}{c} \text{CH}_3 \\ | \\ \text{CH}_3 - \text{C} = \text{CH} - \text{CH}_3 \end{array}$$
- IUPAC-name: 2-Methyl-2-butene
- Other names (eng): 2-Methyl 2-Butene, Trimethylethylene, Isoamylene
- Old name in the mechanism: C5H10-M2D2

C5H10-D1Me3

- Name in mechanism: C5H10-D1Me3
- Molecular formula: C₅H₁₀
- Structure:
$$\begin{array}{c} \text{CH}_3 \\ | \\ \text{CH}_3 - \text{CH} - \text{CH} = \text{CH}_2 \end{array}$$
- IUPAC-name: 3-Methyl-1-butene
- Other names (eng): 3-Methylbut-1-ene
- Old name in the mechanism: C5H10-M3D1, I-C-C5H10, C5H10-M2D3

C5H10-D1

- Name in mechanism: C5H10-D1
- Molecular formula: C₅H₁₀



- IUPAC-name: Pent-1-en
- Other names (eng): 1-pentene

C5H10-D2

- Name in mechanism: C5H10-D2
- Molecular formula: C₅H₁₀
- Structure: CH₃ — CH = CH — CH₂ — CH₃
- IUPAC-name: Pent-2-en
- Other names (eng): cis-2-pentene or trans-2-pentene. It is lumped in the mechanism

C5H10O-A11

- Name in mechanism: C5H10O-A11
- Molecular formula: C₅H₁₀O
- Structure:
$$\begin{array}{c} \text{H} \\ \diagdown \\ \text{O} = \text{C} - \text{CH}_2 - \text{CH}_2 - \text{CH}_2 - \text{CH}_3 \end{array}$$
- IUPAC-name: Pentanal
- Other names (eng): N-Pentanal, Valeraldehyde
- Old name in mechanism : N-C4H9CHO

C5H11-R1

- Name in mechanism: C5H11-R1
- Molecular formula: C₅H₁₁
- Structure: $\dot{\text{C}}\text{H}_2 - \text{CH}_2 - \text{CH}_2 - \text{CH}_2 - \text{CH}_3$
- IUPAC-name: 1-Pentanyl

C5H11-R2

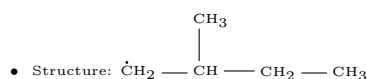
- Name in mechanism: C5H11-R2
- Molecular formula: C₅H₁₁
- Structure: CH₃ — $\dot{\text{C}}\text{H}$ — CH₂ — CH₂ — CH₃
- IUPAC-name: 2-Pentanyl

C5H11-R3

- Name in mechanism: C5H11-R3
- Molecular formula: C₅H₁₁
- Structure: CH₃ — CH₂ — $\dot{\text{C}}\text{H}$ — CH₂ — CH₃
- IUPAC-name: 3-Pentanyl

C5H11-R1Me2

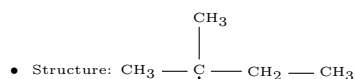
- Name in mechanism: C5H11-R1Me2
- Molecular formula: C₅H₁₁



- IUPAC-name: 2-Methyl-1-butanyl
- Other names (eng): 2-methylbut-1-yl
- Old name in the mechanism: C5H11-M2R1

C5H11-R2Me2

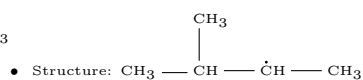
- Name in mechanism: C5H11-R2Me2
- Molecular formula: C₅H₁₁



- IUPAC-name: 2-Methyl-2-butanyl
- Other names (eng): 2-methylbut-2-yl
- Old name in the mechanism: C5H11-M2R2

C5H11-R2Me3

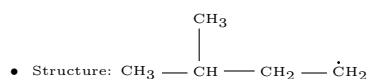
- Name in mechanism: C5H11-R2Me3
- Molecular formula: C₅H₁₁



- IUPAC-name: 3-Methyl-2-butanyl
- Other names (eng): 3-methylbut-2-yl
- Old name in the mechanism: C5H11-M2R3

C5H11-R1Me3

- Name in mechanism: C5H11-R1Me3
- Molecular formula: C₅H₁₁



- IUPAC-name: 3-Methyl-1-butanyl
- Other names (eng): 3-methylbut-1-yl
- Old name in the mechanism: C5H11-M2R4

C5H11O-O1

- Name in mechanism: C5H10O-O1
- Molecular formula: C₅H₁₁O
- Structure: $\text{CH}_2 - \text{CH}_2 - \text{CH}_2 - \text{CH}_2 - \text{CH}_3$
 $\begin{array}{c} | \\ \text{O} \end{array}$
- IUPAC-name: Pentan-1-olate

C5H11O-O2

- Name in mechanism: C5H10O-O2
- Molecular formula: C₅H₁₁O
- Structure: $\text{CH}_3 - \text{CH} - \text{CH}_2 - \text{CH}_2 - \text{CH}_3$
 $\begin{array}{c} | \\ \text{O} \end{array}$
- IUPAC-name: Pentan-2-olate

C5H11O-O3

- Name in mechanism: C5H10O-O3
- Molecular formula: C₅H₁₁O
- Structure: $\text{CH}_3 - \text{CH}_2 - \text{CH} - \text{CH}_2 - \text{CH}_3$
 $\begin{array}{c} | \\ \text{O} \end{array}$
- IUPAC-name: Pentan-3-olate

C5H12

- Name in mechanism: C5H12
- Molecular formula: C₅H₁₂
- Structure: $\text{CH}_3 - \text{CH}_2 - \text{CH}_2 - \text{CH}_2 - \text{CH}_3$
- IUPAC-name: Pentane
- Other names (eng): *n*-pentane
- Old name in the mechanism: N-C5H12

C5H12-Me2

- Name in mechanism: C5H12-Me2
- Molecular formula: C₅H₁₀
- Structure: $\begin{array}{c} \text{CH}_3 \\ | \\ \text{CH}_3 - \text{CH} - \text{CH}_2 - \text{CH}_3 \end{array}$
- IUPAC-name: 2-methyl-butane
- Other names (eng): 2-methyl butane, 2-methylbutane, *iso*-pentane
- Old name in the mechanism: C5H12-m2

B.7 C₆ species

C6H-R1T1T3T5

- Name in mechanism: C6H-R1T1T3T5
- Molecular formula: C₆H
- Structure: $\text{HC} \equiv \text{C} - \text{C} \equiv \text{C} - \text{C} \equiv \dot{\text{C}}$
- IUPAC-name: hexa-1,3,5-triyne-1-yl
- Other names (eng): 1,3,5-hexatriynyl radical
- Old name in mechanism: C6H

C6H2-T1T3T5

- Name in mechanism: C6H2-T1T3T5
- Molecular formula: C₆H₂
- Structure: $\text{HC} \equiv \text{C} - \text{C} \equiv \text{C} - \text{C} \equiv \text{CH}$
- IUPAC-name: 1,3,5-Hexatriyne
- Other names (eng): 1,3,5-Hexatriyne
- Other names (ger): 1,3,5-Hexatriin
- Old name in mechanism: C6H2

C6H3-R1T1D3-D5

- Name in mechanism: C6H3-R1T1D3-D5
- Molecular formula: C₆H₃
- Structure: $\text{H}_2\text{C} = \text{C} = \text{C} = \text{CH} - \text{C} \equiv \dot{\text{C}}$
- IUPAC-name: hexa-3,4,5-trien-1-yne-1-yl
- Old name in mechanism: C6H3

C6H11O-R1K4

- Name in mechanism: C6H11O-R1K1
- Molecular formula: C₆H₁₁O
- Structure: $\text{H}_2\dot{\text{C}} - \text{CH}_2 - \text{CH}_2 - \overset{\text{O}}{\parallel} \text{C} - \text{CH}_2 - \text{CH}_3$
- IUPAC-name: Hexa-1-yl-4-one
- Old name in the mechanism: C3H6COC2H5-1

C6H11O-R1K3

- Name in mechanism: C6H11O-R1K3
- Molecular formula: C₆H₁₁O
- Structure: $\text{CH}_3 - \text{CH}_2 - \text{CH}_2 - \overset{\text{O}}{\parallel} \text{C} - \text{CH}_2 - \dot{\text{C}}\text{H}_2$
- IUPAC-name: Hexa-1-yl-3-one
- Old name in the mechanism: N-C3H7COC2H4-1

C6H11O-R1K2

- Name in mechanism: C6H11O-R1K2
- Molecular formula: C₆H₁₁O
- Structure: $\text{CH}_3 - \text{CH}_2 - \text{CH}_2 - \text{CH}_2 - \overset{\text{O}}{\parallel} \text{C} - \dot{\text{C}}\text{H}_2$
- IUPAC-name: Hexa-1-yl-2-one
- Old name in the mechanism: N-C4H9COCH2

C6H11O-R1K1

- Name in mechanism: C6H11O-R1K1
- Molecular formula: C₆H₁₁O
- Structure: $\text{CH}_3 - \text{CH}_2 - \text{CH}_2 - \text{CH}_2 - \text{CH}_2 - \dot{\text{C}} = \text{O}$
- IUPAC-name: Hexa-1-yl-1-one
- Old name in the mechanism: N-C5H11CO

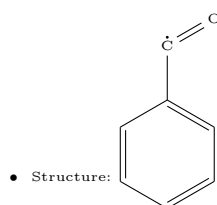
C6H12O-A11

- Name in mechanism: C6H12O-A11
- Molecular formula: C₆H₁₂O
- Structure: $\text{CH}_3 - \text{CH}_2 - \text{CH}_2 - \text{CH}_2 - \text{CH}_2 - \text{C} \begin{matrix} \text{H} \\ \diagup \\ \text{O} \end{matrix}$
- IUPAC-name: Hexanal
- Old name in the mechanism: N-C5H11CHO

B.8 C₇ species

A1CO

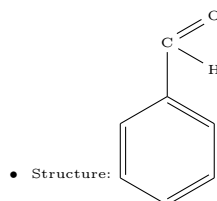
- Name in mechanism: A1CO
- Molecular formula: C₇H₅O



- IUPAC-name: phenylmethanone
- Old name in mechanism: A1CO

A1CHO

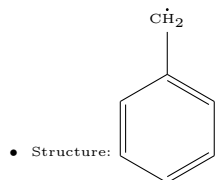
- Name in mechanism: A1CHO
- Molecular formula: C₇H₆O



- IUPAC-name: Benzaldehyde
- Other names (eng): Benzaldehyde
- Old name in mechanism: A1CHO

A1CH2

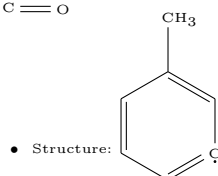
- Name in mechanism: A1CH2
- Molecular formula: C₇H₇



- IUPAC-name: Benzyl
- Other names (eng): Benzyl radical, Phenyl-methyl radical
- Other names (ger): Methyl,phenyl-
- Old name in mechanism: A1CH2

A1CH3-M

- Name in mechanism: A1CH3-M,
- Molecular formula: C₇H₇

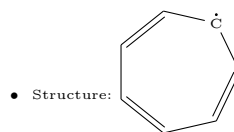


- IUPAC-name: Methylbenzene

- Old name in mechanism: C7H7-A1m1*; A1CH3*-m

CyC7H7-D1D4D6

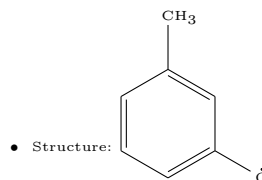
- Name in mechanism: CyC7H7-D1D4D6
- Molecular formula: C₇H₇



- IUPAC-name: 2,4,6-Cycloheptatrien-1-yl
- Other names (eng): cycloheptatrienyl
- Old name in mechanism: C7H7

OA1CH3-M

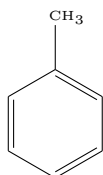
- Name in mechanism: OA1CH3-M
- Molecular formula: C₇H₇O



- IUPAC-name: (3-Methylphenyl)oxy radical
- Other names (eng): 3-Methyl-phenoxy
- Other names (ger): Phenoxy, 3-methyl-
- Old name in mechanism: C7H7O-A1m1o3

A1CH3

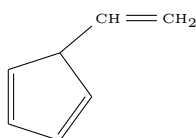
- Name in mechanism: A1CH3
- Molecular formula: C₇H₈



- Structure:
- IUPAC-name: Methyl benzene
- Other names (eng): Toluene
- Old name in mechanism: A1CH3

CH3FC6H6

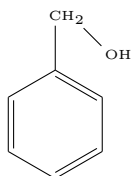
- Name in mechanism: CH3FC6H6
- Molecular formula: C₇H₈



- Structure:
- IUPAC-name: 5-Ethylidene-1,3-cyclopentadiene
- Other names (eng): 6-Methylfulvene

A1CH2OH

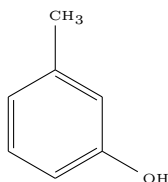
- Name in mechanism: A1CH2OH
- Molecular formula: C₇H₈O



- Structure:
- IUPAC-name: Phenylmethanol,
- Other names (eng): Benzyl alcohol
- Old name in mechanism: A1CH2OH

OHA1CH3-M

- Name in mechanism: OHA1CH3-M
- Molecular formula: C₇H₈O

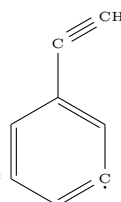


- Structure:
- IUPAC-name: 3-Methylphenol
- Other names (eng): 1-Hydroxy-3-methylbenzene, 3-Hydroxytoluene
- Old name in mechanism: C7H8O-A1m1OH3

B.9 C₈ species

A1C2H-M

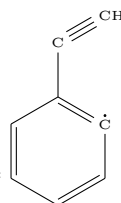
- Name in mechanism: A1C2H-M
- Molecular formula: C₈H₅



- Structure:
- IUPAC-name: m-ethynylcyclohexatriene
- Old name in mechanism: A1C2H-; A1C2H*-m

A1C2H-O

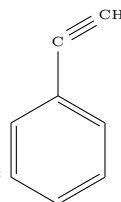
- Name in mechanism: A1C2H-O
- Molecular formula: C₈H₅



- Structure:
- IUPAC-name: o-ethynylcyclohexatriene
- Other names (eng): ortho-Ethynylphenyl
- Other names (ger): phenylethynyl radical, Ethynylphenyl radical
- Old name in mechanism: A1C2H*; A1C2H*-o

A1C2H

- Name in mechanism: A1C2H
- Molecular formula: C₈H₆

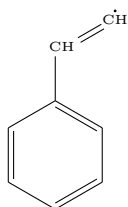


- Structure:
- IUPAC-name: Ethynylbenzene
- Other names (eng): Phenylacetylene, 1-Phenylethyne

N-A1C2H2

- Name in mechanism: N-A1C2H2

- Molecular formula: C_8H_7

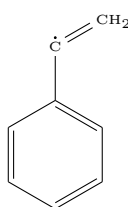


- Structure:
- IUPAC-name: 1-Ethenylbenzene
- Other names (eng): n-Styryl, n-Styral radical ($C_6H_5CH=CH^*$)

I-A1C2H2

- Name in mechanism: I-A1C2H2

- Molecular formula: C_8H_7

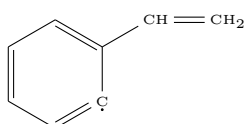


- Structure:
- IUPAC-name: 2-Ethenylbenzene
- Other names (ger): i-Styrenyl Radical

A1C2H3-R

- Name in mechanism: A1C2H3-R

- Molecular formula: C_8H_7

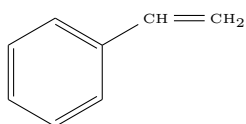


- Structure:
- IUPAC-name: Phenylethene
- Other names (eng): o-Styrene Radical ($C_6H_4CH=CH_2$)

A1C2H3

- Name in mechanism: A1C2H3

- Molecular formula: C_8H_8

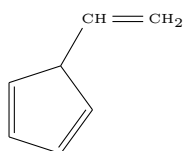


- Structure:
- IUPAC-name: Styrene
- Other names (eng): Styrene, Vinyl benzene; cin-namene; styrol; phenylethene; diarex HF 77; styrolene; styropol; vinylbenzene; phenylethylene

C2H3FC6H6

- Name in mechanism: C2H3FC6H6

- Molecular formula: C_8H_8

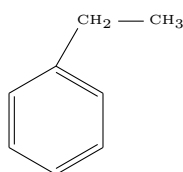


- Structure:
- IUPAC-name: Ethenylfulvene

A1C2H5

- Name in mechanism: A1C2H5

- Molecular formula: C_8H_{10}

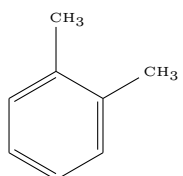


- Structure:
- IUPAC-name: Ethylbenzene

C8H10-A1M1M2

- Name in mechanism: C8H10-A1M1M2

- Molecular formula: C_8H_{10}

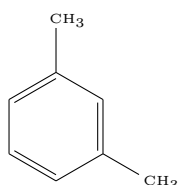


- Structure:
- IUPAC-name: o-Xylene
- Other names (eng): o-Xylol, 1,2-Dimethylbenzene

C8H10-A1M1M3

- Name in mechanism: C8H10-A1M1M3

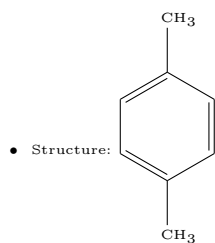
- Molecular formula: C_8H_{10}



- Structure:
- IUPAC-name: m-Xylene
- Other names (eng): m-Xylol, 1,3-Dimethylbenzene

C₈H₁₀-A1M1M4

- Name in mechanism: C₈H₁₀-A1M1M4
- Molecular formula: C₈H₁₀

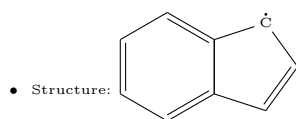


- IUPAC-name: p-Xylene
- Other names (eng): p-Xylol, 1,4-Dimethylbenzene

B.10 C₉ Species

A1R5-

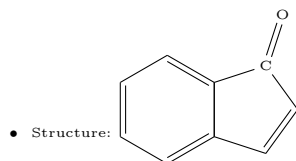
- Name in mechanism: A1R5-
- Molecular formula: C₉H₇



- IUPAC-name: Indene radical

OA1R5

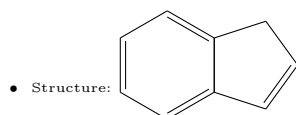
- Name in mechanism: OA1R5
- Molecular formula: C₉H₇O



- IUPAC-name: Inden-1-one

A1R5

- Name in mechanism: A1R5
- Molecular formula: C₉H₈

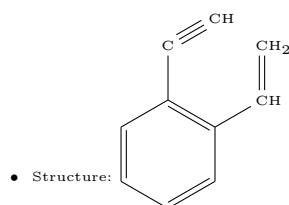


- IUPAC-name: 1-Indene
- Other names (eng): Indene, benzocyclopentadiene, Indonaphthene

B.11 C₁₀ Species

A1C2HAC

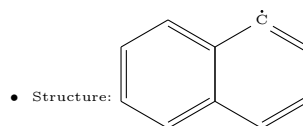
- Name in mechanism: A1C2HAC
- Molecular formula: C₁₀H₇



- IUPAC-name: 1-ethen,2-ethin benzene

A2-X

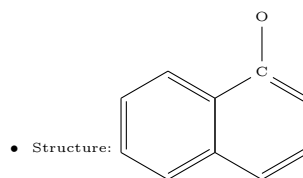
- Name in mechanism: A2-X
- Molecular formula: C₁₀H₇



- IUPAC-name: 1-naphthyl radical

OA2

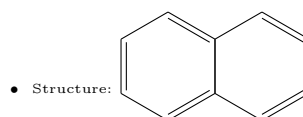
- Name in mechanism: OA2
- Molecular formula: C₁₀H₇O



- IUPAC-name: Naphthalene-1-one

A2

- Name in mechanism: A2
- Molecular formula: C₁₀H₈

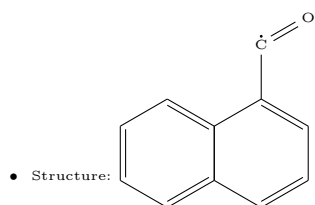


- IUPAC-name: Naphthalene
- Other names (eng): naphthalin, naphthaline, antimit, albocarbon,

B.12 C₁₁ Species

A2CO

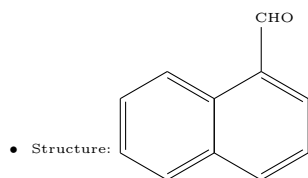
- Name in mechanism: A2CO
- Molecular formula: C₁₁H₇O₁



- IUPAC-name: naphthalen-1-ylmethanone

A2CHO

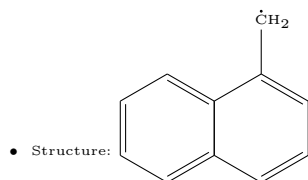
- Name in mechanism: A2CHO
- Molecular formula: C₁₁H₈O₁



- IUPAC-name: 1-Naphthaldehyde

A2CH2

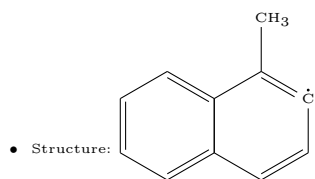
- Name in mechanism: A2CH2
- Molecular formula: C₁₁H₉



- IUPAC-name: 1-methylene Naphthalene

A2CH3-P

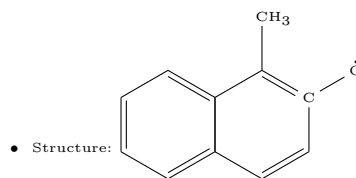
- Name in mechanism: A2CH3-P
- Molecular formula: C₁₁H₉



- IUPAC-name: 1-methyl,2-naphthalenyl radical

OA2CH3

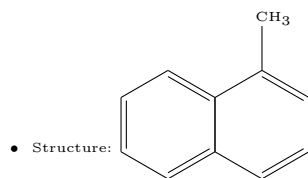
- Name in mechanism: OA2CH3
- Molecular formula: C₁₁H₉O



- IUPAC-name: 1-methyl Naphthalol

A2CH3

- Name in mechanism: A2CH3
- Molecular formula: C₁₁H₁₀

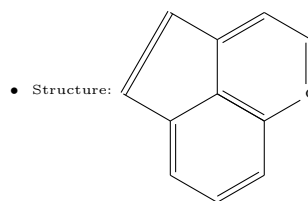


- IUPAC-name: 1-Methylnaphthalene

B.13 C₁₂ Species

A2R5-

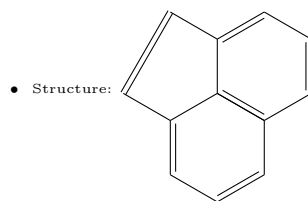
- Name in mechanism: A2R5-
- Molecular formula: C₁₂H₇



- IUPAC-name: Acenaphthylene radical

A2R5

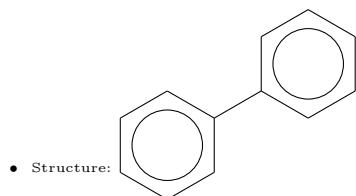
- Name in mechanism: A2R5
- Molecular formula: C₁₂H₈



- IUPAC-name: Acenaphthylene

P2

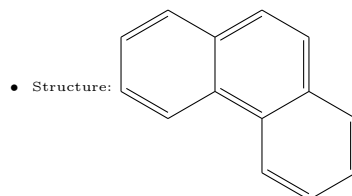
- Name in mechanism: P2
- Molecular formula: $C_{12}H_{10}$



- IUPAC-name: Biphenyl

A3

- Name in mechanism: A3
- Molecular formula: $C_{14}H_{10}$

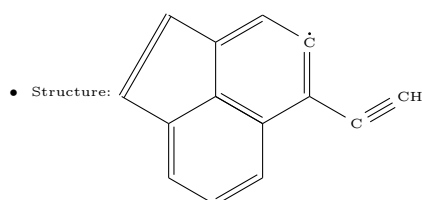


- IUPAC-name: Phenanthrene

B.14 C_{14} species

A2R5C2H-

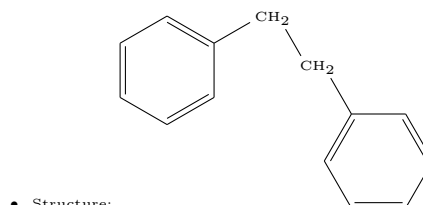
- Name in mechanism: A2R5C2H-
- Molecular formula: $C_{14}H_7$



- IUPAC-name: 5-ethynylacenaphthylene

TOLA2

- Name in mechanism: TOLA2
- Molecular formula: $C_{14}H_{14}$

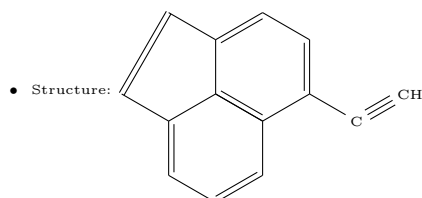


- Structure:
- IUPAC-name: (1,2-Ethanediyl)dibenzene
- Other names (eng): Bibenzyl

- Old name in mechanism: TOLA2

A2R5C2H

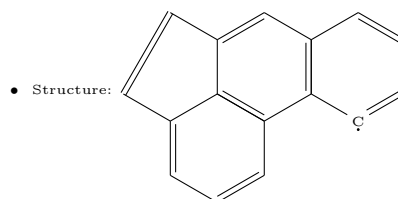
- Name in mechanism: A2R5C2H
- Molecular formula: $C_{14}H_8$



- IUPAC-name: ethynylacenaphthylene

A3R5-

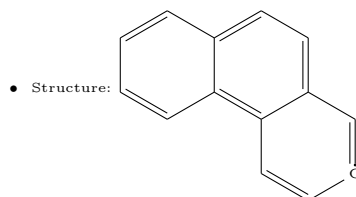
- Name in mechanism: A3R5-
- Molecular formula: $C_{16}H_9^-$



- IUPAC-name: Acephenanthrylene

A3-

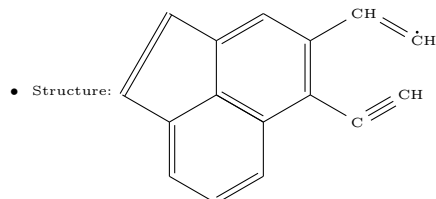
- Name in mechanism: A3-
- Molecular formula: $C_{14}H_9$



- IUPAC-name: 2-Phenanthrenyl

ANC2HAC

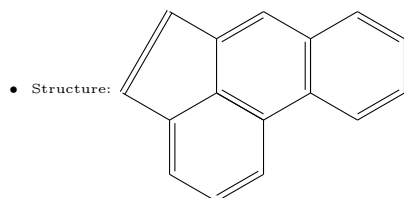
- Name in mechanism: ANC2HAC
- Molecular formula: $C_{16}H_9$



- IUPAC-name: 1-ethen,2-ethin acenaphthylene

A3R5

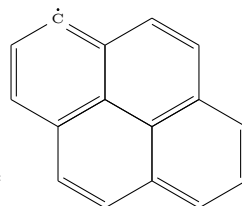
- Name in mechanism: A3R5
- Molecular formula: $C_{16}H_{10}$



- IUPAC-name: Acephenanthrylene

A4-

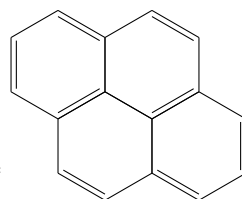
- Name in mechanism: A4-
- Molecular formula: $C_{16}H_9$



- Structure:
- IUPAC-name: Pyrene radical

A4

- Name in mechanism: A4
- Molecular formula: $C_{16}H_{10}$



- Structure:
- IUPAC-name: Pyrene